The druggable antimalarial target 1–deoxy–D–xylulose–5–phosphate reductoisomerase: purification, kinetic characterization and inhibition studies

A thesis submitted in fulfilment of the requirement for the degree of

DOCTOR OF PHILOSOPHY

of

RHODES UNIVERSITY

by

JESSICA LEIGH GOBLE

April 2011

Abstract

Plasmodium falciparum 1–deoxy–D–xylulose–5–phosphate reductoisomerase (PfDXR) plays a role in isoprenoid biosynthesis in the malaria parasite and is absent in the human host, making this parasite enzyme an attractive target for antimalarial drug design. To characterize PfDXR, it is necessary to produce large quantities of the enzyme in a soluble and functional form. However, the over–production of malarial proteins in prokaryotic host systems often results in the formation of truncated proteins or insoluble protein aggregates. A heterologous expression system was developed for the production of active PfDXR using codon harmonization and tight control of expression in the presence of *lac* repressor. Yields of up to 2 mg/l of enzyme were reported using the optimised expression system, which is 8 to 10–fold greater than previously reported yields. The kinetic parameters K_m, V_{max} and k_{cat} were determined for PfDXR; values reported in this study were consistent with those reported in the literature for other DXR enzymes. A three–dimensional model of the malarial drug target protein PfDXR was generated, and validated using structure–checking programs and protein docking studies. Structural and functional features unique to PfDXR were identified using the model and comparative sequence analyses with apicomplexan and non–apicomplexan DXR proteins. Residues Val44 and Asn45, essential for NADPH binding; and catalytic hatch residues Lys224 and Lys226, which are unique to the species of *Plasmodium*, were mutated to resemble those of *E. coli* DXR. Interestingly, these mutations resulted in significant reductions in substrate affinity, when compared to the unmutated PfDXR. Mutant enzymes PfDXR(VN43,44AG) and PfDXR(KK224,226NS) also demonstrated a decreased ability to turnover substrate by 4–fold and 2–fold respectively. This study indicates a difference in the role of the catalytic hatch of PfDXR with regards to the way in which it captures substrates. The study also highlights subtle differences in cofactor binding to PfDXR, compared with the well characterized EcDXR enzyme. The validated PfDXR model was also used to develop a novel efficient *in silico* screening method for potential tool compounds for use in the rational design of novel DXR inhibitors. Following *in silico* screening of 46 potential DXR inhibitors, a two–tiered *in vitro* screening approach was undertaken. DXR inhibition was assessed for the 46 novel compounds using an NADPH–dependant DXP enzyme inhibition assay and antimalarial potential was assessed using *P.falciparum*–infected erythrocyte growth assays. Select compounds were tested in human cells in order to determine whether they were toxic to the host. From the parallel *in silico* and *in vitro* drug screening, it was evident that only a single compound demonstrated reasonable potential binding to DXR (determined

using *in silico* docking), inhibited DXR *in vitro* and inhibited *P. falciparum* growth, without being toxic to human cells. Its potential as a lead compound in antimalarial drug development is therefore feasible. Two outcomes were evident from this work. Firstly, analogues of known antimalarial natural products can be screened against malaria, which may then lead towards the rational design of novel compounds that are effective against a specific antimalarial drug target enzyme, such as PfDXR. Secondly, the rational design of novel compounds against a specific antimalarial drug target enzyme can be untaken by adopting a coupled *in silico* and *in vitro* approach to drug discovery.

Declaration

I declare that this thesis is my own, unaided work. It is being submitted for the degree of Doctor of Philosophy at Rhodes University. It has not been submitted before for any degree or examination in any other university.

_____

Signed on the 5th day of April 2011

Dedication

This thesis is dedicated to

My parents, Jennifer Watson, Clive Goble and Michael Strohman

Acknowledgements

Thank you to my supervisor, Professor Greg Blatch. Your spirit and energy has allowed me to accomplish one of the greatest feats possible. Thank you for encouraging me to always give of my best, even when I thought it was impossible.

Thank you to my friend and co–supervisor, Dr Linda Stephens. You have made this experience fulfilling and exciting.

I wish to extend further acknowledgement to:

- Mr Marius Mutorwa and Mr Ryan Young, at Department of Chemistry, Rhodes University, for synthesizing the compounds used in this study
- Mr Tjaart De Beer, at the Department of Biochemistry, University of Pretoria, for assistance with homology modelling
- Mr Matthew Adendorff, at Department of Chemistry, Rhodes University, for assistance with docking
- Professor Peter Smith and Sumaya Salie, at the Department of Pharmacology, University of Cape Town, for help with parasite culturing
- Mr Sagaran Abboo and Mrs Margot Brooks for technical support
- Collaborators in this work, Dr Aileen Boshoff, Professor Perry Kaye and Professor Mike Davies–Coleman, at the Department of Chemistry, Rhodes University, as well as Professor Abraham Louw, at the Department of Biochemistry, University of Pretoria
- The National Research Foundation (NRF) and South Africa Malaria Initiative (SAMI) for supporting this research

To my siblings, Tarryn Goble, Megan Goble, David Goble, Paige Goble, and best friend, Elizabeth Baron, thank you for your love and support

And the most special mention needs to be extended to Colleen Hepburn, Jennifer Watson and Jane Baron, who spent hours proof reading my thesis

Table of contents

List of figures

List of tables

Symbols and abbreviations

α: alpha

β: beta

γ: gamma

Dxr/ IspC: 1–deoxy–D–xylulose–5–phosphate reductoisomerase

PfDXR: *Plasmodium falciparum* 1–deoxy–D–xylulose–5–phosphate reductoisomerase

EcDXR: *Escherichia coli* 1–deoxy–D–xylulose–5–phosphate reductoisomerase

ZmDXR: *Zymomonas mobilis* 1–deoxy–D–xylulose–5–phosphate reductoisomerase

AtDXR: *Arabidopsis thaliana* 1–deoxy–D–xylulose–5–phosphate reductoisomerase

TmDXR: *Thermotoga maritima* 1–deoxy–D–xylulose–5–phosphate reductoisomerase

DXP: 1–deoxy–D–xylulose–5–phosphate

MVA pathway: mevalonate pathway

MEP pathway: mevalonate–independent pathway

MEP: 2–C–methyl–erythritol 4–phosphate

NADPH: nicotinamide adenine dinucleotide phosphate

PKC: protein kinase C

IC_{50}: half maximal inhibitory concentration

K_i: dissociation constant for the enzyme–inhibitor complex

K_m: concentration of substrate that leads to half–maximal velocity

V_{max}: maximum initial velocity or rate of a reaction

K_{cat}: maximum number of enzymatic reactions catalyzed per second

nM: nano molar

µM: micro molar

mM: milli molar

Kcal/mol: kilo calories per mole

GPI: Glycosylphosphatidylinisotol

Å: Angstroms

Ala (A): Alanine

Arg (R): Arginine

Asn (N): Asparagine

Asp (D): Aspartic acid

Cys (C): Cysteine

Glu (E): Glutamic acid

Gly (G): Glycine

His (H): Histadine

Ile (I): Isoleucine

Leu (L): Leucine

Lys (K): Lysine

Met (M): Methionine

Phe (F): Phenylalanine

Pro (P): Proline

Ser (S): Serine

Thr (T): Threonine

Trp (W): Tryptophan

Tyr (Y): Tyronsine

Val (V): Valine

Outputs

Publications:

1. The druggable antimalarial target PfDXR: overproduction strategies and kinetic characterization. Goble, J.L., Johnson, H., de Ridder, J., Stephens, L.L., Louw, A., Blatch, G.L., Boshoff A. Protein Expression and Purification. Accepted for review by the Journal of Biomedical Science
2. The malarial drug target *Plasmodium falciparum* 1–deoxy–D–xylulose–5–phosphate reductoisomerase (*Pf*DXR): development of a 3–D model for identification of novel, structural and functional features and for inhibitor screening, by Goble, J.L., Adendorff, M.R., de Beer, T.A.P., Stephens L. L., and Blatch, G. L.; Protein and Peptide Letters, 2010, Vol 17, No 1, 109–120
3. Malaria Heat Shock Proteins: Drug Targets that Chaperone other Drug Targets by Pesce, E.–R., Cockburn, I.L., Goble, J.L., Stephens, L.L., and Blatch, G.L. Infectious Disorders – Drug Targets 2010, Vol. 10, No. 3

Conference outputs:

1. Presented: 'The malarial Drug Target Enzyme *Pf*DXR: coexpression strategies to improve protein production'. J.L. Goble, L.L. Stephens, G.L. Blatch; work presented by myself at the SASBMB Conference, Bloemfontein, January, 2010
2. Presented: 'The malarial Drug Target Enzyme *Pf*DXR: Computer to Bench'. J.L. Goble, L.L. Stephens, G.L. Blatch; work presented by myself at the Center for Chemico– and Biomedicinal Research Symposium, Grahamstown, November 2009
3. Presented: 'The Malarial Drug Target *Pf*DXR: Development of a 3–D Model for Identification of Novel, Structural and Functional Features and for Inhibitor Screening'. J.L. Goble, M.R. Adendorff, T.A.P. de Beer, L.L. Stephens, G.L. Blatch; work presented by myself, at the SAICSIT Bioinformatics conference, Vaal, October 2009

CHAPTER 1

LITERATURE REVIEW

1.1 MALARIA

1.1.1 Malaria: the burden

Human malaria can be caused by transmission by four different species of *Plasmodium* protozoa, namely *Plasmodium malariae*, *Plasmodium ovale*, *Plasmodium vivax and Plasmodium falciparum*, with the latter being the most deadly strain (WHO, 2010_1). A fifth species, *Plasmodium knowlesi*, which is known to infect primates, has in recent years been shown to infect humans (Vythilingam *et al.*, 2006). Reports have confirmed that one fifth of the cases of malaria diagnosed in Malaysia are due to *P. knowlesi* (Singh *et al*, 2004), because the mosquito vector responsible for infection, *Anopheles latens*, is endemic to the area (Vythilingam *et al.*, 2006).

In 2008, 108 countries were classified as areas at risk of malaria, with 57% being in Africa, 30% in Asia and 5% in the Americas (SAMI, 2007; WHO, 2010_1). In 2008, there were 247 million cases of malaria reported, with nearly one million resulting in death. In Africa a child dies every 45 seconds of malaria, accounting for more than 20% of all childhood deaths (WHO, 2010_1). Numerous quantitative aspects have been investigated in order to more accurately estimate the burden that malaria places on the world. However, estimations are rough because of a number of known limitations, for example, incomplete coverage of areas at risk and the difficulty in diagnosing malaria post mortem. Results regarding these statistics have highlighted the severity of the malaria burden and the lack of support in the field of research (Ndugwa *et al*., 2007).

In 2006, the World Health Organization issued a statement endorsing the use of indoor residual spraying with dichlorodiphenyltrichloroethane (DDT) for the purpose of malaria vector control in malaria epidemic areas. Due to the relative ineffectiveness of other control strategies on the great burden imposed by malaria, other international organizations supported this endorsement, even though at the Stockholm Convention in 2001 DDT was targeted as a persistent organic pollutant requiring eventual elimination (Sadasivaiah *et al.*, 2007). However, with an increasing mosquito resistance to insecticides, including DDT and pyrethroids, malaria control proves to be a continuous setback (WHO, 2010_1).

According to the WHO (2010_1), global eradication of malaria is unachievable, because of the emergence of drug resistance in *P. falciparum*. The emergence of drug resistance means that many antimalarial drugs and prophylactics have become less effective. Many new generation drugs are often associated with significant side effects, such as gastrointestinal stress (doxycycline), fatal heart rhythms (halofantrine) and neurological disturbances (mefloquine) (Doolan and Hoffman, 2001). The incidence of increased insecticide resistance means that insecticides are no longer effective against the vector (Doolan and Hoffman, 2001). These factors emphasize the urgent need for development of malaria vaccines and new effective antimalarial drugs (Doolan and Hoffman, 2001).

1.1.2 Current research and development (R&D)

There is a global need to encourage additional research in the development of pharmaceutical products against neglected diseases – such as tuberculosis, malaria, leishmaniasis, and trypanosomiasis – that affect millions of people annually, particularly in poverty–stricken countries with poorly developed health care systems (Kesselheim, 2008). Coartem (a combination of lumefantrine and artemether) is an antimalarial drug that is commonly used in the treatment of malaria. Still today its wholesale price is US$ 2.40 per treatment and is often marketed at five times this value in the private sector. Its patent however expires in 2010, but it is expected that the price will not fall very quickly. Because malaria is a disease of poverty, even a price of $1 per treatment is unacceptable. Chloroquine, for example, costs less than $0.10 per treatment and so investment in antimalarial drug discovery and development is small (Balasegaram *et al*., 2006).

In a study done by Trouiller *et al*. (2002), the outcomes of pharmaceutical R&D over 25 years was analysed. It was found that of 1393 drugs marketed between 1975 and 1999, only 16 were for tropical diseases and tuberculosis. According to the study, pharmaceutical companies argued that R&D is "too costly and risky to invest in low–return neglected diseases" (Trouiller *et al*., 2002). A number of positive initiatives have however been put in place in the last decade; the Food and Drug Administration (FDA) Amendments Act of 2007 is a programme that will afford companies the opportunity to apply for a "voucher" entitling the company to sponsorship for research into drug development for tropical diseases (Kesselheim, 2008). A major setback with this initiative is however the fact that the voucher will only see rewards on successful endeavours and the voucher will also not be weighted based on the "usefulness" of the drug. For example, if a novel antimalarial drug which is

highly effective against malaria, but it degrades in the sun and needs to be taken six times per day, will earn a voucher, but will not be considered for reapplication for a follow–on that may be even more effective. Another alternative to such an initiate could be for government to work with non–profit organisations who are involved in developing drugs/treatments for neglected diseases (Kesselheim, 2008). GlaxoSmithKline is however putting money and resources into free malaria research. In the past 2 years GlaxoSmithKline have screened more than two million molecules against asexual blood stage *P. falciparum*, with the investigation revealing 13 500 active compounds demonstrating more than 80% growth inhibition. It has been said that sharing this data could trigger significant advances in malaria research, such as those that came from the human genome project (Fidock, 2010).

In order for malaria research to advance, it is not only necessary to build a public repository of knowledge and data (Fidock, 2010), it is also essential to bridge the gap between chemical and biochemical investigators, in a multidisciplinary research approach (MIM, 2009). For this reason, understanding the biochemistry of the parasite responsible for malaria is a major building block in the advancement of malaria research.

1.1.3 The *Plasmodium* life cycle

Plasmodium protozoal parasites *P. falciparum*, *P. vivax, P. ovale, and P. malariae* encompass a life cycle which is split between a vertebrate host and an insect vector. The *Plasmodium* species' infect primarily a human host, with the exception of *P. malariae*, which can affect other higher primates (Cann, 1996).

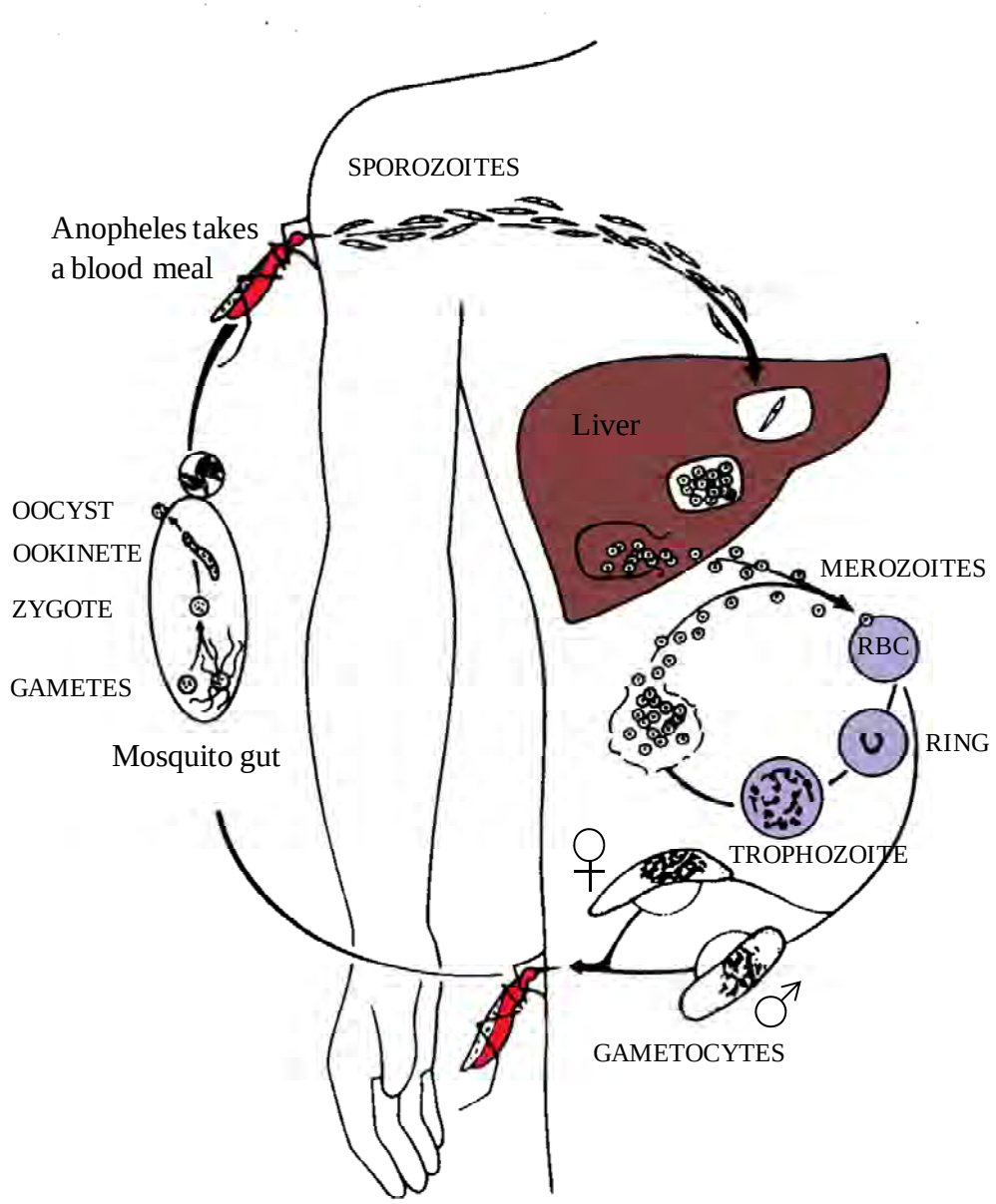

Figure 1.1: The life–cycle of *P.falciparum* in the human host and in the insect vector (modified from Wirth, 2002).

The basic life cycle of the parasite (Figure **1.1**) begins with the anopheles mosquito; sporozoites bud from oocysts located in the mosquito midgut. When a mature oocyst bursts, sporozoites are released into the hemolymph and travel to the salivary glands, where they come to rest. Sporozoites remain viable for weeks, while the anopheles mosquito awaits its next blood meal. When the infected mosquito takes a blood meal, the sporozoites are injected into the skin of the vertebrate host (Kappe *et al*, 2003). Once in the host blood stream, the sporozoites invade the liver and penetrate hepatocytes where they multiply within host cells for up to 16 days (Cann, 1996), in a replicative process called schizogony. Subsequently, segmentation of the cytoplasm, gives rise to merozoites, which then re–enter the blood.

Merozoites then penetrate the erythrocyte and the parasite then transforms into the trophozoite or feeding stage, ingesting large amounts of hemoglobin. The processing of hemoglobin occurs in the parasite food vacuole and involves transforming the by–product heme, into the non–toxic crystalline form, called haemozoin. The parasite cell then undergoes schizogony resulting in the rupturing of the erythrocyte and subsequent release of merozoites into the blood, which then invade new erythrocytes. Erythrocytic schizogony is synchronized, meaning that erythrocytes generally rupture synchronously, releasing merozoites into the bloodstream. Some merozoites differentiate into male and female gametocytes, while others actuate to infect other erythrocytes (Wirth, 2002). The sexual stage gametocytes, which have no further activity in the human host, re–enter another mosquito vector after it has bitten the infected host. Within the gut of the vector, the gametocytes become fertilized, resulting in an ookinete. The ookinete penetrates the cell wall of the midgut, where it develops into an oocyst. Sporogeny within the oocyst results in the release of sporozoites, which then migrate to the salivary glands of the vector, after the oocyst has ruptured; the system now ready for another cycle of infection (Cann, 1996).

1.2 VACCINES AND ANTIMALARIAL DRUGS

1.2.1 Malaria vaccines

Malaria research is predominantly two–tier; firstly, research is being carried out in the field of antimalarial drug design and secondly, in the development of a vaccine that is effective against malaria. It has been necessary to look closely at the parasite's life cycle in order to procure an appropriate vaccine strategy. The traditional approach to vaccine development has been to target specific aspects of the parasite development, including the pre–erythrocytic, asexual and sexual stages (WHO, 2010_2).

Different classes of vaccines exist, including: inactivated vaccines; live vector–based vaccines, which include attenuated and heterologous vaccines; subunit/component vaccines; conjugate vaccines; and DNA vaccines. In malaria, inactivated vaccines typically result from the killing of blood stage parasites using methods such as formaldehyde treatment (Ghaffar and Haqqi, 2010). Live vector vaccines involve chemically weakening a blood stage parasite such that the immune system can elicit an immune response – attenuation involves reducing the virulence of a pathogen while still keeping it viable (Badgett *et al*., 2002), while a heterologous prime boost vaccine introduces a virus, in order to provide protection from the

parasite (Ho *et al*., 2008). A subunit vaccine typically involves isolating a specific protein from the parasite and presenting it to the immune system so that an immune response is elicited. And alternative to this is recombinantly engineering a protein gene from a virus. In this case, the parasite will produce the protein, to which the immune system will develop antibodies (The College of Physicians of Philadelphia, 2010). A conjugate vaccine involves covalently attaching an antigen to a protein carrier, whereby the carrier protein provides the epitopes required for immune system recognition (Goldblatt, 2000). DNA vaccines involve introducing genetically engineered DNA in order to induce an immune response – this type of vaccination typically induces a greater number of immune response types when compared to other vaccine strategies (Alarcon *et al*., 1999).

In malaria vaccine production, two strategies are typically investigated, including live attenuated whole parasite vaccines and subunit vaccines. Most subunit vaccines are developed to mimic naturally acquired immunity from long term exposure while whole parasite vaccines induce immune responses that are greater than that from naturally acquired immunity (reviewed by Matuschewski and Mueller, 2007). The success of whole parasite vaccines was reported by Nussenzweig and co–workers in 1967, whereby an immune response against malaria was achieved in a rodent malaria model, subsequent to irradiation of sporozoites. The group reported that mice were completely immunized with repeat doses of γ–irradiated sporozoites. Subsequent to this was the development of genetically attenuated parasites (GAPs) (Mueller *et al*., 1995), which have overcome the short fallings of the live attenuated sporozoite vaccines with regards to safety and batch–to–batch variation. GAPs have superseded γ–irradiated sporozoites in that they are consistently produced, they are genetically stable and they have greater potency (reviewed by Matuschewski and Mueller, 2007). In the case of subunit vaccines, numerous vaccine strategies have been undertaken that involve targeting the *Plasmodium* parasite at different stages of the parasite lifecycle; these include strategies that target the pre–erythrocytic stage, the liver stage and the blood stage of the parasite.

In the case of pre–erythrocytic vaccine strategies, an antibody response at the level of the sporozoites could potentially result in no hepatocyte (liver) invasion. A vaccine that targets the liver–stage of the parasite would facilitate the parasite not reaching the blood, hence preventing clinical symptoms (Taylor–Robinson, 2002). This type of vaccine would be superlative for travellers as it would prevent the development of the clinical disease and

partial immunity would at least reduce morbidity (WHO, 2010_2). An erythrocytic (asexual blood stage) vaccine typically involves eliciting an antibody response against attenuated merozoites or malarial surface antigens, with the resultant T–cell response resulting in no development of the parasite in the erythrocyte. This type of vaccine would be most effective as a "disease reduction vaccine" in countries where malaria is endemic (WHO, 2010_2). Sexual stage vaccines aim to prevent or decrease transmission of the parasite to other hosts. This type of vaccine has public health benefits in future planning (WHO, 2010_2).

Convincing evidence suggests that a vaccine for humans, against malaria, is indeed feasible. Firstly, naturally acquired immunity has been reported in individuals living in malaria–endemic countries, where immunity is progressively built up in the first 20 years of life. This immunity appears to be linked to antigenic stimulation, however understanding the molecular basis of naturally acquired immunity is still preliminary (WHO, 2010_2). Secondly, reports of malaria resistance by the sickle cell trait (genotype HbAS) have allowed researchers to isolate antibodies from people demonstrating a natural immunity to malaria for the creation of new vaccines (Williams *et al*., 2005). Researchers have speculated that resistance involves factors such as a reduced ability of *P. falciparum* parasites to grow and multiply in HbAS erythrocytes, while other observations suggest that it might also involve the accelerated acquirement of malaria–specific immunity (Williams *et al*., 2005). Lastly, clinical trials to date have shown that 90% protection against infection could be conferred to human test subjects under laboratory conditions, following immunization using irradiated sporozoites (WHO, 2010_2).

There are however a number of issues in the vaccine development process, such as; malaria parasites are often able to evade the host's immune system (Ferreira *et al*., 2002), recombinant expression of *Plasmodium* antigens proves to be very difficult (Girard *et al*., 2007), there is a lack of useful animal models in which to test potential drugs (WHO, 2010_2), there is insufficient clinical trial capacity, which is also linked to serious administrative issues at a level of local ethical committee reviewing (Girard *et al*., 2007) – all these factors limit the development of clinically useful vaccines. With respect to natural immunity, the malaria parasite is able to evade the host's immune system by polymorphism of target antigens, meaning that no natural immunity can be conferred upon the human host (Ferreira *et al*., 2004). There is also a major lack in the understanding of the types of immune response elicited, which means that it is difficult to come up with an effective strategy in vaccine

development. Difficulty also lies in producing the appropriate protective antigens *in vitro,* especially in the case of conformationally dependent epitopes (Girard *et al*., 2007). Once antigens have been purified *in vitro* and vaccine candidates developed, these need to be tested in an appropriate animal model. Animal models are essential because the immune response needs to be analysed within a similar physiological environment in which the vaccine will exist. Animals are however not always susceptible to human pathogens and this requires careful selection of strain or species pathogens (Brewer and Schijns, 2009).

Numerous pre–erythrocytic vaccine candidates have been researched and include vaccine candidates against *P.falciparum* circumsporozoite protein (CSP) as well as a number of other vaccines based on the CSP antigen (WHO, 2010_2). Another pre–erythrocytic multiple–antigen DNA vaccine was designed to encode five different liver–stage antigens: CSP, liver stage antigens 1 and 3 (LSA–1 and –3), exported protein 1 (EXP1), and the sporozoite surface protein 2 (SSP2, also known as thrombospondin–related adhesive protein, TRAP) (Parker *et al*., 2001). Additional targeted antigens for pre–erythrocytic vaccine development include the liver stage antigens 1 and 3 (LSA–1 and –3), the sporozoite and liver stage antigen (SALSA) and the sporozoite threonine and asparagine rich protein (STARP). The most advanced vaccine development against asexual stages of the parasite include vaccines against apical membrane antigen 1 (AMA–1) (Malkin *et al*., 2005), merozoite surface protein 3 (MSP–3) (Druilhel *et al*., 2005), MSP–2 (WHO, 2010_2), as well as MSP–1 against *P.falciparum* (WHO, 2010_2) and *P. vivax* (Bastos *et al*., 2007). Transmission–blocking candidates that target the sexual stages of the parasite include vaccines against: *P.falciparum* surface protein antigens Pfs25 and Pfs28 as well as the *P. vivax* homologues Pvs25 and Pvs28 (WHO, 2010_2).

The world's most clinically advanced malaria vaccine candidate to date is however against the CSP antigen that is found at the surface of the sporozoite and of the infected hepatocyte. The Mosquirix (RTS,S) vaccine was developed by GlaxoSmithKline (GSK) and is expected to complete late–stage trials in 2011 involving 16,000 people. It is currently underway in seven African countries: Burkina Faso, Gabon, Ghana, Kenya, Malawi, Mozambique and Tanzania. Recent Phase II studies showed that RTS,S demonstrated a 53% success in preventing clinical episodes of malaria; with a future goal of 80% success by 2025 (GSK, 2009).

1.2.2 Drugs available in the treatment of malaria

While the world awaits the successful production of a vaccine against malaria, the use of antimalarial drugs remains the only method of treatment for this disease of burden. Current antimalarial drugs most commonly target the asexual stages of the parasite (Rosenthal, 2003); Table **1.1** summarises the existing antimalarials, the drug target pathway and enzyme.

Chemotherapies against asexual stages of malaria involve targeting numerous pathways that exist in the parasite membrane, cytosol, food vacuole, mitochondrion and plastid–like organelle, the apicoplast. Proteins involved in phospholipid synthesis and membrane transport represent antimalarial targets of the parasite membrane (Table **1.1**). Extensive phospholipid synthesis is required in the malaria parasite in the development of numerous membranes, including those that enclose the parasitophorous vacuole, the cytosol and numerous other subcellular compartments (Sahu *et al*., 2008). Antimalarials that target the unique membrane transport proteins have been reported, despite the fact that knowledge of the many transport mechanisms remains limited (Gero *et al*., 2003).

Subsequent to antimalarial treatment of asexual parasites, disease transmission can still prevail for several weeks, resulting in further spread of the disease in a community. A multifaceted approach could be taken such as combination therapies that target gametocytes or exoerythrocytic parasite stages in addition to asexual blood stage parasites. This approach may lead toward an overall reduction in morbidity and mortality at a community level. Numerous limitations exist in this approach, for example, mature gametocytes are resistant to current antimalarial drugs, excluding primaquine, which is not commonly used because of the severe side effects imparted by the drug (Williamson, 2008).

Table 1.1 Summary of existing antimalarials and the pathway that they target in asexual blood stage parasites.

Target location	**Pathway/mechanism**	**Target molecule**	**Existing therapies**	**References**
Food vacuole	Heme polymerization	Hemozoin	Quinolines	De *et al*., 1998
	Hemoglobin hydrolysis	Plasmepsins	Protease inhibitors	Haque *et al*., 1999
		Falcipains	Protease inhibitors	Rosenthal, 2001
	Endocytosis	Macromolecular tracers	Artemisinins	Hoppe *et al*., 2004
Parasite membrane	Phospholipid synthesis	Choline transporter	G25	Sahu *et al*., 2008
	Membrane transport	Unique channels	Dinucleoside dimers	Gero *et al*., 2003
Cytosol	Folate metabolism	Dihydrofolate reductase (DHFR)	Pyrimethamine, cycloguanil, trimethoprim, chlorproguanil	Cowman, 1998; Milhous and Kyle, 1998
		Dihydropteroate synthase (DHPS)	Sulfa compounds	Cowman, 1998
		Thymidylate synthase (TS)	5–Fluoroorotate	Jiang *et al*., 2000
	Shikimate pathway	5–Enolpyruvyl shikimate 3–phosphate synthase	Glyphosate	Sahu *et al*., 2008
	Glycolysis	Lactate dehydrogenase	Azoles	Becker and Kirk, 2004; Cameron *et al*., 2004
Mitochondrion	Electron transport	Cytochrome *c* oxidoreductase	Hydroxynapthoquinones	Milhous and Kyle, 1998
Apicoplast	Protein synthesis	Apicoplast ribosome	Antibiotics	Sahu *et al*., 2008
	DNA synthesis	DNA gyrase	Quinolones	Sahu *et al*., 2008
	Transcription	RNA polymerase	Rifampin	Sahu *et al*., 2008
	Type II fatty acid biosynthesis	β–Ketoacyl–ACP synthases III (FabH)	Thiolactomycin	Waller *et al*., 2003
		Enoyl–ACP reductase (FabI)	Triclosan	Waller *et al*., 2003
	Isoprenoid synthesis	1–Deoxy–D–xylulose–5–phosphate reductoisomerase	Fosmidomycin	Jomaa *et al*., 1999
	Protein farnesylation	Farnesyl transferase	Peptidomimetics	Chakrabarti *et al*., 2002

1.2.3 Malaria chemoprophylaxis

Antibiotics, including tetracycline and its derivatives are still commonly used as antimalarial drugs, both in the treatment of and as a prophylaxis against malaria (Bloland, 2004). A number of prophylactics are used, most commonly, by travellers visiting malaria–endemic countries. The choice of prophylaxis is generally area–specific and is hence *Plasmodium* specific (WHO 2010_3). Prophylactic drugs that act on the pre–erythrocytic liver forms are called *causal* prophylaxis, while drugs that act on the erythrocytic blood forms are called *suppressive* prophylaxis. Suppressive prophylaxis is used predominantly for prevention of *P. falciparum* malaria, which resides predominantly in sub–Saharan Africa. Causal prophylaxis is typically chosen in the prevention of P. *vivax* or *P. vivax*/*P.falciparum* malaria (Castelli *et al*., 2010).

The most common prophylactic treatments typically involve combination therapies and may include: 1) chloroquine/proguanil (Nivaquine® + Paludrine®, or Savarine®), which is prescribed for *P.vivax* endemic areas with low *P.falciparum* prevalence and no widespread chloroquine resistance; 2) Mefloquine (Lariam® or Mephaquine®) is effective against *P.* falciparum and other *plasmodial* infections in malarial endemic areas, with the exception of some focal areas of South East Asia and Africa; 3) Atovaquone/proguanil (Malarone®) is effective in *P.falciparum* chloroquine resistance areas; 4) Doxicycline® is a tetracycline antibiotic that is effective in *P.falciparum* chloroquine–resistant areas even if cases of prophylactic failures are reported; 5) Primaquine® has therapeutic use for the treatment of *P. vivax* and *P. ovale* infections; 6) Tafenoquine® is an 8–aminoquinoline and is effective both as causal and suppressive prophylaxis for *P.vivax* and *P.falciparum*; 7) Chloroquine is a 4–aminoquinoline, and is effective in areas dominated by *P. vivax* or in areas where *P.falciparum* is still sensitive to chloroquine – it is however typically used in combination with other prophylactics such as proguanil or doxycycline (WHO 2010_3; Castelli *et al*., 2010)

However, due to the development of antimalarial drug resistance, both in treatment and in prophylaxis, much confusion for both Doctors and travellers arises as to which is the most effective drug, which areas necessitate special precautions and which drugs result in the most serious side effects (Castelli *et al*., 2010).

1.2.4 Antimalarial drug resistance

Antimalarial drug resistance can be defined as the "ability of a parasite strain to survive and/or multiply despite the administration and absorption of a drug given in doses equal to or higher than those usually recommended; but within tolerance of the subject". The drug in question must "gain access to the parasite or the infected red blood cell for the duration of the time that is necessary for its normal action" (Bruce–Chwatt *et al*., 1986).

The first accounts of antimalarial drug resistance were only publicised 1986 in *Parasitology Today*, despite the fact that the emergence of resistance occurred in the 1950s. *P.falciparum* was becoming resistant not only to chloroquine, but also to almost all existing alternative treatments with the exception of quinine (Ambroise–Thomas and Rossignol, 1986). Yet despite significant progress in the molecular analysis of the *Plasmodium* parasite, the problem of drug–resistant malaria is unquestionably worse now than was reported in 1986 (Wongsrichanala *et al*., 2002).

Quinine was used as an antimalarial drug since the seventeenth century. Resistance to quinine was reported throughout the twentieth century, but consistent reports of treatment failure, mainly in Southeast Asia, were reported from 1965. Chloroquine resistance was first reported in Southeast Asia and South America in the 1950s and eventually spread to all of sub–Saharan Africa by 1988 (Hyde, 2005).

Despite the rapid spread of pyrimethamine and sulfadoxine resistance in Southeast Asia in the 1960s, the combination therapy was still widely used into the 1990s to combat chloroquine–resistant parasites in Africa. Artemisinin and its derivatives were used in monotherapy treatment in the 1970s; however, due to the very short half–life of the drug in human plasma, artemisinin derivatives are only used in combination therapies. Until 2005, no clinical resistance had been observed (Hyde, 2005), however, more recently Dondorp *et al*. (2009) publicised that a reduction in efficacy of artemisinin combination therapies had been reported on the Cambodia–Thailand border, which is said to be a historical site for antimalarial drug resistance. Mefloquine and atovaquone resistance was reported shortly after their release and atovaquone is now used clinically only in combination with proguanil (Depetrillo *et al*, 2010). LapDap is a chlorproguanil/dapsone combination treatment and has been used effectively against pyrimethamine/sulfadoxine–resistant infections. Unfortunately

the combination is not 100% efficacious because it targets the same enzymes as pyrimethamine/sulfadoxine drugs (Figure **1.2**) (Hyde, 2005).

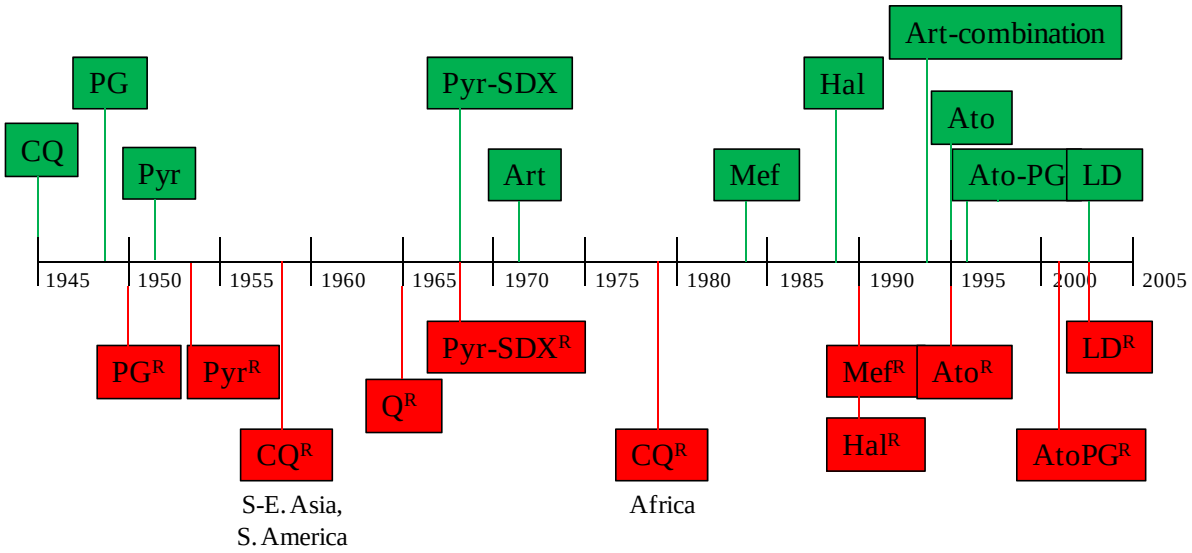

Figure 1.2: Approximate dates of introduction of antimalarial drugs as clinical agents and observations of treatment failure.
Antimalarial drugs that were used from 1945 to 2005 include: chloroquine (CQ), proguanil (PG), pyrimethamine (Pyr), sulfadoxine (SDX), artemisinin (Art), mefloquine (Mef), halofantrine (Har), atovaquone (Ato), LapDap (LD) and are shown in *green*, with their respective reported resistances shown in *red* (adapted from Hyde, 2005).

The most common mechanism of drug resistance involves spontaneous mutations that confer resistance (or reduced sensitivity) to specific drugs or classes of drugs; these can be either single or multiple mutations. The biochemical mechanism of resistance has been well documented for antimalarials such as chloroquine, the antifolates, atovaquone (Bloland, 2001) and quinine (Bennett *et al*., 2007).

Chloroquine belongs to the family of antimalarial drugs called the quinolines (De *et al*., 1998). Chloroquine resistance is associated with the parasites' increased ability to pump chloroquine out of the erythrocytes at a rate that does not allow the drug to reach toxic levels. The result of this is an inability of chloroquine to inhibit heme polymerization, which is the mechanism of action of the drug in question (Bloland, 2001). This is accomplished through two transporter proteins on the digestive vacuole, namely chloroquine resistance transporter (CRT) and the P–glycoprotein homologue 1 (Pgh1) (Johnson *et al*., 2008; Martin *et al*., 2009) and originates through mutations in the *pfcrt* gene (Bennett *et al*., 2007). Antifolate drugs are typically used in combination therapies against DHFR and DHPS (Cowman, 1998). Specific combinations of mutations have been associated with varying degrees of resistance (reviewed by Sridaran *et al*., 2010). In some cases, partial resistance has been conferred by simply

expressing more of the relevant enzyme and thus increasing the ratio of enzyme to inhibitor (Cowman, 1998). Atovaquone, forms part of the hydroxynapthoquinone drug family and acts by inhibiting the cytochrome *bc1* complex of the electron transport chain (Milhous and Kyle, 1998). Resistance is conferred by single point mutations in the cytochrome–b gene, and while resistance develops rapidly when used alone, a combination strategy results in a very slow resistance development (Bloland, 2001). Quinine belongs to the same family as chloroquine, the quinolines; and quinine resistance and chloroquine resistance are often (but not always) seen together. Yet the mechanism of conferring resistance was poorly understood until recently (Bennett *et al*., 2007). Quinine resistance is associated with a mutation on chromosome 13 as a partner (with *pfcrt*), which predominantly harbours a gene encoding a *P. falciparum* Na^+/H^+ exchanger (PfNHE) (Ferdig *et al*., 2004; Bennett *et al*., 2007).

Numerous factors have contributed to antimalarial drug resistance and include human behaviour, parasite biology, vector biology, pharmacokinetics and economics (Bloland, 2001). Because of this increasing problem of antimalarial drug resistance, the need for new and effective drugs against existing targets and new targets is escalating (Macreadie *et al*., 2000).

1.2.5 Identifying novel antimalarial targets

Antimalarial drug development is restricted by a number of aspects; first and foremost the new drug needs to be safe, it needs to demonstrate efficacy, it needs to be cheap, and it needs to demonstrate additional properties important for the specific disease indication. It is generally accepted that new antimalarials should be dosed orally in a single–daily dosing regimen, for no more than 3 days (Wright, 2005). It would also be prudent to consider the potential inclusion of features to counter the parasite's ability to adapt. The new drug also needs to be effective against current drug–resistant strains (Cowman *et al*., 1998).

Antimalarial drug development ranges from minor modifications of existing agents, to the development of novel agents against new targets (Olliaro and Yuthavong, 1999). The optimization of combination therapies, development of existing drug target analogues, and the testing of compounds originally developed against other diseases, include some of the potential minor modifications to existing targets (Rosenthal, 2003); while the development of new targets involves synthesizing rationally designed drug target molecules, as well as

discovering natural products that are efficient against malaria (Olliaro and Yuthavong, 1999). Natural products chemistry in drug discovery has lead to the development of numerous natural product–derived compounds, some of which are in phase III clinical trials or have been developed as drugs (Butler, 2004). For example, the antimalarial compound arteether is a fast–acting schizontocide that is specifically utilized for the treatment of chloroquine resistant *P.falciparum* malaria and cerebral malaria. Arteether is a synthetic derivative of artemisinin, a product of the Chinese plant *Artemisia annua* (Robert and Meunier, 1998).

Numerous approaches are being taken to identify novel antimalarial targets, including strategies that target unique aspects of the parasite biology (Rangarajan and Padmanaban, 2001). Potential chemotherapeutic targets include enzymes of the digestive vacuole, enzymes involved in macromolecular and metabolite synthesis and enzymes responsible for signalling and other membrane processes (Olliaro and Yuthavong, 1999).

1.2.6 Food vacuole drug targets

Drug discovery has lead researchers to look at possible target enzymes in the heme biosynthetic pathway (Sato and Wilson, 2002). In the acidic food vacuole, erythrocyte hemoglobin is hydrolyzed into heme, which is then polymerized into insoluble hemozoin pigment and globin, which is further hydrolyzed to individual amino acids. Antimalarial drugs that act against this process typically prevent hemozoin formation, resulting in an accumulation of heme, which is toxic to the parasite (Tekwani and Walker, 2005). Despite the fact that parasites have become chloroquine resistant, it must be noted that the drug was used for more than 50 years, with very slow development of resistance (Rosenthal, 2003).

The food vacuole also appears to be the target of artemisinin (Table **1.1**), which tenders very potent activity without any reported drug resistance; in November 2010, the world Health Organization made a call to all malaria–endemic countries imploring then to monitor antimalarial drug efficacy such that artemisinin resistance could be detected early (WHO, 2010_4). Artemisinin and its derivatives confer antimalarial effects by free–radical damage. It has been suggested that the alkylation of plasmodial proteins is the result of the free–radical accumulation (Bhisutthibhan *et al*., 1998).

Hemoglobin degradation is essential for the intraerythrocytic development of the malaria parasite. This process is mediated by a number of proteases of the food vacuole (Moura *et*

al., 2009), including; aspartic proteases (plasmepsins) (Table **1.1**) (Banerjee *et al*., 2002; Moura *et al*., 2009), metalloproteases (falcilysin) (Eggleson *et al*., 1999), cysteine proteases (falcipains) (Shenai *et al*., 2000), as well as the recently discovered dipeptidyl aminopeptidase 1 (DPAP1) (Klemba *et al*., 2004). Falcipain–2 and falcipain–3 (Table **1.1**) are cysteine proteases that are essential hemoglobinases of *P*. *falciparum*, and represents potential antimalarial drug targets (Singh and Rosenthal, 2001). It has been shown that cysteine and aspartic protease inhibitors exert synergistic antimalarial effects *in vitro* and *in vivo* (Semenov *et al*., 1998) and it may be prudent to develop a combination antimalarial which incorporates the inhibition of both proteases (Rosenthal, 2003). Moura *et al*. (2009) showed, by way of a plasmepsin knockout *P.falciparum* stain, that the antimalarial activity of previously characterized aspartic protease inhibitors was independent of the effect that they had on the plasmepsins. This work led to the identification of non–food vacuole plasmepsins against which, adaptive inhibitors could be designed (Moura *et al*. 2009).

1.2.7 Parasite membrane drug targets

In order to produce the membranes that enclose the parasitophorous vacuole the malaria parasite needs to undergo extensive phospholipid synthesis. Phosphatidylcholine is the most abundant lipid in the in the parasite membrane and antimalarial drugs that target phospholipid synthesis, function by inhibiting choline transport (Vial and Calas, 2001). The lead compound, G25 (Table **1.1**) was found to be effective both *in vitro* and *in vivo* by blocking choline transport; choline being the precursor for phosphatidylcholine (Rosenthal, 2003).

The invasion of an erythrocyte by a malaria parasite results in major alterations in the permeability of the host's cell membrane. The infected erythrocyte membrane demonstrates a significant increase in permeability to low molecular weight solutes such as inorganic ions, nutrients and metabolic waste. It is believed that this is accomplished through the introduction of channels both into and out of the red blood cell. Recent evidence suggests that it is both the host's endogenous channels as well at the parasite's encoded proteins that make this possible (Martin *et al*., 2009). The membrane transport system is therefore necessary to facilitate the uptake of solutes and nutrients from the extracellular medium and the disposal of metabolic wastes. The properties of these parasite–induced transport systems are significantly different from those in normal human cells, making it a valid target for antimalarial drug development (Gero *et al*., 2003).

The parasite encodes in excess of 100 membrane transport proteins, some of which have been proposed to be suitable drug targets. Unfortunately, most inhibitors against membrane proteins have demonstrated poor specificity and low affinity (Martin *et al*., 2009). However, a series of dinucleoside phosphate dimers have been found to be highly toxic to the parasite and experimental evidence has confirmed that they are incapable of entering normal mammalian cells (Gero *et al*., 2003). A number of newly identified transport protein families have been identified including those of the α–type small conductance mechanosensitive ion channels (Rayavara and Desai, 2008), CorA metal transporter proteins, copper transporters, β–type mitochondrial and plastid porin proteins, as well as vacuolar iron transporters (reviewed by Martin *et al*., 2009). Of these transporter families, 11 of these transporters have been predicted to be localized to the apicoplast, 17 to the mitochondrion, 8 to the digestive vacuole and 5 to the ER/Golgi (Martin *et al*., 2009). It may be practical to assess their potential as drug target proteins, because little or no research into these proteins has been done. This may lend toward the development of antimalarial drugs against new targets.

1.2.8 Cytosolic drug targets

Numerous metabolic pathways are located in the cytosol, however, many of these pathways are highly conserved among organisms, making them inefficient drug targets (Rosenthal, 2003). One pathway that has proven to be an effective target is that of folate metabolism (Plowe, 2001), where protein targets include GTP cyclohydrolase I (GCHI), DHFR, DHPS and TS (Hyde *et al*., 2008). The enzymes of the folate biosynthetic pathway are essential for DNA synthesis and are therefore considered to be valid drug targets. Antifolate drugs have been fashioned against DHFR, DHPS and TS (Table **1.1**); however, other enzymes in this pathway have not been considered until recently (Hyde, 2005). Loss in efficacy for DHFR and DHPS inhibitors has been reported (Plowe, 2001) and as discussed previously, even combination therapies against DHFR and DHPS have been associated with resistance (Cowman, 1998). The GCHI enzyme of the folate pathway has however come under scrutiny in the last decade as a candidate for antimalarial drug design because it has only 30% similarity with the human and *Escherichia coli* homologues (Lee *et al*., 2001).

The shikimate pathway also presents an attractive target for malaria chemotherapy because of the absence of the pathway in mammals. The shikimate pathway, also called the aromatic biosynthetic pathway, constitutes a series of seven enzymatic reactions that produce the aromatic precursor chorismate from simple products of carbohydrate metabolism. In plants,

the pathway is localized to the chloroplast; however, in the parasite the pathway is predicted to occur in the cytoplasm, as is seen with fungi and bacteria. A series of fluorinated analogs of shikimate have been tested against malaria and two were found to be effective antimalarial agents (Table **1.1**) (McConkey, 1999).

Lactate dehydrogenase (LDH) (Table **1.1**) is an enzyme that is involved in glycolysis and is a cytosolic pathway that is of interest in antimalarial drug design. Several inhibitors of LDH have been reported to demonstrate antimalarial activity *in vitro* (Razakantoanina *et al*., 2000). LDH utilizes NADH (nicotinamide adenine dinucleotide) as a cofactor and boasts a unique NADH binding site, which offers the opportunity for the design of selective compounds (Deck *et al*., 1998).

The *Plasmodium* parasite is dependent on high amounts of polyamines for growth and accomplishes this through polyamine synthesis. This pathway is of interest when it comes to antimalarial drug development because it differs highly from the mammalian pathway such that in the parasite, *S*–adenosylmethionine decarboxylase and ornithine decarboxylase (AdoMetDC/ODC) makes up a single bifunctional protein, while in mammals, AdoMetDC and ODC are two proteins (Müller *et al*., 2008). Cytostatic effects with curative rates have however been reported for the traditional inhibitors, meaning that combination therapies with polyamine analogues in murine malaria models had to be employed (Bitonti *et al*., 1989). Another enzyme of the pathway that has come under scrutiny is spermidine synthase (SpdSyn). The SpdSyn inhibitor cyclohexylamine resulted in complete arrestment of parasite development (Becker *et al*., 2010).

The purine salvage and pyrimidine synthetic pathways have also come under observation for identification of potential drug targets (Keough *et al.*, 1999) because of the unique features of the parasite enzymes coupled to their essential role in parasite survival, but not in the human host (Rosenthal, 2003). *Plasmodium* parasites cannot synthesize purines and therefore rely on the host in order to obtain these vital DNA building blocks. *P.falciparum* obtains it purines from hypoxanthine, and hypoxanthine–guanine phosphoribosyltransferase (HGPRT) and is therefore an obvious drug target (Keough *et al*., 1999). In the case of pyrimidine synthesis, the pyrimidine synthetic enzymes of *Plasmodium* parasites are different from those found in the human host and therefore lend toward their potential as drug targets. Interestingly, pyrimidine synthesis works synergistically with mitochondrial electron

transport and a possible combination drug that targets pyrimidine synthesis and mitochondrial electron transport could possibly be explored (Rosenthal, 2003).

1.2.9 Mitochondrial drug targets

There appears to only be a single target in the mitochondrion namely ubiquinol–cytochrome *c* oxidoreductase (complex III) (Table **1.1**). An antimalarial drug that has been found to be very effective against this target is atovaquone, which is used in combination therapies because of drug resistance problems (Rosenthal, 2003). The mitochondrion is a valid drug target organelle because it houses the apparatus for genome replication, repair, recombination, transcription, and translation. A number of unusual features of the components of this apparatus have been discovered through genome sequence analyses, warranting further investigation of the mitochondrion for drug discovery and development (Mather *et al*., 2007).

1.2.10 Apicoplast drug targets

Apicomplexan parasites harbour a plastid–like organelle called an apicoplast which is derived from the endosymbiosis of cyanobacterium (Ralph *et al*., 2004). The function of the apicoplast has been debated since its discovery in the 1970s. The plastid is involved in a number of processes including; synthesis of haem for mitochondrial respiration (Wilson *et al*., 1991), fatty–acid synthesis and starch storage (Köhler *et al*., 1997), and the production of aromatic amino acids (Palmer, 1992). The heritage of the apicoplast means that many of its bacterial–like enzymes are fundamentally different from that of the mammalian host, making them potential drug targets (Ralph *et al*., 2004).

The *P. falciparum* genome sequence has been elucidated and revealed that the malaria–causing parasite has three genomes; the nuclear genome (14 chromosomes), mitochondrial DNA genome (6 kb) and the plastid–like genome (35 kb) (Gardner *et al*., 1998). Interestingly, most apicoplast–destined proteins are coded for by the nuclear genome (Wilson *et al*., 1996) and are transported to the organelle, via molecular mechanisms that are not fully understood (Spork *et al*., 2009). Proteins destined for the apicoplast do however boast a targeting signal sequence that results in its transport to the desired destination (Wilson *et al*., 1996). An *in silico* study predicted that an endoplasmic reticulum (ER)–associated protein degradation (ERAD) system exists in the parasite, which is directly involved the transport of nuclear–encoded proteins to the apicoplast (Spork *et al*., 2009).

The existence of the plastid–like genome may explain why some antibacterial compounds that otherwise do not attack eukaryotes have an antimalarial effect (Rosenthal, 2003). The tetracyclines, clindamycin, macrolides and chloramphenicol inhibit various steps of prokaryote–like protein synthesis, while quinolone inhibits DNA gyrase, and rifampin inhibits RNA polymerase (Table **1.1**) (Rosenthal, 2003).

Type II fatty acid biosynthesis occurs in the apicoplast and has obvious chemotherapeutic applications because it is absent in humans. The antibiotic thiolactomycin, targets the enzyme FabH (Waller *et al*., 1998), while the other subunit, FabI (Table **1.1**) is the target for the antibiotic triclosan (Surolia and Surolia, 2001).

The non–mevalonate pathway is a metabolic pathway which ultimately leads to the synthesis of the isoprenoid precursor molecules isopentenyl diphosphate (IPP) and dimethylallyl diphosphate (DMAPP) (Singh *et al*., 2006). 1–Deoxy–D–xylulose 5–phosphate reductoisomerase (DXR) catalyzes the reaction whereby 1–deoxy–D–xylulose 5–phosphate (DXP) is reduced to 2–C–methylerythritol 4–phosphate (MEP) using a distinct pathway that is dissimilar to that of the mevalonate pathway employed in the human host. This, coupled to the fact that isoprenoids are essential for survival of the malaria parasite, make it a potent drug target. The antibiotic, fosmidomycin (Table **1.1**) has been shown to be an effective inhibitor of DXR *in vivo* in a rodent malaria model; however, the apparent need for frequent and prolonged dosing means that its use as a monotherapy is limited (Jomaa *et al.*, 1999; Wiesner and Jomaa, 2007). Recently, the use of microarrays to identify mutations was employed in a study of drug resistance. The study allowed for the elucidation of the molecular and biochemical basis of the *P.falciparum* parasite's resistance to fosmidomycin. Fosmidomycin–resistant parasites demonstrated an increase in gene copy number of the putative target *P.falciparum* DXR *(*PfDXR) as a plausible mechanism for *in vitro* derived resistance. This amplification event is used commonly by parasites such that they increase the transcription of important genes in order to counteract the effects of the drug. The parasite is able to do so because the environment of the human host is relatively stable (Dharia *et al*., 2009). The elucidation of the mechanism of fosmidomycin resistance is important so that an appropriate combination therapy can be employed against malaria (Borrmann *et al*., 2005).

1.2.11 Emerging drug target enzymes

A very interesting group of proteins that have emerged as potential drug targets in recent years are the *Plasmodium chaperones* (reviewed by Pesce *et al*., 2010). The chaperones, including heat shock proteins (Hsps) are ubiquitous in almost all cells, with *P.falciparum* encoding 43 Hsp40s, 6 Hsp70s, and 3 Hsp90s. Chaperones are involved in a number of cellular processes including; protein folding, protein translocation, signal transduction, as well as in the cellular stress response. Hsps are highly conserved across the species, some differences do however exist in *P.falciparum* Hsps, including unique structural characteristics and parasite specific features that could make them fitting targets in antimalarial drug design (reviewed by Pesce *et al*., 2010).

The isolation and characterization of the 90 kDa heat shock protein 90 (Hsp90) has lead to the discovery of an extensive N–terminal acidic domain, which is specific to the *Plasmodium* Hsp90 (Acharya *et al*., 2007). Inhibitors of Hsp90 that have been reported include; geladanamycin and its clinical derivative 17–allylamino–17–demethoxy–geladanamycin (17–AAG) as anti–cancer drugs (Solit and Chiosis, 2008). Geladanamycin in combination with ascomycin (an inhibitor of the plasmodial immunophilin FKBP35, which is associated with PfHsp90) has also been shown to be effective at reducing *P.falciparum* growth (Kumar *et al*., 2005). The development of antimalarial drugs to target Hsp90 poses a challenge in that the drug will need to effectively target *Plasmodium* Hsp90 and not human Hsp90 (Pesce *et al*., 2010).

The 70 kDa heat shock protein 70 (Hsp70) is probably the most well characterized Hsp (Tavaria *et al*., 1996). The immuno–suppressive drug, 15–deoxyspergualin (DSG) is a specific modulator of Hsp70 and was found to have both *in vitro* (Midorikawa *et al*., 1998) and *in vivo* (Midorikawa and Haque, 1997) inhibitory effects on malaria. Similarly, in a recent study, a library of pyrimidinone compounds was screened against malaria and of the 157 compounds tested, 9 demonstrated IC_{50} (concentration at which there is 50% inhibition) values in a range of 30 nM to 1.6 µM (Chang *et al*., 2009). It has been suggested that the *Plasmodium* Hsp70 protein PfBiP (Figure **1.6**) may be involved in the export of parasite proteins into the erythrocyte (Shonhai *et al*., 2007) and may therefore be worth exploring as an antimalarial target (Pesce *et al*., 2010). Both the Hsp70 and Hsp40 chaperones are essential for survival of the parasite; it therefore may be prudent to target the Hsp40–Hsp70

interaction (Botha *et al*., 2007). This may be difficult based on the fact the *P.falciparum* Hsp70 shares a very similar homology to the human homologue (Chiang *et al*., 2009). The chaperone activity of PfHsp70–1 (Figure **1.6**) is however sufficiently different to the human Hsp70 and it codes for a different Hsp40 binding site, so it may therefore be worth exploring the synthesis of small modulators of PfHsp70–1 (Pesce *et al*., 2010).

Hsp40 is a 40 kDa chaperone and is classified into one of 4 groups, including; type I, type II, type III and type IV. Hsp40s are typically made up of 4 domains, namely: The N–terminal J domain, a glycine/phenylalanine–rich region (GF domain), a cysteine–rich zinc–binding domain and a C–terminal domain. Because the J domain is said to be essential in the Hsp40–Hsp70 interaction (Cheetham and Caplan, 1998), it may be possible to target such functional domains as the J domain, in drug discovery (Pesce *et al*., 2010). This however, cannot be said for the type IV Hsp40s because they lack a functional J domain (Cheetham and Caplan, 1998). To date, it appears that no inhibitors of Hsp40 have been published in antimalarial drug discovery.

Protein kinases are another group of proteins that perform vital roles cellular processes including growth regulation and differentiation (Geyer *et al*., 2005; Christian and Laurent, 2007). Many kinases have not been characterized; however, sufficient information exists that have allowed for the identification of unique families of plasmodial kinases, hence making this a targeted group in antimalarial drug design (Jirage *et al*., 2010). A group of kinases that have been heavily targeted in drug design are the cyclin–dependent protein kinases (CDKs), whose vital cellular role involves the regulation of progression of the cell cycle (reviewed by Morgan, 1997). CDKs that have been targeted in antimalarial drug design include; PfPK5, the CDK/mitogen–activated protein kinase (MAPK) hybrid protein PfPK6, the MO15–related Pfmrk, as well as numerous cyclin–related kinases (Pfcrk–1, Pfcrk–3, Pfcrk–4, and Pfcrk–5) (Knockaert *et al*., 2002). Inhibitors against PfPK5 include; purvalanol, hymenialdisine, and indirubin–30–monoxime. PfPK6 has been shown to be effectively inhibited by roscovitine and olomoucine (Hardcastle *et al*., 2002), while Pfmrk has been shown to be inhibited by a group of compounds containing a lactam moiety (Xiao *et al*., 2001), as well as by a number of other compound groups including; purines, quinolinones, flavones, oxindoles, and chalcones (reviewed by Waters and Geyer, 2003; Keenan *et al*., 2005).

A novel *in silico* approach was taken to facilitate drug discovery and involved a computational approach which prioritized potential metabolic drug target enzymes. A pathway/genome database (PGDB) has been constructed for *P.falciparum* 3D7, using its annotated genomic sequence. A computational algorithm was applied and resulted in the identification of 216 "chokepoint enzymes". Chokepoint enzymes are those that are potentially essential to the parasite and are therefore potential drug targets (Yeh *et al*., 2004). In 2009, the Bioinformatics and Functional Genomics group in Germany, improved the precision of the prediction results, and presented a refined list of 22 new potential candidate targets for *P. falciparum*, half of which have publicized reasonable evidence to be valid targets against other diseases (Fatumo *et al*., 2009).

Despite sufficient progress in the development of new drugs, the mechanism of action of existing drugs is poorly understood. Also, the rate of development of new drugs does not match the decline in effectiveness of antimalarial drugs. An obstacle in the rapid development of novel antimalarials is the lack of specialists and funding in the field of R&D (Macreadie *et al*., 2000). At present only 10% of global R&D resources are directed at malaria, even though it accounts for 90% of the global disease burden (SAMI, 2007). Evidence of bias against the diseases of poverty has been reported by the World Health Organization, whereby there has been widespread systematic prejudice in medical journals against diseases that dominate the least–developed regions of the world (Horton, 2003).

1.3 THE ANTIMALARIAL DRUG TARGET ENZYME PfDXR

1.3.1 Targeting the non–mevalonate pathway

Isoprenoids are the most chemically diverse group of compounds present in all organisms and have essential roles in membrane structure, redox chemistry, reproductive cycles, growth regulation, signal transduction and defense mechanisms (Rodriguez–Concepcion *et al*, 2000). Isopentenyl diphosphate (IPP) is the general precursor required for isoprenoid biosynthesis, which occurs via either the mevalonate (MVA) or mevalonate–independent (MEP) pathway (Disch *et al.*, 1998). Organisms such as mammals and fungi use the MVA pathway for isoprenoid biosynthesis (Vial *et al.*, 1984), while numerous bacteria, green algae, and higher plants utilize the alternative MEP pathway (Disch *et al.*, 1998).

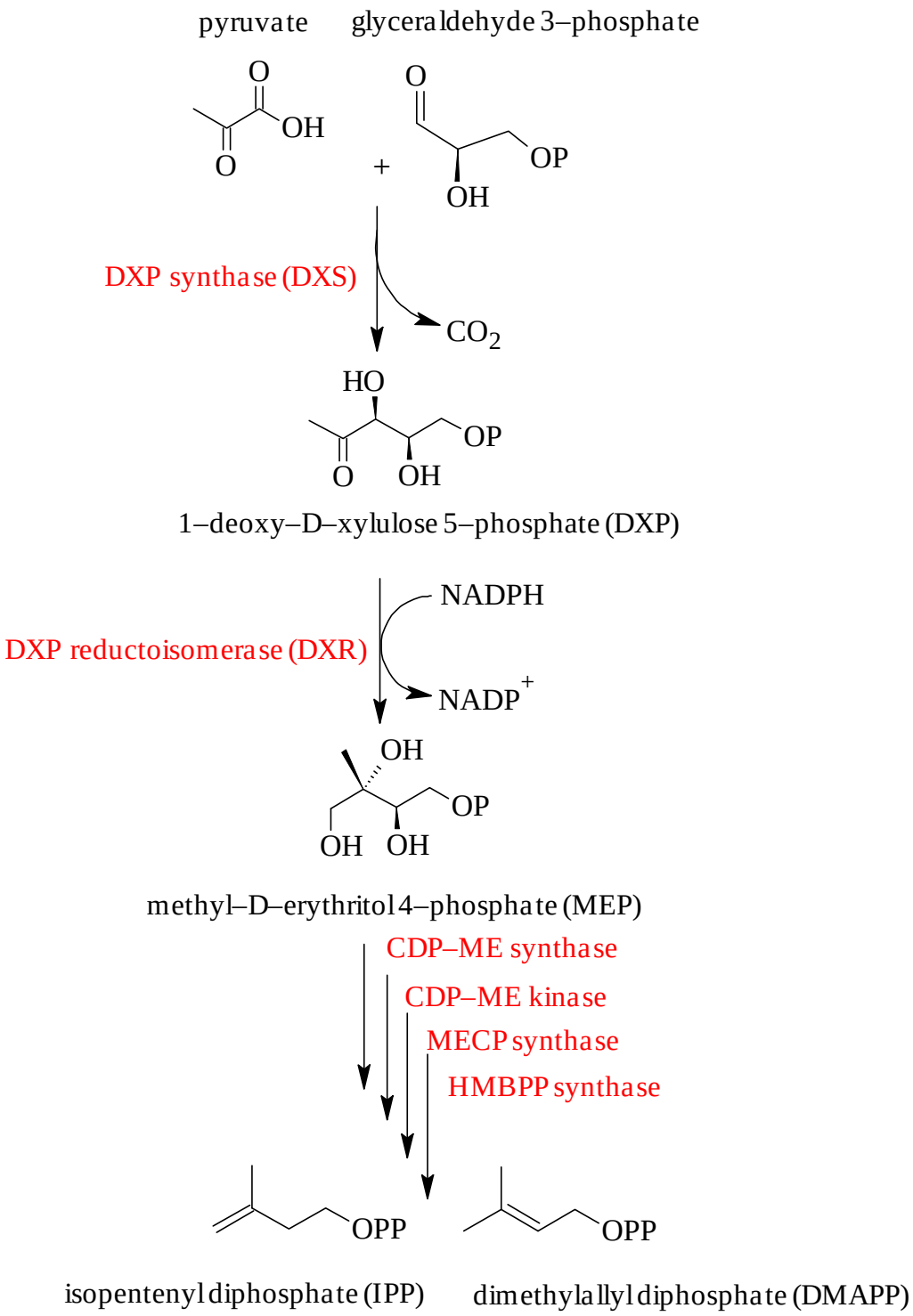

Figure 1.3: The biosynthesis of isoprenoids via the MEP pathway.
The condensation of pyruvate and glyceraldehydes–3–phosphate, by DXS results in the formation of DXP. DXP then undergoes rearrangement and reduction by NADPH (nicotinamide adenine dinucleotide phosphate) to form MEP. This step is catalyzed by DXR (enzyme of interest). The subsequent five reaction steps result in the formation of IPP and DMAPP isoprenoids, via 4–diphosphocytidyl–2–*C*–methyl–D–erythritol (CDP–ME), 4–diphosphocytidyl–2–*C*–methyl–D–erythritol 2–phosphate (CDP–ME2P), 2–*C*–methyl–D–erythritol–2,4–cyclodiphosphate (MECP), and 1–hydroxy–2–methyl–2–(E)–butenyl 4–diphosphate (HMBPP) (adapted from Singh *et al*., 2007).

The MEP pathway (Figure **1.3**) is comprised of seven enzymatic steps, which begin with the formation of 1–deoxy–D–xylulose–4–phosphate (DXP) by condensation of pyruvate and glyceraldehyde by DXP synthase (DXS) (Takahashi *et al.*, 1998). The subsequent step is catalyzed by DXR and involves an intramolecular rearrangement and NADPH–dependent reduction of DXP to MEP (2–C–methyl–erythritol 4–phosphate) (Argyrou and Blanchard, 2004).

The MEP pathway in *P. falciparum* differs greatly from the human isoprenoid biosynthesis via the MVA pathway, which proceeds through acetyl–CoA with mevalonate as a key intermediate (Hunter, 2007). Because of the crucial role that isoprenoids play in survival of organisms, the synthetic steps involved in isoprenoid biosynthesis could be targeted in antimalarial drug design (Dubey, 2002). The genetic validation of DXR was accomplished using a single cross–over strategy, such that plasmid integration at the DXR locus only resulted when gene function was preserved. From the study it was hence concluded that DXR is essential for intraerythrocytic development of *P. falciparum* (Odom and Van Voorhis, 2010), further validating the enzyme as a drug target enzyme.

Research conducted on the MEP pathway demonstrates a relatively young field of research (Jomaa *et al.*, 2007). DXS and DXR have been expressed as recombinant enzymes in *Pseudomonas aeruginosa* (Altincicek *et al.*, 2000) and inhibitors against the two enzymes have been published, including fluoropyruvate as an inhibitor of DXS and fosmidomycin against DXR (Altincicek *et al.*, 2000). Evidence for the reversibility of the DXR–catalyzed reaction in *E. coli* and *Mycobacterium tuberculosis*, with a reaction equilibrium that is essentially in favor of MEP production, has resulted in an increase in interest in this particular reaction step in drug discovery (reviewed by Singh *et al.*, 2007). It is this reaction that has come under increased examination as a target for novel antimalarial drug design (Rohmer *et al.*, 2004). The last two catalytic steps of the MEP pathway are mediated by two enzymes that catalyze unique radical–type reactions. These enzymes contain oxygen–sensitive iron–sulphur clusters and are therefore highly sensitive to oxygen, meaning that previous attempts to purify catalytically–active enzymes have failed (Jomaa *et al.*, 2007); until very recently, where Seemann and her group (2009) were able to characterize the last enzyme of the pathway, where ^{57}Fe Mössbauer spectroscopy was used to investigate the LytB enzyme in whole *E. coli* cells, as well as in the anaerobically purified enzyme

1.3.2 Catalytic Mechanism of DXR

In a study by Argyrou and Blanchard (2004), *M. tuberculosis* DXR (MtDXR) was expressed in *E. coli* and purified using conventional column chromatography and characterized by performing mechanistic and structural studies on the enzyme. It was concluded that MtDXR requires a divalent metal ion for catalysis and Co^{2+}, Mn^{2+} and Mg^{2+} have all been shown to activate the enzyme (Argyrou and Blanchard, 2004). This corresponds to the findings for *E. coli* DXR (EcDXR) put forward by Reuter *et al.* (2002), where active site residues were shown to complex with Mn^{2+} ions. However, *in vivo* studies have suggested that Mg^{2+} is the most relevant divalent cation for DXR catalysis in *E. coli* (Koppisch *et al.*, 2002), *M. tuberculosis* (Argyrou and Blanchard, 2004), *Synechocystis* sp. PCC6803 (Yin and Proteau, 2003) and *P.falciparum* (Singh *et al.*, 2006). DXR catalyses the reaction, whereby DXP substrate undergoes both molecular rearrangement and reduction. Firstly, the C3–C4 bond is broken and a new bond between C2 and C4 of the substrate forms, resulting in a MEP aldehyde intermediate. Following this rearrangement, the aldehyde intermediate is then reduced by the NADPH cofactor to form the product MEP, as illustrated in Figure **1.4**.

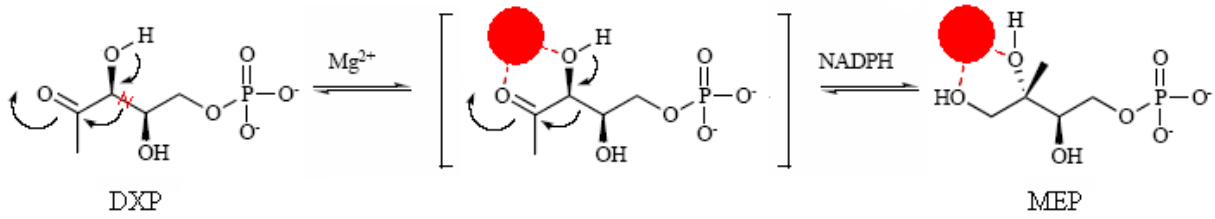

Figure 1.4: The reaction catalyzed by DXR, including the divalent magnesium cation (red) (modified from Singh *et al.*, 2007).

The possibility of using 1–deoxy–D–xylulose (DX) substrate instead of DXP was investigated independently by Querol *et al.* (2002) and Takahashi *et al.* (1998), after DX was reported to be used by a wild–type *E. coli* strain by Schwender *et al.* (1997). Querol *et al.* (2002) found no oxidation of NADPH resulted and it was hence concluded that DXP is the correct substrate for DXR. The crystal structure of EcDXR, with Mn^{2+} and fosmidomycin bound, provided evidence that fosmidomycin binds in a fashion closely related to the substrate DXP (Steinbacher *et al.*, 2003).

1.3.3 Structural Characterization of DXR

A number of DXR crystal structures have been solved from numerous DXR enzymes including: *E. coli*, *M. tuberculosis*, *Zymomonas mobilis* and *Thermotoga maritima* (Reuter *et al*., 2002; Yajima *et al*., 2002; Ricagno *et al*., 2004; Mac Sweeney *et al*., 2005; Henriksson *et al*., 2007; Takenoya *et al*., 2010). In a recent study by Yajima *et al*. (2007), for the first time, EcDXR was crystallized with Mg^{2+}, as well as NADPH cofactor and fosmidomycin inhibitor. Previous DXR crystal structures that have been solved have been complexed with either a divalent metal ion, or substrate, or inhibitor and include: EcDXR complexed with a sulphate ion and NADPH (Yajima *et al*., 2002); the apo form of EcDXR (Reuter *et al*., 2002); EcDXR complexed with Mn^{2+} and fosmidomycin (Steinbacher *et al*., 2003); EcDXR complexed with a sulphate ion and biphosphate ion (Yajima *et al*., 2004); *Z. mobilis* DXR (ZmDXR) complexed with NADPH (Ricagno *et al*., 2004); EcDXR complexed with NADPH and DXP substrate (Mac Sweeney *et al*., 2005); EcDXR complexed with NADPH and fosmidomycin (Mac Sweeney *et al*., 2005); MtDXR complexed with a sulfate ion (Henriksson *et al*., 2006); MtDXR complexed with Mn^{2+} and NADPH (Henriksson *et al*., 2007_2); MtDXR complexed with peptidyl–prolyl *cis–trans* isomerase A (Henriksson, 2007_1); *Yersinia pestis* DXR complexed with Mg^{2+} and inhibitor 1,2–ethanediol (Osipiuk *et al*., 2009); and *T. maritima* (TmDXR) complexed with NADPH (Takenoya *et al*., 2010). In 2010, the crystallization and preliminary X–ray crystallographic study was carried out on *P.falciparum* DXR and the group is currently performing structural analysis by molecular replacement (Umeda *et al*., 2010). This information is however not yet publically available, meaning that the use of a homology model remains feasible. Two homology models were created, which in the interim, has allowed for the facilitation of structure–function predictions and inhibitor binding properties (Singh *et al*., 2007; Goble *et al*., 2010). One of the models was however not made publically available and there were very few PfDXR inhibitor binding studies available (fosmidomycin and FR900098) for the authors to use in validation of their model (Singh *et al*., 2007).

Numerous structural and biochemical analyses on various DXR enzymes have also been documented in literature. These include: EcDXR (Yajima *et al*., 2002; Reuter *et al*., 2002; Steinbacher *et al*., 2003; Mac Sweeney *et al*., 2005), ZmDXR (Grolle *et al*., 2000; Ricagno *et al*., 2004), *Synechocystis* sp. PCC6803 DXR (SyDXR) (Fernandes *et al.*, 2005), as well as very limited analysis on PfDXR (Jomaa *et al*., 1999). According to biochemical studies, EcDXR exists as an 86 kDa homodimer in its quaternary form (Figure **1.5A**), where each

monomer presents itself in a 43.5 kDa v–shape (Reuter *et al.*, 2002). The DXR monomer comprises three domains, namely the amino–terminal dinucleotide binding domain (residues 1–150), the carboxyl terminal four–helix bundle (residues 328–400), and a connective domain, which accommodates most of the active site and is also involved in dimerisation of the enzyme. The connective domain also incorporates a flexible loop, called the catalytic hatch, which is said to move over the active site after the substrate has bound (Yajima *et al.*, 2002). The accepted substrate binding site for the enzyme is in a cleft where concurrence of the three domains occurs (Figure **1.5B**).

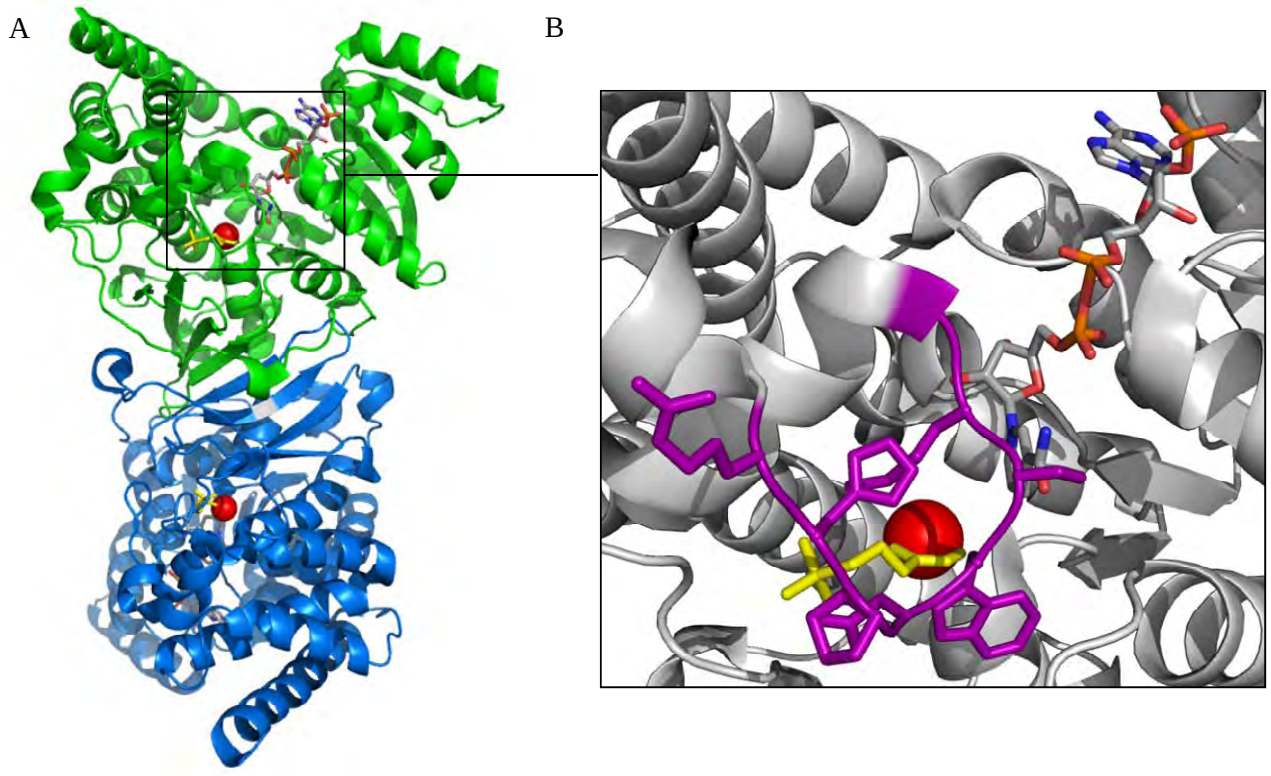

Figure 1.5: The well documented dimeric EcDXR enzyme with cofactors and fosmidomycin bound.
Ribbon representation of the EcDXR crystal structure (adapted from Yajima *et al.*, 2007). (A) The homodimeric structure of DXR is made up of two monomers with the one subunit coloured *green*, with the other subunit coloured *blue*. NADPH (coloured by *element*) and fosmidomycin (coloured *yellow*) atoms are shown as sticks, with the coordinating magnesium ion shown in *red* (B) Zoomed into the active site, the catalytic hatch (coloured *purple*) (Arg207–Met213) closes over the active site, once fosmidomycin has moved into the active site. Figures were prepared using PyMol.

Crystallization of EcDXR in complex with the inhibitor fosmidomycin (Mac Sweeney *et al.*, 2005) revealed that the phosphonate moiety of fosmidomycin was bound at the active site by residues Ser186, Gly187, Ser222, Met225, Asn227, Lys228 and Ile250 (reviewed by Singh *et al.*, 2007). The catalytic cleft conceals mostly hydrophilic amino acids that are strictly

conserved among all DXR enzymes in literature; a summary of these residues can be seen in Table **1.2**. An important difference to be noted includes interactions with Gly197 and His219 that were established in PfDXR that have to date, not been observed in any published DXR crystal structures (Singh *et al.*, 2006). These interactions were however not observed in the other PfDXR homology model that has been published in the literature (Goble *et al*., 2010); however, the study reported that these interactions were observed with fosmidomycin's closest analogue, FR900098. The residues that are responsible for enzyme catalysis are highly conserved among DXR enzymes and include Ser199, Ser235, Asn240 and Lys241 in PfDXR (Ser186, Ser222, Asn227 and Lys228 in EcDXR according to Table **1.2**). The literature reports that a number of residues are essential in active site formation and instead of having a direct interactive role rather perform a structural role. Such residues include His153, His209, Trp212, Met214 His257 and Pro274 in *E. coli* (Yajima *et al*., 2002). Glu231 has been implicated in a number of functions including direct enzyme catalysis (Yajima *et al*., 2002; Steinbacher *et al*., 2003), structural support (Goble *et al*., 2010) and divalent metal coordination (Reuter *et al*., 2002; Steinbacher *et al*., 2003; Mac Sweeney *et al*., 2005) (Table **1.2**).

As mentioned previously, the presence of a divalent cation is essential for active site formation and catalysis, where Asp150, Glu152, Glu231 (Steinbacher *et al*., 2003, Mac Sweeney *et al*., 2005) and Gly234 (Reuter *et al*., 2002), along with three water molecules form an octahedral coordination complex (with the divalent ion) in EcDXR. Similar residues have been implicated in metal ion coordination in TmDXR and include Asp142, Glu144 and Glu209 (Asp150, Glu152 and Glu217 in *E. coli*) (Takenoya *et al*., 2010). By a network of salt bridges, numerous residues are positioned to play a supportive role metal ion binding; in *E. coli*, these residues include Lys125, His153, and Lys228 (Reuter *et al*., 2002) (Table **1.2**).

The binding of NADPH has also been associated with the structuring of the active site (Steinbacher *et al*., 2003) and includes a number of amino acids. Gly11 and Ser12 coordinate the diphosphate moiety, while Ala35 and Gly36 interact with the 2'–phosphate of the NADPH adenosine mononucleotide moiety; Gly14 had also been said to be essential in divalent metal ion coordination (Reuter *et al*., 2002) (Table **1.2**).

Table 1.2: Analysis of critical amino acids in DXR and their predicted role.

Putative Function	Identified Amino Acid	Organism	Predicted Role	Reference
NADPH cofactor binding	Gly11, Ser12	*E. coli*	Coordinates the pyrophosphonate moiety of NADPH	Reuter *et al*., 2002
	Gly14	*E. coli*	Forms an important part of the NADPH binding motif	Reuter *et al*., 2002
	Ala35 and Gly36	*E. coli*	Accommodates the 2' phosphate moiety of NADPH	Reuter *et al*., 2002
	Thr10, Gly11, Gly36, Ile101, Ala105	*E. coli*	Pentose phosphate of adenine forms five hydrogen bonds to Thr10, Gly11 and Gly36 and the adenine ring interacts hydrophobically with Ile101 and Ala105	Yajima *et al*., 2007
	Trp212 and Met214	*E. coli*	Stacking functions essential in forming hydrophobic contacts with nicotinamide moiety of NADPH	Steinbacher *et al*., 2003
Coordination with the divalent metal ion	Asp150, Glu152 and Glu231	*E. coli*	Bound Mg^{2+} accompanied with three water molecules make an octahedral coordination with the three residues	Reuter *et al*., 2002; Steinbacher *et al*., 2003; Mac Sweeney *et al*., 2005
	Glu234	*E. coli*	Said to also coordinate the divalent metal ion, along with the other residues (Asp150, Glu152 and Glu231)	Reuter *et al*., 2002
	Asp142, Glu144 and Glu209 (Asp150, Glu152 and Glu217 in *E. coli*)	*T.maritima*	Bound Mg^{2+} accompanied with three water molecules make an octahedral coordination with the three residues	Takenoya *et al*., 2010
	Lys125, His153, and Lys228	*E. coli*	By a network of salt bridges, support the residues that coordinate with the metal ion	Reuter *et al*., 2002
Coordination with the substrate DXP or fosmidomycin or both	Ser186, Ser222, Asn227 and Lys228	*E. coli*	Catalytic residues that interact with the substrate DXP or fosmidomycin via a hydrogen bonding network with the phosphonate moiety, via oxygen atoms	Steinbacher *et al*., 2003; Yajima *et al*., 2007

Gly187, Met225, and Ile250	*E. coli*	Along with the other catalytic residues (Ser186, Ser222, Asn227 and Lys228), interact with the phosphonate moiety of fosmidomycin	Mac Sweeney *et al*., 2005
His209 and His153	*E. coli*	Important for enzyme catalysis as they have been implicated in having a structural role	Yajima *et al*., 2002
Trp212, His257 and Pro274	*E. coli*	Perform a stacking role which orders the active site structure (only in the presence of NADPH)	Steinbacher *et al*., 2003
His208–Met214	*E. coli*	His208–Met214 is considered to be the catalytic hatch that functions to open/close the active site of DXR and along with Trp212 and Met214 bind directly to fosmidomycin	Yajima *et al*., 2007
His209 and Pro274	*E. coli*	Perform a support role to Trp212 and Met214	Yajima *et al*., 2007
Trp204 (Trp212 in *E. coli*)	*Synechocystis* sp. PCC6803	Involved in the substrate binding and is essential for closing the loop over the active site, possibly forming a highly specific binding pocket (may also have a role in discriminating substrates for DXR)	Fernandes *et al*., 2005
Gly197 and His219 (Gly187 and His209 in *E. coli*)	*P. falciparum*	Involved in binding fosmidomycin and have to date, not been observed in any published DXR crystal structures	Singh *et al*., 2006

1.3.4 Kinetic Characterization of DXR

The steady state behaviour of many enzymes can be best represented by the hyperbolic relationship between the steady–state velocity and the concentration of substrate, cofactor or reversible modifier. For enzymes that follow typical Michaelis Menten kinetic behaviour, the maximum velocity (V_{max}) and the Michaelis constant (K_m) can be quantified (Eisenthal *et al*., 1974). The Michaelis constant is often thought of as being the dissociation constant for the substrate–enzyme complex where the lower the K_m, the greater the affinity that the substrate has for the enzyme (Smith and Wood, 1991). The maximal velocity cannot be looked at on its own because of its clear dependency on substrate concentration. A more appropriate measure of enzyme efficiency is the turnover number (k_{cat}), which is a direct measure of the catalytic production of product under saturating enzyme conditions. Another useful parameter for enzyme analysis is the second order rate constant, k_{cat}/K_m, which is summarised as the specificity constant indicative of an enzyme's efficiency (Smith and Wood, 1991). A rapid reaction turnover (large value of k_{cat}) or a high affinity for substrate (small value of K_m) will result in greater enzyme efficiency (large k_{cat}/K_m).

Kinetic characterization of numerous DXR enzymes has been undertaken has from 1998 and continues still today, with no values being reported to date for PfDXR. Values that have been experimentally quantified in the literature are summarised in Table **1.3.**

Table 1.3: Kinetic values quantified experimentally for DXR enzymes in the literature, including K_m (mM), turnover number (1/[s]) and catalytic efficiency K_m/k_{cat}). Parameters were quantified in the presence of Mn^{2+}, Mg^{2+} or Co^{2+}.

Organism	**Substrate**	**Specific Activity (µmol/min/mg)**	**K_m (mM)**	**k_{cat} (1/[s])**	**K_m/k_{cat}**	**Reference**
E. coli	1–deoxy–D–xylulose 5–phosphate	4 – 18	0.003 – 0.250	29 – 38	0.22 – 0.99	Takahashi *et al*., 1998; Kuzuyama *et al*., 2000; Hoeffler *et al*., 2002; Koppisch *et al*., 2002; Fox and Poulter, 2005; Walker and Poulter, 2005; Wong and Cox, 2007
Z. mobilis	1–deoxy–D–xylulose 5–phosphate	19.5	0.3			Grolle *et al.*, 2000
Streptomyces coelicolor	1–deoxy–D–xylulose 5–phosphate	25.8	0.19	19.2	0.1	Cane *et al.*, 2001
Synechocystis sp.	1–deoxy–D–xylulose 5–phosphate	20 – 22	0.134 – 12	0.16 – 17	0.037	Yin and Proteau, 2003; Fernandes *et al*., 2005; Phaosiri and Proteau, 2004
M. tuberculosis	1–deoxy–D–xylulose 5–phosphate		0.004 – 0.240	2.1 – 5.3	0.05	Dhiman *et al*., 2005; Henriksson *et al*., 2006; Argyrou and Blanchard, 2004
T.maritima	1–deoxy–D–xylulose 5–phosphate	8 – 10.5 x 10^{-3}	40	0.29	0.0075	Takenoya *et al*., 2010
Francisella tularensis	1–deoxy–D–xylulose 5–phosphate		0.104	2	1.2	Jawaid *et al*., 2009
A. thaliana	1–deoxy–D–xylulose 5–phosphate	2.1 – 5.6	0.132	4.4		Rohdich *et al.*2006
Coleus forskohlii	1–deoxy–D–xylulose 5–phosphate		0.147			Engprasert *et al*., 2005

According to an online enzyme database (Chang *et al*., 2009); there are no recorded entries for the PfDXR homologue, with respect to kinetic data. To date, only one laboratory has characterized kinetic parameters for PfDXR, where IC_{50} values were calculated using an NADPH–dependent assay with recombinant PfDXR protein (Gieβmann *et al*., 2008).

1.4 HETEROLOGOUS PROTEIN EXPRESSION

1.4.1 Production of target proteins in different expression systems

E. coli is the principle bacterial expression system used in molecular biology (Billman–Jacobe, 1996) because of its ability to produce large quantities of expressed protein in short times (Verma *et al*, 1998). This is because many of its biological processes have been extensively studied and are well understood. The *E. coli* expression system however, is not sufficient for cloning and expression of all recombinant proteins, because the system is not capable of post–translational modification (Geisse *et al*., 1996). Other bacterial expression systems have been used with success; for example, *Mycobacterium bovis* BCG and *Salmonella typhimurium* have been utilized as vaccine vectors in order to deliver recombinant proteins to specific sites in higher organisms (Billman–Jacobe, 1996). When choosing an appropriate expression system, specific aspects need to be considered, namely: the problem of gene maintenance, the control of expression and the cellular destination of the recombinant protein (Billman–Jacobe, 1996).

If bacterial expression is unsuccessful, other host expression systems need to be considered. Common eukaryotic alternatives include; *Pichia pastoris* and *Saccharomyces cerevisiae* yeast strains, the baculovirus expression system in insect cells, human cells, as well as cell–free systems (Gräslund *et al*., 2008). Cell–free systems have been used comprehensively to express and purify thousands of proteins and this system is particularly useful when producing proteins that are toxic to *E. coli*. Cell–free systems have also been used to produce PCR–amplified linear DNA fragments, without needing to clone into a vector (Gräslund *et al*., 2008).

Numerous studies have been undertaken in order to directly compare various expression systems. In a study by Morton and Potter (2000), bacterial (*E. coli*), yeast (*S. cerevisiae*, *P. pastoris*), insect (*Spodoptera frugiperda*), and mammalian (COS7 cells) expression systems were utilized in order to overproduce the enzyme rabbit liver carboxylesterase. Expression in

E. coli and *S. cerevisiae* resulted in little or no activity of the mammalian carboxylesterase, while expression in *P. pastoris*, *S. frugiperda* (baculovirus expression) and COS7 cells resulted in the purification of active enzyme. However, only the baculovirus–infected *S. frugiperda* expression system resulted in purification of milligram quantities of active enzyme (Morton and Potter, 2000). Thousands of recombinant proteins have to date, been successfully purified from baculovirus–infected insect cells; ranging from cytosolic enzymes to membrane–bound proteins (Kost *et al.*, 2005). The advantages of this virus–based expression system are that it is safe, easy to use and adaptable to facilitate large scale–up. Insect cells are able to perform general functions including folding, modifying, and assembly and trafficking of newly synthesized proteins. However, the protein processing pathways are not necessarily equivalent to that of the higher eukaryote; for example, the N–glycosylation pathway (Kost *et al.*, 2005). A number of studies have published accounts of improved protein production following cotransfection with baculovirus–expressing chaperones. For example, human lipoprotein lipase was coexpressed with calreticulin (Zang *et al.*, 2003); similarly, Epstein–Barr virus replication protein BZLF1 (Yokoyama *et al.*, 2000) and human tumour suppression protein LKB1 (Martinez–Torrecauadrada *et al.*, 2005) were coexpressed with the human chaperone combinations Hsp70/Hsp40 and Hsp70/Hsdj (human homologue of bacterial DnaJ). In both these cases, marked improvement in yield of functionally active human enzymes was accomplished using the human chaperones. The insect expression system appears to be a popular choice in the production and purification of human proteins; very little literature however exists for expression of malarial proteins in insect cells.

Mammalian expression systems comprise an array of different cell lines that are used for protein production; the most commonly used cell lines include: Chinese hamster ovary (CHO) cells, baby hamster kidney (BHK) cells, human embryonic kidney (HEK) 293 cells, mouse L–cells and myeloma cell lines like J558L or Sp2/0. Less frequently employed cell lines include: NIH 3T3 cells, lymphoblastoid cell lines, and murine erythroleukemia (MEL) cells (Geisse *et al.*, 1996). It has been said that when employing a mammalian expression system, the structure of the target protein needs to be considered when choosing the expression cell line. One needs to consider aspect such the degree of post–translational modification that is required, for example, disulfide bonding and protein glycosylation. Furthermore, the expression plasmid construction should be carefully designed as to fully utilize the expression system of choice (Geisse *et al.*, 1996). Similarly, mammalian expression systems are not popular for malarial protein production, perhaps due to the fact

that the degree of post–translational modification in higher eukaryotes is not the same as that of the malarial system (Kost *et al.*, 2005). Other non–bacterial expression systems are relatively simple to use, however, they are significantly more time consuming resulting in a decrease in their popularity (Gräslund *et al*., 2008).

1.4.2 Methods to improve protein expression

Despite the success that has been reported using other host expression systems, heterologous production of proteins in a bacterial expression system remains dominant, even for complicated proteins such as malarial enzymes. This is because the bacterial expression systems are simple, they boast rapid growth and overexpression is most often associated with overproduction of the recombinant protein (Ahuja *et al.*, 2006). However, a major limitation associated with overproduction of recombinant protein is the formation of insoluble non–functional clusters of protein known as inclusion bodies, which accumulate due to the attraction of exposed hydrophobic regions of a misfolded protein (Carrió and Villaverde, 2002). Another problem faced is degradation by the proteolytic machinery of the cell (Georgiou and Valax, 1996).

The overproduction of parasitic proteins, specifically those of *P. falciparum*, proves to be a challenge because of a number of different aspects. One of these includes the codon bias of prokaryotic host expression systems, meaning codons that are preferentially used by *P.falciparum* are not used in highly expressed genes by *E. coli* (Baca and Hol, 2000). The heterologous expression of 1000 *P.falciparum* proteins in *E. coli* was carried out in a single study and 337 of these target proteins were expressed, however, only 37 remained soluble (Mehlin *et al.*, 2006). The parameters that were used in choosing the target proteins included size, where proteins had to be reasonably small (less than 450 amino acids); proteins could not have more than 30% identity to any other protein that has been published in the Protein Data Bank; and they had to be non–membrane proteins. From this study, it was concluded that there was a reasonable correlation between the gene's A/T (adenine and thiamine) content (%) and the corresponding protein solubility (Mehlin *et al.*, 2006).

The mRNA of *P.falciparum* is characterized by its high A/T content and it encodes an abundance of lysine and arginine repeats, which often leads to the early termination of translation resulting in the formation of truncated protein forms or insoluble inclusion bodies (Flick *et al*., 2004). Amino acid codons used most frequently in *P. falciparum* are different

from those used in other organisms (Narum *et al.,* 2001). Experimental strategies that have been adopted in order to overcome these obstacles include: rare codon tRNA supplementation (Baca and Hol, 2000), codon optimization (Narum *et al.,* 2001; Nicoll *et al.,* 2006) and codon harmonization (Angov *et al.,* 2008).

Rare codon tRNA supplementation involves coexpression of the target protein with a RIG plasmid that encodes rare transfer RNAs for arginine (R), isoleucine (I) and glycine (G) (Baca and Hol, 2000). This strategy was used successfully for the production of full–length *P.falciparum* Hsp70, where a considerable reduction in lower molecular weight degradation products was reported after coexpression with the RIG plasmid (Matambo *et al.,* 2004). Codon optimization is an experimental strategy in which the coding region of a target protein is designed to include the most frequently used codons of the host cell (Nicoll *et al.,* 2006). Narum *et al.* (2001) reported that optimising the codon usage of *P. falciparum* merzoite proteins to that of mammalian systems improved the expression and immunogenicity of gene fragments in DNA vaccines used on mice. However, the expression of numerous other malaria proteins was not improved through codon optimization (Birkholtz *et al.,* 2008). Codon harmonization is an alternative strategy that involves substituting codons with synonymous ones that have the same or similar usage frequencies in the expression host, while maintaining the integrity of the pause site profile of a native sequence (Angov *et al.,* 2008). Codon harmonization permits translation in the heterologous host in a similar way to the native host, and thereby potentially enhances protein folding, unlike the product of an optimized gene (Angov *et al.,* 2008).

Site–directed mutagenesis has also been shown to be useful in enhancing solubility of recombinant proteins, by replacing non–polar amino acids with charged ones such as lysine (Dale *et al.,* 1994_1). Protein aggregation can also be minimized by adjusting growth parameters, such as temperature (Lilie *et al.,* 1998; Okita *et al.,* 2004; de Marco, 2007_1) or growth media (Moore *et al*., 1993). It has also been documented by Hanning and Makrides that coexpression of recombinant proteins with molecular chaperones, has positively improved protein yield (Hanning and Makrides, 1998).

1.4.3 Molecular chaperones

Molecular chaperones are divided into a number of highly conserved families and are present in all living cells, those under normal or stress conditions (Boshoff *et al*., 2004). Molecular

chaperones function by facilitating the folding and refolding of proteins in the cell and have been implicated in vital cellular processes such as protein synthesis, protein translocation, protein folding and protein degradation (Fink, 1999). Molecular chaperones distinguish between folded and unfolded proteins by recognising the hydrophobic surfaces that are characteristic of unfolded proteins (Boshoff *et al*., 2004). Newly translated proteins frequently enter non–productive folding pathways which result in their misfolding and ultimate aggregation. The assistance of chaperones is therefore necessary such that proteins are able to reach their active configuration; they do so by guiding the target protein along the productive folding pathway (Houry, 2001).

Hsps are a group of highly conserved proteins that are ubiquitous in all cells and whose main role is to act as molecular chaperones (Shonhai *et al*., 2007). In eukaryotes, Hsps are named according to molecular size, for example, Hsp70 is 70 kDa in size and the bacterial homologue of Hsp70 is DnaK. Hsp40 is 40 kDa in size, with its bacterial homologue being named DnaJ. Similarly, the bacterial homologue of Hsp60 is named GroEL (Szabo *et al*., 1994). In prokaryotes the most physiologically important and ubiquitous chaperones can be divided into two teams: DnaK–DnaJ–GrpE and GroEL–GroES, which have distinct but co–operative functions (Nishihara *et al*., 1998).

DnaK and DnaJ work in combination, where DnaJ delivers the substrate protein to its partner DnaK. DnaK then binds the substrate via hydrophobic protein sequences of four to five residues flanked by basic residues. Statistically, these binding motifs occur once every 36 residues, although most are buried in folded proteins (Rüdiger *et al*., 1997). In so doing, DnaK stabilizes the unfolded protein giving it sufficient time to fold correctly. GrpE is a nucleotide exchange factor that functions to promote dissociation of adenosine 5'–diphosphate (ADP) from the nucleotide–binding cleft of DnaK (Harrison, 2003). DnaK–DnaJ–GrpE (KJE) chaperone system was classified as the most important chaperone system in the cell for suppressing protein aggregation (Thomas *et al.*, 1997). The *E. coli* chaperone ClpB assists the KJE system in solubilising and refolding aggregated proteins (Watanabe *et al*., 2000) and is also thought to rescue proteins from high molecular weight aggregates (Bukau *et al.*, 2006). The small heat shock proteins IbpA and IbpB are considered “holder chaperones” that also bind protein aggregates and along with KJE/ClpB, facilitate refolding (Schlieker *et al.*, 2002). In a study by Deuerling *et al.* (1999), it was found that DnaK, only

in combination with trigger factor (TF), promoted proper folding of proteins, but neither was essential for folding and viability at intermediate growth temperatures.

The prokaryotic homologue of Hsp60, GroEL, assists in the proper folding of nascent polypeptides. Analysis of its tertiary structure shows that it forms a 3D barrel structure with a hydrophilic interior, with GroES (Hsp10) forming the lid (Weissman *et al*., 1995). Substrates bind GroEL via hydrophobic interactions on the interior rim of the hydrophilic chamber (Burston and Clarke, 1995) and require subsequent binding of GroES and ATP to trigger the release of the protein into the cavity. The folding intermediate then has about 10 seconds to fold as ATP (adenosine triphosphate) is hydrolysed to ADP (adenosine diphosphate); the dissociation of ADP and the binding of ATP, triggers the release of GroES and the folded polypeptide (Burston and Clarke, 1996; Weissman *et al*., 1995). It has however been shown that GroEL assists only in the folding of a minority of proteins (Deuerling *et al*., 1999); a possible reason for this may be the fact that GroEL has an upper size limit of 60 kDa (Houry *et al*., 1999). The KJE and GroEL–GroES (ELS) systems, along with TF is therefore said to be the primary chaperones for *de novo* folding in *E. coli* (Haacke *et al.*, 2009).

1.4.4 *P.falciparum* molecular chaperones

As with all other organisms, *P. falciparum* is abundant in these cellular helpers. As mentioned previously, the Hsps have become targeted in recent years for antimalarial drug design, as well as in coexpression studies with other proteins, including antimalarial drug target proteins (reviewed by Pesce *et al*., 2010). According to Pesce *et al*. (2010), there may be some value in understanding the complexity of the chaperone networks and partnerships such that resident chaperones can be used to improve the soluble production of antimalarial target proteins *in vitro.* Figure **1.6** summarizes the localization of some of the important chaperone families.

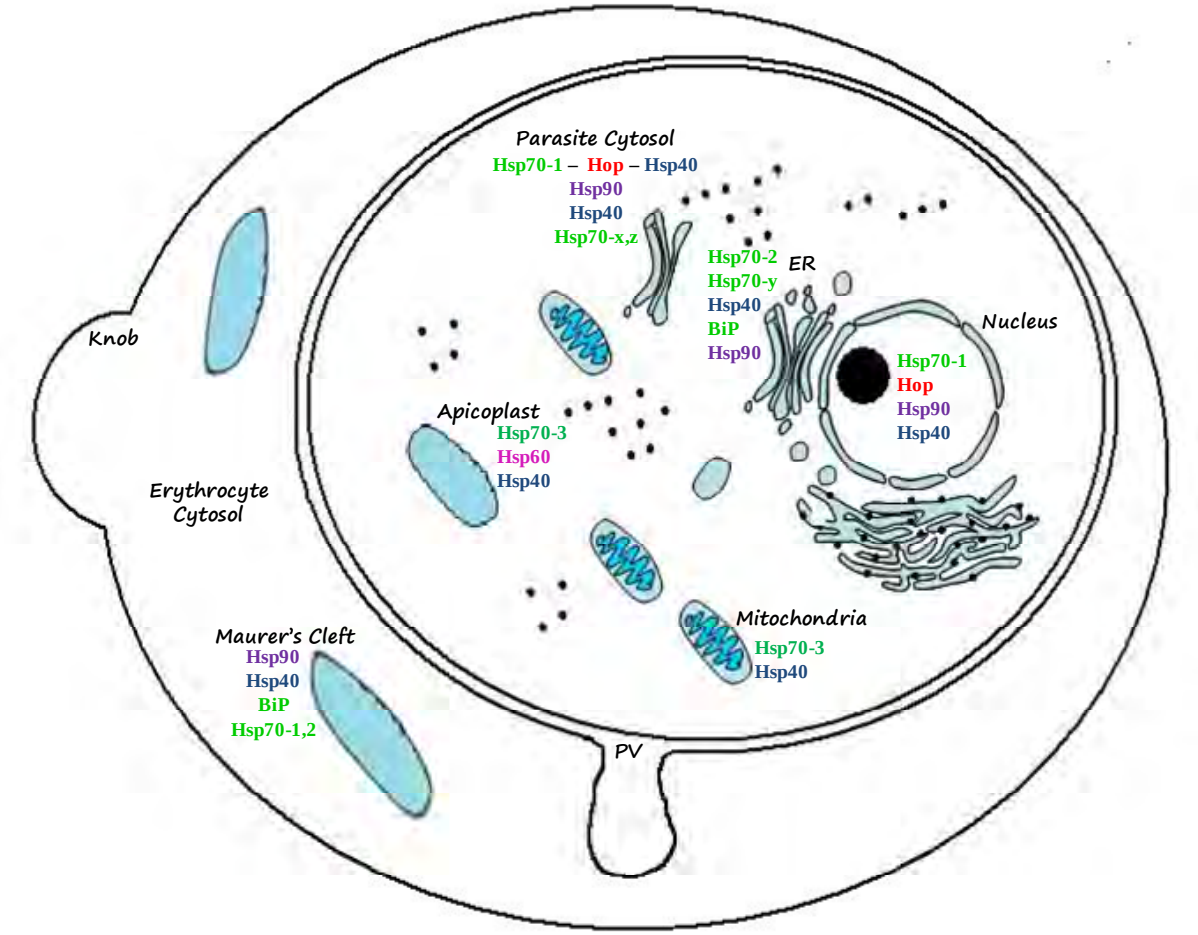

Figure 1.6: Chaperones in malaria for a *P. falciparum*–infected erythrocyte.
Only organelles of interest are shown, where Hop (heat shock organising protein) is shown in *red*, Hsp40s in *blue*, Hsp70s in *green* and Hsp90s in *purple* (Kumar *et al.*, 1991; Cunnea *et al* 2003; Hosoda *et al.*, 2003; Hiller *et al*., 2004; Vincensini *et al*., 2005; Nyalwidhe *et al*., 2006; Sargeant *et al.*,2006; Acharya *et al*., 2007; Botha *et al*., 2007; Powers and Workman, 2007; Tuteja, 2007; Bhattacharjie *et al*., 2008; Pesce *et al*., 2008; Misra and Ramachandran, 2009).

1.5 RESEARCH MOTIVATION

There is a global need to invest in additional research in the development of pharmaceutical products against diseases of poverty like malaria (Kesselheim, 2008); however, because of the low–returns and costliness of such research, pharmaceutical companies are not always willing to invest resources into this neglected disease (Trouiller *et al*., 2002). The recent genetic validation of PfDXR (Odom and Van Voorhis, 2010) means that this enzyme has become a particularly interesting antimalarial drug target.

Numerous inhibitors of DXR have been published in the literature, most of which share structural similarity with either the DXP substrate (Hoeffler *et al*., 2002; Wong *et al*., 2004; Phaosiri and Proteau, 2004; Fox and Poulter, 2005) or the antibacterial agent fosmidomycin (Reichenberg *et al*., 2001; Ortmann *et al*., 2003; Kurz *et al*., 2003_1; Kurz *et al*., 2003_2; Mincheva *et al*., 2003; Ortmann *et al*., 2005; Merckle *et al*., 2005; Woo *et al*., 2006; Devreux *et al*., 2006). Fosmidomycin is the benchmark against which all other DXR inhibitors are compared because it has been shown to inhibit PfDXR both *in vitro* and *in vivo* (Jomaa *et al*., 1999). Fosmidomycin has however been shown to demonstrate a reduction in pharmacological efficacy (reviewed by Singh *et al*., 2007) and so the search for potent inhibitors against DXR continues.

However, the difficulty involved in purifying malarial protein remains a major setback in drug discovery (Mehlin *et al*., 2006) and PfDXR is no exception (reviewed by Singh *et al*., 2007). Because of this, it has taken more than 10 years to produce a PfDXR crystal structure, which has not yet been structurally validated (Umeda *et al*., 2010). As a result of the crystal structure not yet being available, a three–dimensional PfDXR homology model would have to suffice. In this work, a homology model was created and validated using structure–checking programmes and docking of 34 known DXR inhibitors. The model was used to create an *in silico* screening tool for the rational design of novel DXR inhibitors. Numerous coexpression strategies were then employed in order to express soluble, functional PfDXR protein; coexpression with *lac* repressor resulted in the greatest protein solubility because of its ability to tightly control protein expression. Up to 4 mg per litre of protein could be purified using this strategy, which was then used for the *in vitro* kinetic characterization of PfDXR.

Site–directed mutagenesis was undertaken using the information obtained from the theoretical model and features that are unique to PfDXR were identified, which included major differences in the PfDXR catalytic hatch and NADPH binding site. Subsequent to rigorous analysis of the PfDXR active site, a compound library was synthesized and screened both *in silico* and *in vitro* for DXR inhibition potential and antimalarial potential. An *in silico* and *in vitro* parallel approach was hence employed to provide vital information which links theoretical and experimental evidence for an important antimalarial target enzyme PfDXR; this approach may assist in drug discovery in the future.

1.6 AIMS AND OBJECTIVES OF THIS WORK

A parallel approach to antimalarial drug screening was taken in this work:

Firstly, a three–dimensional PfDXR homology model was created and validated, which was then used to screen for potential lead compounds against the antimalarial drug target enzyme PfDXR. This was accomplished under the following objectives:

1. CREATION AND VALIDATION OF A PFDXR HOMOLOGY MODEL USING MODELLER, with the specific objectives of rigorously analysing the PfDXR active site; for the prediction of function using structural alignment strategies with apicomplexan and non–apicomplexan DXRs from the literature; and for development of a novel method for inhibitor screening
2. *IN SILICO* SCREENING OF A POTENTIAL DXR INHIBITOR LIBRARY, with the specific objectives of developing a link between structure and inhibition potential; as well as for further rigorous analysis of the PfDXR active site

Secondly, a high yield of functional PfDXR was purified for further characterization of the enzyme's active site and for the purpose of screening novel inhibitors for *in vitro* DXR–inhibition and *P. falciparum*–growth inhibition. This was done under the following objectives:

3. HETEROLOGOUS PROTEIN PRODUCTION AND PURIFICATION OF PFDXR, with the specific objectives of codon harmonization of the PfDXR gene; cloning the codon harmonized PfDXR coding region into the pQE30 expression system; co–expressing PfDXR with malarial and bacterial chaperones, as well as with the lac repressor protein in order to improve the yield of folded, functional protein

4. STRUCTURALLY AND KINETICALLY CHARACTERIZE THE PFDXR, with the specific objectives of characterizing PfDXR kinetically; using site–directed mutagenesis to create PfDXR mutants for the determination of structurally significant residues
5. PFDXR INHIBITION STUDIES USING NOVEL INHIBITORS , with the specific objectives of screening potential PfDXR inhibitors *in silico* using the PfDXR theoretical model; and for the determination of DXR–inhibition potential of novel ligands
6. GROWTH INHIBITION ASSAYS USING *P. FALCIPARUM*–INFECTED ERYTHROCYTES, with the specific objectives of determining antimalarial potential of novel PfDXR inhibitors

CHAPTER 2

IN SILICO ANAYSIS OF PfDXR IN LINKING STRUCTURE AND FUNCTION

2.1 INTRODUCTION

Not long after the discovery of DXR, reports of natural inhibitors emerged; the most potent inhibitor against PfDXR is still the antibacterial agent fosmidomycin (Figure **2.1**), isolated from *Streptomyces lavendulae* (Jomaa *et al.*, 1999). Replacement of the formyl–hydrogen (H) of fosmidomycin by a methyl group (CH_3) yielded the inhibitor FR900098 which was even more potent than fosmidomycin *in vitro* (Figure **2.1**) (Okuhara *et al.*, 1980). To date, several DXR inhibitor libraries have been identified (Jomaa *et al.*, 1999; Herforth *et al.*, 2004; Silber *et al.*, 2005; Haemers *et al.*, 2006; Gieβmann *et al.*, 2008), yet fosmidomycin and its analogue FR900098 have been shown to still be the most potent (reviewed by Singh *et al.*, 2007). These compounds have however been shown to exhibit reduced pharmacological properties (reviewed by Singh *et al.*, 2007) and fosmidomycin was also shown to only have a resorption rate of 10 – 30%. Therefore their potential to become drugs is considered to be poor (Murakawa *et al.*, 1982; Jomaa *et al.*, 1999).

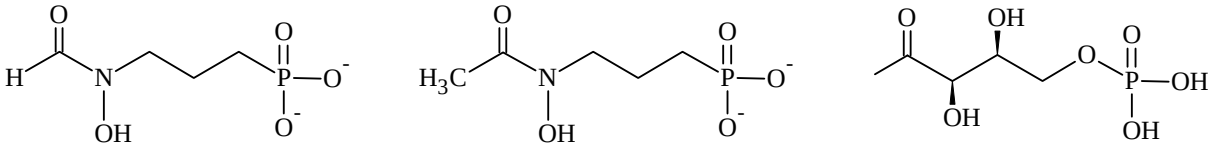

Figure 2.1: Structures of the most potent DXR inhibitors, fosmidomycin and its acetyl analogue FR900098 and the structure of the substrate DXP.

In general, PfDXR inhibitors can be classified into two groups; structural analogues of the substrate DXP (Figure **2.1**) (Hoeffler *et al.*, 2002; Phaosiri and Proteau, 2004; Wong *et al.*, 2004; Fox and Poulter, 2005) and structural analogues of fosmidomycin (Reichenberg *et al.*, 2001; Kurz *et al.*, 2003_1; Kurz *et al.*, 2003_2; Mincheva *et al.*, 2003; Ortmann *et al.*, 2003; Ortmann *et al.*, 2005; Merckle *et al.*, 2005; Woo *et al.*, 2006; Devreux *et al.*, 2006).

Important structural elements of DXR inhibitors have been identified and include a hydroxamic acid functionality (hydroxylamine inserted into a carboxylic acid), and a phosphonate group (Kurz *et al.*, 2003_1; Kurz *et al.*, 2003_2; Wiesner and Jomaa, 2007). The

crystal structure of EcDXR revealed that the hydroxamic acid moiety displaced two water molecules in the octahedral coordination of the divalent metal ion, where the N–formyl oxygen was trans to Glu231 and the N–formyl nitrogen was trans to Asp150 (Steinbacher *et al.*, 2003). Hoeffler *et al.* (2002) found that the presence of a hydroxyl group was essential for the rearrangement reaction and that it most likely acted as a Lewis acid (electron–pair acceptor) in the chelation of the divalent cation. The presence of the nitrogen atom has been shown to be crucial towards binding of inhibitors in the active site, most likely by changing the arrangement of the active site pocket (Zubrzycki and Blatch, 2001). Modifications of the hydroxamic moiety have also resulted in the synthesis of benzoxazolone, benzothione, hydroxamic acid and oxazolopyridinone functionalities (Courtois *et al.*, 2004; Kuntz *et al.*, 2005).

In the EcDXR crystal structure, the phosphonate moiety was shown to be anchored by numerous hydrogen bonding interactions to Ser186, Ser222, Asn227, and Lys228 (Steinbacher *et al.*, 2003). It has been shown that the two negatively charged oxygens of the phosphonate group are necessary for good inhibition of DXR (Perruchon *et al.*, 2008). In the case of most enzymes that boast a phosphate binding site, the incidence of many flexible Gly residues is common (Flitsch *et al.*, 1987), resulting in no specific recognition for the charged phosphate partner. This means that in drug discovery, the synthesis of compounds with neutral heterocyclic parts to target the phosphate binding pocket is common (Harvey *et al.*, 1966). However, in the case of the DXR active site, the presence of the divalent metal ion for coordination means that the maintenance of the phosphonate moiety is the general strategy of choice (Gieβmann *et al.*, 2008). Also, because of the susceptibility of the O–P bond to phosphatase cleavage (seen with DXP), the C–P bond of the phosphonate is commonly used in inhibitor design (Meyer *et al.*, 2003).

However, because of the bioavailability of fosmidomycin (most likely due to its high water solubility) (Na–Bangchang *et al.*, 2008), the initiation and design of phosphonate prodrugs was undertaken, which included for example, ester prodrugs (Reichenberg *et al.*, 2001; Ortmann *et al.*, 2003; Ortmann *et al.*, 2005), biphosphonates (Ling *et al.*, 2005) and carboxylic acids (Kurz *et al.*, 2003_2). The rationale behind this was that the ester linkages would be cleaved *in vivo* by non–specific plasma esterases, yielding the phosphonic acid moiety. Some of these phosphonate mimics (particularly the diphenyl phosphonate analogues) appeared to be even more active than fosmidomycin and FR900098 (Reichenberg

et al., 2001). Contradictory to this, Courtois *et al.* (2004) found that, in some cases, hydrolysis of the diethyl phosphonate analogues to the acid led to a reduction in inhibitory activity in plant cells.

Another structural aspect of novel DXR inhibitors that needs to be considered is the length of the carbon chain that links the hydroxamic acid and phosphonate group. Chain length has been linked to inhibitory activity, where the longer chained compounds appear to become less active against DXR (Woo *et al.*, 2006). Upon analysis of the space–fill rendition of the EcDXR crystal structure (Wiesner and Jomaa, 2007), it is clear that there is limited space available for inhibitors much larger than fosmidomycin. Mac Sweeney *et al.* (2005) reported that inhibitors with long carbon chains would most likely displace NADPH or bind to the open hatch conformation of the enzyme. This was however addressed by Gieβmann *et al.* (2008) who reported that significant inhibitory activity of an O–phenyl–substituted fosmidomycin analogue (24h) (which possessed and elongation of the hydroxamic moiety) possibly resulted from the support of a hydrophobic binding pocket reasonably far away from the active site pocket (Gieβmann *et al.*, 2008).

While modifications to the carbon chain length have been undertaken, modifications addressing the three carbon spacer are scarce. This has however been addressed in recent years; Devreux (2006) synthesized a library of cyclopropyl analogues containing a three–membered ring between C1 and C2 in order to restrict rotational freedom; and Haemers *et al.* (2006) on the other hand, concentrated rather on bulkiness and synthesized a library of fosmidomycin analogues containing a phenyl moiety at the α–position. It was concluded that the presence of the aromatic group may assist in the ability of compounds to cross the parasite membranes (Haemers *et al.*, 2006) because of its improvement in lipophilicity (Foye *et al.*, 2008). The low lipophilicity typical of fosmidomycin, which leads to difficulty in crossing phospholipid membranes and also adds to its poor absorption, was the motivation for development of lipophilic DXR inhibitors (Deng *et al.*, 2009). Interestingly enough, these compounds demonstrated reasonable activity against numerous pathogenic bacteria.

Silber *et al.* (2005) took their research into drug discovery further using protein–based docking with various DXR crystal structures and ligand–based 3D QSAR (quantitative structure–activity relationship), coupled to AFMoC (adaptation of fields for molecular comparison) to assess the structure–activity relationship of 34 DXR inhibitors with the target

enzyme. This *in silico* approach allowed Silber *et al.* (2005) to link the molecular interaction properties and ligand structure with inhibitory activity.

With the structural analysis of the preliminary X–ray crystal structure of *P.falciparum* DXR still underway (Umeda *et al.*, 2010); it was necessary to create an appropriate PfDXR homology model for the facilitation of predictions about structure–function relationships and for determination of inhibitor binding properties. This approach has been used previously and a PfDXR model developed and successfully used in *in silico* docking studies with various inhibitors, including fosmidomycin and FR900098 (Singh *et al.*, 2006). However, this model was not made publically available and there were very few PfDXR inhibitor binding studies available (fosmidomycin and FR900098) (Jomaa *et al.*, 1999) for the authors to use to validate of their model. Since this PfDXR modelling study, further experimental inhibitor binding studies have been conducted on PfDXR (Gieβmann *et al.*, 2008). The lack of a publically available PfDXR crystal structure or homology model provided the opportunity to produce a more vigorously validated PfDXR model for use in further structure, function and inhibitor screening studies.

The primary objectives of this work involved firstly identifying structural and functional features unique to PfDXR and secondly, developing an *in silico* docking system to identify, by screening, novel inhibitors of DXR. A three–dimensional homology model for PfDXR was created using MODELLER (version 9v2), which was verified by way of a Ramachandran plot and by way of docking–based validation. Using comparative sequence and structural analysis with apicomplexan and non–apicomplexan DXR proteins sourced from a literature review, structural and functional features unique to PfDXR were identified. This included the identification of insert regions, unique to apicomplexan DXRs, as well as significant structural differences with respect to the catalytic hatch and NADPH binding site, which were consistent in the apicomplexans. The PfDXR active site was also rigorously analysed, so that a structure–based approach could be taken for determination of novel inhibitors. This was accomplished by comparative docking of 34 known DXR inhibitors into PfDXR and EcDXR. Following this, a screen of 46 compounds was undertaken using the PfDXR homology model in an attempt to understand and potentially predict the effectiveness of novel inhibitors *in vitro* (see Chapter 5).

2.2 EXPERIMETNAL PROCEDURES

2.2.1 Primary validation and structural analysis of the predicted active site of PfDXR

It can be assumed that the tertiary structure of two proteins is similar if their sequences share a significant degree of similarity (Kroemer *et al.*, 1996). Subsequent to sequence alignment using ClustalX (Thompson *et al*., 1997), a PfDXR homology model was created using MODELLER (version 9v2) (Sali and Blundell, 2001), with the crystal structures of EcDXR (accession number: 1Q0Q_A) (Mac Sweeney *et al.*, 2005), ZmDXR (accession number: 1R0K_A) (Ricagno *et al.*, 2004) and *E. coli* IspC (accession number: 1ONP_A) (Steinbacher *et al.*, 2003) used as templates; sequence similarity of 36.2%, 36.6% and 35.2% was found for EcDXR, ZmDXR and IspC respectively, when compared to PfDXR. These models could hence allow for the structural prediction of a reasonable PfDXR homology model because medium–accuracy comparative models are based on 30 to 50% sequence identity (Baker and Sali, 2001). The initial PfDXR model was energy minimized using the *InsightII*/DISCOVER module, with 500 steps of steepest decent, at 22^{o}C. The homology model was assessed using WHATIF (version 6.0), PROCHECK (Vriend, 1990; Laskowski *et al.*, 1993) and the Ramachandran plot. Model images were rendered using PyMOL (version 0.98) (DeLano, 2003) and Accelrys Visualizer/Material Studios (version 2.0) (www.accelrys.com).

2.2.2 Comparative sequence analysis for prediction of function

The 417 amino acid sequence of PfDXR proposed here was aligned against the apicomplexan DXRs from *P. vivax* (accession number: XM_001615665), *P. berghei* (accession number: XM_673952) and *P. yoelii* (accession number: XM_720958), as well as the plant homologue *Arabidopsis thaliana* (accession number: AJ242588) and bacterial homologues *Z. mobilis* (accession number: 1R0K_A) and *E. coli* (accession number: 1JVS_A). Sequence alignments were derived using the ClustalW (Thompson *et al.*, 1994) and BLOSUM matrices were used to score the alignments, with the parameters for ‘gap open’, ‘gap extension’, and ‘gap distance’ set at 10, 0.5, and 8 respectively. The obtained alignments were manually inspected to ensure consistency with known structural information. Gene Runner (version 3.1) was used to analyse sequences with respect to open reading frames, composition and motif searches.

2.2.3 Docking–based model validation and inhibitor screening

For PfDXR homology modelling, the EcDXR crystal structure in complex with the substrate DXP was used (accession number: 1Q0Q_A), while docking was undertaken using the same EcDXR crystal structure in complex with fosmidomycin (accession number: 1Q0L_A) (Mac Sweeney *et al.*, 2005). This was done so that the modelling protocol could be appropriately validated; the protocol was validated by docking the minimized fosmidomycin structure back into the original protein crystal structure (accession number: 1Q0L_A). From the reference crystal structure for EcDXR (accession number: 1Q0L_A), fosmidomycin was removed from the binding site and the molecule was desolvated; the NADPH cofactor was retained – this was the EcDXR template that was used for this work. All structures of known DXR inhibitors (from the literature) were sketched in Accelrys Visualizer/Material Studios (version 2.0), with the phosphonate moieties in the deprotonated state and were DFT–minimized at the B3LYP/6–31G(d) level using Gaussian 03 (www.gaussian.com). Docking studies were performed on an Intel Core 2 Duo 3GHz workstation, equipped with OCZ 8800GTX 768MB DDR3 graphics. Using AutoDock 4.2 (Morris *et al.*, 1998), the AutoDock tool set was used to merge non–polar hydrogens such that all permitted torsions were allowed in the docking studies. The protein active site and surrounding residues were mapped using the AutoGrid 4.2 algorithm, incorporating a grid box of dimensions 60 x 60 x 60 units along the x, y and z axes, respectively. Atom maps were generated for all potential interactions between the ligand and the active site residues, where catalytic residues (Ser186, Ser222, Asn227 and Lys228 for EcDXR; Ser199, Ser235, Asn240 and Lys241 for PfDXR) and the metal coordinating residue (Glu231 for EcDXR; Glu244 in PfDXR) were kept flexible. The dockings were executed using a Lamarckian algorithm to create populations containing 150 individuals and allowing for a maximum of 2.5×10^6 energy evaluations. For each ligand, 10 docks were generated with visual analysis and ligand scoring data being used to decide upon the optimal conformation for each docking run.

Unless otherwise stated, atoms were coloured by element where oxygen (O) = red; nitrogen (N) = blue; phosphate (P) = orange; hydrogen (H) = light grey; carbon (C) = dark grey; chlorine (Cl) = green; fluorine (F) = cyan; and bromine (Br) = brown.

2.3 RESULTS

2.3.1 Primary validation of the predicted PfDXR model

According to the NCBI database, there are 24 published three–dimensional molecular structures for the DXR enzyme available (NCBI, 2010), none of which are from the *P. falciparum* homologue. This provided the platform from which the creation of the PfDXR homology model was initiated. Following sequence alignment, a predicted PfDXR three–dimensional structure was generated and appropriately validated. The first measure for model verification involved analysis of the tertiary structure using WHATIF and WHAT CHECK. The Ramachandran plot of psi and phi backbone conformational angles for each residue in the protein indicated that a normal distribution was apparent (Figure **2.2A**). The data from the Ramachandran plot (summarised in Figure **2.2B**) indicated that the PfDXR model presented here was comparable to the EcDXR crystal structure (accession number: 1Q0L_A), with respect to most favoured regions (87.4%), generously allowed regions (10.3%), and additionally allowed regions (1.5%) and for the stereochemical quality of the model, as observed using the PROCHECK protein structure checking programme. Only three residues (0.8%) were in disallowed conformations and these included Ser112, Glu387 and Glu390 (Figure **2.2A** and **2.2B**). With respect to the protein secondary structure, all three disallowed conformations were only fractionally out of the generously allowed region. All three residues were identified on a surface loop, suggesting that it would be unlikely that these residues could modify the internal protein core or secondary structure of the protein. The superimposition of the predicted PfDXR homology model and EcDXR (accession number: 1Q0L_A) suggested that they shared very similar structures overall (data not shown), validating the proposed three–dimensional tertiary arrangement of PfDXR. This assumption could be made because the PfDXR tertiary structure was modelled using a number of DXR templates from several well studied organisms.

A

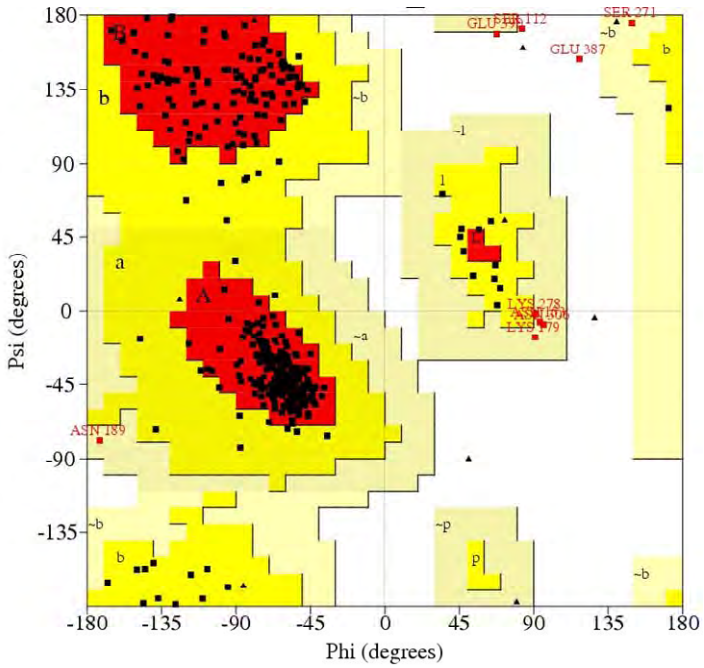

B

		EcDXR	PfDXR
Total Number of Residues		398	417
Most favoured regions	[A,B,L]	332 (93 %)	339 (87.4%)
Generously allowed regions	[~a,~b,~l,~p]	24 (6.7 %)	40 (10.3%)
Additional allowed regions	[a,b,l,p]	1 (0.3 %)	6 (1.5%)
Disallowed regions	[XX]	0 (0 %)	3 (0.8%)
Glycine residues		21	15
Proline residues		18	13
End-residues (excl. Gly & Pro)		2	1
Overall Score (PROCHECK)		0.19	-0.48
Mainchain G-factor Score		0.20	-0.72

Figure 2.2: Primary validation of the predicted PfDXR model.
(A) Conformational map (Ramachandran plot) of the psi and phi backbone conformational angles for each residue in the modelled PfDXR, where "most favoured" (coloured in *red*), "generously allowed" (*yellow*), "additionally allowed" (*beige*), and "disallowed" (white) regions are described. (B) Ramachandran plot statistics for EcDXR crystal structure (accession number: 1Q0L_A) and PfDXR homology model (presented in this work). The overall PROCHECK score of less than –0.50 is recommended and investigation is needed for a score of more than –1.0; both EcDXR and PfDXR score within the accepted reference scores. The G–factor score is a measure of the overall normality of the structure and is the average of all the different G–factors for each residue in the structure.

The native *P.falciparum* DXR enzyme (489 amino acids) (accession number: XM_001348779.1) (Gardner *et al.*, 1998) codes for a 71 amino acid leader peptide, which is said to comprise an N–terminal extension resembling an endoplasmic reticulum signal peptide and a 44 amino acid sequence exhibiting characteristics of a plastidial targeting sequence (Schwartzbach *et al.*, 1998; Jomaa *et al.*, 1999). Expression of PfDXR with the leader sequence appeared to be toxic to *T. gondii* (Jomaa *et al.*, 1999) and for this reason, PfDXR was modelled without the inclusion of the leader sequence. Following validation of

the PfDXR homology model, an attempt to link the tertiary structure and possible function was examined more closely. Sequence alignment with known DXR enzymes that have had their crystal structures defined was the platform from which the potential structure–function relationship of PfDXR could be surmised.

2.3.2 Comparative sequence analysis for prediction of function

A great deal of literature exists for the characterization of numerous DXR enzymes, the most well studied being EcDXR (Kuzuyama *et al.*, 1998; Takahashi *et al.*, 1998; Yajima *et al.*, 2002; Steinbacher *et al.*, 2003; Mac Sweeney *et al.*, 2005). From the literature, it is evident that catalytic residues and structural residues are highly conserved among the homologues (Figure **2.3**) and PfDXR is no exception. Upon careful inspection of the amino acid sequence alignment, it became evident that some differences did however exist with respect to the NADPH binding motif residues, as well as an area on the catalytic hatch which is highly conserved. Of those residues that are reported in the literature to bind NADPH, the apicomplexans presented a highly conserved Val and Asn at positions 43 and 44 (for PfDXR), while the *E. coli* and plant homologues replaced these with an Ala and Gly (Figure **2.3**). Similarly, some apicomplexans had large, highly charged residues (Lys residues at 224 and 226 on PfDXR) in an area of high conservancy on the catalytic hatch (His209 – Gly215 on EcDXR), where the bacterial and plant homologues boasted small polar residues instead (Figure **2.3**).

Further analysis of the sequence alignment revealed that the PfDXR, as well as the other apicomplexans, contained sequence insertions that were not evident in the bacterial and plant homologues (Figure **2.3**). These insertions appeared at the following positions on the PfDXR sequence: residues 30–32, 184–193 and 382–383 (Figures **2.3** and **2.4**). At residues 291–293 on the *A. thaliana* (AtDXR) sequence (at 307 on the PfDXR sequence), the plant homologue contained an insertion that did not appear in any of the other homologues (Figure **2.3**).

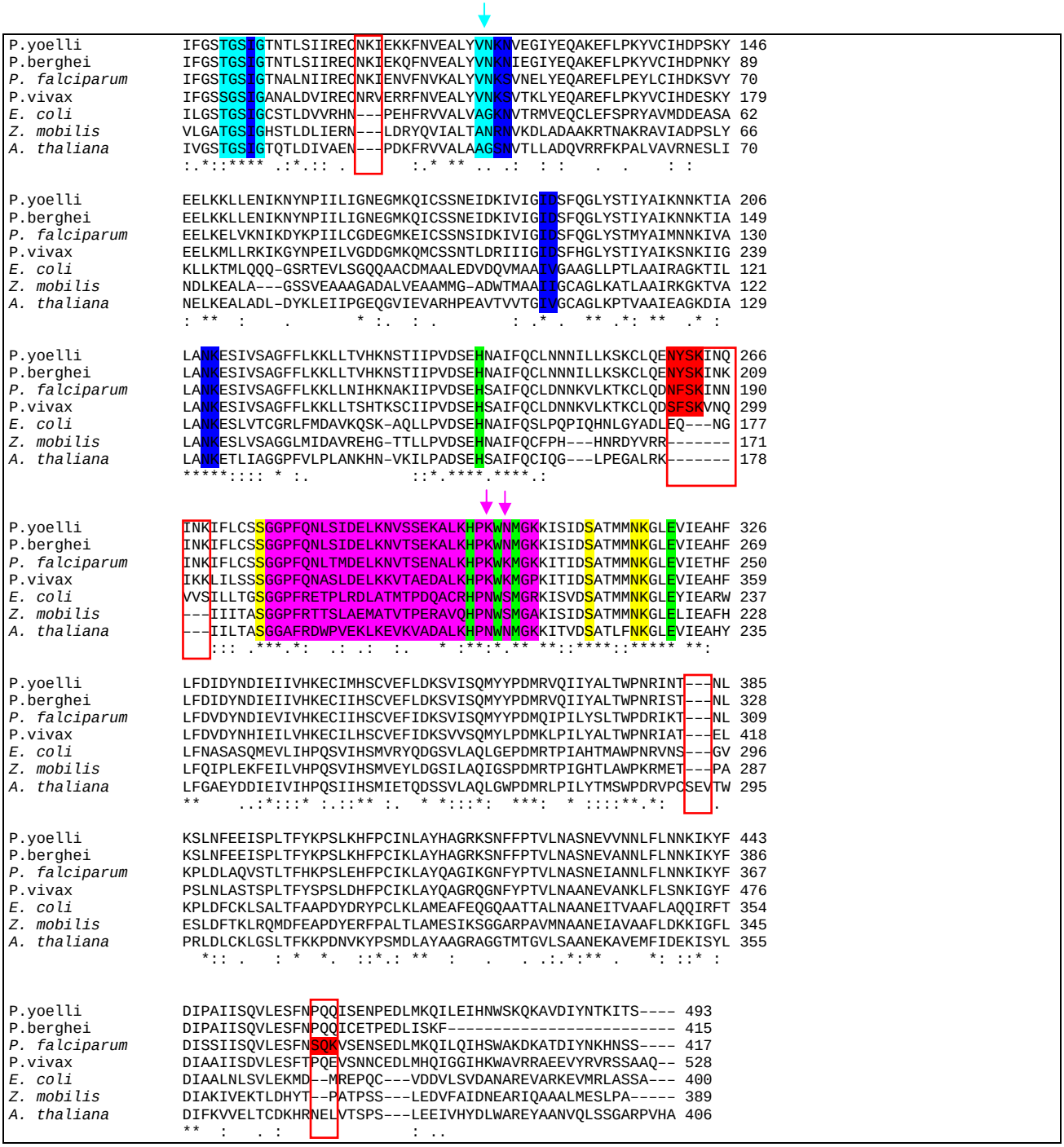

Figure 2.3: Comparative sequence analysis for prediction of function.

Multiple sequence alignment of *P.falciparum* DXR using ClustalW and BLOSUM matrices for scoring. The consensus sequence characterizes identical residues as '*****', strongly similar residues as '**:**' and weakly similar residues as '**.**'. Residues are highlighted according to catalytic or structural function and include: residues that bind NADPH cofactor highlighted in *light blue* (Reuter *et al.*, 2002) and *dark blue* (Goble *et al.*, 2010), structural residues important in active site formation (*green*) and catalytic residues (*yellow*) (Yajima *et al.*, 2002; Steinbacher *et al.*, 2003). The catalytic hatch (*pink*) is said to move over the active site once the substrate has bound (Reuter *et al.*, 2002). Significant differences in residues, between the *E. coli* and apicomplexan homologues, are highlighted using arrows and include: Ala35, Gly36 (arrow in *light blue*), Asn211 and Ser213 (arrows in *pink*) for EcDXR. Sequence insert regions specific to apicomplexans appear in blocks (*red*), with potential N–glycosylation sites (NFSK/NYSK) and protein kinase C phosphorylation site (SQK) within insert region coloured *red*. Alignment was performed with homologous sequences from other organisms, namely: *P. vivax* (accession number: XM_001615665), *P. berghei* (accession number: XM_673952), *P. yoelii* (accession number: XM_720958), *A. thaliana* (accession number: AJ242588), *Z. mobilis* (accession number: 1R0K_A) and *E. coli* (accession number: 1JVS_A). All sequences are truncated forms that do not include portions of the N–terminus.

When the PfDXR sequence was inspected for possible motifs (using visual analysis and using the Gene Runner motif search tool), a potential N–glycosylation site (N–{P}–[ST]–{P}) at residues 184–187 and protein kinase C (PKC) phosphorylation site ([ST]–x–[RK]) at residues 382–384, were located within the sequence insertion regions (Figures **2.3** and **2.4**), where P = the site of phosphorylation and x = any residue.

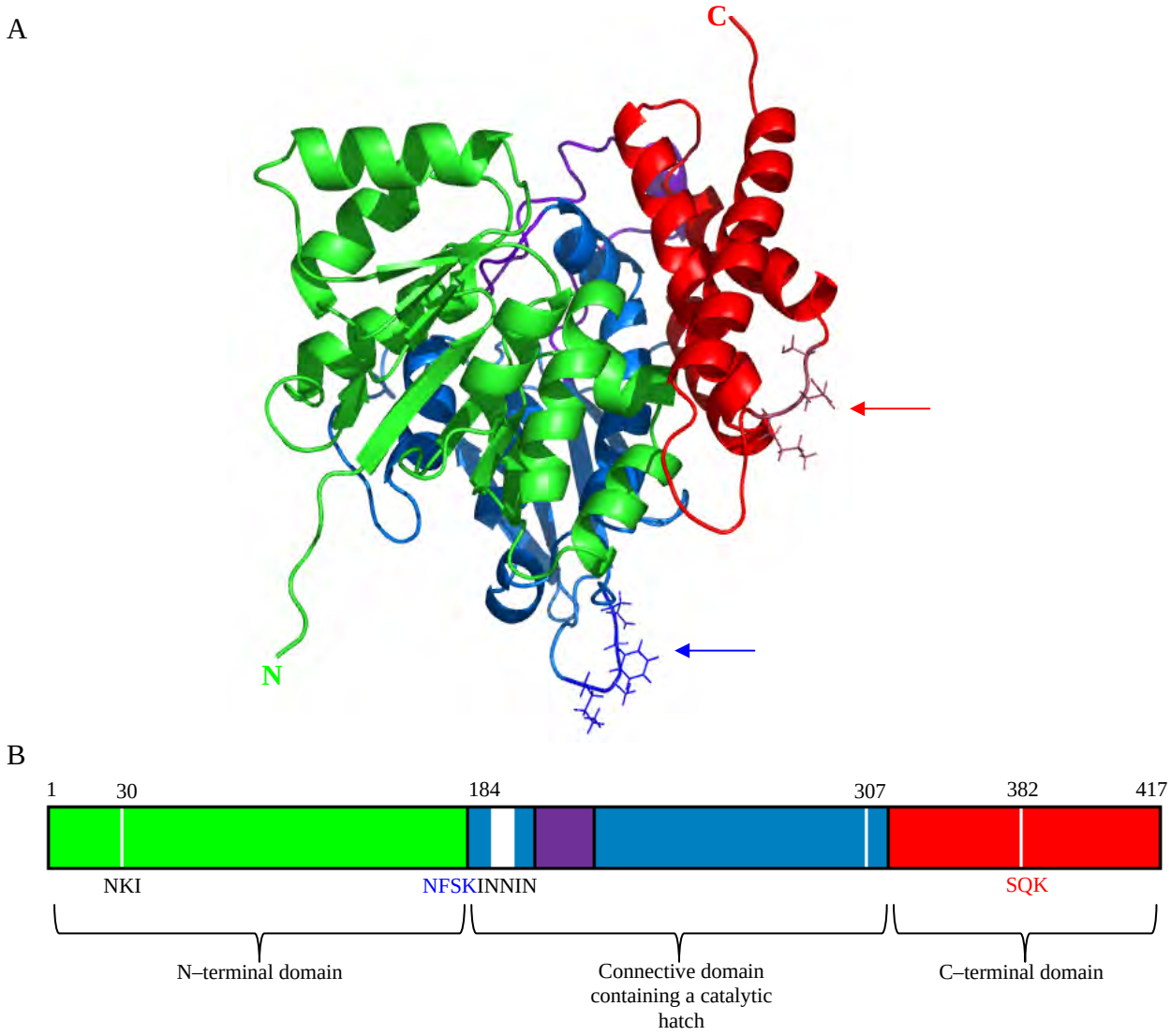

Figure 2.4: Three–dimensional analysis of predicted surface motifs.
(A) Ribbon representation of the 417 amino acid PfDXR monomer coloured by domain: N–terminal dinucleotide binding domain (*green*), a connective domain (*blue*) which includes a 30 residue catalytic hatch (*purple*), and a C–terminal four–helix bundle domain (*red*). Motifs on the protein surface that occur at sequence insert regions are highlighted (side chains shown), where an N–glycosylation site (NFSK) (*dark blue*) and a protein kinase C phosphorylation site (SQK) (*raspberry*) is shown in sticks and designated by an arrow. (B) Linear representation of PfDXR monomer coloured by domain, with the location of the insert regions labelled by residue position (relative to PfDXR) and residue name. The PfDXR insert regions occur at residue positions 30, 184 and 382 and residues are labelled appropriately. At residue position 307 (on the PfDXR sequence), *At*DXR presents an insert that does not appear in other homologues.

The other apicomplexans shared the same N–glycosylation motif at the same alignment position; however the PKC phosphorylation motif was specific to the PfDXR homologue (Figure **2.3** and **2.4**). The tertiary analysis of the apparent v–shaped PfDXR monomer confirmed that these two potential motifs were predicted to be on the protein surface, consistent with being a site of post–translational modification (Figure **2.4A**).

2.3.3 Structural analysis of the predicted PfDXR homology model

The EcDXR enzyme presents itself as an 86 kDa homodimer, with three domains making up each monomer (Reuter *et al.*, 2002); these include an N–terminal dinucleotide binding domain (residues 1–150), a C–terminal four–helix bundle (residues 328–400) (Yajima *et al.*, 2002), and a connective domain (residues 151–327), which accommodates most of the active site and is also involved in dimerisation of the enzyme (Reuter *et al.*, 2002). The PfDXR model proposed here presents itself as a 46.7 kDa v–shaped monomer, as is seen with the EcDXR homologue (Figure **2.4A**) (Reuter *et al.*, 2002). The residues that correspond to the regions in the *P. falciparum* sequence are as follows: residues 1–160 in the PfDXR sequence comprises the N–terminal domain; residues 161–340, the connective domain; and residues 341–417 make up the C–terminal domain (Figure **2.4**). According to the literature, the connective domain also contains a catalytic hatch, which is said to move over the active site after the substrate/inhibitor has bound (Yajima *et al.*, 2002). The connective domain of PfDXR appears to contain this catalytic hatch (199–229 for PfDXR) (Figures **2.5** and **2.6**), which is highly conserved (from His222–Gly228) (Figure **2.3**) in the position that is immediately adjacent to the active site. However differences do exist as mentioned previously (including residues Lys224 and Lys226, which are Asn211 and Ser213 EcDXR equivalents). It is evident from Figure **2.5** that the bulkiness of the hatch residues, Lys224 and Lys226, differs significantly from that of the EcDXR equivalents Asn211 and Ser213. Asn211 is within 9.15 Å of the inhibitor (when FR900098 is bound) and similarly, Lys224 is within 9.56 Å of the docked inhibitor, for PfDXR and EcDXR respectively (Figure **2.5**).

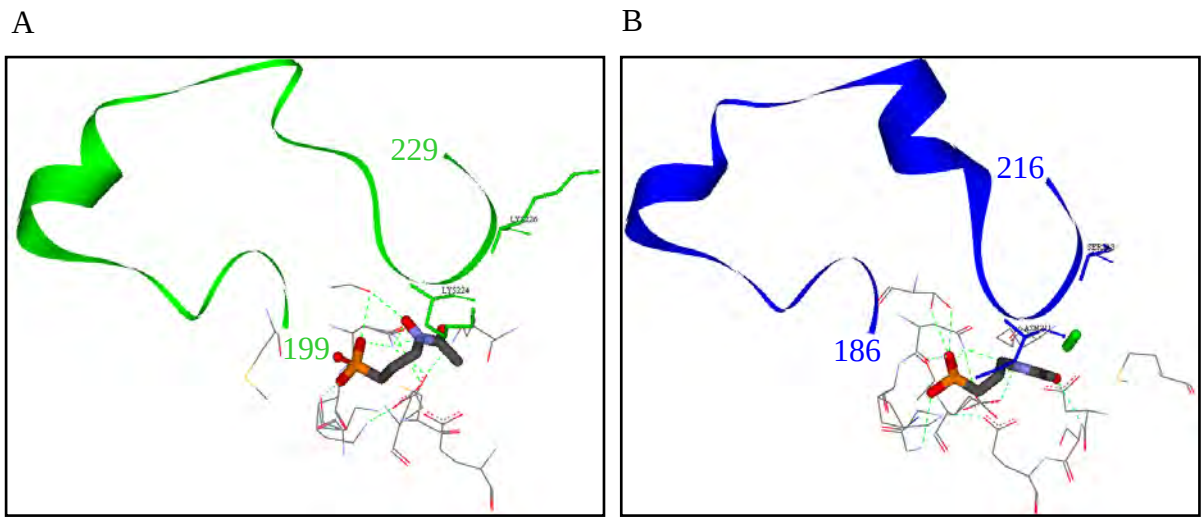

Figure 2.5: The catalytic hatch closes over the active site once the substrate/inhibitor has bound.
(A) FR900098 docked into PfDXR, showing residues within 4 Angstroms of the inhibitor, as well as the hatch in ribbon representation (*green*) from residues 199 to 229, with the side chains of hatch residues Lys224 and Lys226 shown in *green*. Hydrogen bonding is shown in green. (B) FR900098 docked into EcDXR, showing residues within 4 Angstroms of the inhibitor, as well as the hatch in ribbon representation (coloured *blue*) from residues 186 to 216, with the side chains of hatch residues Asn211 and Ser213 shown in *blue*. Hydrogen bonding is shown in green.

As with the proposed EcDXR models in the literature (Reuter *et al.*, 2002; Yajima *et al.*, 2002; Mac Sweeney *et al.*, 2005), the connective domain of the PfDXR model also accommodates all of the active site residues, namely Ser199, Ser235, Asn240, Lys241, Glu244 (Ser186, Ser222, Asn227, Lys228, Glu231 in EcDXR) (Figure **2.6**) (Yajima *et al.*, 2002; Steinbacher *et al.*, 2003). Other structurally significant residues in EcDXR include His153, His209, Trp212, His257 and Pro274 (His163, His222, Trp225, His270 and Pro287 in PfDXR), which are essential in the formation of the active site architecture (Yajima *et al.*, 2002; Steinbacher *et al.*, 2003). It is evident from Figure **2.6** that the architecture of the PfDXR and EcDXR active sites are very similar, where the catalytic residues and structural residues named have very similar orientations and positions. While the active DXR enzyme presents itself as a homodimer, for the purpose of this modelling work, the monomeric form of the enzyme was analysed. While this appears to be a potential limitation of this modelling approach, it is evident from Figure **1.5A** that the two monomers interact in such a way that the subunit interactions would not impact the architecture of the active site. This is evident upon the superimposition of the experimentally determined three–dimensional EcDXR crystal structure onto the PfDXR homology model, where the active site architecture remains intact (Figure **2.6** and **2.7**).

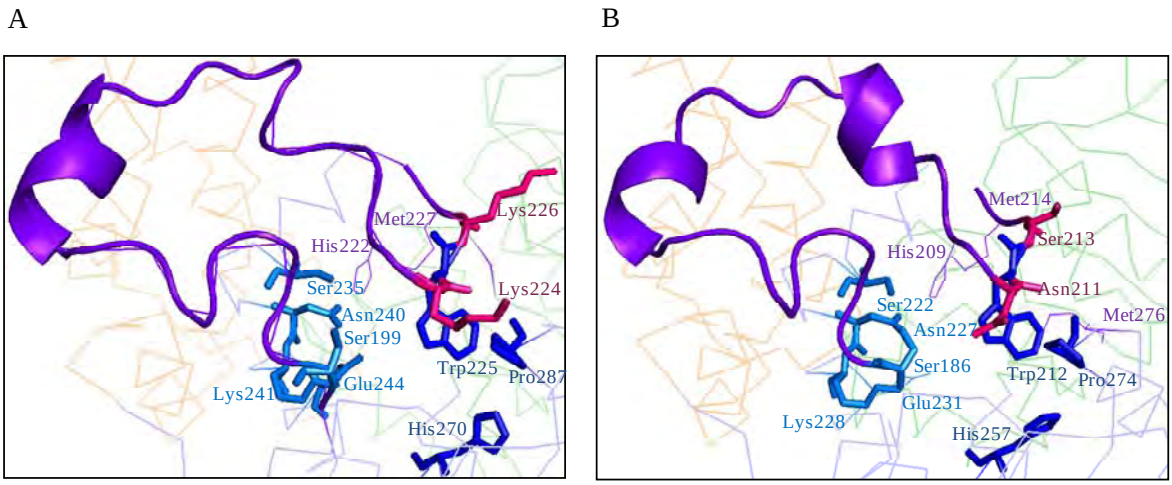

Figure 2.6: Structural analysis of the predicted active site of PfDXR.
(A) Stick representation of PfDXR monomer coloured by domain, zoomed into the catalytic site: N–terminal dinucleotide binding domain (coloured *pale green*), connective domain (*pale blue*) which includes a 30 residue catalytic hatch (shown in ribbon representation and coloured *purple*), and C–terminal four–helix bundle domain (*pale red*). The side chains for hatch residues His222 (*purple*), Trp225 and Met227 are shown (*dark blue*). The Lys224 and Lys226 residues are shown in sticks (*pink*) because they are different in size and charge when compared to the *E. coli* homologue (*pink*). Catalytic residues that are shown in sticks include: Ser199, Ser235, Asn240, Lys241 and Glu244 (*light blue*). Structural residues that are shown in sticks include: His270 and Pro287 (*dark blue*). Hydrogens are not shown. (B) Stick representation of EcDXR monomer coloured by domain, zoomed into the catalytic site: N–terminal dinucleotide binding domain (*pale green*), connective domain (*pale blue*) which includes a 30 residue catalytic hatch (shown in ribbon representation and coloured *purple*), and C–terminal four–helix bundle domain (*pale red*). The side chains for hatch residues His209 (*purple*), Trp212 and Met214 are shown (*dark blue*). In some docking studies, Met276 (*purple*) has been shown to close over the active site instead of Met214. The hatch residues, Asn211 and Ser213 are shown in sticks (*pink*) because they differ from the topologically equivalent PfDXR residues, Lys224 and Lys226. Catalytic residues that are shown in sticks include: Ser186, Ser222, Asn227, Lys228 and Glu231 (*light blue*). Structural residues that are shown in sticks include: His257 and Pro274 (*dark blue*). Hydrogens are not shown.

Adjacent to the substrate/inhibitor active site, exists the NADPH binding motif. According to the literature, NADPH binding motif residues for EcDXR include: Thr10, Gly11, Ser12, Gly14, Ala35 and Gly36 (Reuter *et al.*, 2002). The equivalent residues in PfDXR are: Thr15, Gly16, Ser17, Gly19, Val43 and Asn44. It is clear from this that major differences in the NADPH binding motif exist when comparing EcDXR and PfDXR, where the small side chains of Ala35 and Gly36 are replaced for significantly larger residues in PfDXR (shown in sticks in Figure **2.7**). When compared to the orientation of residues that exist within 4 Å of the cofactor in PfDXR versus EcDXR, it is apparent that there is a high degree of conservancy when comparing the two homologues. However, the two predicted NADPH binding residues, Val43 and Asn44, inhabit very different orientations with respect to their EcDXR equivalents, especially Asn44. In this work, NADPH established 9 hydrogen bonding interactions with EcDXR, which included: Thr10, Ser12 (x2), Ile13, Lys37, Asn38,

Ile101, Lys125 and Gly215 (Figures **2.3** and **2.7**). In the case of most of the above–mentioned residues, hydrogen bonding with the cofactor occurred via the main chain groups as opposed to the side chains, which are in many cases not capable of hydrogen bonding. While there appear to be no clear interactions between EcDXR and motif residues mentioned in the literature, those critical motif residues do reside within 4 Å of the bound NADPH. With PfDXR, similar protein–cofactor interactions were observed, with hydrogen bonding of the protein to residues Gly16, Ser17, Ile18, Asn44, Ser46, Asp111 and Asn133 (Gly11, Ser12, Ile13, Gly36, Asn38, Val102 and Asn124 in EcDXR) (Figures **2.3** and **2.7**). As with the EcDXR NADPH binding residues that have been mentioned in the literature, all PfDXR equivalent residues also reside within 4 Å of the bound NADPH.

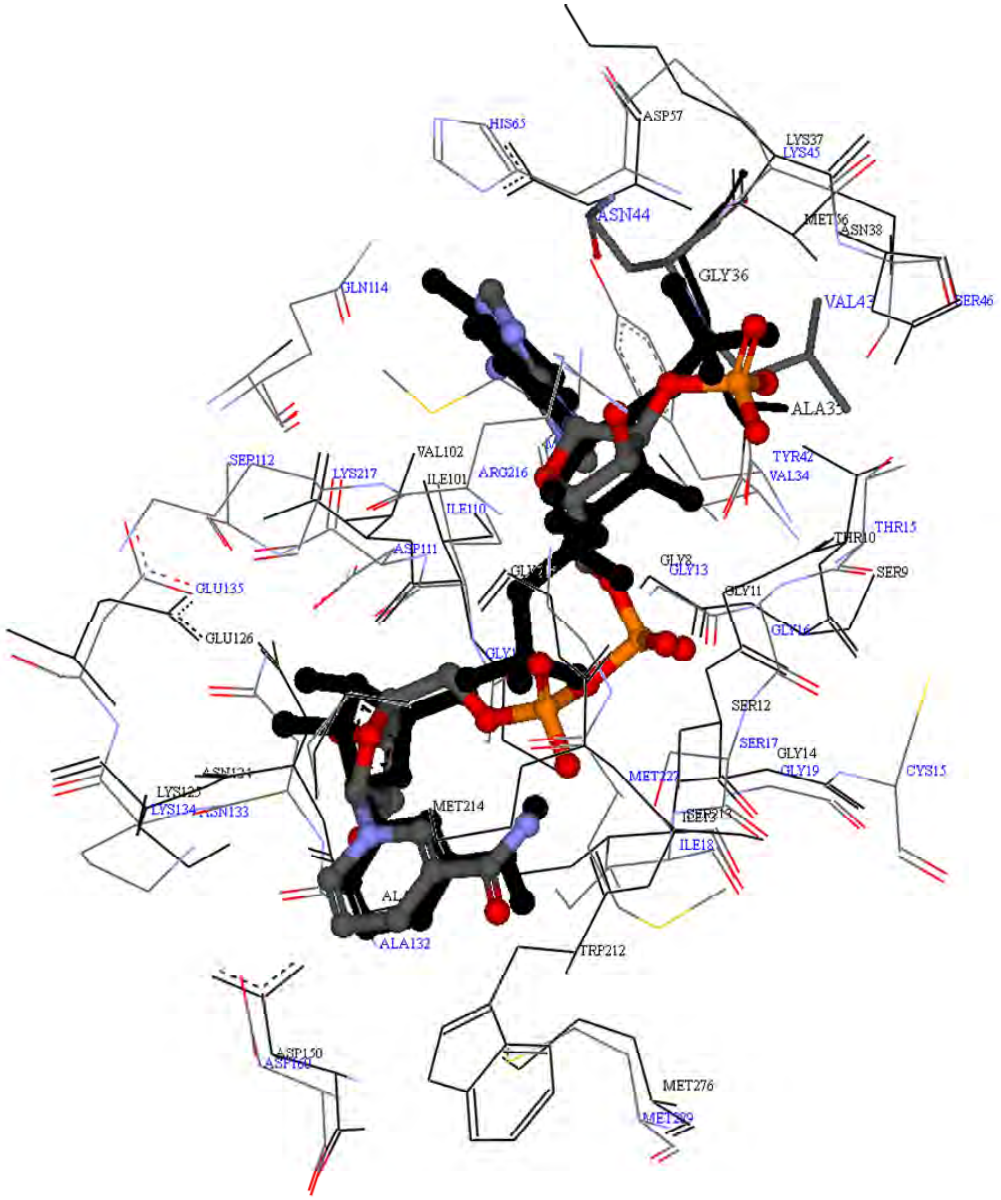

Figure 2.7: Superimposition of EcDXR with bound NADPH onto the PfDXR equivalent with bound NADPH shows a very similar orientation (legend on next page).

Schematic view of NADPH (coloured by *atom type*) bound to PfDXR at the NADPH binding motif. Resides within 4 Å of the ligand are shown and are coloured by *atom type* and labelled *blue*. The schematic view of NADPH (coloured *black*) bound to EcDXR (1Q0L) is superimposed onto the PfDXR equivalent such that orientations are identical. Resides within 4 Å of the ligand are and are coloured and labelled *black*. Ala35 and Gly36 (in EcDXR) are known to interact directly with NADPH and are shown in sticks because they differ in size and orientation when compared to the PfDXR equivalents Val43 and Asn44.

After rigorous analysis of the PfDXR homology model's highly conserved substrate and NADPH binding sites, docking–based model validation was carried out using 34 known inhibitors of DXR published in the literature.

2.3.4 Docking–based model validation and inhibitor screening

The reliability of the docking protocol was validated by removing fosmidomycin from the modelled EcDXR (accession number: 1Q0L_A) in the literature. Fosmidomycin was then re–docked into the protein, as well as into the modelled PfDXR and analysed. Similarly, this protocol was applied to 34 other ligands (Figure **2.8**); for each docking run, 10 possible docks were generated. The best docking mode was chosen based on the binding affinity demonstrated by the ligand, orientation of the ligand in the active site, and the number of potential bonding interactions. Upon analysis, structurally similar ligands, *i.e.* from the same research group, appeared to exhibit similar orientations in both the PfDXR and EcDXR active sites.

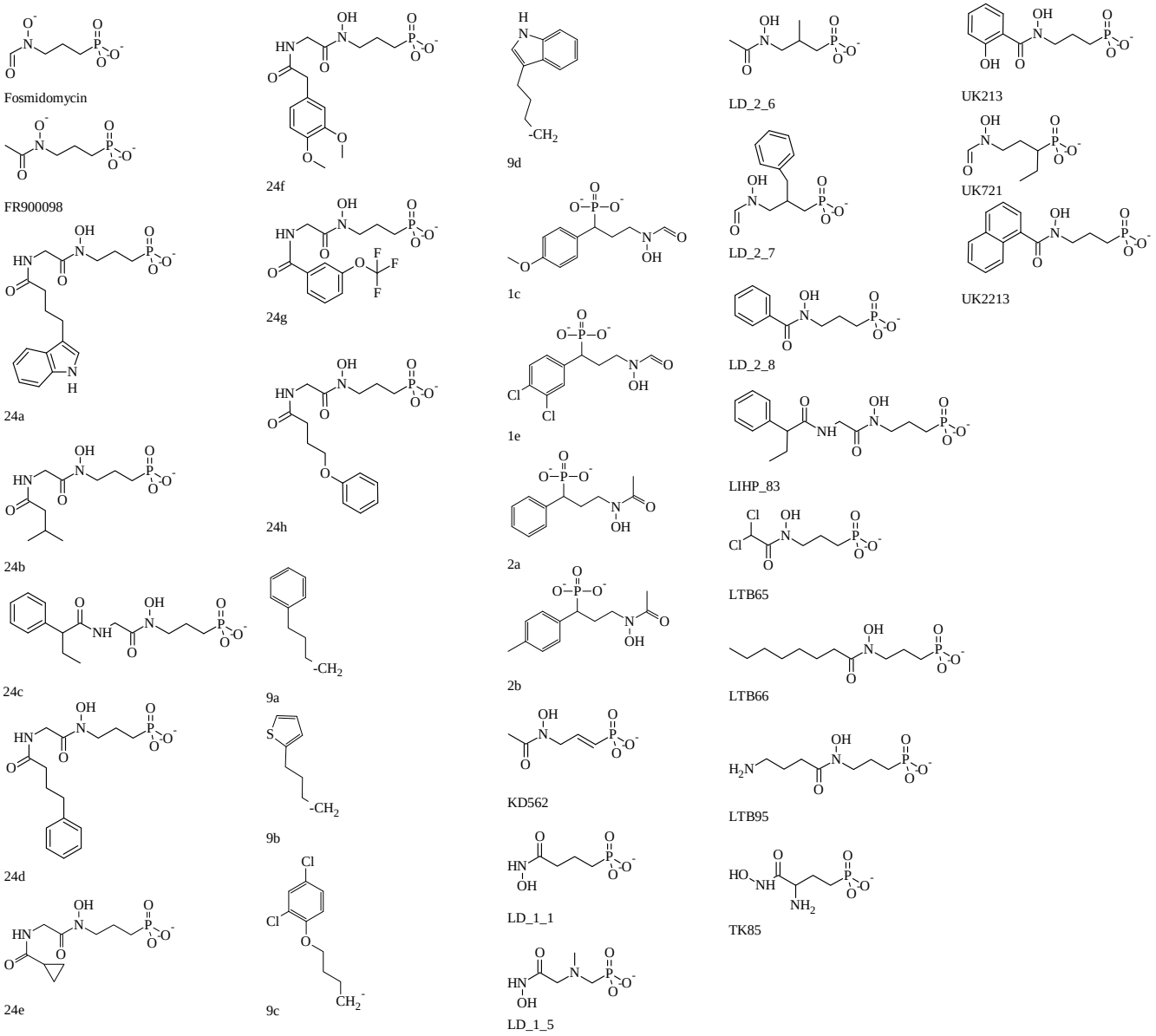

Figure 2.8: The chemical structures of novel DXR inhibitors from the literature.
Inhibitors used for docking studies (in columns from left to right), namely fosmidomycin, FR900098, Gieβmann *et al.* (2008) ligands 24a–h, Herforth *et al.* (2004) ligands 9a–d, Haemers *et al.* (2006) fosmidomycin analogues 1c, 1e, 2a, 2b and Silber *et al.* (2005) ligands KD562, LD_1_1, LD_1_5, LD_2_6, LD_2_7, LD_2_8, LIHP_83, LTB65, LTB66, LTB95, TK85, UK213, UK2213, UK721. Structures were drawn using ACD/ChemSketch freeware software version 11.01.

All ligands were quantified with respect to binding affinity and the number of hydrogen bonding interactions. The theoretical inhibition potential of each ligand was graphically classified into quadrants using these two parameters (Figure **2.9**). For EcDXR, those ligands that demonstrated the lowest binding energy (kcal/mol) with the highest incidence of interaction resided in the bottom right quadrant and included: LTB95, LD_2_6, FR900098, LD_1_1, KD562, UK213, TK85, LD_2_7, UK721, fosmidomycin and LTB65 (Figure **2.9A)**. For PfDXR, ligands that demonstrated a good binding affinity and reasonable strength of

binding included: LTB95, 2a, TK85, UK721, fosmidomycin, FR900098 and LD_2_7 (Figure **2.9B**). In all the above mentioned docking simulations, critical interactions between the enzyme and the ligands' phosphonate moiety were documented, as were interactions with the N–formyl oxygen. It is evident from Figure **2.9** that those ligands which have been reported to be efficient at inhibiting DXR, such as FR900098 and fosmidomycin (highlighted in yellow), resided within the expected quadrant. This method of screening was therefore validated as a useful tool to screen compound libraries *in silico*.

When fosmidomycin was docked into PfDXR the phosphonate moiety of the ligand interacted with the following residues: Ser199, Ser235, Asn240 and Lys241; the exact EcDXR equivalent residues, namely: Ser186, Ser222, Asn227 and Lys228 also interacted with phosphonate moiety when fosmidomycin was docked into EcDXR. Interactions with FR900098 included: Ser199, Gly200, Ser235, Asn240 and Lys241 for PfDXR (Figure **2.10A**), while EcDXR interacted with Ser151, Gly185, Ser186, Ser222, Asn227, Lys228 and Glu231 (Figure **2.10B**). In the case of the phosphate mimics 24a–h (Gieβmann *et al.*, 2008), α–substituted fosmidomycin analogues (Haemers *et al.*, 2006) and DXR inhibitors (Silber *et al.*, 2005), it was evident that a phosphonate moiety carrying a significant negative charge, as well as a nitrogen atom carrying a partial/induced negative charge, was required for reasonable binding of the active site residue. This was validated by the fact that when the 3'–amido–3'–deoxy–N_6–(1–naphthylmethyl) adenosine derivatives 9a–d (Herforth *et al.*, 2004) were docked into EcDXR and PfDXR, very few hydrogen bonding interactions were observed. This compound library was originally derived for the purpose of blocking the NADPH binding site; however, in this study all compounds demonstrated a preference for DXR active site and preferentially bound there.

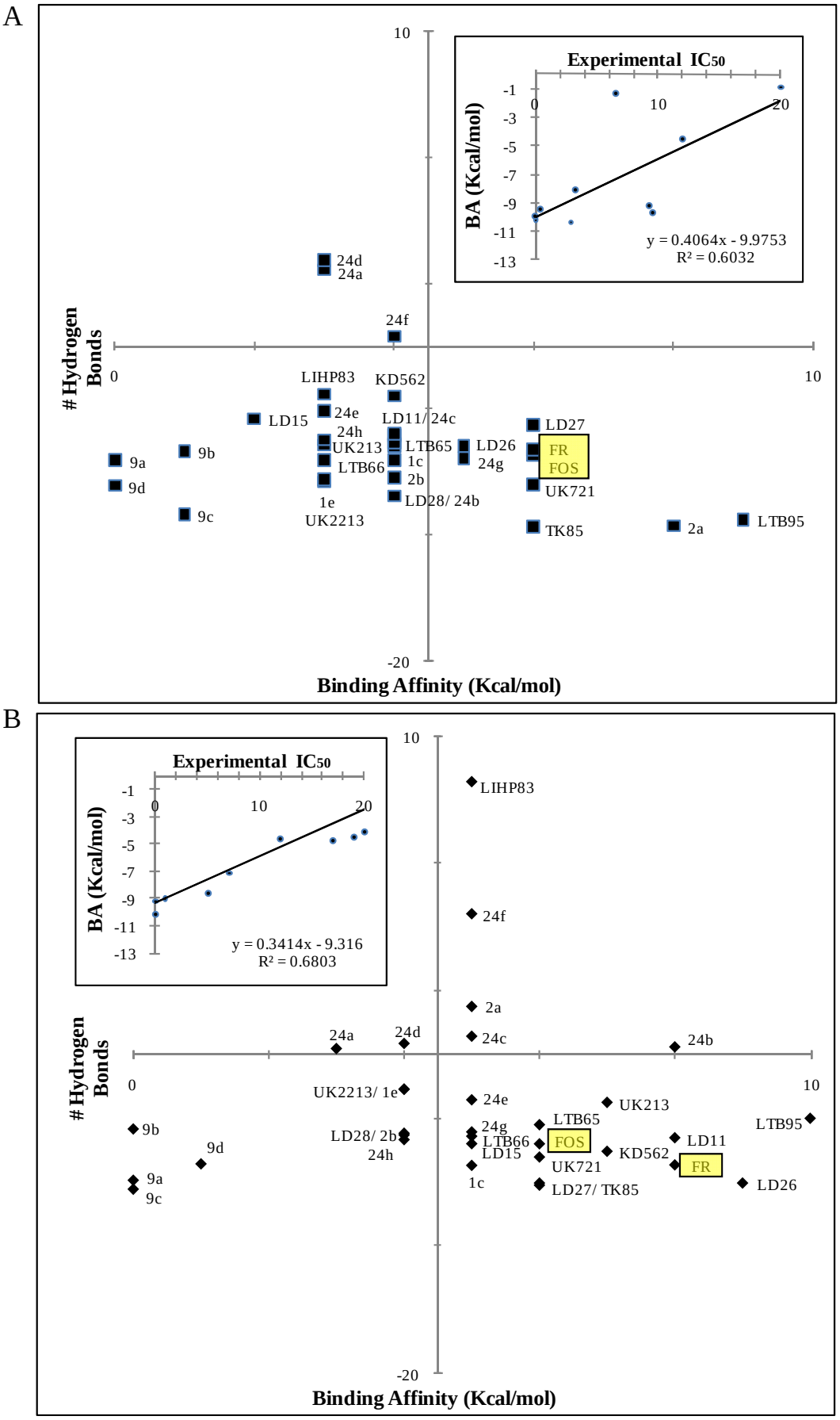

Figure 2.9: Docking–based model validation and DXR inhibitor screening (legend on next page).

(A) For PfDXR, graph showing the correlation between binding affinity (in kcal/mol) and the number of hydrogen bonds for 32 potential DXR inhibitors docked into EcDXR. (B) For EcDXR, graph showing the correlation between binding affinity (in kcal/mol) and the number of hydrogen bonds for 32 potential DXR inhibitors docked into PfDXR. Inhibitors include: fosmidomycin (highlighted *yellow*), FR900098 (highlighted *yellow*), DXR inhibitors KD562, LD_1_1, LD_1_5, LD_2_6, LD_2_7, LD_2_8, LIHP_83, LTB65, LTB66, LTB95, TK85, UK213, UK2213, UK721 (Silber *et al.*, 2005), 3'–amido–3'–deoxy–N6–(1–naphthylmethyl) adenosine 9a–d (Herforth *et al.*, 2004), α–substituted fosmidomycin analogues 1c, 1e, 2a, 2b (Haemers *et al.*, 2006), and non–hydrolyzable phosphate mimics 24a–h (Gieβmann *et al.*, 2008). The potential DXR inhibitors are classified into one of four quadrants: top left = poor binding affinity with poor hydrogen bonding; top right = poor binding affinity with good hydrogen bonding; bottom left = good binding affinity with poor hydrogen bonding; bottom right = good binding affinity with good hydrogen bonding. (insert A and B) Graph showing a correlation between binding affinitiy (in kcal/mol) and known experimental IC_{50} value determined by Gieβmann *et al.* (2008) for fosmidomycin, FR900098 and non–hydrolysable phosphonate mimics 24a–h docked into PfDXR and EcDXR respectively.

Visual assessment of the docked ligands into PfDXR and EcDXR provided some evidence regarding bulkiness of the ligand side chain and the potential bonding interactions that were possible with the respective proteins. From these trends it could be assumed that the DXR enzyme does not efficiently accommodate ligands boasting bulky side chains and in many cases, ligands conformationally altered from the minimized state in order to enter the active site. For example, the EcDXR backbone with 24g docked was superimposed onto the PfDXR backbone equivalent with 24g docked, with the protein orientations being identical. Analysis of the docking log showed that when 24g was docked into PfDXR, the ligand adopted a reasonably linear arrangement comparable with that of the undocked minimised ligand (Figure **2.10C**). However, when docked into EcDXR, 24g assumed an entirely new conformation, as can be seen in Figure **2.10D**. However, in the case of PfDXR, the elongated conformation of 24g was such that the phosphonate moiety did not move into the small active site pocket (indicated by the black circle in Figure **2.10C**), while with EcDXR, the altered conformation of 24g allowed the ligand's phosphonate group to move into the active site, with which it shared the fluorine side chain group (indicated by the black circle in Figure **2.10D**).

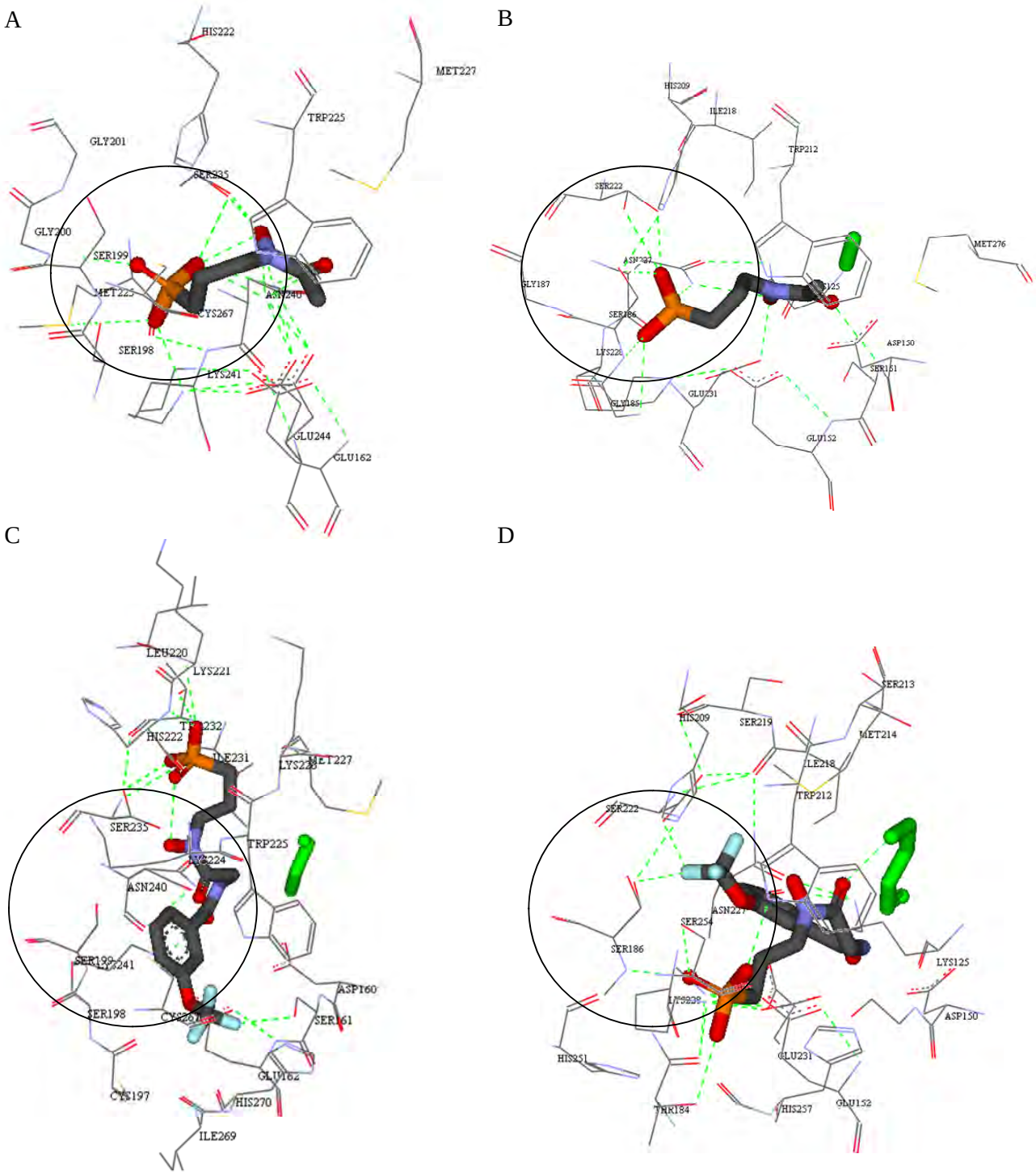

Figure 2.10: The potential interactions between PfDXR and bound inhibitors, FR900098 and 24g.
(A) Schematic view of FR900098 bound to PfDXR active site. (B) Schematic view of FR900098 bound to EcDXR (1Q0L) active site (identical orientation to that of PfDXR with FR900098 bound). (C) Schematic view of phosphate mimic 24g bound to PfDXR active site. (D) Schematic view of phosphate mimic 24g bound to EcDXR (1Q0L) active site (identical orientation to that of PfDXR with 24g bound). For all schematics, resides within 4 Å of the ligands are shown and labelled, with hydrogen bonds dotted in green. Those atoms of NADPH within 4 Å of the ligand are shown in solid green. For orientation purposes, the catalytic residues have been circled in black, such that Ser199, Ser235, Asn240 and Lys241 (for PfDXR) and Ser186, Ser222, Asn227 and Lys228 (for EcDXR) form the border of the circled area as a broad indication of the active site pocket.

Binding affinity was then plotted against experimental IC_{50} (Figure **2.9 inserts**) in order to assess whether a link between theoretical inhibition and actual inhibition existed. A single set of ligand data was therefore analysed (Gieβmann *et al.*, 2008) and the actual IC_{50} values (μM) for the DXR inhibitors were plotted against the theoretical binding affinity (kcal/mol) determined by this study. The inhibition of EcDXR demonstrated a reasonable correlation of 0.68, while PfDXR showed a less significant correlation between binding affinity and IC_{50} of 0.60.

2.4 DISCUSSION

A three–dimensional model of the malarial drug target protein PfDXR was created and sufficiently validated using the Ramachandran plot. Analysis of the tertiary structure of PfDXR allowed for the conclusion that all the catalytically and structurally significant residues involved in binding the substrate/inhibitor or cofactor, are highly conserved among bacterial (*E. coli* and *Z. mobilis*), plant (*A. thaliana*) and apicomplexan homologues (*P. vivax*, *P. berghei* and *P. yoelii*). The *P.falciparum* DXR enzyme is no different, where PfDXR catalytic residues Ser199, Ser235, Asn240, Lys241 (Ser186, Ser222, Asn227, Lys228 in EcDXR), presented almost identical conformations when the PfDXR homology model was superimposed onto the EcDXR crystal structure. These catalytic residues were found to interact with almost every known DXR inhibitor presented in the study, predominantly by way of the phosphonate moiety that was typical in most DXR inhibitors used in this study. It must however be noted that in the experimental determination of an enzyme's crystal structure, buffers that are slightly acidic (pH 5.5 – 6.5) are typically used; this environment may interfere with an enzyme's functionality. However in a study by Dhiman *et al* (2005), a pH range for MtDXR between 5 and 9 was reported, meaning that even in slightly acidic conditions, enzyme functionality is unlikely to be affected.

The literature reports that the DXR enzyme active site presents a phosphate binding pocket, structured to accommodate the DXP phosphate group. However, because of the susceptibility of the O–P bond to phosphatase cleavage, the non–cleavable C–P bond of the phosphonate moiety is commonly used in inhibitor design (Meyer *et al.*, 2003). In this work, the data illustrated that a phosphonate moiety carrying a significant negative charge, as well as a nitrogen atom carrying a partial/induced negative charge, was required for reasonable binding to the active site residue. This has also been documented in the literature for

fosmidomycin and FR900098 in a DFT study, which quantified the partial charges for each atom of the respective inhibitors (Zubrzycki *et al.*, 2001). The presence of these charged or partially charged groups, as compared to the carbon atom, may provide an active site environment suitable for tight binding.

This was confirmed by the docking of the 3'–amido–3'–deoxy–N_6–(1–naphthylmethyl) adenosine derivatives 9a–d (Herforth *et al.*, 2004) into PfDXR and EcDXR. These NADPH binding site inhibitors contained no phosphonate moiety or charged nitrogen, which resulted in very few hydrogen bonding interactions with the catalytic residues at the DXR active site. The ligands from this group were not bulky and therefore entered the active site efficiently, yielding a reasonable binding affinity. The apparent lack of hydrogen bonding meant that the ligands could move freely between the active site and external environment. Interestingly, all these compounds had a preference for binding at the active site, as opposed to the NADPH binding motif, when the docking grid box was enlarged to include the NADPH binding pocket. Given this, it is surprising that the compounds of this group still displayed moderate antimalarial activity against *P. falciparum* (micromolar range) and some inhibitory activity against DXR (Herforth *et al.*, 2004), especially if they had a preference for the active site. This may have been as a result of the ligands entering both the active site and NADPH binding pocket, resulting in an amplified inhibitory effect. The activity was however weak when compared to fosmidomycin, which has been shown to have antimalarial activity against *P. falciparum* in the nanomolar range (Jomaa *et al.*, 1999; Haemers *et al.*, 2006; Gieβmann *et al.*, 2008).

In a recent study by Gieβmann *et al.* (2008), IC_{50} values (μM) were quantified for fosmidomycin, FR900098 and a range of other non–hydrolyzable phosphate mimics using an NADPH–dependent assay. The study concluded that FR900098 was two to three times more active against the malaria parasite than fosmidomycin. Fosmidomycin was shown to have similar inhibition in the malaria parasite and bacterial DXR (Gieβmann *et al.*, 2008). In this study, fosmidomycin and FR900098 maintained similar binding affinities, ligand efficiencies and number of hydrogen bonds for EcDXR and PfDXR respectively (Gieβmann *et al.*, 2008).

Coupled with fosmidomycin and FR900098, the docking of other non–hydrolysable phosphate mimics (24a–h) into EcDXR and PfDXR were used for docking–based validation of the PfDXR model. Statistically, the difference in order of magnitude, for EcDXR and

PfDXR experimental IC_{50} values, should be consistent with computational binding affinities. For example, the binding affinities for 24c docked into EcDXR and PfDXR was –4.15 and –12.16 kcal/mol respectively. This meant that theoretically PfDXR has a 2.9–fold greater inhibition potential because it utilized significantly less energy to bind at the active site. Experimentally, 24c was found to demonstrate a 2.2–fold higher inhibition of PfDXR when compared to EcDXR (Gieβmann *et al.*, 2008). The other phosphate mimics (24a–h), demonstrated the same trend (data not shown), indicating that the theoretical PfDXR model behaves in the same manner as the PfDXR enzyme does experimentally. However, while EcDXR demonstrated a reasonable correlation between IC_{50} (μM) and theoretical binding affinity (kcal/mol), PfDXR did not demonstrate a confident correlation. This may provide evidence for the difference in accuracy when using a known crystal structure versus a homology model of a protein for analysis. It was therefore necessary to further validate the PfDXR homology model, especially given the poor correlation described for PfDXR. Docking–based model validation was therefore carried out using 34 inhibitors known to be competent DXR inhibitors *in vitro*. Data analyses resulted in the development of a visual screening tool, sufficient to classify DXR inhibitors into quadrants, based on the ligands' potential binding affinity (kcal/mol) and number of potential hydrogen bonding interactions. Fosmidomycin and its acetyl analogue FR900098 are known to be the benchmark against which all DXR inhibitor studies are compared. Because these two DXR inhibitors resided within the expected quadrant (demonstrating good binding affinity and a great number of hydrogen bonding interactions), it could be said that this method of quantification provided a model against which one could differentiate between active and inactive inhibitors. Hence this efficient methodology could be used to screen for potential tool compounds for use in the rational design of novel DXR inhibitors.

Closer analysis of the inhibitor binding, coupled to the information reported in the literature may present the ultimate validation of the PfDXR homology model proposed in this work. As in the literature, when FR900098 was docked into EcDXR and PfDXR, the ligand maintained a similar orientation to that of fosmidomycin (Singh *et al.*, 2006), with the phosphonate moiety binding the highly charged but small active site pocket. Upon docking of fosmidomycin and FR900098 into PfDXR, it became evident that Glu244 (Glu231 in EcDXR) played a supporting role to stabilise the catalytic Lys, while the literature reports that Glu231 is involved in divalent metal ion coordination (Yajima *et al.*, 2002; Steinbacher *et al.*, 2003). In AutoDock 4.2, Mg^{2+} is assigned an automatic Gasteiger charge of 0. This

means that an unrealistic environment is created whereby the octahedral complex of negatively charged residues of Asp163, Glu165 and Glu244 (Asp150, Glu152 and Glu231 in EcDXR) cannot interact with the positively charged divalent cation (Steinbacher *et al.*, 2003). This was seen when fosmidomycin and FR900098 were docked into the EcDXR and PfDXR structures respectively, containing both the Mg^{2+} and NADPH cofactors. With the automatic assignment of the 0 Gasteiger charge, neither ligands docked with reasonable binding efficiency nor were there adequate hydrogen bonding, when compared to the docking confirmation of the respective enzymes with the divalent metal ion removed. Because of this, docking studies were carried out using the respective enzymes with bound NADPH only.

In the literature, NADPH cofactor binding in EcDXR occurs via: backbone amides of Gly11 and Ser12 (Gly16 and Ser17 in PfDXR), which coordinate the NADPH diphosphonate moiety (Reuter *et al.*, 2002); Ala35 and Gly36 (Val43 and Asn44 in PfDXR) which accommodate the 2' phosphate (Reuter *et al.*, 2002); Thr10 (Thr15 in PfDXR), which anchors the 2' phosphonate moiety (Yajima *et al.*, 2002); and Gly14 (Gly19 in PfDXR), which forms an important part of the NADPH binding motif (Reuter *et al.*, 2002; Kuzuyama *et al.*, 2000). In this work, the NADPH pyrophosphonate moiety was coordinated by Ser12 and Ile13 in EcDXR and Gly16, Ser17 and Ile18 in PfDXR (Gly11, Ser12 and Ile13 in *E. coli*). In the case of Ile (in both EcDXR and PfDXR), hydrogen bonding via the main chain electronegative nitrogen, potentially occurred as an alternative (EcDXR) or additional (PfDXR) interaction to Gly11 or Gly14 (Gly19 or Gly22); the literature reported additional interactions of NADPH with PfDXR residues Ile15, Met224, and Met286 (Singh *et al.*, 2006) (Ile18, Met227, and Met289 for PfDXR in this work). The 2' phosphate was coordinated by: Lys37 and Asn38 in EcDXR; and Asn44 and Ser46 in PfDXR. In EcDXR, again interactions occurred via the main chain electronegative nitrogen of Lys37 and Asn38, possibly as an alternative to Ala35 and Gly36 – which can also only interact via the main chain because of the lack of electronegative groups on their respective side chains. It is worth noting however that Ala35 and Gly36 were still within hydrogen bonding distance (4 Å) of NADPH. In the case of PfDXR, the interaction of NADPH with Asn44 (Gly36 in EcDXR) was consistent with that reported in the literature for EcDXR. The interaction of Ser46 also occurred via the main chain electronegative nitrogen and could have been an alternative interaction to the main chain electronegative nitrogen of Val43 (Ala35 in EcDXR). Additional hydrogen bonding interactions for PfDXR included interactions between the 2'–hydroxyl group of the adenosine sugar ring, with Asp111 and Asn133. Similarly, in EcDXR the same 2'–hydroxyl

interacted with Lys125, while the 3'–hydroxyl interacted with Ile101. These additional interactions have not been reported in the literature.

The propinquity of the NADPH binding site to the DXR active site is evident because structurally important residues including Trp212, Met214 and Met276 for EcDXR are within hydrogen bonding distance of bound NADPH. The same can be said of PfDXR residues Met227 and Met289 – Trp225 however does not appear to be within 4 Å of NADPH. No interactions with the NADPH adenine ring were evident in this work, although in the literature interactions with strands β1, β 2 and β 5 were reported for ZmDXR (Ricagno *et al.*, 2004). Interestingly, those residues that form the octahedral complex with Mg^{2+} in EcDXR (Asp150, Glu152 and Glu231) (Reuter *et al.*, 2002) reside within 5 Å of NADPH, which may explain why no interactions exist between the enzyme and the NADPH adenine ring. This could potentially make the enzyme–substrate–cofactor complex too rigid, which it evidently is not if one considers the significant movement of the catalytic hatch upon substrate binding (Yajima *et al.*, 2002), as discussed in Chapter 4. Superimposition of the docked cofactor into EcDXR and into PfDXR confirmed that the orientation of NADPH in both homologues was comparable.

The NADPH binding motif is highly conserved among DXR enzymes, and it is therefore interesting that with there are significant differences with respect to Ala35 and Gly36 for EcDXR, where all the apicomplexans incorporate a Val and an Asn instead. This is particularly interesting because Asn has a considerably larger side chain when compared to the Gly equivalent and upon docking; it was evident that it had an orientation that was notably different to the Ala35 equivalent. Thus it is reasonable to conclude that the protein–cofactor interactions were similar for the EcDXR and PfDXR homologues, with some major differences in the architecture of the NADPH binding motif.

As with the catalytic and cofactor binding residues, structurally important residues His163, His222, Trp225, His270 and Pro287 (His153, His209, Trp212, His257 and Pro274 in EcDXR) also existed in almost identical conformations subsequent to PfDXR superimposition onto the EcDXR structure. In the literature, interactions with Gly197 (Gly200 in PfDXR) and His219 (His222 in PfDXR) have been observed for the PfDXR–NADPH–fosmidomycin complex (Singh *et al.*, 2006), in addition to the interaction with the catalytic residues Ser199, Ser235, Asn240, Lys241 (Ser186, Ser222, Asn227, Lys228 in

EcDXR) (Steinbacher *et al*., 2003). These additional interactions (with Gly200 and His222) were not observed upon fosmidomycin docking, they were however observed upon docking of other ligands such as FR900098 and 24f (for Gly200) docked into PfDXR, and 24g and UK2213 both presented apparent interactions with His222 in PfDXR. The hydrogen bonding interaction between His209 (His222 in PfDXR) and the phosphate moiety of the substrate is said to be the reason for the closing of the hatch once the substrate has entered (Kuzuyama *et al.*, 2000; Yajima *et al.*, 2002), shielding the reactants completely from the solvent environment (Reuter *et al.*, 2002). Hence this supports the theory that the ligands boasting large conformations, such as 24g or 24h, could prevent the correct organization of the active site subsequent to inhibitor binding. This may be because the side chains of active site residues protruded out of the active site binding pocket, potentially creating a highly charged environment that results in the catalytic hatch behaving in an altered manner. In other cases, some ligands with bulky side chains conformationally altered from the minimized state and engaged in intramolecular bonding to facilitate entry into the active site.

According to the available literature, the catalytic hatch moves over the active site after the substrate/inhibitor has bound (Yajima *et al.*, 2002) and the hatch, as well as the nicotinamide moiety of NADPH are both required for the correct positioning of the active site (Steinbacher *et al.*, 2003). Catalytic hatch residues Trp212 and Met214 in EcDXR (Trp225 and Met227 in PfDXR) perform a vital stacking role when the active site is shaped (Steinbacher *et al.*, 2003). Upon docking of various inhibitors into EcDXR, it was evident that non–hatch residue Met276 provided a potential substitute for Met214. Further analyses of the mostly conserved catalytic hatch presented an interesting difference in the PfDXR hatch, where the small polar uncharged Asn and Ser residues in EcDXR (Asn211 and Ser213), were substituted for large, positively charged Lys in PfDXR (Lys224 and Lys226). With Asn211 being within 9.56 Å of the ligand and similarly, with Lys224 being within 9.15 Å of the ligand, for EcDXR and PfDXR respectively, no direct intermolecular interactions would be possible. However, the difference in the bulkiness and charge may have resulted in the PfDXR catalytic hatch behaving in a slightly modified manner to that of other species', especially given the degree of movement of the Lys224 residue upon inhibitor binding. Ser213 in EcDXR and Lys226 in PfDXR did not appear to form part of the active site architecture as they exist at the C–terminal portion of the hatch. Mutation of these Lys hatch residues in PfDXR could possibly result in the perturbation of the enzyme's K_m (concentration of substrate that leads to half–maximal velocity), as well as the k_{cat} (substrate

turnover) and enzyme efficiency. Because the hatch is associated with substrate specificity (Fernandes *et al*., 2005), the disruption of the tertiary structure of the hatch may result in a significant loss in the enzyme's ability to perform efficiently.

Following structural analysis of the PfDXR substrate and cofactor binding sites, which was comparable to the well studied EcDXR crystal structure, an attempt to link structure to function was carried out. Structural and functional features unique to PfDXR were identified using the protein tertiary structure and comparative sequence analyses with apicomplexan and non–apicomplexan DXR proteins. A potential N–glycosylation site and PKC phosphorylation site were identified on the surface of the protein. The cellular location of a target protein, as well as enzyme activity and associations with other proteins can be altered through phosphorylation by protein kinases (EMBL, 2008). Protein kinases play a functional role in a multitude of processes, including cell proliferation, division, differentiation and apoptosis (Manning *et al.*, 2002). PfDXR potentially boasts a surface PKC phosphorylation motif at a region of sequence insertion. None of the other homologues showed evidence of the motif at a similar position, suggesting that this may be an attribute specific to PfDXR. The motif, however, was not predicted to occur on an extended loop. Experimentally, PKC demonstrates a preference for the phosphorylation of serine/threonine when these residues are located close to a C–terminal basic residue (Woodgett *et al.*, 1986, Kishimoto *et al.*, 1985). The potential PKC phosphorylation motif of PfDXR contains only a single C–terminal basic lysine, suggesting that it may be a relatively poor substrate for PKC.

Unlike the sequence coding for a potential PKC phosphorylation site, the prospective N–glycosylation site presents itself on an extended loop region that was evident when the EcDXR crystal structure was superimposed onto the three–dimensional PfDXR homology model. Although glycosylation appears to be rare in *P. falciparum*, a basic N–glycosylation pathway does exist (Templeton *et al.*, 2004). The occurrence of this motif at the protein surface suggests that it could potentially be an active glycosylation site. Glycosylation at this motif could be involved in the facilitation of protein folding or improved solubility (Fournillier *et al.*, 2001). Alternatively, it could be involved in PfDXR targeting to the apicoplast after it has moved through the secretory pathway (Fournillier *et al.*, 2001).

Protein targeting in malaria parasites involves numerous compartments and is highly complex (van Dooren *et al.*, 2000). Examples of known targeting methods in *P. falciparum* include

post–translational addition of a GPI (Glycosylphosphatidylinisotol) anchor (Karsten *et al.*, 1998), sorting by timing (Le Cabec *et al.*, 1996), oligosaccharide–mediated signalling (glycosylation) (Dahms *et al.*, 1989), and targeting via motifs embedded in the amino acid sequence of the protein (van Dooren *et al.*, 2000). Perhaps the most well studied example of amino acid motif–based targeting is the apicoplast (Waller *et al.*, 1998, Jomaa *et al.*, 1999). Even though trafficking to the apicoplast is better understood than with other compartments, much remains unknown (Wienk *et al.*, 1999). Most proteins of the apicoplast are encoded in the nucleus and are imported into the apicoplast following post–translational modification (van Dooren *et al.*, 2000). Numerous *P. falciparum* proteins contain an N–terminal hydrophobic region (signal peptide) that functions to target the secretory pathway (von Heijne, 1985). Studies have confirmed that further signalling is required for transport to the apicoplast, over and above targets into the secretory system; this is known as a sub–terminal targeting system (McFadden, 1999_1; McFadden, 1999_2). Targeting motifs are readily interchangeable (McFadden, 1999_1; McFadden, 1999_2), however, no obvious amino acid motifs have been identified. It has been speculated that evidence for these motifs may lie in the secondary or three–dimensional tertiary structures (Wienk *et al.*, 1999), where mutagenesis experiments may provide some information regarding the residues that are important for trafficking (van Dooren *et al.*, 2000).

N–linked glycosylation occurs in both eukaryotes and archaea, but very rarely in bacteria (Marshall, 1972). This may be the rationale for the absence of the motif in the EcDXR sequence at a surface position. Other *Plasmodium* apicomplexans, which include *P.yoelli*, *P. berghei* and *P. vivax*, exhibit an N–glycosylation motif at the same position as *P. falciparum*. Interestingly, the position of the motif, which is consistent with all apicomplexa, appears at an insertion region that is not a feature of the bacterial or plant homologues. Experimental evidence suggests that *P.falciparum* possess both a secretory and glycosylation pathway (Gowda and Davidson, 1999; Templeton *et al.*, 2004) that involves trafficking of apicoplast–destined proteins through four membranes, resulting from the secondary endosymbiotic origin of the apicoplast (van Dooren *et al.*, 2000). This may be a potential reason for the evolution of the sequence insertions in the *Plasmodium species*. In conclusion, a well validated homology model, coupled to the information obtained from sequence analyses, may provide the platform from which a protein's structure and function can be linked.

CHAPTER 3
HETEROLOGOUS PRODUCTION OF PfDXR TARGET ENZYME

3.1 INTRODUCTION

Recombinant protein expression places a rigorous energetic burden on the host expression system and misfolding is often a direct consequence of overproducing a recombinant protein because the host's folding machinery is inadequate at such high expression rates (de Marco, 2007_1). Many attempts have been made to increase yield of correctly folded, functional protein by co–production with chaperones; however, the success has been limited (reviewed by de Marco *et al.*, 2007_2). In coexpression studies, the limited success of using this method for protein overproduction has been suggested to be a result of incorrect chaperone combinations (de Marco and de Marco, 2004). It has been said that not any combination is suitable for a specific protein and that interactions are dependent on the specific features of the protein during folding (de Marco and de Marco, 2004).

The molecular chaperones used can either be heterologous or homologous to the target protein of interest. When overproduction of a target protein is induced in a host, the cell's endogenous chaperone system can become overloaded, thereby limiting the amount of soluble protein that can be produced (Carrió and Villaverde, 2002). The ideal cell for overproduction allows for the overexpression of the target protein as well as the molecular chaperone(s). The use of more than one plasmid is therefore most often required, but the success of this approach may be limited by the need to utilize plasmids with compatible but significantly different origins (de Marco and de Marco, 2004). The overproduction of molecular chaperones has been used successfully to enhance the yield of numerous target proteins (Nishihara *et al*., 1998; Ahn *et al*., 2004; Martínez–Torrecuadrada *et al*., 2005; Schrodel *et al*., 2005; Hu *et al*., 2007). However this technique has also been found to be highly protein and chaperone specific (Carrió and Villaverde, 2002; de Marco and de Marco, 2004).

The use of *E. coli* chaperone combinations to improve the solubility of other bacterial target proteins has been largely documented in the literature. For example, *Staphylococcus aureus*

trimethoprim–resistant type SI DHFR (Dale, *et al.*, 1994_2), and *Agrobacterium tumefaciens* *N*–carbamoyl–D–amino acid amidohydrolase AM10 (Sareen *et al.*, 2001) were coexpressed with the ELS system and in both cases the production of active protein was greatly improved upon. Numerous eukaryotic target enzymes have also been used successfully when coexpressed with the ELS and/or KJE chaperone combinations. For example, maize protoporphyrinogen IX oxidase (de Marco *et al*., 2000), Japanese cedar pollen, Cryj2 (Nishihara *et al.*, 2000), *Saccharomyces cerevisiae* GTR1 (de Marco and de Marco, 2004) and *Xenopus laevis* Xklp3B (de Marco and de Marco, 2004). In all the above–mentioned experiments, significant improvements in yield of folded, functional protein were reported. Human proteins that have been overproduced using chaperone coexpression include: human kinases Csk, Fyn, Lck and Btk (de Marco and de Marco, 2004; reviewed by de Marco *et al*., 2007_2), p50csk protein tyrosine kinase (Amrein *et al*., 1995), phosphomannose isomerase (Proudfoot *et al*., 1996), and CLIPB14 serine protease (Schrödel *et al*., 2005). Hayhurst and Harris (1999) successfully used the *E. coli* Skp chaperone to improve the solubility of single–chain antibody fragments (scAb) specific for the herbicide atrazine. From the study, the authors hypothesized that Skp may be useful in the purification of other problematic periplasmically expressed proteins (reviewed by de Marco *et al*., 2007_2).

In a study by de Marco *et al.* (2007_2), coexpression of an entire network of *E. coli* chaperones in different combinations were used to improve the yield of 64 different recombinant target proteins. Chaperone combinations included: KJE; KJE/ClpB; ELS; KJE/ClpB/ELS (high amounts); KJE/ClpB/ELS (lower amounts); IbpAB; IbpAB/ELS; and IbpAB/KJE/ClpB/ELS. Chaperone coexpression, combined with a two–step procedure in which protein synthesis and protein refolding were coupled, resulted in increased solubility of up to 70%. Chaperone coexpression coupled to a one–step procedure, however demonstrated significantly less improvement in solubility (reviewed by de Marco *et al*., 2007_2).

A number of literature reviews however have stated that the success of this chaperone–based protein expression method is highly protein specific (Wall and Pluckthun, 1995; Makrides, 1996; Gräslund *et al*., 2008). This provided the motivation for Haacke *et al.* (2009) to investigate whether chaperone coexpression can be applied to any target protein or whether the method is protein specific; 10 members of a single protein family (kinases) were coexpressed with different chaperone combinations, namely: KJE/ELS, KJE/ELS/TF, KJE/ELS/ClpB; KJE/ELS/ClpB/TF. The study showed that subsequent to chaperone

coexpression some kinases showed a two–fold increase in yield of functional protein, other kinases showed improvements in expression but not in solubility (57%), while a significant proportion showed no improvement in expression or solubility. The authors therefore concluded that it is not possible to predict whether recombinant protein production will be improved upon by using chaperone coexpression (Haacke *et al.*, 2009). In the case of each target protein, optimization of each individual expression system is often required to benefit from this technique (reviewed by de Marco *et al*., 2007_2).

It is possible that chaperone coexpression may be improved upon by utilizing homologous chaperone combinations that are native to the cellular compartment in which the target protein exists. It is therefore necessary to be acquainted with the localization of the target cell's chaperone machinery and the co–chaperone partnerships that exist in the cell. Although the coexpression of *P. falciparum* molecular chaperones for improved solubility and yield of malaria drug target proteins is appealing, it has to be considered that the expression of such molecular chaperones may also be very problematic in *E. coli* because the prokaryotic *E. coli* expression system is not capable of post–translational modification of eukaryotic proteins (Geisse *et al*., 1996). To our knowledge, no chaperone coexpression studies have been undertaken which have utilized homologous malarial chaperones for production of folded, functional *P.falciparum* proteins. Hence this technique may be employed in drug discovery for the successful purification of potential drug target proteins, for the rational design of inhibitors as novel and potent antimalarial drugs.

In this study, the successful overproduction and purification of soluble active PfDXR was endeavoured upon using codon harmonization and numerous coexpression strategies; including coexpression with molecular chaperones from both *E. coli* and *P. falciparum*, as well as coexpression with *lac* repressor to control transcription. An NADPH–dependent DXP enzyme activity assay was then used to confirm the successful purification of a functional target enzyme, with the well characterized EcDXR enzyme as a control.

3.2 EXPERIMENTAL PROCEDURES

3.2.1 Materials, special reagents and chemicals

All general chemicals used in this study were of the highest analytical grade. The reagent and supplier information can be seen in Table **C.1**, Appendix C. Restriction enzymes used in this study (*Sac*I, *Bam*HI, *Eco*RI, *Sal*I, *Hind*III and *Aat*II) and their respective buffers were obtained from New England Biolabs. The plasmids that were used for this work included: pQE30, which was purchased from Qiagen; pGEM–T Easy, which was purchased from Promega; pQE9–EcDXR, which was a kind gift from Jomaa Pharmaka GmbH; pMRBAD–PfHsp70–1, which was constructed by Dr Addmore Shonhai; pGro7, pKJE7 and pG–KJE8, which were purchased from Takara Bio Inc. The overview for each plasmid used in the study is summarised in Table **3.1**.

Table 3.1: Plasmids encoding the target proteins of interest, the molecular chaperones and *lac* repressor investigated in this study.

Plasmid	Protein	Promoter	Inducer	Origin of replication	Resistance marker	Source
pG–KJE8	DnaK–DnaJ–GrpE	*araB*	L–arabinose	p15A	Chloramphenicol	Takara Bio Inc.
pGro7	GoEL–GroES	*araB*	L–arabinose	p15A	Chloramphenicol	Takara Bio Inc.
pKJE7	DnaK–DnaJ–GrpE	*araB*	L–arabinose	p15A	Chloramphenicol	Takara Bio Inc.
pMRBAD–PfHsp70–1	PfHsp70–1	*araB*	L–arabinose	p15A	Kanamycin	A Shonhai
pREP4	*lac* repressor	*araB*	L–arabinose	p15A	Kanamycin	Qiagen
pQE9–EcDXR	EcDXR	T5	IPTG	ColE1	Ampicillin	H Jomaa
pQE30–hPfDXR	PfDXR	T5	IPTG	ColE1	Ampicillin	This study

3.2.2 The construction of an expression plasmid with a codon harmonised PfDXR coding region

3.2.2.1 Codon harmonisation of the PfDXR coding region

The codon harmonization algorithm used in this study was implemented as a PHP–script driven web interface and is available at (www.sami.org.za/equalize). This algorithm follows a codon frequency matching approach whereby codons are assigned on the basis of closest matching codon preference fraction when comparing the source and target codon preference tables. Each wild–type codon is substituted with a synonymous codon having the closest codon preference match between the source and target codon preference tables. This approach preserves the pause site profile of a wild–type gene in the synthetic gene designed for heterologous expression. Pause sites are predicted by calculating pausing propensity of a sliding window by applying a modified codon adaptation index (CAI) approach.

The PfDXR (AF111813) coding region was converted to its harmonized version (PfDXR) using the highly expressed *E. coli* codon preference as target codon preference table. The Shine–Delgarno (SD) removal module of the website indicated no putative false start sequences in the harmonized version of the gene. The final step in the design pipeline was the removal of selected restriction sites required for downstream subcloning steps and subsequent addition of *Bam*HI and *Sac*I restriction sites to the 5' and 3' ends to facilitate directional insertion into pQE30. The full length harmonized version of the coding region was synthesized by GENEART (www.geneart.com). The codon harmonised DXR coding region fragment was inserted into a pGA15 vector. The plasmid DNA was purified (Pure Yield™ Plasmid Midiprep, Promega) from transformed bacteria and the final 0804945–DXR–pGA15 construct was verified by DNA sequencing. This was done in collaboration with the University of Pretoria, South Africa, by Mr Jaco de Ridder, under the supervision of Professor Abraham Louw.

3.2.2.2 Insertion of the codon harmonized PfDXR coding region into the pQE30

For the construction of the pQE30–PfDXR plasmid, the harmonised coding region for PfDXR was first amplified by polymerase chain reaction (PCR) from plasmid 0804945–DXR–pGA15 using the following primers: forward primer hPfDXR*Bam*HIF (5'– GGA TCC GGC GCT ATC AAG AAA C –3') and reverse primer hPfDXR*Sal*IR (5'– GTC GAC TTA AGA GCT GTT GTG –3'). The primers were designed using the Gene Runner software package (version 3.05). It was our initial intention to clone the full length coding region, via *Bam*HI and *Sac*I restriction sites. However, it was decided that because the full length PfDXR coding region is toxic to *E. coli* cells (Jomaa *et al*., 1999), the PfDXR coding region was constructed to exclude the first 71 amino acid leader sequence and the inclusion of *Bam*HI and *Sal*I restriction sites in the forward and reverse primers respectively. Primers were synthesised and purchased from IDT and the properties of the respective primers are summarised in Table **3.2**.

Table 3.2: Analysis of hPfDXR*Bam*HIF and hPfDXR*Sal*IR primer properties.

Properties	**hPfDXR*Bam*HIF**	**hPfDXR*Sal*IR**
Number of bases	22–mer	21–mer
GC Content	54.5%	47.6%
AT+GC Tm	68^{o}C	62^{o}C

PCR was conducted using *Taq* DNA PCR system (Amersham Biosciences) and PCR amplifications performed in the GeneAmp PCR system 9700 (PE Applied Biosystems). The PCR reaction mixture (50µl) contained the following: 100 ng plasmid DNA, 1 µM forward primer, 1 µM reverse primer, 2.5 units *Taq* DNA polymerase (Qiagen), 0.2 mM dNTPs, 1x reaction buffer (200 mM Tris–HCl, 100 mM KCl, 100 mM $(NH_4)_2SO_4$, 15 mM $MgCl_2$; pH 8.7 at 20°C) containing 15 mM $MgCl_2$) and sterile milli–Q water to a final volume of 50 µl. Cycling parameters used for the PCR reaction were as follows: 1 cycle of 1 minute at 95^{o}C; followed by 30 cycles of denaturation, annealing and extension (30 seconds at 95^{o}C, 1 minute at 52^{o}C and 2 minutes at 72^{o}C); 1 cycle of 5 minutes at 72^{o}C; followed by a hold at 4^{o}C.

The PCR amplified PfDXR coding sequence was visualised using short wave ultraviolet (UV) after resolution by 0.8% agarose gel electrophoresis (AGE) (Appendix **A4**) and excised from the gel and transferred into a pre–weighed 1.5 ml microcentrifuge tube. Purification of the DNA was performed using a DNA Gel Extraction Kit (Fermentas), according to the manufacturer's instructions. Elution efficiency was increased by performing a second elution step. The gel purified PCR amplified PfDXR coding region (2µl) was diluted 100 times using sterile milli–Q water and quantification of DNA was performed using a GeneQuant (Pharmacia Biotech). DNA concentration was determined using the formula: A_{600nm} x dsDNA factor (50 µg/ml) x dilution factor (100).

The gel purified PCR amplified PfDXR coding region was ligated to the pGEM–T Easy cloning vector (Promega) in a reaction containing 50 ng pGEM–T Easy cloning vector, 100 ng DNA encoding PfDXR coding region, 3 units T4 DNA ligase and 2x ligation buffer (60 mM Tris–HCl, 20 mM $MgCl_2$, 20 mM dithiothreitol, 2 mM ATP, 10% polyethylene glycol, pH 7.8). Ligation control reactions included a negative control with no insert DNA and a positive control using control insert DNA (Promega). The ligation reactions were incubated at 4^{o}C overnight and transformed into super–competent *E. coli* JM109 commercial cells (50 µl), according to the protocol described in Appendix **A1**. A single colony from the transformed cells was inoculated into sterile 2x YT broth (5 ml) containing the appropriate antibiotic(s) and incubated at 37^{o}C with shaking overnight (180–200 rpm). The bacterial cells were collected by centrifugation (12 000 x g at room temperature for 1 minute) and plasmid DNA was purified using the Qiagen DNA minipreparation protocol, according to the manufacturer's instructions. The plasmid DNA was stored at –20^{o}C, after diagnostic

restriction analysis and AGE (see Appendix **A3** and **A4**). The pGEMT–hPfDXR construct was verified by DNA sequencing (see Appendix **A5**).

The PfDXR coding region was excised from the pGEM–T Easy cloning vector by double digestion with *Sal*I and *Bam*HI restriction enzymes, by bulk digestion of pGEMT–hPfDXR plasmid DNA (1 µg). The pQE30 vector DNA (1 µg) was digested with the same restriction enzymes in order to create complementary ends for ligation. The digested DNA encoding the PfDXR coding region, and pQE30 vector sequence was visualised on a 0.8% agarose gel containing 0.5 µg/ml ethidium bromide in the presence of 0.5x TBE buffer at 100 V. Purification of the DNA was performed using DNA Gel Extraction Kit (Fermentas), according to the manufacturer's instructions. The gel purified DNA encoding the PfDXR coding region, and pQE30 cloning vector sequence were ligated in a reaction containing 50 ng DNA encoding pQE30 cloning vector, 100 ng DNA encoding the PfDXR coding region, 3 units T4 DNA ligase and 2x ligation buffer. Ligation control reactions included a negative control with no insert DNA and a positive control using control insert DNA (Promega). The ligation reactions were incubated at 4^{o}C overnight and transformed into super–competent *E. coli* JM109 cells (50 µl). The pQE30–PfDXR plasmid DNA was isolated from *E. coli* JM 109 transformants and stored at –20^{o}C, after diagnostic restriction analysis and AGE (Appendix **A3** and **A4**).

3.2.3 Heterologous expression and purification of recombinant PfDXR

3.2.3.1 Heterologous production of PfDXR with and without coexpression

E. coli XL1 Blue cells (100 µl) (Appendix **A2**) were transformed with pQE30–PfDXR plasmid DNA using *the population effect* according to the protocol summarized in Appendix **A1**. A volume of the overnight culture was then inoculated into 240 ml sterile 2x YT broth containing 100 µg/ml ampicillin, such that the absorbance was at 0.1. The culture was grown at 37^{o}C with shaking on a platform (180–200 rpm) until the A_{600nm} was between 0.4 and 0.7 absorbance units (AU). A pre–induction sample was taken (1 ml) and 1 mM isopropyl–β–D–thiogalactopyranoside (IPTG) was added to induce production of PfDXR.

For coexpression studies *E. coli* XL1 Blue cells, containing pMRBAD–PfHsp70, pGro7, pKJE7, pG–KJE8 or pREP4, were transformed with pQE30–PfDXR plasmid DNA using *the population effect* according to the protocol summarized in Appendix **A1**. A volume of the overnight culture was then inoculated into 240 ml sterile 2x YT broth containing 100 µg/ml

ampicillin and 50 µg/ml kanamycin or 34 µg/ml chloramphenicol, according to Table **3.1**, such that the absorbance was at 0.1. The culture was grown at 37^{o}C with shaking on a platform (180–200 rpm) until the A_{600nm} was approximately 0.4 AU. A pre–induction sample was taken (1 ml) and 0.2% $_{L}$–arabinose in order to induce the chaperone. The culture was further incubated at 37^{o}C with shaking on a platform (180–200 rpm) until the A_{600nm} was approximately 0.8 AU was reached; the culture was then inoculated with 1 mM IPTG in order to induce production of PfDXR.

Samples after hourly induction were taken for six hours and again overnight. All induction samples were quantified at A_{600nm} and were then centrifuged at 12 000 x g at room temperature for 1 minute. Each pellet was resuspended in sterile phosphate–buffered–saline (PBS) (137 mM NaCl, 2.2 mM KCl, 4.3 mM Na_2HPO_4, and 1.4 mM KH_2PO_4, pH 7.4); at 150µl PBS per 0.5 AU at A_{600nm}. The whole cell extracts were then analyzed using sodium dodecyl sulphate polyacrylamide gel electrophoresis (SDS–PAGE) according to the protocol summarized in Appendix **A6**. The presence of His–tagged PfDXR protein was confirmed using western analysis according to the protocol summarized in Appendix **A7**. In the case of the coexpression study with PfHsp70, the presence of PfHsp70 was confirmed using anti–PfHsp70 according to the protocol summarized in Appendix **A7**.

PfDXR solubility was assessed after induction of 4 hours; *E. coli* cells were harvested via centrifugation in an Avanti® JE centrifuge from Beckman Coulter at 6000 rpm at 4^{o}C for 15 minutes. The cell pellet was resuspended in wash buffer (1/20th culture volume) (20 mM Tris–HCl, 300 mM NaCl, 10 mM imidazole, 1 mM $MnCl_2$, pH 7.6, 1 mM PMSF). Cells were frozen overnight, and thawed in the presence of 1 mg/ml lysozyme in 1.5 ml aliquots. Aliquots were thawed on ice and sonicated at 60 amperes (Vibra Cell, Sonics and Materials, USA) at 4^{o}C for 3 x 30 seconds. Cell debris was pelleted after centrifugation at 12 000 x g at 4^{o}C for 15 minutes. Soluble and insoluble (resuspended in 1.5 ml PBS) fractions for the different samples were visualized by SDS–PAGE and western analysis, as described in Appendix **A6** and **A7**.

3.2.3.2 Nickel affinity–based purification of PfDXR

E. coli M15[pREP4] cells (100 µl) were transformed with pQE30–PfDXR plasmid DNA using *the population effect* according to the protocol summarized in Appendix **A1**. A volume of the overnight culture was then inoculated into 240 ml sterile 2x YT broth containing 100

µg/ml ampicillin, such that the absorbance was at 0.1. The culture was grown at 37^{o}C with shaking on a platform (180–200 rpm) until the A_{600nm} was between 0.4 and 0.6 AU, at which stage production of PfDXR was induced with 1 mM IPTG. Subsequent to PfDXR solubilization (as described above), soluble protein was purified using a competitive elution strategy (50 mM Tris, 300 mM NaCl, 500 mM imidazole). Two different nickel affinity–based strategies were employed in PfDXR purification; this first made use of a 1 ml His–trap^{TM} HP column (GE Healthcare), where nickel affinity chromatography was performed on an ÄKTA basic FPLC (fast protein liquid chromatography). PfDXR protein was eluted using a gradient elution from 0 to 500 mM imidazole in 10 ml. The second method made use of a His–spin protein miniprep^{TM} and was carried out according to the manufacturer's instructions (Zymo Research) (Appendix **A8**). Following both strategies, the eluted protein was buffer–exchanged into assay buffer (20 mM Tris–HCl, 300 mM NaCl, 10 mM imidazole, 1 mM $MnCl_2$, pH 7.6) via size exclusion chromatography/gel filtration chromatography (GFC) at 4˚C using a Sephadex G–25 medium (Amersham Biosciences) column (10 cm x 1 cm); twenty, 1 ml fractions were collected. Proteins were monitored at A_{280nm} (100 µl, 96–well microtitre UV plate; Corning Costar) and protein concentration was assessed using a Bradford's protein assay (Appendix **A9**).

3.2.3.3 NADPH–dependent DXP enzyme assay

The assay, which monitors NADPH reduction, as DXP is converted to MEP, is described in full in Appendix **A10**. This experiment was done in triplicate for four separate batches of PfDXR protein. Specific activity (µmol/min/mg) for each enzyme was calculated using the straight line of the graph which plotted average absorbance at 340 nm over 10 minutes.

3.3 RESUTLS

3.3.1 The construction of an expression plasmid with a codon harmonised PfDXR coding region

3.3.1.1 Codon harmonisation of the PfDXR coding region

Codon harmonization was used in an attempt to improve the protein production of folded function PfDXR target enzyme. When comparing the sequence of the codon optimized coding region of PfDXR versus the codon harmonized coding region of PfDXR (Figure **B.1**, Appendix B**)**, it is evident that the harmonized sequence has only 71% identity with that of the codon optimized coding region of PfDXR. Following successful codon harmonization, it was necessary to clone the codon harmonized coding region of PfDXR into an appropriate expression vector.

3.3.1.2 Insertion of the codon harmonized PfDXR coding region into the pQE30

The choice of plasmid vector here was based on the presence of a T5 promotor, as well as a Histidine$_6$–tag for the purpose of affinity purification. The cloning strategy that was employed is summarised in Figure **3.1**.

DNA sequencing was used to confirm the correct cloning of the pQE30–hPfDXR plasmid such that the protein translation was in frame and there were no mutations. According to Figure **B.2** (Appendix B), the presence of the *Bam*HI and *Sal*I restriction sites occur at nucleotide position 145 and 1405 respectively. The pQE30–hPfDXR plasmid map and diagnostic restriction enzyme analysis can be seen in Figure **B.3** (Appendix B).

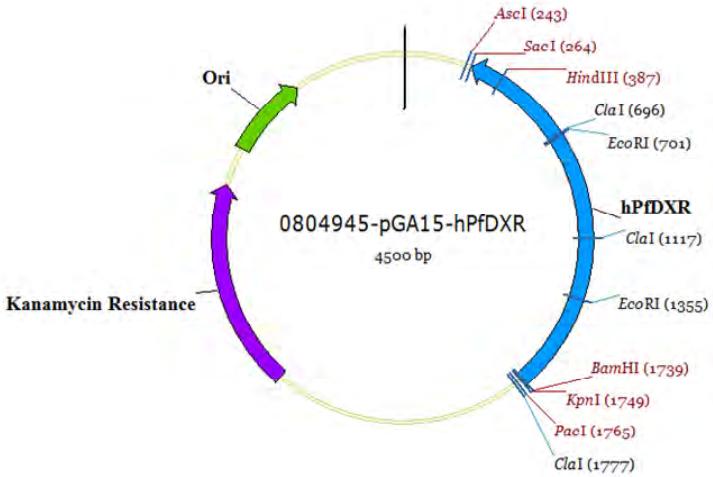

PCR amplification of PfDXR with removal of leader sequence and addition of *Bam*HI and *Sal*I restriction sites

Gel purification of PCR product

Ligation of PfDXR coding region into pGEM-T Easy

Release of PfDXR coding region by a double digest with *Bam*HI and *Sal*I

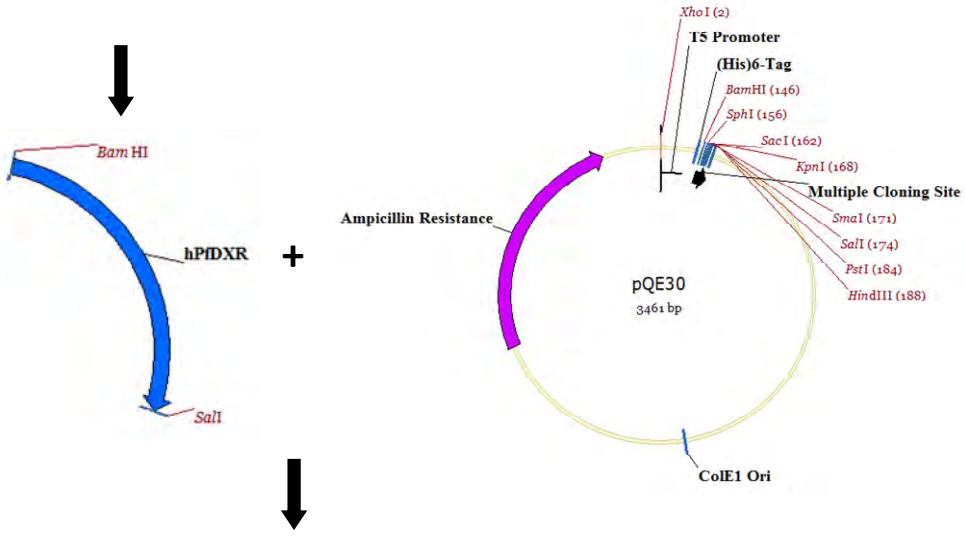

Ligation of *Pf*DXR coding region into pQE30 plasmid via *Bam*HI and *Sal*I restriction sites

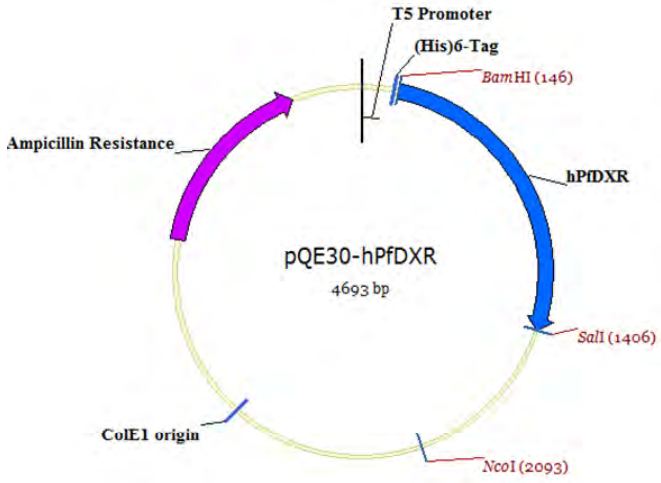

Figure 3.1: Cloning strategy for the creation of the pQE30–hPfDXR construct (legend on next page).

The codon harmonised PfDXR coding region was PCR–amplified from the 0804945–pGA15–hPfDXR plasmid (using the primers hPfDXR*Bam*HI and hPfDXR*Sal*IR), resulting in the deletion of the 71 amino acid leader sequence, as well as the insertion of a *Bam*HI and *Sal*I restriction sites at the 5' and 3' ends of the coding region respectively. The gel purified PCR product was then ligated into pGEM–T Easy as a means of interim storage. The PfDXR coding region was then released from the pGEM–T–hPfDXR by double digesting with *Bam*HI and *Sal*I. The digestion product was then ligated into pQE30 via the same restriction enzyme pair to yield the pQE30–hPfDXR plasmid.

After the successful confirmation of the pQE30–hPfDXR construct, it was necessary to assess whether the codon harmonization of the PfDXR gene improved the expression and solubility of PfDXR.

3.3.2 Heterologous expression and purification of recombinant PfDXR

3.3.2.1 PfDXR was insoluble after heterologous production

Initial experiments using the codon optimized PfDXR coding region, which was inserted into the pQE31 plasmid (pEQ31–oPfDXR), revealed that the PfDXR protein expressed from the optimized coding region resulted in very little expression and little to no production of soluble protein (data not shown). In an attempt to enhance the solubility of PfDXR, the coding region was therefore harmonized. According to SDS–PAGE analysis of the induction profile of PfDXR expressed from pQE30–hPfDXR, it was evident that the protein was not overexpressed (Figure **3.2**) and resulted in decreased protein levels compared to PfDXR expressed from pEQ31–oPfDXR (data not shown). Western analysis using anti–His_6 antibodies confirmed the presence of PfDXR after 1 hour of induction, where the greatest protein expression transpired 4 hours post–induction (Figure **3.2, lane 6**). Solubility analysis was therefore assessed after 4 hours, which evidently indicated that almost all the PfDXR protein expressed remained in the insoluble fraction (Figure **3.2, lane 11**). Purified EcDXR was used as a positive control (Figure **3.3, lane 1**) and it migrated as a 45 kDa band.

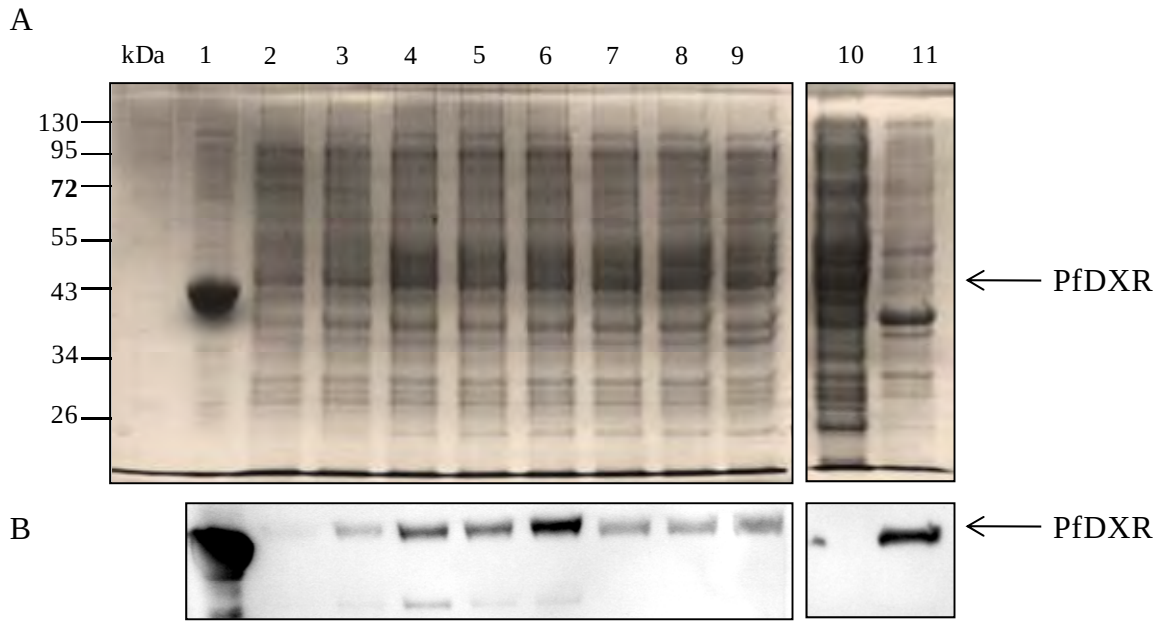

Figure 3.2: Analysis of PfDXR expression and solubility in *E. coli* cells.
IPTG induced logarithmic phase *E. coli* XL1 Blue[pQE30–hPfDXR] whole cell lysate and solubility analyses fractions were analysed by denaturing SDS–PAGE (A) and western analysis (B). The molecular mass marker was resolved on the left (kDa). Purified *Ec*DXR (44.6 kDa) was used as a positive control (lane 1). The pre–induced *E. coli* XL1 Blue[pQE30–hPfDXR] whole cell lysate is shown in lane 2 (at time = 0; A_{600nm} = 0.4), with samples after hourly induction by 1 mM IPTG shown in lanes 3 to 8 (1 to 6 hours), and overnight induction shown in lane 9. Following sonication and centrifugation, soluble supernatant fractions (lane 10) and insoluble fractions (lane 11) were analysed. The presence of the PfDXR monomer (46.7 kDa) was confirmed by western analysis and is shown by the arrow.

Having shown that PfDXR aggregated in *E. coli* cells when heterologously produced, the next step was to determine whether a viable expression strategy could be procured in order to acquire folded functional target protein for further characterization.

3.3.2.2 Coexpression of PfDXR using *E. coli* and malarial chaperones

Because of the nature and function of chaperones, the coexpression of PfDXR with the *E. coli* molecular chaperone combinations KJE and ELS was employed in an attempt to improve the heterologous production of the target enzyme.

Coexpression of PfDXR with KJE resulted in successful overexpression of DnaK (70 kDa), DnaJ (40 kDa), as well as GrpE (26 kDa) and according to SDS–PAGE analysis all chaperones mentioned also remained soluble after lysis (Figure **3.3, lane 10**). Despite the presence of the KJE in the soluble fraction, the chaperones appeared to be unable to improve the solubility of PfDXR as the majority of the target protein produced resided in the insoluble

fraction (Figure **3.3, lane 11**). When compared to Figure **3.2**, where PfDXR was produced alone, PfDXR protein production was considerably less when coexpressed with KJE.

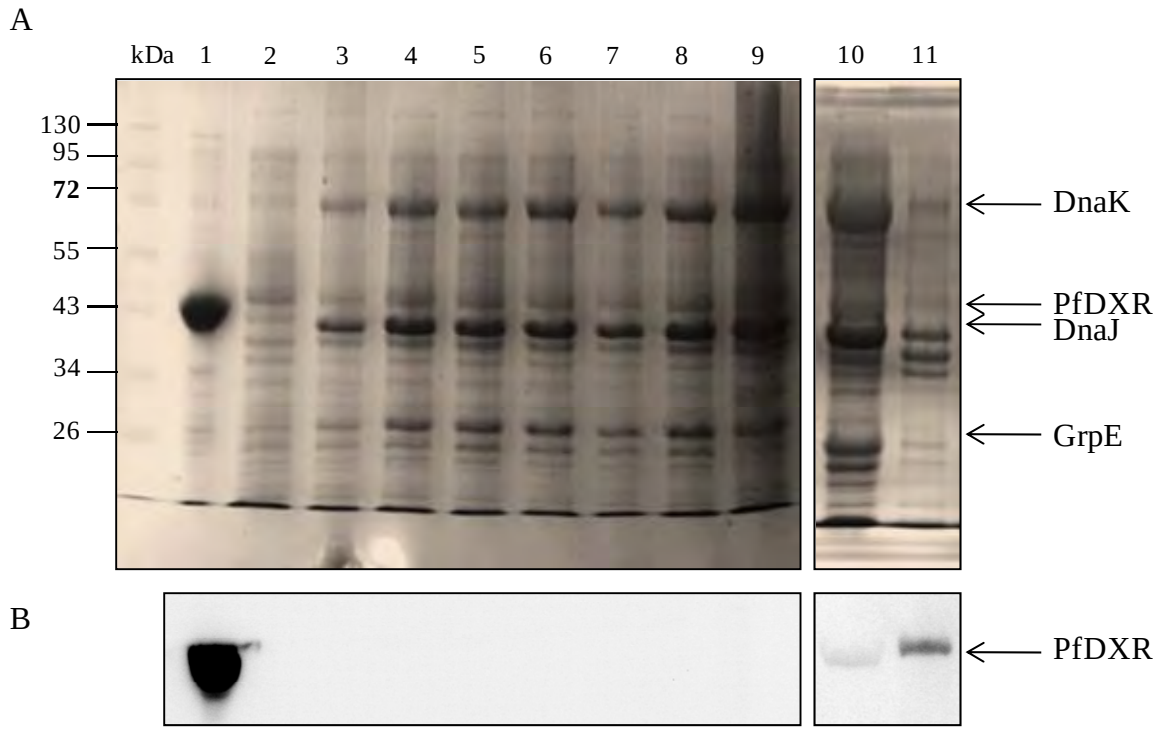

Figure 3.3: Analysis of PfDXR expression and solubility after co–expression with the *E. coli* molecular chaperones DnaK, DnaJ and GrpE.

L—arabinose and IPTG induced logarithmic phase *E. coli* XL1 Blue[pQE30–hPfDXR][pKJE7] whole cell lysate and solubility analyses fractions were analysed by denaturing SDS–PAGE (A) and western analysis (B). The molecular mass marker was resolved on the left (kDa). Purified *Ec*DXR (44.6 kDa) was used as a positive control (lane 1). The pre–induced *E. coli* XL1 Blue[pQE30–hPfDXR][pKJE7] whole cell lysate is shown in lane 2 (at time = 0; A_{600nm} = 0.4), with samples after hourly induction by 0.2% $_{L}$–arabinose (at time = 0) and 1 mM IPTG (at time = 1) shown in lanes 3 to 8 (1 to 6 hours post L—arabinose induction), and overnight induction shown in lane 9. Following sonication and centrifugation, soluble supernatant fractions (lane 10) and insoluble fractions (lane 11) were analysed. The presence of the PfDXR monomer (46.7 kDa) was confirmed by western analysis and is shown by *black* arrows. The efficient induction of the *E. coli* chaperones DnaJ (70 kDa), DnaK (40 kDa) and GrpE (25 kDa) are shown by *black* arrows.

In contrast to the KJE coexpression profile, the co–production of ELS with PfDXR resulted in the successful solubilization of PfDXR. The amount of PfDXR protein produced was however considerably less than the amount of protein produced from the coexpression of the codon optimized PfDXR coding region with ELS (data not shown). However, the total quantity of soluble protein was still comparable because only ~50% of PfDXR expressed from pQE31–oPfDXR remained soluble, while ~80% of PfDXR expressed from the codon harmonized equivalent remained soluble (Figure **3.4, lane 10**).

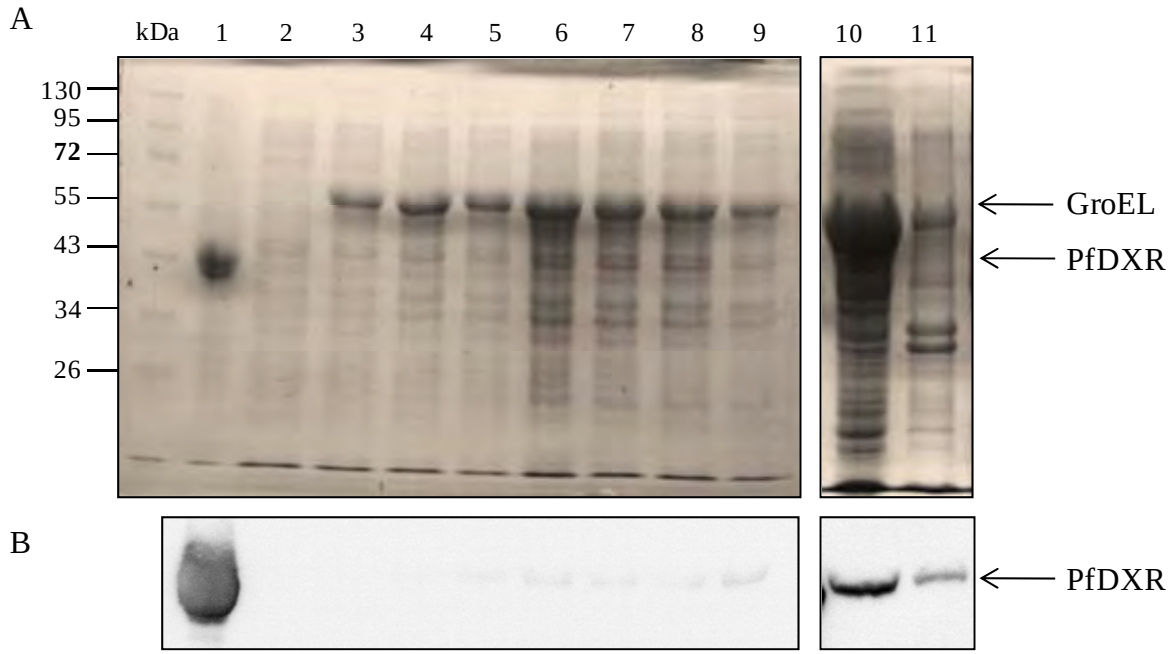

Figure 3.4: Analysis of PfDXR expression and solubility after co–expression with the *E. coli* molecular chaperones GroEL and GroES.

L—arabinose and IPTG induced logarithmic phase *E. coli* XL1 Blue[pQE30–hPfDXR][pGro7] whole cell lysate and solubility analyses fractions were analysed by denaturing SDS–PAGE (A) and western analysis (B). The molecular mass marker was resolved on the left (kDa). Purified *Ec*DXR (44.6 kDa) was used as a positive control (lane 1). The pre–induced *E. coli* XL1 Blue[pQE30–hPfDXR][pGro7] whole cell lysate is shown in lane 2 (at time = 0; A_{600nm} = 0.4), with samples after hourly induction by 0.2% $_{L}$–arabinose (at time = 0) and 1 mM IPTG (at time = 1) shown in lanes 3 to 8 (1 to 6 hours post L—arabinose induction), and overnight induction shown in lane 9. Following sonication and centrifugation, soluble supernatant fractions (lane 10) and insoluble fractions (lane 11) were analysed. The presence of the PfDXR monomer (46.7 kDa) was confirmed by western analysis and is shown by *black* arrows. The efficient induction of the *E. coli* chaperones GroEL (60 kDa) is shown by a *black* arrow, while the 10 kDa GroES was not sufficiently resolved and cannot be seen.

The next strategy endeavoured to decipher whether an even greater improvement in total PfDXR protein could be accomplished using the homologous *P.falciparum* molecular chaperone PfHsp70–1. Based on SDS–PAGE analysis of the induction profile, PfHsp70–1 was not overexpressed, while there was significant overexpression of PfDXR, from as early as 2 hours post– induction (Figure **3.5, lane 4**). When considering the more sensitive western analysis, it is evident that there was in fact increasing expression of PfHsp70–1 an hour post–induction, which was maintained overnight. However PfDXR expressed well for the first 6 hours (Figure **3.5, lanes 3–8**), then expression decreased overnight (Figure **3.5, lane 9**). The co–production of PfHsp70–1 with PfDXR unfortunately resulted in unsuccessful solubilization of PfDXR, and all target protein precipitated with the insoluble proteins (Figure **3.5, lane 11**).

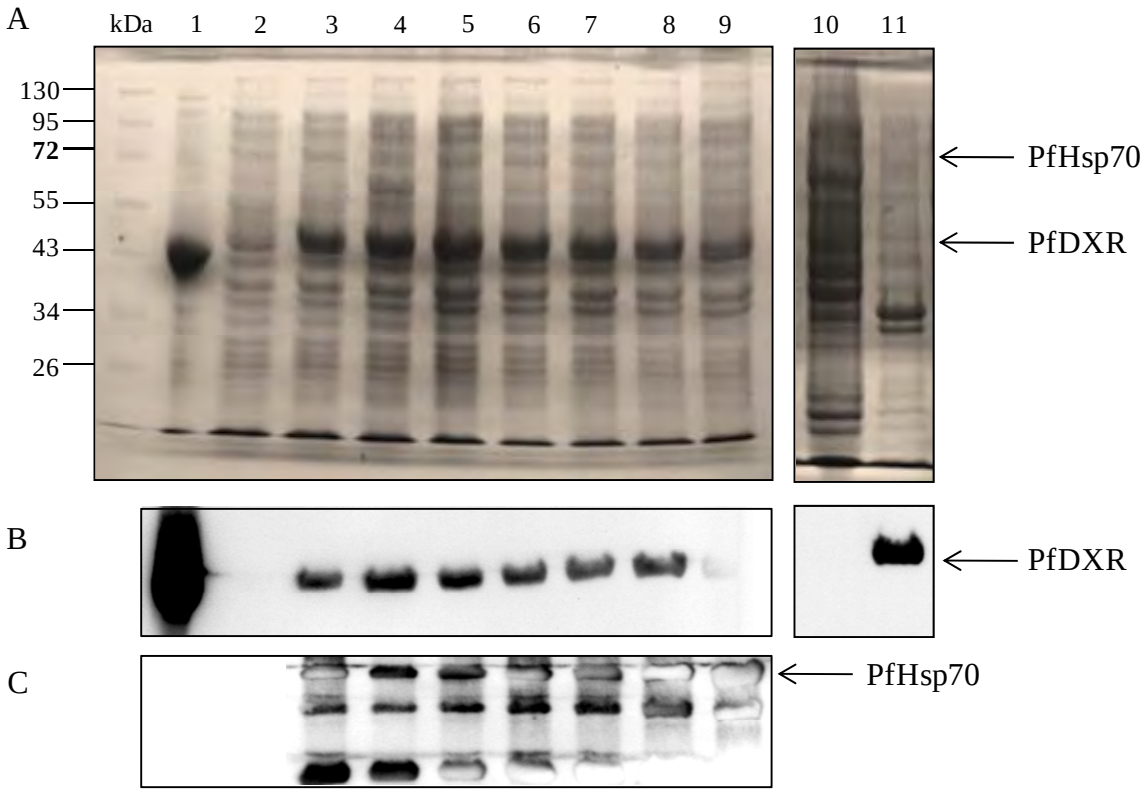

Figure 3.5: Analysis of PfDXR expression and solubility after co–expression with the malarial chaperone PfHsp70–1.

L—arabinose and IPTG induced logarithmic phase *E. coli* XL1 Blue[pQE30–hPfDXR][pGro7] whole cell lysate and solubility analyses fractions were analysed by denaturing SDS–PAGE (A) and western analysis for PfDXR (B) and PfHsp70 (C). The molecular mass marker was resolved on the left (kDa). Purified *Ec*DXR (44.6 kDa) was used as a positive control (lane 1). The pre–induced *E. coli* XL1 Blue[pQE30–hPfDXR][pGro7] whole cell lysate is shown in lane 2 (at time = 0; A_{600nm} = 0.4), with samples after hourly induction by 0.2% $_{L}$–arabinose (at time = 0) and 1 mM IPTG (at time = 1) shown in lanes 3 to 8 (1 to 6 hours post L—arabinose induction), and overnight induction shown in lane 9. Following sonication and centrifugation, soluble supernatant fractions (lane 10) and insoluble fractions (lane 11) were analysed. The presence of the PfDXR monomer (46.7 kDa) was confirmed by western analysis and is shown by *black* arrows. The presence of the malarial chaperone PfHsp70 was confirmed by western analysis and is shown by *black* arrows.

While some of the above–mentioned coexpression strategies using heterologous and homologous chaperone combinations improved the expression of PfDXR, none resulted in successful solubilization of the target enzyme sufficiently enough to warrant continuing with the strategy in PfDXR purification.

3.3.2.3 Tight control of transcription of PfDXR by coexpression with *lac* repressor

The tight control of gene expression was the final coexpression strategy attempted. The coexpression of the *lac* repressor protein with PfDXR was employed in the hope that it would enhance expression and solubility of PfDXR. The transcription of the *hPfdxr* gene was halted by the presence of the *lac* repressor protein in the *E. coli* host, until expression was induced

by IPTG. As expected, prior to induction of target protein (i = 0), there was no expression of PfDXR (Figure **3.6, lane 2**). This is in contrast to the expression profile of PfDXR expressed alone, where the leaky expression of the PfDXR gene resulted in some basal transcription of PfDXR pre–induction (Figure **3.2, lane 2**); while this was not completely compelling in the above–mentioned figure, it was evident in almost all other expression studies for PfDXR alone (data not shown). According to Figure **3.6**, it is clear that there was significant overexpression of PfDXR in the presence of *lac* repressor, with the greatest expression occurring after 4 hours (Figure **3.6, lane 6**). Western analysis using anti–His antibodies confirmed that more than 90% of the PfDXR protein produced remained soluble (Figure **3.6, lane 10**).

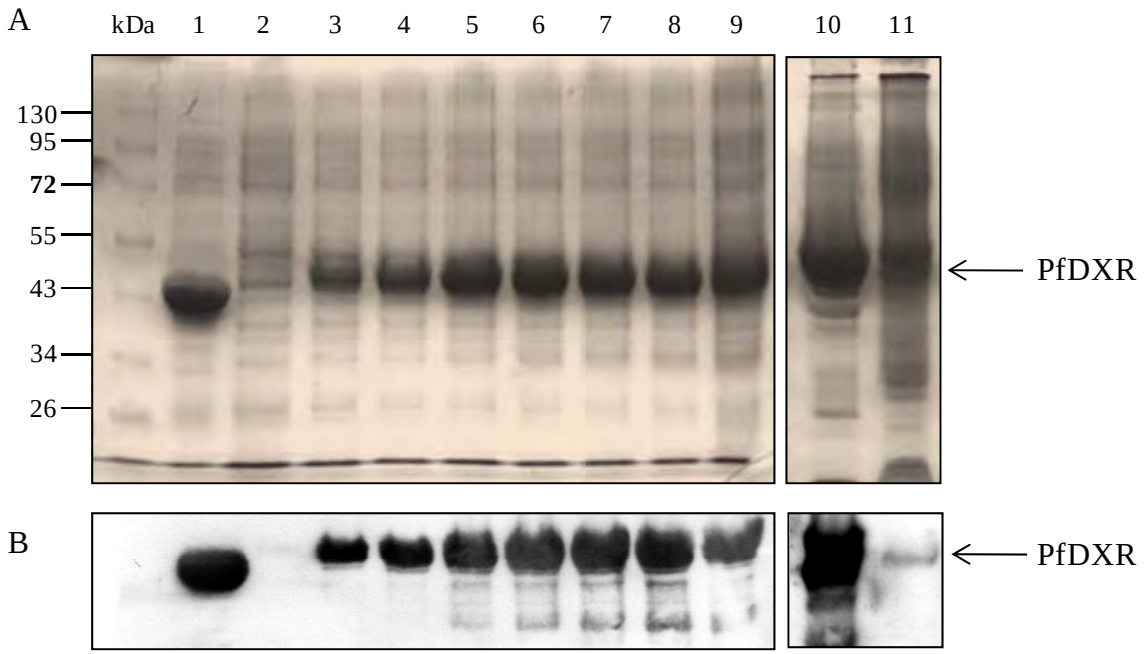

Figure 3.6: Analysis of PfDXR expression and solubility after co–expression with the *lac*I repressor protein.
IPTG induced logarithmic phase *E. coli* M15 [pQE30–hPfDXR][pREP4] whole cell lysate and solubility analyses fractions were analysed by denaturing SDS–PAGE (A) and western analysis (B). The molecular mass marker was resolved on the left (kDa). Purified *Ec*DXR (44.6 kDa) was used as a positive control (lane 1). The pre–induced *E. coli* M15 [pQE30–hPfDXR][pREP4] whole cell lysate is shown in lane 2 (at time = 0; A_{600nm} = 0.4), with samples after hourly induction by 0.2% $_{L}$–arabinose (at time = 0) and 1 mM IPTG (at time = 1) shown in lanes 3 to 8 (1 to 6 hours post L—arabinose induction), and overnight induction shown in lane 9. Following sonication and centrifugation, soluble supernatant fractions (lane 10) and insoluble fractions (lane 11) were analysed. The presence of the PfDXR monomer (46.7 kDa) was confirmed by western analysis and is shown by *black* arrows.

Based on the heterologous expression results put forward here, it was concluded that the coexpression strategy utilizing the *lac* repressor protein would be used for the subsequent purification of PfDXR for the purpose of kinetic characterization.

3.3.2.4 Nickel affinity purification of PfDXR after coexpression with *lac* repressor

Two separate nickel affinity protocols were employed in this work, both generating significantly different results. The first strategy made use of a 1 ml His–trap™ HP column coupled to FPLC, with PfDXR protein being eluted using a gradient elution from 0 to 500 mM imidazole concentration. The second method made use of a His–spin protein miniprep™, which involved a single elution event at 500 mM imidazole concentration. After protein quantification by SDS–PAGE analysis and confirmation by Bradford's protein assay, protein purity and protein concentration were quantified. The His–spin method resulted in the purification of consistently pure protein (~90%) (data not shown) at consistent yields (0.15–0.25 mg/l), the His–trap method resulted in the purification of significantly more PfDXR; ~2 mg/l of starting culture volume (Figure **3.7, lane 6**), with the same degree of purity as seen with the other method. The major disadvantage of this method was however that the nickel affinity purification step was carried out at room temperature; meaning that the activity of the target enzyme may have been compromised.

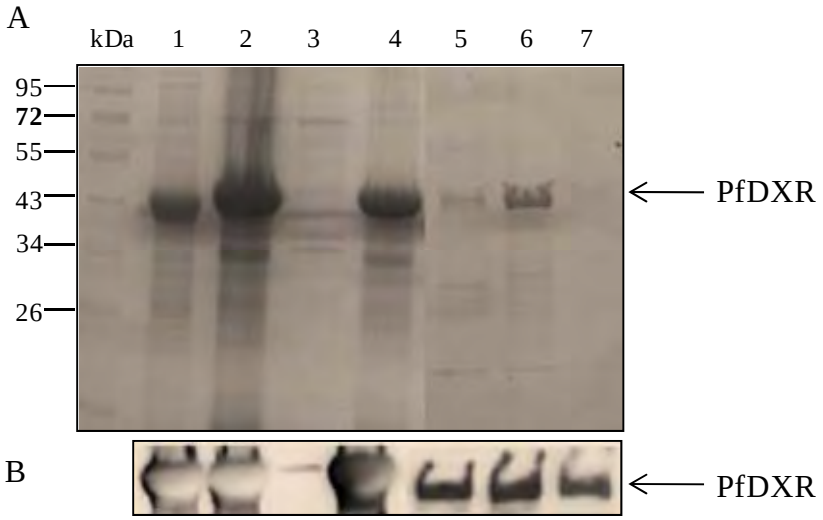

Figure 3.7: Purification by nickel affinity chromatography of PfDXR produced during co–expression with the *lac* repressor protein.

His–tagged PfDXR was purified by way of nickel affinity chromatography. The PfDXR purification profile was analysed by denaturing SDS–PAGE (A) and western analysis (B). The molecular mass marker was resolved on the left (kDa). Purified *Ec*DXR (44.6 kDa) was used as a positive control (lane 1). The post–induced *E. coli* M15 [pQE30–hPfDXR][pREP4] whole cell lysate is shown in lane 2 (at time = 4; A_{600nm} = ± 2). Following sonication and centrifugation, the insoluble supernatant fractions (lane 3) and soluble fractions (lane 4) were analysed. Nickel affinity purified samples subsequent to gel filtration are shown in lanes 6, 7 and 8. The presence of the PfDXR monomer (46.7 kDa) was confirmed by western analysis and is indicated by *black* arrows.

PfDXR protein was purified successfully using two different purification methods. Using the His–trap method resulted in protein yields that were 20–fold greater when compared to the

His–spin method; this was evident when comparing the SDS–PAGE profile for qualification and confirmation. However, when analysing the specific activity of the final purified protein, the His–spin method, which was carried out at 4^{o}C (1.04 ± 0.04 µmol/min/mg), resulted in a 4–fold greater activity per mg of protein, when compared to the His–trap method (0.25 ± 0.03 µmol/min/mg).

3.4 DISCUSSION

Numerous strategies were employed in this study to enhance the expression and solubility of the PfDXR enzyme. Codon bias can be problematic during the production of recombinant proteins in *E. coli* (Baca and Hol, 2000) because *P.falciparum* is characterized by a high A/T content (Flick *et al*., 2004). Codon harmonization was therefore one of the approaches taken to improve upon the production of soluble protein from this problematic malarial enzyme (Angov *et al.*, 2008). The method used for harmonization was such that there was preservation of the pause site profile of the native sequence; with the intention that the correct arrangements of the protein secondary structures would be maintained. Analysis of the sequence alignment of the codon optimized versus the codon harmonised coding regions for PfDXR revealed that they share 71% sequence identity, while still preserving the protein sequence. This strategy was however unsuccessful as codon harmonization in this work, resulted in a reduction in the total amount of PfDXR produced. However neither codon optimization nor harmonization resulted in the production of soluble PfDXR (data not shown), confirming the recalcitrant nature of the PfDXR protein.

Often the host cell's chaperone system becomes overloaded during recombinant protein production, limiting the amount of soluble protein that can be produced (Carrió and Villaverde, 2002). The overproduction of molecular chaperones, as a coexpression technique, has been used successfully for a wide range of proteins (reviewed by de Marco *et al*., 2007$_2$); however it is difficult to predict which chaperone family will recognise a particular protein (Haacke *et al.*, 2009). It has been said that in the case of each target protein, optimization of each individual expression system is often required to benefit from this technique (reviewed by de Marco *et al*., 2007$_2$).

According to Botha *et al.* (2007), PfHsp70–3 (NP 701211) and PfHsp70–y (MAL13P1.540) are potentially localized to the apicoplast, however, Spork (2008) hypothesized that

PhHsp70–y was unlikely to be an apicoplast protein due to the presence of endoplasmic reticulum KDEL retrieval sequence. DnaK is the prokaryotic equivalent to Hsp70, so one could hypothesize that DnaK could assist in PfDXR functionality by assisting with its correct folding during translation. However, the presence of soluble KJE failed to enhance the expression or solubility of PfDXR, neither from the optimized gene (data not shown) nor from the harmonized gene. In contrast to this, ELS recognised PfDXR as a substrate and significantly enhanced its solubility. Unfortunately the total protein expressed was significantly less than that of PfDXR alone, although more than in the presence KJE**.** Due to the size of the cavity formed by GroEL, this chaperone family has an upper size limit for substrates of ~60 kDa (Houry *et al*., 1999), therefore allowing PfDXR, which is 47 kDa in size, to act as a substrate. DnaK is more likely to recognise protein substrates larger than 70 kDa (Mayer *et al*., 2000) and this may explain why PfDXR was not recognised as a substrate by the KJE chaperone family. In addition to this is the fact that PfDXR may not have DnaK binding motifs (Deuerling *et al*., 2004). It could also be possible that the overexpression of the chaperones (at t = 0) resulted in the overloading of the *E. coli* expression system's protein synthesis machinery, such that when PfDXR expression was induced (at t = 1), no transcription machinery was available. In summary, while ELS coexpression resulted in some expression improvement when compared to KJE, neither chaperone combinations resulted in enhancement sufficient to warrant their further use. It may be possible that *E. coli* chaperones are not capable of folding malarial proteins and that a strategy should be employed that uses homologous molecular chaperones.

The use of the homologous chaperone PfHsp70–1 in a coexpression study with PfDXR showed compelling evidence for the positive production of PfDXR. Unfortunately, western analysis confirmed that all of the target protein was essentially insoluble. Chaperones that have been said to be residents of the apicoplast include: PfHsp70–3 (Botha *et al*., 2007), Hsp40–5 (PFD0465w) (Botha *et al*., 2007) and the Hsp60 named Cpn60 (Sato and Wilson, 2005). PfHsp70 used in this study was cytosolic PfHsp70–1 (Botha *et al*., 2007) and therefore may not have been suitable when trying to express the apicoplast target protein PfDXR. There is evidence to suggest that PfHsp70–1 interacts with numerous apicoplast destined proteins in plants, via a transit peptide sequence. *P.falciparum* transport is quite different from that seen in plants where apicoplast–destined proteins contain both a transit peptide immediately upstream of the leader sequence (Foth *et al*., 2003). It is therefore not possible to speculate that the two systems work in a similar manner and that Hsp70

recognises the apicoplast targeted proteins. It has been suggested that PfBiP (a *P.falciparum* Hsp70) is responsible for the export of *Plasmodium* proteins into the erythrocyte. This, together with the fact that PfBiP has been shown to interact with more *Plasmodium* proteins than the other PfHsp70s (e.g. Hsp70–1 and Hsp70–3) (reviewed by Pesce *et al*., 2010), makes it seem highly unlikely that Hsp70–1 is capable of binding and correctly folding the apicoplast–destined PfDXR. Based on the results of this study, however, the most probable molecular chaperone folding partner may be the *P. falciparum* homologue of GroEL (PfHsp60) because it is localised in the apicoplast (Sato and Wilson, 2005), and because GroEL has been shown to be capable of binding proteins of up to 60 kDa in size (Houry *et al*., 1999).

The most successful strategy to improve expression and solubility of PfDXR was undoubtedly the coexpression of PfDXR with the *lac* repressor protein, which halts basal transcription in the *E. coli* host expression system. In the presence of *lac* repressor, the basal level of expression is tightly controlled (Spehr *et al*., 2000), such that subsequent to the induction of PfDXR, significant overexpression of the target enzyme resulted, with the greatest overexpression occurring 4 hours post induction. This tightly controlled expression system was therefore employed production and purification of PfDXR. It is possible that this system led to the greatest control of the levels of PfDXR, and the enzyme was induced at the correct time during growth of the cells to enable the production of soluble protein. In the absence of the *lac* repressor protein, the levels of PfDXR were not controlled in the cell.

When comparing the total protein by SDS–PAGE analysis, it was evident that the total protein purified after GFC was approximately 70 to 80% that of the total soluble protein isolated subsequent to cell lysis. The use of SDS–PAGE as a method of direct quantification is however not an accurate gauge because of loading discrepancies which will most certainly affect the amount of PfDXR protein resolved on the gel. Therefore, the activity of the target protein needs to be considered, using an assay that is specific for the enzyme of interest; in this work, the NADPH–dependent DXP assay was used. The purity of PfDXR was assessed to be ~90%, for both the His–trap and His–spin methods of purification, however, as a consequence of the His–trap nickel affinity step being carried out at room temperature, the enzyme did not demonstrate maximal enzyme activity to the same degree as protein purified by means of the His–spin method. The advantage of the His–trap method however, was that it allowed for the purification of ~ 2 mg of protein per litre of starting culture and it is also

more amenable to scale–up. This method would therefore be sufficient if a large quantity of target enzyme was required for drug screening experiments such as nuclear magnetic resonance (NMR) binding assays, by which novel compounds that demonstrate specificities for the target enzyme could be identified (reviewed by van Dongen *et al*., 2002). The His–spin method on the other hand only allowed for the purification of up to 0.5 mg of PfDXR per litre of starting culture, but the enzyme was 4–fold more active. For the accurate quantification of enzyme's kinetic parameters, it would therefore be prudent to sacrifice yield for activity. In future work, the His–trap method could be further optimized so that a scale up procedure could be followed that is conducted at 4^{o}C. Ideally, the same yields could be obtained as described here for the His–trap method, but with activity in the range that was obtained for the His–spin method in this work.

In conclusion, the results of this study showed that the influence of various strategies to improve solubility cannot be predicted but must be optimized for each particular recombinant protein. For the His–trap method, the yield of PfDXR per litre of culture (up to 2 mg), was 8 to 10–fold higher than previously reported yields in the literature (Gieβmann *et al*., 2008), further validating the success of this coexpression technique, however activity was significantly sacrificed for an increase in yield.

CHAPTER 4

MUTAGENESIS STUDIES FOR RATIONAL PFDXR ENGINEERING

4.1 INTRODUCTION

A number of crystal structures of DXR enzymes have provided respectable information regarding the structure of the enzyme active site and a number of studies have been undertaken to better understand the role of these active site residues in an attempt to link structure to function. Site–directed mutagenesis is one method that can be applied experimentally for the purpose of enzyme characterization (Kuzuyama *et al*., 2000) and this approach has been used extensively in the literature and is summarised in Table **4.1**. When relating structure to function, mutations of the DXR enzyme can be categorised, including: residues that interact with cofactors (NADPH or the divalent metal ion), residues that interact directly with the DXR substrate or inhibitors (fosmidomycin was used in this study), residues that are involved in active site architecture, and residues that are involved in the closing of the catalytic hatch over the active site **(**Kuzuyama *et al*., 2000; Proteau *et al*., 2004; Fernandes *et al.*, 2005; Fernandes and Proteau, 2006; Jawaid *et al*., 2009).

Because the binding of the NADPH cofactor has been extensively studied in the literature for *E. coli* (Takahashi *et al*., 1998; Yajima *et al*., 2002; Steinbacher at al., 2003) and because the residues of the NADPH binding motif are highly conserved, it can be assumed that the NADPH binding site is consistent throughout the DXR families. Very little analysis by way of site–directed mutagenesis has been undertaken for assessing the effects of mutating the NADPH binding motif (Table **4.1**.), possibly because the *in vitro* analysis of DXR using NADPH has been so well documented in the literature for numerous DXR enzymes including: *Hevea brasiliensis* (Cordoba *et al*, 2009), *Ginkgo biloba* (Kim *et al*., 2006), *Rauvolfia verticillata* (Liao *et al*., 2007), *A. thaliana* (Rohdich *et al*., 2006), *E. coli* (Takahashi *et al*., 1998; Hoeffler *et al*., 2002; Fox and Poulter, 2005), *M. tuberculosis* (Argyrou and Blanchard, 2004), *Z. mobilis* (Grolle *et al*., 2000), *Synechocystis* sp. (Fernandes and Proteau, 2006), *C. forskohlii* (Engprasert *et al*., 2005) and *P. falciparum* (Singh *et al*., 2006; Gieβmann *et al*., 2008). Also, numerous DXR crystal structures have been solved in the presence of NADPH (Yajima *et al*., 2002; Ricagno *et al*., 2004; Henriksson *et al*., 2006; Takenoya *et al*., 2010). Cofactor studies using NAD+ and NADP+ for *A. thaliana* (Rohdich *et al*., 2006), *M. tuberculosis* (Argyrou and Blanchard, 2004), *Pseudomonas aeruginosa*

(Altincicek *et al*., 2000), *Z. mobilis* (Grolle *et al*., 2000) and *E. coli* (Takahashi *et al*., 1998; Hoeffler *et al*., 2002; Fox and Poulter, 2005), resulted in a significant reduction of enzyme activity, corroborating that NADPH is the preferred cofactor. For example, Takahashi *et al.* (1998) reported that DXR has a preference for NADPH, as opposed to NADH, where a decrease in reaction rate of 100–fold was recorded.

Upon analysis of divalent metal ion preference, it was clear that Ca^{2+}, Ni^{2+}, Zn^{2+}, Cu^{2+} or Fe^{2+} could not be utilized (Takahashi *et al*., 1998). The literature suggests that only Mn^{2+}, Co^{2+} and Mg^{2+} could be utilized (Brenda Enzyme Database, 2008). Extensive mutagenesis studies for *Synechocystis* sp. has been undertaken in the literature for Asp152, Glu154 and Glu233 (Fernandes and Proteau, 2006). It was concluded that the divalent metal ion is essential for catalysis, such that the ion interacts in an octahedral complex with one Asp and two Glu residues (Yajima *et al*., 2002; Steinbacher *et al*, 2003 Ricagno *et al*., 2004; Takenoya *et al*., 2010). Interestingly, mutation of these three residues individually, in *Synechocystis* sp. (Asp152, Glu154 and Glu223) resulted in complete loss of enzyme activity, while in *E. coli*, mutation studies for the Glu223 equivalent (Glu231) resulted in only a reduction substrate turnover (k_{cat}) with no change in the K_m (substrate's affinity for the enzyme) (reviewed by Singh *et al*., 2007) (Table **4.1**). Contradictory to the statement that Glu231 is involved in metal coordination (Takahashi *et al*., 1998; Kuzuyama *et al*., 2000; Proteau *et al*., 2004), Reuter *et al*. (2002) reported that the reduction in turnover but not substrate affinity suggested that Glu231 is involved in catalysis rather than substrate or cofactor binding.

Site–directed mutagenesis studies for the *E. coli* enzyme revealed the importance of numerous conserved His and Glu residues for activity (Querol *et al*., 2002), as is evident in Table **4.1**. Mutation of His209, His153 and His257 in *E. coli* (Kuzuyama *et al*., 2000; Proteau *et al*., 2004) resulted in a drastic reduction in enzyme efficiency (k_{cat}/K_m), as a direct result of a small decrease in substrate affinity (K_m) and a drastic reduction in turnover rate (k_{cat}). This information allowed the authors to conclude that these residues were not directly involved in enzyme catalysis, but rather played a vital role in structural integrity of the active site because the change in K_m was not significantly different to that of the wild type, but there was a reduction in k_{cat}/K_m (Kuzuyama *et al*., 2000).

The successful crystallization of numerous EcDXR enzymes in the presence of the DXP substrate or fosmidomycin inhibitor have been completed (Steinbacher *et al*., 2003;

Henriksson *et al*., 2006; Yajima *et al*., 2007; Takenoya *et al*., 2010), rendering it futile to carry out mutagenesis studies on catalytic residues. In a recent study by Jawaid *et al*. (2009), the *F. tularensis* DXR was kinetically characterized, confirming Ser177 (Ser186 in *E. coli*) as a site of phosphorylation. The inactivity of the S177D and S177E mutant proteins (Table **4.1**) allowed the authors to hypothesize that the MEP pathway is responsible for post–translational control of isoprenoid precursor production. This metabolic control, via reversible phosphorylation of a Ser residue, has been documented in the MVA pathway (Clarke and Hardie, 1990). Interestingly, Ser153 on SyDXR (Ser151 in *E. coli*), which is not characterized as one of the catalytic residues (Ser186, Ser222, Asn227 and Lys228 in EcDXR) has been said to interact with both fosmidomycin via the N–formyl carbonyl moiety and with and DXP substrate via the C2 carbonyl (Mac Sweeney *et al*., 2005), while Steinbacher *et al*. (2003) reported that Ser151 rather forms a pronounced hydrophilic cavity behind fosmidomycin. Mutation of the hydroxyl group of Ser153 in SyDXR resulted in a drastic reduction in the catalytic efficiency (k_{cat}/K_m), which allowed Fernandes and Proteau (2005) to conclude that Ser153 is responsible for optimal arrangement of active site, with the most likely hydrogen–bonding partner being His249 (His257 in *E. coli*).

Mutations of the catalytic hatch, as well as the crystal structures derived for various DXR enzymes, have allowed authors to better understand the catalytic mechanism of DXR upon substrate/inhibitor binding. If one compares the crystal structure of the apo form of EcDXR (Reuter *et al*., 2002), with that of the EcDXR crystal structure with an inhibitor (Steinbacher *et al*., 2003) or ion bound (Yajima *et al*., 2002), it is evident that the catalytic hatch closes over the active site in the presence of an inhibitor/substrate/ion (reviewed by Singh *et al*., 2007). In SyDXR, mutation of Trp204 (Trp212 in *E. coli* DXR) allowed Fernandes *et al*. (2005) to conclude that the smaller the substitute residue was, the more substrate affinity was lost (Table **4.1**). The study confirmed that the highly conserved Trp residue was involved in substrate/inhibitor binding and substrate differentiation (Fernandes *et al*., 2005). Mutation of another hatch residue, Met206 in SyDXR (Met 214 in *E. coli*), again resulted in a drastic reduction in catalytic efficiency and substrate affinity (Table **4.1**). The authors concluded that the catalytic hatch was essential for catalysis and substrate specificity (Fernandes and Proteau, 2006). The authors of this work conversely related specificity to enzyme efficiency (k_{cat}/K_m) (Fernandes and Proteau, 2006). To completely quantify specificity, a number of different substrates, in addition to DXP would need to be assessed.

Table 4.1: Analysis of critical amino acids in DXR and their predicted role from site–directed mutagenesis experiments.

Identified Amino Acid	Organism	Predicted Role	Experimental Result	Reference
Gly14	*E. coli*	NADPH binding	G14D resulted in insoluble protein **suggesting** it is part of the NADPH binding motif and that it contributes to maintenance of the secondary or tertiary structure	Kuzuyama *et al*., 2000
Asp152 (Asp150 in *E. coli*)	*Synechocystis* sp. PCC6803	Interaction with the divalent metal ion	D152A resulted in no activity. D152N resulted in little activity, an increase in K_m and significant decrease in k_{cat}/K_m. This **suggests** that the metal ion is essential for catalysis	Fernandes and Proteau, 2006
Glu154 (Glu152 in *E. coli*)	*Synechocystis* sp. PCC6803		E154Q resulted in almost no activity. E154D resulted in no change in K_m, but demonstrated a significant reduction in k_{cat}/K_m. This **suggests** that the positioning of the carboxylate is critical for activity	Fernandes and Proteau, 2006
Glu231	*E. coli*		E231K resulted in a drastic decrease k_{cat} but no change in its K_m, **suggesting** that it is essential for catalysis	Kuzuyama *et al*., 2000; Proteau *et al*., 2004
Glu223 (Glu231 in *E. coli*)	*Synechocystis* sp. PCC6803		E223H and E223Q resulted in no activity, **suggesting** that the residue is essential in catalysis	Fernandes and Proteau, 2006
Ser153 (Ser151 in *E. coli*)	*Synechocystis* sp. PCC6803	Interaction with the substrate DXP or inhibitor (fosmidomycin)	S153A, S153N and S153T resulted in little to no activity. S153N and S153T demonstrated a reasonable decrease in k_{cat}/K_m, while the decrease in k_{cat}/K_m for S153A was drastic, **suggesting** that the residue is vital for optimal arrangement of active site and catalysis	Fernandes and Proteau, 2006
Ser177 (Ser186 in *E. coli*)	*F.tularensis*		S177D and S177E resulted in complete loss of enzyme activity, **suggesting** that the residue is involved in catalysis and is a possible phosphorylation site for isoprenoid regulation	Jawaid *et al*., 2009

His209	*E. coli*	Maintenance of active site architecture	H209Q resulted in significant decrease in k_{cat}/K_m, and a moderate increase in K_m, **suggesting** that it might play a structural role	Kuzuyama *et al*., 2000; Proteau *et al*., 2004
His153	*E. coli*		H153Q resulted in a moderate decrease in k_{cat}/K_m, and no change in K_m **suggesting** that it plays a crucial role in catalysis	Kuzuyama *et al*., 2000; Proteau *et al*., 2004
His155 (His153 in *E. coli*)	*Synechocystis* sp. PCC6803		H155A resulted in an insignificant decrease in K_m, with no change in k_{cat}/K_m, **suggesting** that the residue is not as critical as in *E. coli*	Fernandes and Proteau, 2006
His257	*E. coli*		H257Q resulted in a drastic decrease in k_{cat}/K_m, and interestingly, a decreased K_m, **suggesting** that it affects the structure of the catalytic pocket	Kuzuyama *et al*., 2000; Proteau *et al*., 2004
Trp204 (Trp212 in *E. coli*)	*Synechocystis* sp. PCC6803	Closing of the catalytic hatch over the active site	W204L, W204V, and W204A resulted in little activity. K_m increased significantly as the size of the amino acid side chain decreased. W204L and W204A resulted in drastic reduction in k_{cat}/K_m. This **suggests** that the residue is essential for substrate/inhibitor binding and in discriminating substrates for DXR	Fernandes *et al*., 2005
Met206 (Met214 in *E. coli*)	*Synechocystis* sp. PCC6803		M206V resulted in no activity. M206A resulted in a significantly increased K_m, with a significant decrease in k_{cat}/K_m, **suggesting** that the proper catalytic hatch arrangement is essential for activity	Fernandes and Proteau, 2006

The rigorous analysis of the PfDXR homology model (see Chapter 2) allowed for the identification of significant differences between the EcDXR crystal structure and that of the theoretical PfDXR model. Two interesting differences included the NADPH binding motif residues Val43 and Asn44 in PfDXR were replaced with resides containing small side chains in EcDXR, namely Ala35 and Gly36. The two predicted NADPH binding residues, Val43 and Asn44 were also shown to inhabit very different orientations with respect to their EcDXR equivalents. A highly conserved segment of the catalytic hatch reveals another interesting difference where Asn211 and Ser213 in EcDXR are substituted for two large, positively charged Lys residues in PfDXR. Again, orientation of these residues was significantly different. The aim of this work therefore involved mutation of PfDXR residues by site–directed mutagenesis, to resemble those found in EcDXR. The mutant proteins were then kinetically characterized so that the effects of the mutations could be properly quantified. To our knowledge, these particular amino acid residues present in PfDXR have not been mutated previously and the results could play a role in the rational design of novel DXR inhibitors.

4.2 EXPERIMENTAL PROCEDURES

4.2.1 Materials, special reagents and chemicals

All general chemicals used in this study were of the highest analytical grade. The reagent and supplier information can be seen in Table **C.1**, Appendix C.

4.2.2 Oligonucleotide–directed mutagenesis

For the construction of the pQE30–hPfDXR(VN43,44AG) plasmid, the double mutation, to change Val43/Asn44 to Ala43/Gly44, was created via whole plasmid linear amplification–based (non–PCR) site–directed mutagenesis using the forward primer 5'– GTT AAA GCT CTC TAC GCC GGC AAG TCT GTC AAC G –3' and reverse primer 5'– CGT TGA CAG ACT TGC CGG CGT AGA GAG CTT TAA C –3' (synthesised and purchased from Inqaba Biotec). Similarly, the pQE30–hPfDXR(KK224,226NS) plasmid with the Lys224/Lys226 to Asn224/Ser226 double mutation was created using the forward primer 5'– GCT CTG AAG CAT CCA AAT TGG AGT ATG GGC AAG AAA ATC –3' and reverse primer 5'– GAT TTT CTT GCC CAT ACT CCA ATT TGG ATG CTT CAG AGC–3' (synthesised and purchased from Inqaba Biotec). The primers were designed using the Gene Runner software package (version 3.05).

The mutagenesis reaction mixture was set up as follows: 200 ng pQE30–hPfDXR plasmid DNA, 1 µM forward primer, 1 µM reverse primer, 2.5 units *Pfu* DNA polymerase (Promega), 10 mM dNTPs, 5 µl 10x reaction buffer with $MgSO_4$ (200 mM Tris–HCl [pH 8.8 at 25°C], 100 mM KCl, 100 mM $(NH_4)_2SO_4$, 20 mM $MgSO_4$, 1.0% Triton® X–100, 1 mg/ml nuclease–free BSA), 2.5 µl [v/v] DMSO, 25 mM $MgCl_2$, and sterile milli–Q water to a final volume of 50 µl. Cycling parameters used for the mutagenesis reaction were as follows: 1 cycle of 30 seconds at 95°C; followed by 18 cycles of denaturation, annealing and extension (30 seconds at 95°C, 1 minute at 52°C and 5 minutes at 68°C); 1 cycle of 7 minutes at 68°C; followed by a hold at 4°C. DNA amplification was performed in the GeneAmp PCR system 9700 (PE Applied Biosystems).

The mutagenesis product (40 µl) was treated with 10 units *Dpn*I restriction enzyme, and subsequent to centrifugation at 12 000 x g at room temperature for 1 minute, the *Dpn*I treatment reaction mixture was incubated at 37°C for 12 – 16 hours. A volume of the *Dpn*I treatment reaction mixture was transformed into super–competent *E. coli* JM109 commercial cells (50 µl), according to the protocol described in Appendix **A1**. A single colony from the transformed cells was inoculated into sterile 2x YT broth (5 ml) containing the appropriate antibiotic(s) and incubated at 37°C with shaking overnight (180–200 rpm). The bacterial cells were collected by centrifugation (12 000 x g at room temperature for 1 minute) and plasmid DNA was purified using the Qiagen DNA minipreparation protocol, according to the manufacturer's instructions. Samples were analysed by AGE (see Appendix **A4**) and the presence of the desired mutation and the lack of any undesired second site mutations on the plasmid was confirmed by DNA sequencing (see Appendix **A5**).

4.2.3 Heterologous expression and purification of recombinant PfDXR mutant proteins

E. coli M15[pREP4] cells (100 µl) were transformed appropriate with plasmid DNA [pQE9–EcDXR, pQE30–hPfDXR or pQE30–hPfDXR(VN43,44AG) or pQE30–hPfDXR (KK224,226,NS)] using *the population effect* according to the protocol summarized in Appendix **A1**. A volume of the overnight culture was then inoculated into 240 ml sterile 2x YT broth containing 100 µg/ml ampicillin, such that the absorbance was at 0.1 AU at A_{600nm}. The culture was grown at 37°C with shaking on a platform (180–200 rpm) until the A_{600nm} was approximately 0.4 to 0.6 AU, at which stage production of PfDXR was induced by 1 mM IPTG.

PfDXR solubility was assessed after induction of 4 hours; *E. coli* cells were harvested via centrifugation in an Avanti® JE centrifuge from Beckman Coulter at 6000 rpm at 4°C for 15 minutes. The cell pellet was resuspended in wash buffer (1/20th culture volume) (20 mM Tris–HCl, 300 mM NaCl, 10 mM imidazole, 1 mM $MnCl_2$, pH 7.6, 1 mM PMSF). Cells were frozen overnight, and thawed in the presence of 1 mg/ml lysozyme in 1.5 ml aliquots. Aliquots were thawed on ice and sonicated at 60 amperes (Vibra Cell, Sonics and Materials, USA) at 4°C for 3 x 30 seconds. Cell debris was pelleted after centrifugation at 12 000 x g at 4°C for 15 minutes. Soluble and insoluble (resuspended in 1.5 ml PBS) fractions for the different samples were visualized by SDS–PAGE and western analysis, as described in Appendix **A6** and **A7**.

Subsequent to PfDXR solubilization, soluble protein was purified using the His–spin protein miniprep™ and was carried out according to the manufacturer's instructions (Zymo Research) (Appendix **A8**). Following nickel affinity–based purification, the eluted protein was buffer–exchanged into assay buffer (20 mM Tris–HCl, 300 mM NaCl, 10 mM imidazole, 1 mM $MnCl_2$, pH 7.6) via size exclusion chromatography/gel filtration chromatography (GFC) at 4˚C using a Sephadex G–25 medium (Amersham Biosciences) column (10 cm x 1 cm); twenty, 1 ml fractions were collected. Proteins were monitored at A_{280nm} (100 µl, 96–well microtitre UV plate; Corning Costar) and protein concentration was assessed using a Bradford's protein assay (Appendix **A9**).

4.2.4 NADPH–dependent DXP enzyme assay

The assay, which monitors NADPH reduction, as DXP is converted to MEP is described in full in Appendix **A10**. Experiments were carried out in triplicate for two separate batches of purified enzyme, with the standard deviation shown. Specific activity (µmol/min/mg) for each enzyme was calculated using the straight line of the graph which plotted average absorbance at 340 nm over 10 minutes (ΔA/min).

For the cofactor assays, the experiment was carried out as described in Appendix **A10**; however, Mg^{2+}, Co^{2+} and Mn^{2+} were all tested in independent experiments, in triplicate, in the same plate and under identical conditions. All cofactors were tested at 3 mM and 1 mM concentrations, with no noted difference.

Michaelis Menten and Lineweaver–Burk plots were used to quantify the kinetic constants V_{max}, K_m, and k_{cat}, for both EcDXR and PfDXR. This was done using Prism software, version 5 (www.graphpad.com). For this experiment, varying DXP substrate concentrations were used including: 200, 300, 500, 750, 1000, 1500, 2000, 2500 and 3000 µM.

4.3 RESULTS

4.3.1 Cofactor preference of PfDXR

DXR catalyzes the second step of the MEP pathway whereby the substrate DXP undergoes intramolecular rearrangement and reduction to result in MEP; this reaction step utilizes NADPH, as well as a divalent cation (Kuzuyama *et al*., 2000). DXP is not only an intermediate in the biosynthesis of isopentenyl diphosphate and dimethylallyl diphosphate; it is also involved in the biosynthesis of thiamin in vitamin B1 synthesis and pyridoxine in vitamin B6 synthesis (Hill *et al*., 1996; Cane *et al*., 1999; Cane *et al*., 2000 White, 1978).

Enzymatic activity was assessed in the presence of various divalent cations. Literature demonstrates that numerous cofactor studies have been performed for other DXR enzymes (Takahashi *et al*., 1998; Argyrou and Blanchard, 2004; Takenoya *et al*., 2010); however to date, cofactor studies using PfDXR have only been examined *in silico* (Singh *et al*., 2006). Enzyme activity was therefore quantified in the presence of three cofactors all known to result in activity for numerous DXR enzymes *in vitro* (Chang *et al*., 2009). According to Figure **4.1**, PfDXR was only able to utilize Mn^{2+} and Mg^{2+} as a divalent cation but not Co^{2+}, which resulted in only trace amounts of enzyme activity. EcDXR, on the other hand, was able to utilize all three cofactors, Mn^{2+}, Co^{2+} and Mg^{2+}, with Mn^{2+} resulting in the greatest activity.

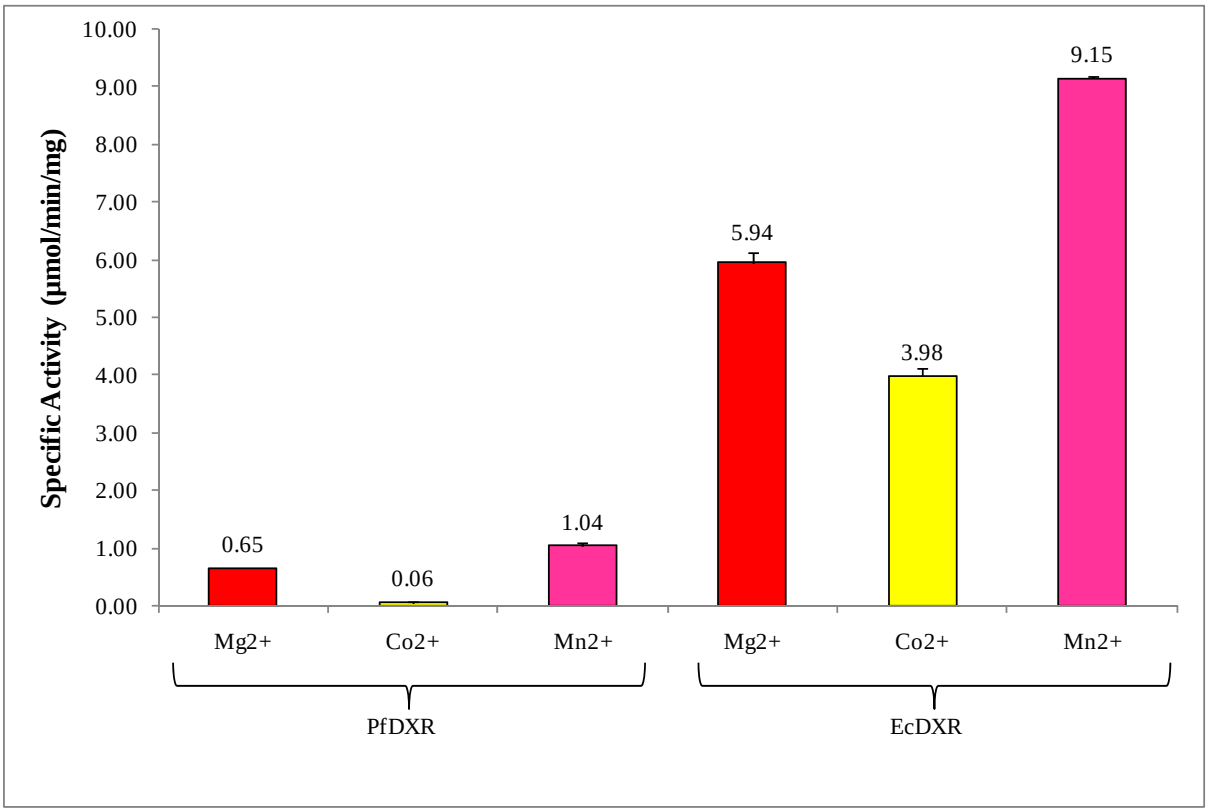

Figure 4.1: The ability of PfDXR and EcDXR to utilize the divalent ions Mn^{2+}, Mg^{2+} and Co^{2+}.
Cofactor studies for PfDXR and EcDXR were carried out using different divalent cations (Mn^{2+}, Mg^{2+} and Co^{2+}) at a concentration of 1 mM each. The experiment was performed in triplicate for two separate batches of purified enzyme, with the standard deviation shown.

Subsequent to the determination of the divalent cation preferences for EcDXR and PfDXR, enzymes were purified and kinetically characterized, in order to quantify the effect that the respective mutations had on activity.

4.3.2 Analysis of structural differences between PfDXR and EcDXR via rational protein engineering

In this work, two novel mutant proteins were engineered to more closely resemble the EcDXR enzyme. The first double mutation engineered the PfDXR NADPH binding residues, Val43 and Asn44 to resemble the EcDXR equivalents, Ala35 and Gly36 (VN43,44AG). The second double mutation resulted from mutation of two charged Lys hatch residues (Lys224 and Lys226), to the polar uncharged EcDXR complements, Asn211 and Ser213 (KK224,226NS) (Figure **4.2**). Mutagenesis studies that have been undertaken, in an attempt to analyze substrate utilization, involved mutating the highly conserved catalytic hatch residues Trp204 and Met206 in SyDXR (Trp212 and Met214 in *E. coli*) (Fernandes *et al.*, 2005; Fernandes and Proteau, 2006) (Figure **4.2**). Similarly, limited mutagenesis studies of

the NADPH binding motif have been endeavoured upon, where mutation of Gly14 to Ala resulted in the mutant protein being insoluble (Kuzuyama *et al*., 2000) (Figure **4.2**).

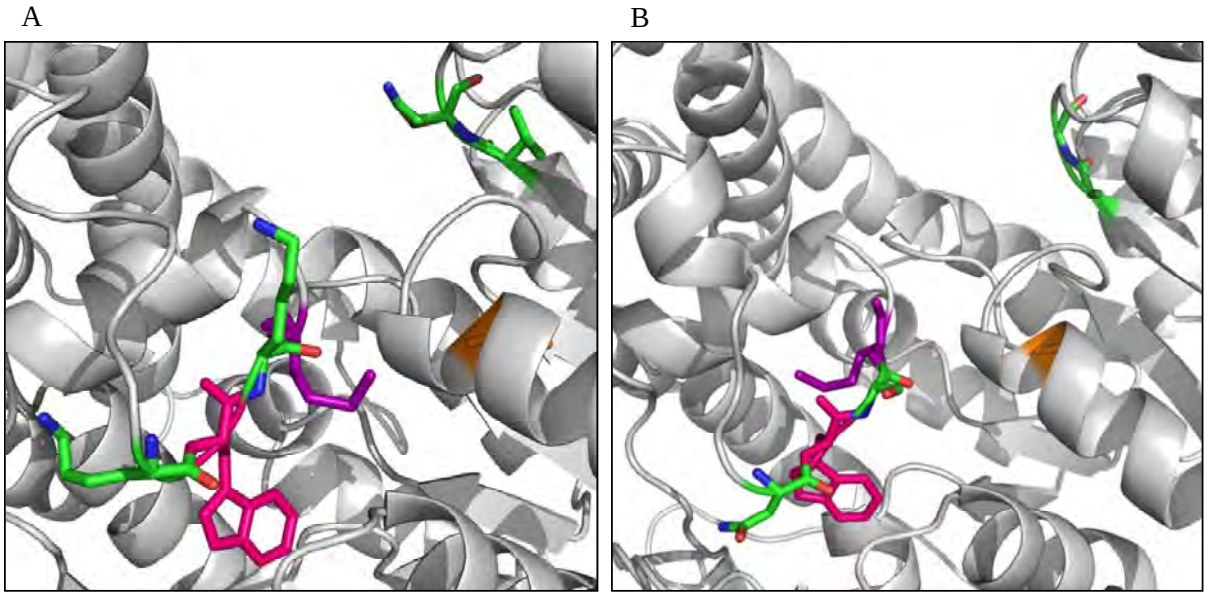

Figure 4.2: Structural differences in the EcDXR and PfDXR catalytic hatch and NADPH binding motif.
(A) Ribbon representation of the PfDXR homology model (created using MODELLER) zoomed into the active site, with the catalytic hatch residues Trp223 (*pink*), Met225 (*purple*), Lys224 (coloured *by element*) and Lys226 (coloured *by element*), and NADPH binding motif residues Gly19 (*orange*), Val43 (coloured *by element*) and Asn44 (coloured *by element*) shown in sticks. (B) Ribbon representation of the EcDXR crystal structure (adapted from Mac Sweeney *et al*., 2005) zoomed into the active site, with the catalytic hatch residues Trp212 (*pink*), Met214 (*purple*), Asn213 (coloured *by element*) and Ser215 (coloured *by element*), and NADPH binding motif residues Gly14 (*orange*), Ala35 (coloured *by element*) and Gly36 (coloured *by element*) shown in sticks. Figures were prepared using PyMol.

According to Figure **4.2A**, the NADPH binding residues Val43 and Asn44 occupy a very different orientation when compared to the EcDXR equivalent residues Ala35 and Gly36 (Figure **4.2B**). Similarly, the catalytic hatch residues Lys224 and Lys226 (Figure **4.2A**), which have large, positively charged side chains, demonstrate a significantly different orientation when compared to the EcDXR equivalents Asn213 and Ser215 (Figure **4.2B**). It is evident that upon binding of the inhibitor and cofactor to PfDXR, significant movement of Lys226 occurs. Potential hydrogen bonding interactions between Ser213 and Ser12, as well as between Asn211 and Ser254/Pro252 exist when fosmidomycin and NADPH are docked into EcDXR (Figure **4.3A**). When comparing the conformation of PfDXR with and without fosmidomycin bound (Figures **4.3B** and **4.3C**), it is evident that the conformation of the Lys hatch residues is significantly different. Subsequent to fosmidomycin entering and binding the PfDXR active site, a potential hydrogen bonding interaction between Pro223 and the side chain nitrogen of Lys224 takes place. However, when no ligand is docked into the PfDXR active site, the position of Lys224 is significantly different and no noted hydrogen bonding

interactions occur (Figure **4.3C**). Hence it can be concluded that upon binding of an inhibitor and cofactor, the PfDXR catalytic hatch changes conformation significantly in order to facilitate its movement over the active site, as is described in the literature (Yajima *et al*., 2002).

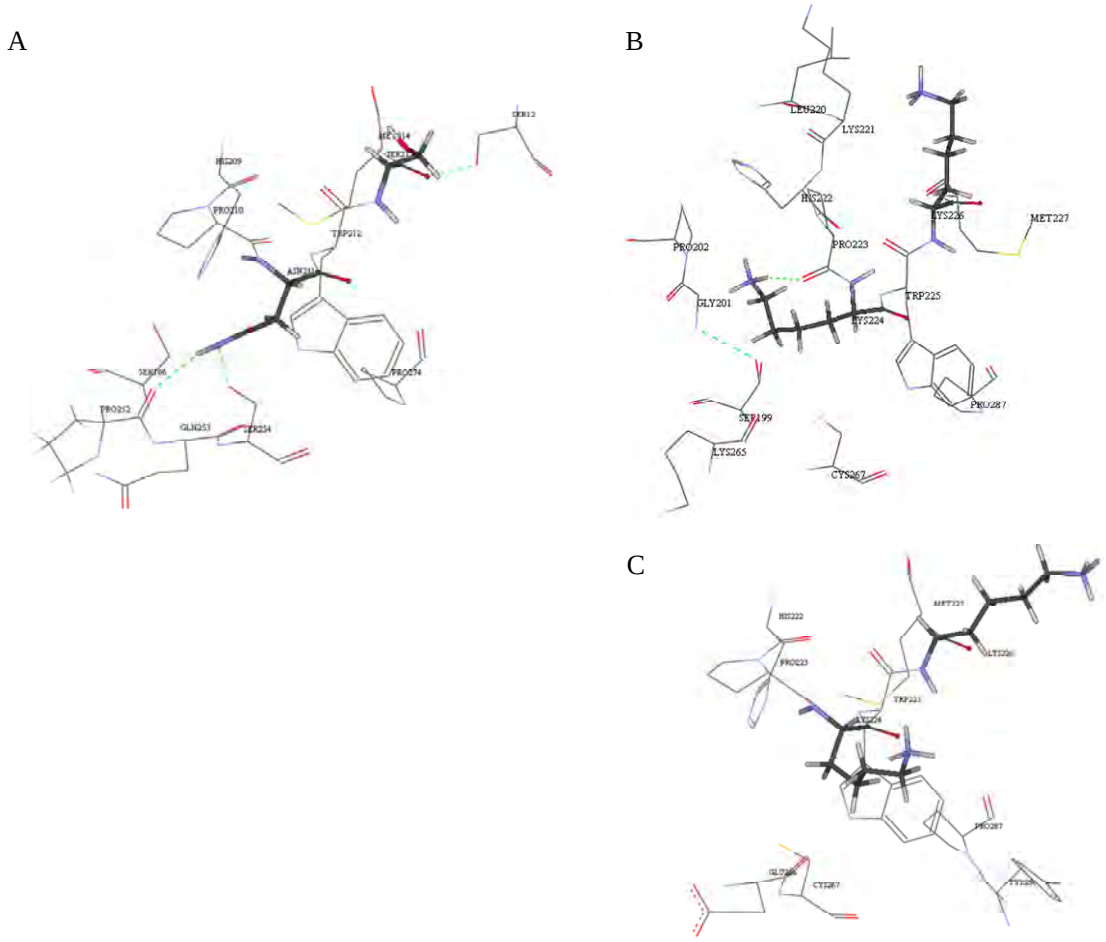

Figure 4.3: Movement of the PfDXR catalytic hatch upon inhibitor binding (legend on next page).
(A) FR900098 docked into *Ec*DXR, showing only the residues within 4 Angstroms of Asn211 and Ser213. Hydrogen bonding is shown in green. (B) FR900098 docked into PfDXR showing only the residues within 4 Angstroms of Lys224 and Lys226. Hydrogen bonding is shown in green. (C) Three–dimensional PfDXR model with only NADPH with no ligand and no cofactor docked, showing only the residues within 4 Angstroms of Lys224 and Lys226. Hydrogen bonding is shown in green.

Subsequent to structural analysis of the highly uncharacterized PfDXR and the well studied EcDXR counterpart, rational protein engineering was endeavoured upon in an attempt to understand and quantify the effects that these structural differences posed. The kinetic characterization of PfDXR was undertaken, with EcDXR included as a control enzyme. The kinetic characterization of the PfDXR mutant enzymes PfDXR(VN43,44AG) and PfDXR(KK224,226NS) was taken on simultaneously in an effort to link the structural differences to function.

4.3.3 Kinetic characterization of PfDXR and PfDXR mutant proteins

Kinetic analyses of EcDXR, PfDXR and PfDXR mutant enzymes PfDXR(VN43,44AG) and PfDXR(KK224,226NS), were undertaken using Michaelis Menten enzyme kinetics (Figure **4.4**). It is evident that EcDXR followed a typical Michaelis Menten hyperbolic curve (Figure **4.4A**), while PfDXR resulted in a very flat curve, with little change in activity from 200 to 3000 µM of substrate (Figure **4.4B**). Concentrations at 50, 75 and 100 µM did not yield a straight–line curve for PfDXR and ΔA/min could hence not be quantified at such extreme sub–saturating conditions. These points were therefore excluded from the Michaelis Menten and Lineweaver–Burk plots for all enzymes tested, including EcDXR, PfDXR and PfDXR mutant proteins. The mutant protein PfDXR(VN43,44AG) (Figure **4.4C**) shared the same flattened curve with PfDXR while the PfDXR(KK224,226NS) mutant protein (Figure **4.4D**) demonstrated a curve more closely resembling EcDXR.

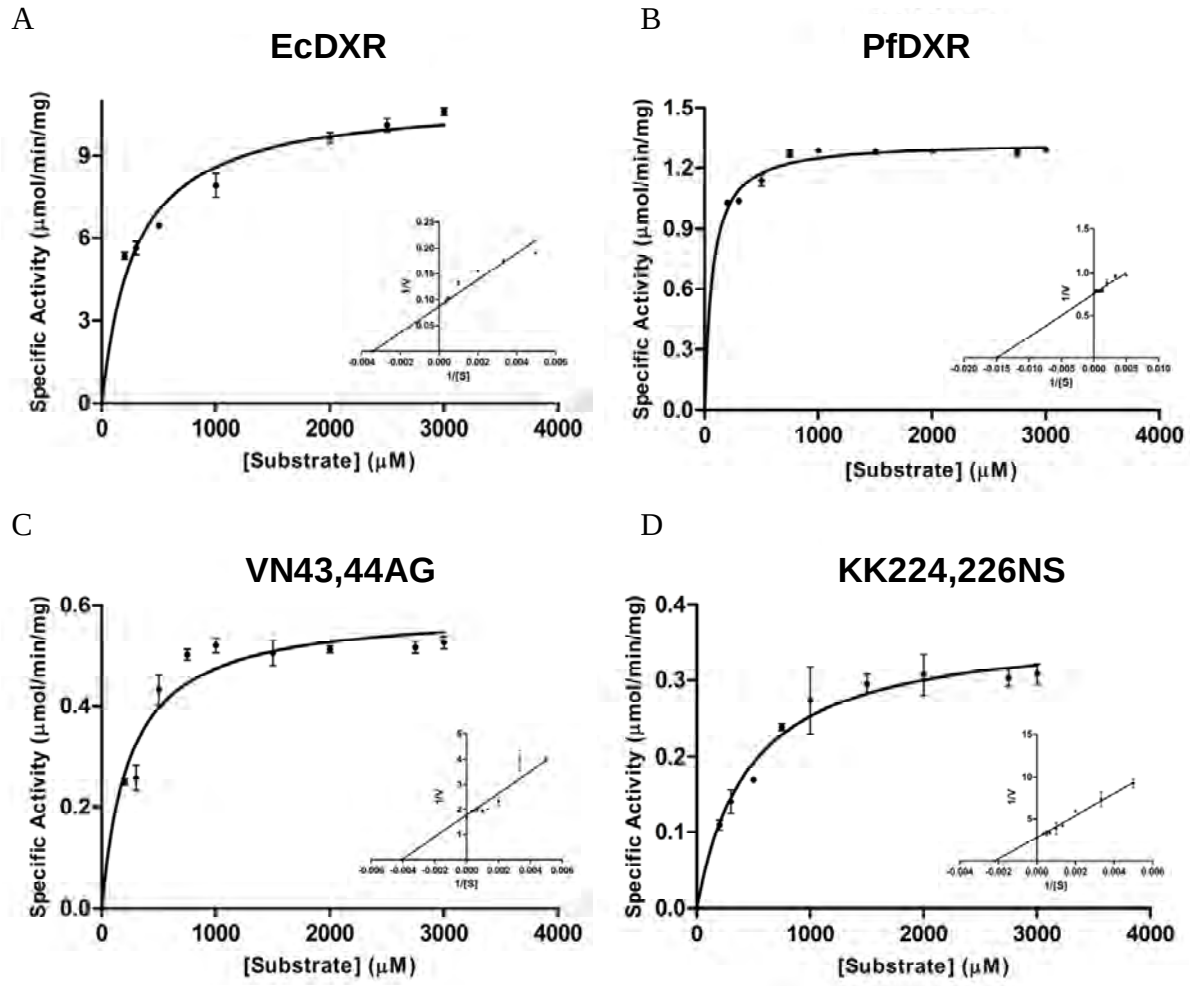

Figure 4.4: Kinetic characterization of EcDXR, PfDXR, and PfDXR mutant proteins PfDXR(VN43,44AG) and PfDXR(KK224,226NS)

Michaelis–Menten and Lineweaver–Burke plots (insert) for EcDXR (A), PfDXR (B), PfDXR(VN43,44AG) (C) and PfDXR(KK224,226NS) (D) at substrate concentrations ranging from 20 – 3000 µM DXP. Prism software, version 5 was used to generate the figures. The experiment was completed in triplicate for two separate batches of purified enzyme, with the standard deviation shown.

Subsequent to the purification of PfDXR (see Chapter 3) a specific enzyme activity of 1.04 ± 0.04 µmol/min/mg was reported for PfDXR, in the presence of Mn^{2+}, while EcDXR demonstrated a 9–fold greater activity of 9.15 ±0.105 µmol/min/mg, which is consistent with ratios reported in the literature (Jomaa *et al*., 1999). In order to assess the kinetics of PfDXR, V_{max}, K_m, k_{cat} and k_{cat}/K_m values were calculated (Table **4.2)**. K_m values have been reported in the literature for numerous DXR enzymes, with values for EcDXR ranging from 0.0031 mM to 0.294 mM (Chang *et al*., 2009). Our results show a K_m of 0.294 mM for EcDXR and 0.067 mM for PfDXR; these values being consistent with the literature, while there appears to be no kinetic parameters reported for PfDXR (Chang *et al*., 2009). The maximal velocity of the reaction whereby DXR converts DXP to MEP was determined to be 1.33 ± 0.10 µmol/min/mg and 11.04 ± 0.13 µmol/min/mg for PfDXR and EcDXR respectively (Table

4.2). In the case of both enzymes, the average specific activity was approximately 20% lower than the maximal velocity of the reaction. This was due to sub–saturating levels of DXP substrate in the assay, which means that the maximal velocity of the reaction was not reached. The kinetic parameter k_{cat}, which is described as the time required by an enzyme molecule to "turnover" one substrate molecule, was also quantified for both enzymes. The literature reports values for other DXR enzymes in the range of 0.04 to 38 s^{-1} for organisms including; *M. tuberculosis*, *Synechocystis* sp., *A. thaliana* and *E. coli* (Fernandes *et al*., 2005; Fox and Poulter, 2005; Walker and Poulter, 2005; Henriksson *et al*., 2006). In this study, we reported values of 17.12 and 2.063 units per second (s^{-1}) for EcDXR and PfDXR respectively (Table **4.2)**, which is consistent with values reported in the literature for EcDXR. K_m can be described as the concentration of substrate at which a half maximal reaction velocity occurs and is often (but not always) a measure of the affinity that the enzyme has for substrate. It is evident that EcDXR has an 8–fold greater K_m when compared to PfDXR, which is interesting because both enzymes share similar catalytic efficiencies (k_{cat}/K_m) of 0.059 and 0.031 for EcDXR and PfDXR respectively (Table **4.2**).

Table 4.2: Summary of EcDXR, PfDXR, PfDXR(VN43,44,AG) and PfDXR(KK224,226NS) kinetic parameters and divalent cation preferences.

	EcDXR	**PfDXR**	**PfDXR(VN43,44AG)**	**PfDXR(KK224,226NS)**
Mg^{2+} (µmol/min/mg)	5.94 ± 0.19	0.65 ± 0.02		
Co^{2+} (µmol/min/mg)	3.98 ± 0.13	0.06 ± 0.03		
Mn^{2+} (µmol/min/mg)	9.15 ± 0.05	1.04 ± 0.04	0.43 ± 0.04	0.14 ± 0.04
V_{max}	11.04 µmol/min/mg	1.33 µmol/min/mg	0.59 µmol/min/mg	0.37µmol/min/mg
K_m	0.294 mM	0.067 mM	0.245 mM	0.461 mM
k_{cat}	17.120 $^{-s}$	2.063 $^{-s}$	0.915 $^{-s}$	0.572 $^{-s}$
k_{cat}/K_m	0.0587	0.0308	0.0037	0.0013

The two PfDXR mutant proteins were also kinetically characterized in order to assess the effect that the respective double mutations posed on enzyme catalysis. The NADPH binding mutant enzyme PfDXR(VN43,44AG) resulted in approximately a 2–fold decrease in maximal reaction velocity (V_{max}) and a 4–fold increased K_m (representative of a decrease in substrate affinity), when compared to the unmutated PfDXR. Interestingly, the PfDXR(VN43,44AG) mutant protein (0.245 mM) resulted in a K_m that more closely resembled EcDXR (0.294 mM), when compared to the wild type PfDXR (0.067 mM). The catalytic hatch mutant protein PfDXR(KK224,226NS) similarly resulted in a 4–fold decrease

in V_{max} and 7–fold increase in K_m (indicative of a decrease in its affinity for substrate) (Table **4.2**). The turnover of DXP (k_{cat}) was reduced with the introduction of the respective mutations, where a 2–fold and 4–fold decrease in k_{cat} was evident for PfDXR(VN43,44AG) and PfDXR(KK224,226NS) respectively, when compared to the wild type PfDXR (Table **4.2**). Because of the increase in K_m and decrease k_{cat}, the amplified result led to a 9–fold and 24–fold decrease in catalytic efficiency (k_{cat}/K_m) for PfDXR(VN43,44AG) and PfDXR(KK224,226NS) respectively (Table **4.2**), when compared to the unmutated PfDXR.

4.4 DISCUSSION

The use of rational protein engineering enables one to structurally study an enzyme. Common rational design strategies include: reshaping the substrate binding site; interfering with cofactor specificity; or introducing charged residues into an active site in order to alter substrate specificity. This is achievable through the use of a three–dimensional structure or a reasonable model derived from sequence alignment (Cedrone *et al*., 2000). Recently, a preliminary X–ray crystallographic study of PfDXR, in the presence of NADPH was carried out with plans to prepare crystals in the presence of metal ions (Umeda *et al*., 2010); the protein yields or enzyme activity were however not reported in this study. The necessitation for tertiary structure analysis of the PfDXR enzyme was therefore facilitated using a PfDXR homology model described in Chapter 2. The docking of known inhibitors into the theoretical PfDXR active site provided structural information that illustrated some important differences between the much studied EcDXR enzyme and PfDXR. The *in silico* analysis of the PfDXR tertiary structure confirmed that the orientations of the two NADPH binding residues in PfDXR (Val43 and Asn44) were significantly different to their EcDXR counterparts (Ala35 and Gly36). Similarly, in a highly conserved part of the catalytic hatch, two Lys residues (Lys224 and Lys226) in PfDXR were significantly different to the smaller EcDXR equivalents (Asn211 and Ser213), which also exhibited significantly different orientations. Upon binding of fosmidomycin into the PfDXR homology model, it was evident there was a greater degree of movement of the two Lys residues; this may be to facilitate movement of NADPH into its binding pocket adjacent to the enzyme's active site.

Numerous site–directed mutagenesis studies have been undertaken for DXR including: residues responsible for cofactor binding, structural residues that support the catalytic residues, residues that interact with the substrate, and residues of the catalytic hatch

(Kuzuyama *et al*., 2000; Reuter *et al*., 2002; Yajima *et al*., 2002; Steinbacher *et al*., 2003; Fernandes *et al*., 2005; Singh *et al*., 2006). No literature however is available for the rational protein engineering of the PfDXR enzyme. Subsequent to the identification of structural differences between the PfDXR tertiary structure and EcDXR crystal structure, site–directed mutagenesis was used to further analyse the relationship between structure and function. A NADPH–dependent DXP enzyme assay was used to assess the effects of various mutations of the PfDXR enzyme, with the well characterized EcDXR enzyme as a control. Complete inhibition of EcDXR and PfDXR by fosmidomycin *in vitro*, validated the assay and provided a benchmark to which all other potential DXR inhibitors were compared. Subsequent to the efficient purification of the respective enzymes, specific enzyme activity was assessed in order to determine whether folded, functional protein was produced. In this study, PfDXR (1.04 ± 0.04 µmol/min/mg) demonstrated a specific activity 9–fold less than that of EcDXR (9.15 ± 0.05 µmol/min/mg), which is consistent with the literature (Jomaa *et al*., 1999). Jomaa *et al*. (1999) reported a specific activity for recombinant *P. falciparum* DXR (6 U/mg), the units were however not specified and protein purity was only 80%. It may be possible that the presence of this His_6–tag negatively influences activity of the purified PfDXR enzyme, but it is most likely improbable because according to the homology modeling study, the tag appears to protrude away from the enzyme. Also, values reported for the His_6–tagged EcDXR are comparable with those reported in the literature. Both mutant enzymes demonstrated a decrease in specific activity when compared to the wild type PfDXR enzyme; where a reduction in specific activity of approximately 2–fold and 10–fold were reported for PfDXR(VN43,44AG) and PfDXR(KK224,226NS) respectively.

Cofactor studies of PfDXR have only been examined *in silico* (Singh *et al*., 2006). Takenoya (2010) examined the effect of cofactors on the activity of the hyperthermophile *T. maritima* DXR and the enzyme could utilize either Mn^{2+} or Mg^{2+} as a divalent cation, but not Co^{2+}. The EcDXR enzyme could utilize Mn^{2+}, Co^{2+} and Mg^{2+}, with Mn^{2+} resulting in the highest activity; no enzyme activity was reported in the presence of Ca^{2+}, Ni^{2+}, Zn^{2+}, Cu^{2+} or Fe^{2+} (Takahashi *et al*., 1998). In two independent homology modeling studies the active site of PfDXR was found to be very similar to that of EcDXR (Singh *et al*., 2006; Goble *et al*., 2010), and it was expected that the same cofactor preference would be seen. This was however not the case, and the findings in this experiment concluded that EcDXR was able to utilize all three cofactors, Mn^{2+}, Co^{2+} and Mg^{2+}, while PfDXR was only able to utilize Mn^{2+} and Mg^{2+} as a divalent cation, but not Co^{2+}, which is consistent with that of TmDXR. While

only single divalent metal concentrations were addressed in this work, numerous studies in the literature have reported standard cation concentrations of 1 mM, hence making it feasible to do so in this work.

For an enzyme to follow Michaelis Menten kinetics, steady state conditions need to be reached. This means the concentration of the substrate–bound enzyme does not change (Michaelis and Menten, 1913). In this work, EcDXR demonstrated kinetics behaviour that was consistent with that of a Michaelis Menten enzyme. PfDXR on the other hand resulted in a flat curve, with the double reciprocal plot (Lineweaver–Burke) demonstrating a concentration of points that were not clearly resolved. According to Bardsley *et al*. (1980) deviations from typical Michaelis Menten kinetics is common in that simple kinetics schemes can produce complicated curves. Similarly, the mutant protein PfDXR(VN43,44AG) generated a non–typical Michaelis Menten hyperbolic curve that was comparable with the unmutated PfDXR, with only a nominal improvement in the points' distribution. Interestingly though, the curve resolved for the catalytic hatch mutant protein PfDXR(KK224,226NS) more closely resembled that of the EcDXR Michaelis Menten curve; the Lineweaver–Burke plot for EcDXR and PfDXR(KK224,226NS) confirmed this by demonstrating a comparable distribution (to each other) with a strong correlation occurring between the reaction velocity and substrate concentration. It may be possible that the mutation of the catalytic hatch could have resulted in the mutant enzyme becoming mechanistically altered so that the enzyme behaved in a manner more closely related to EcDXR. Without sufficient experimental evidence however, one can only speculate at this time. As mentioned, lower concentrations of substrate were tested for PfDXR and the PfDXR mutants, however, in all cases the resultant data that was not quantifiable.

It may therefore be sensible to analyze the kinetic parameters K_m, k_{cat} and k_{cat}/K_m, which may provide some insight into understanding the mechanisms of each of the respective enzymes under review. Analysis of enzymatic activity confirmed that PfDXR exhibited K_m and k_{cat} values that were similar to those of other DXRs in the literature (Chang *et al*., 2009). However, PfDXR demonstrated a very low maximal reaction velocity (V_{max}). This means that PfDXR is not capable of converting large amounts of substrate into product in the cell. This is evident in the value obtained for the k_{cat}, which was 8–fold less than that obtained for EcDXR. The similarity in the enzyme efficiency (k_{cat}/K_m) for EcDXR and PfDXR may be

because PfDXR demonstrated a greater affinity for substrate as reflected in the lower K_m, which offsets its low turnover rate (k_{cat}).

When comparing the K_m of the non–mutated PfDXR with the mutant proteins, it is evident that the NADPH binding mutant protein PfDXR(VN43,44AG) resulted in a K_m only slightly greater than that of the unmutated PfDXR, while the catalytic hatch mutant protein PfDXR(KK224,226NS) resulted in a K_m that was 7–fold greater than that of the unmutated equivalent. According to Fernandes and Proteau (2006), the catalytic hatch is essential for catalysis and for substrate specificity; however, one cannot make assumptions with regards to substrate specificity unless experimentally numerous substrates have been tested. The Michaelis constant, K_m is defined as the concentration at which a half maximal reaction velocity occurs (Michaelis and Menten, 1913); however, it has been indirectly associated with the affinity of an enzyme for a substrate. If this is the case, then one may be able to speculate that increased K_m demonstrated by the catalytic hatch mutant protein PfDXR(KK224,226NS) may have been as a result of the enzyme's decreased affinity for DXP, possibly because the altering the catalytic hatch may have interfered with the ability of the hatch to close over the active site once the substrate had bound.

When considering the effect that the chosen mutations have on the catalytic efficiency (k_{cat}/K_m) of PfDXR mutant enzymes, it is evident that PfDXR(VN43,44AG) and PfDXR(KK224,226NS) induced a significant decrease in catalytic efficiency, when compared to the unmutated PfDXR. In the case of PfDXR(KK224,226NS), the 24–fold decrease in enzyme efficiency (k_{cat}/K_m) appeared to be due to the significant reduction in the enzyme's affinity for the substrate (K_m) coupled to a decreased substrate turnover (k_{cat}). PfDXR(VN43,44AG) however, shared a similar K_m to that of the unmutated enzyme, therefore the 9–fold decrease in catalytic efficiency (k_{cat}/K_m) appeared to be a direct result of substrate turnover (k_{cat}) and not due to substrate affinity. In the literature, mutation of the cofactor–binding residues resulted in either insoluble protein or a drastic reduction in k_{cat} (Kuzuyama *et al*., 2000; Fernandes and Proteau, 2006). One would therefore expect an even greater drop in turnover (k_{cat}) for the NADPH mutant protein than was reported in this study; interestingly, this is not the case. This may be because the mutations did not induce a large enough change in the binding motif, as with the G14D mutant (Kuzuyama *et al*., 2000), which included a large charged Asp residue in place of the small uncharged Gly. The NADPH binding motif may have only been partially disrupted by the introduction of the Val

– an aliphatic hydrophobic residue (as with Ala) – and Asn, a polar but uncharged residue (as with Gly).

In a mutagenesis study for SyDXR Trp204, the W204F mutant protein demonstrated a 2–fold decrease in substrate turnover (k_{cat}), a 2–fold increase in K_m and 40–fold decrease in catalytic efficiency (k_{cat}/K_m) when compared to the unmutated DXR (Fernandes *et al*., 2005). These ratios are consistent with the PfDXR(KK224,226NS) kinetics data put forward in this study. The authors reported that with a decrease in the size of the aliphatic side chain, for the W204L, W204V, and W204A mutant proteins, there was a decrease in enzyme activity (Fernandes *et al*., 2005). In light of this, it was presupposed that the mutation of the two large, positively charged Lys residues for the smaller polar EcDXR equivalents, Asn and Ser, may have elicited a greater decrease in overall catalytic efficiency. While a 24–fold decrease in enzyme efficiency (k_{cat}/K_m) was reasonably large, when compared to the values reported in the literature (280–fold decrease for M206A and a 7000–fold decrease for W204A) (Fernandes and Proteau, 2006), the change was not as drastic. It can however be hypothesized that the change in catalytic efficiency indicated that the two Lys residues form a vital part of the catalytic hatch and mutation to a residue such as Ala, may have resulted in an even greater reduction in k_{cat}/K_m, more comparable with values reported in the literature.

This work however presents a major limitation in that because specific activity values reported for PfDXR are very low and data could not be captured for substrate concentrations lower than 200 µM. For PfDXR, the concentration of substrate that yielded a half maximal velocity (K_m = 0.67 µM) was 3 times less than that of the lowest data point value (200 µM), meaning that a degree of error may be anticipated. Initial screening however enabled us to quantify PfDXR specific activity at concentrations equivalent to its K_m, with the higher values being comparable to those reported in this work; this was however not achieved for all three purification batches reported here and therefore the data was not included. Therefore, it is acceptable to draw accurate conclusions about PfDXR kinetics from this work, despite the fact that the data at lower concentrations (below 200 µM) was excluded.

In conclusion, *in silico* analysis was used to identify differences in the PfDXR tertiary structure, when compared to the well documented EcDXR. Rational protein engineering was therefore used to better understand the importance of these residues and their impact on the enzymes' kinetics. The catalytic hatch mutant protein PfDXR(KK224,226NS) resulted in a

far greater reduction in catalytic efficiency when compared to the NADPH binding mutant protein PfDXR(VN43,44AG). In the case of the hatch mutant, it may be possible to completely disrupt the hatch by introducing small, non–polar residues such as Ala. The fact that the NADPH binding mutant did not produce a more efficient DXR (by mutating the NADPH binding motif to more closely resembles EcDXR), is probably because these two mutations may not have been sufficient to functionally alter PfDXR to resemble EcDXR.

CHAPTER 5

THE *IN SILICO* AND *IN VITRO* PARALLEL SCREENING OF NOVEL DXR INHIBITORS

5.1 INTRODUCTION

Since the discovery of fosmidomycin in the late 1970's (Okuhara *et al*., 1980), numerous compound libraries have been reported to be effective against the DXR target enzyme. However, due to the recalcitrant nature of *P. falciparum* DXR, inhibitor screening has predominantly been carried out using other DXR homologues, such as *E. coli* and *Synechocystis* sp. (reviewed by Singh *et al*., 2007). Table **5.1** summarizes numerous efforts in DXR inhibitor synthesis and screening.

Fosmidomycin has been reported to inhibit PfDXR, EcDXR, MtDXR and SyDXR at a half maximal inhibitory concentration (IC_{50}) of 32 – 310 nM (Chang *et al*., 2009), thus providing a reasonable backbone from which to develop new inhibitor libraries. Most inhibitor libraries described in the literature represent analogues of fosmidomycin that incorporate a phosphonate moiety; however, some groups have moved away from compounds containing this highly charged group (Woo *et al*., 2006), because it has been associated with poor uptake into cells, resulting in the poor bioavailability of novel drugs that target DXR (Knipe and Howley, 2007). Woo *et al.* (2006) assessed the inhibitory activity of compounds boasting phosphate (6, 7), carboxylate (8), a sulfamate (9) head groups (Table **5.1**). However it was found that the phosphonate group was necessary for inhibitory activity where K_i values (indicative of the inhibitory dissociation of the enzyme–substrate complex), for the respective groups where quantified. While phosphate derivatives exhibited K_i values even lower than fosmidomycin, the carboxylate and sulfamate compounds resulted in significantly increased values in K_i of approximately 4000–fold and 50 000–fold respectively (Table **5.1**). Other sulfone and sulfonamide derivatives resulted in poor inhibitory activity when compared to fosmidomycin and FR900098, the benchmark against which all inhibition studies are compared (Perruchon *et al*., 2008).

The effects of altering the hydroxamic tail group (N–formyl/N–hydroxyl) found that the N–formyl/N–methyl (10), N–acetyl/N–methyl (11) and reversed hydroxamate (12) inhibitors resulted in very poor inhibition in the mM range. Extensions at the hydroxamic tail end

reported little success (Ortmann *et al*., 2007; Gieβmann *et al*., 2008) (Table **5.1**). However, other groups have reported successful use of this strategy. For example, some phosphonohydroxamic acid analogues demonstrated EcDXR inhibition comparable to fosmidomycin (Kuntz *et al*., 2005)

Inhibitors resulting from changes to the 3–carbon spacer have resulted in good inhibition, where α–substituted analogues containing a phenyl moiety resulted in only nominally decreased inhibition activity (IC_{50}); the size of the phenyl side chains had a direct effect on inhibition efficiency as well. The same compound series was tested *in vitro* for antimalarial potential and it was found that compounds that contained chlorinated phenyl side chains resulted in up to 12–fold greater antimalarial activity when compared to fosmidomycin (Haemers *et al*., 2006). Other successful changes to the 3–carbon spacer include the cyclopropyl analogues published by Devreux *et al* (2006); both DXR inhibition and antimalarial activity were reported for some compounds in the nM range. Reverse analogues of fosmidomycin (Behrendt *et al*., 2010) also possess phenyl substitutions at the α–position, which may promote their lipophilicity, potentially facilitating their entry into cells (Behrendt *et al*., 2010), as was hypothesized by Haemers *et al*. (2006). These reverse analogues were tested against EcDXR and PfDXR and resulted in inhibition activity comparable with fosmidomycin. Interestingly enough, the compounds were 50 to 80–fold more effective at inhibiting PfDXR when compared to EcDXR inhibition. The finding by Gieβmann *et al*. (2008) did however not report the same variation in IC_{50} values for EcDXR and PfDXR; in this study, inhibitors responded similarly for each of the respective enzymes.

Numerous groups have been involved in the synthesis of DXP substrate analogues, with little or no success. Analogues lacking hydroxyl C3/C4 (Hoeffler *et al*., 2002), as well as fluoro analogues (Wong *et al*., 2004; Fox and Poulter, 2005; Walker and Poulter, 2005) inhibited EcDXR and SyDXR in the high μM range, with some only demonstrating half maximal inhibitory concentrations in the mM range. Attempts have also been made to inhibit DXR via the blocking of the cofactor binding site Herforth *et al*. (2004) reported the synthesis of more than 40 N_6–substituted adenosine derivatives of NADPH. While some compounds resulted in efficient inhibition of EcDXR, none resulted in antimalarial activity in the nM range. Interestingly though, one of the type IV adenosine derivatives, which demonstrated antimalarial activity in the low μM range, was significantly smaller in size when compared to the lead type IV structure (Herforth *et al*., 2004).

Table 5.1: Summary of DXR inhibition (IC_{50}) and antimalarial activity (μM) for DXR inhibitors reported in the literature. n.d. = not determined.

Group and Structure	Inhibitor	DXR Inhibition			Antimalarial Activity	
		IC_{50} (μM) EcDXR*	**IC_{50} (μM) PfDXR**	**IC_{50} (μM) SyDXR***	**IC_{50} (μM)**	***P. fal* strain**
Fosmidomycin and acetyl analogue (Jomaa *et al*., 1999)						
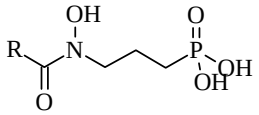 FR900098: R = CH_3 2b: R = phenyl 2C: R = benzyl	chloroquine				0.200 ± 0.030	DD2
	fosmidomycin				0.290 ± 0.130	DD2
	FR900098				0.090 ± 0.020	DD2
Fosmidomycin methyl–phenyl analogue (Tahar and Basco, 2007)						
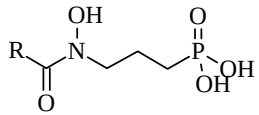 α–(p–methyl–phenyl)	fosmidomycin				0.301 ± 0.112	fresh clinical isolates
	FR900098				0.118	
	TH II46				0.249	
Phosphonohydroxamic acid analogues (Kuntz *et al*., 2005)						
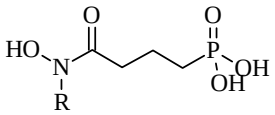 7: R = H 8: R = CH_3	fosmidomycin	0.032				
	7	0.170				
	8	0.048				
α–Substituted fosmidomycin analogues (Haemers *et al*., 2006)						
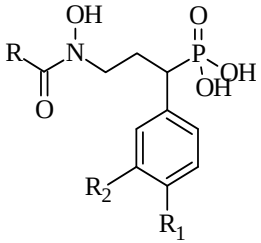 1: R = H 2: R = CH_3 a: R_1 = R_2 = H b: R_1=Me; R_2 =H c: R_1= OMe; R_2 = H d: R_1=Cl; R_2 = H e: R_1 = R_2 = Cl	fosmidomycin	0.030 ± 0.008			0.360	DD2
	FR900098	0.030 ± 0.008			0.180	DD2
	2a	0.311 ± 0.012			0.350	DD2
	2b	0.396 ± 0.061			0.220	DD2
	1c	0.156 ± 0.043			0.200	DD2
	2C	0.459 ± 0.109			0.270	DD2
	2d	0.099 ± 0.026			0.095	DD2
	1e	0.059 ± 0.020			0.028	DD2
	2e	0.119 ± 0.019			0.090	DD2

Cyclopropyl analogues of fosmidomycin (Devreux *et al*., 2006)

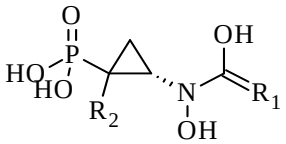

4: *rac cis*; $R_1 = CH_3$; R_2 = phenyl
3a: *rac trans*; $R_1 = CH_3$; $R_2 = H$
3b: $R_1 = CH_3$; $R_2 = H$
3c: $R_1 = R_2 = H$
3d: R_1 = ethyl; $R_2 = H$

fosmidomycin	0.048		0.048	DD2
FR900098	0.058		0.028	DD2
3a	0.160		n.d.	
3b	0.050		0.032	DD2
3c	0.313		2.1	DD2
3d	>3		n.d.	
4	>3		n.d.	

Fosmidomycin analogues (Woo *et al*., 2006)

6/7: 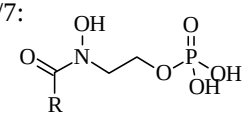

8: 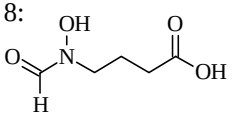

9: 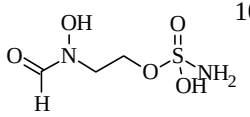

10/11: 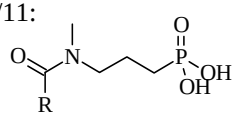

12: 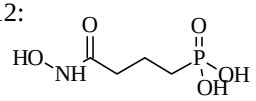

6/10: R = H
7/11: R = CH_3

	K_i (μM) SyDXR
fosmidomycin	0.057
FR900098	0.9
6	0.019
7	0.002
8	240
9	2 800
10	5 000
11	3 600
12	4

Fosmidomycin derivatives with spacious acyl residues (Ortmann *et al*., 2007)

7: 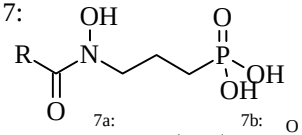

7a: 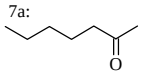

7b: 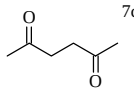

7c: 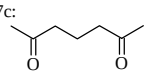

7d: 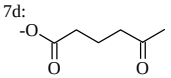

7e: 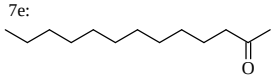

7f: 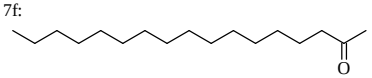

7g: 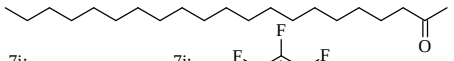

7h: 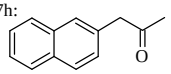

7i: 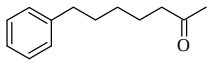

7j: 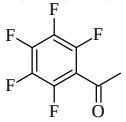

fosmidomycin	0.035
FR900098	0.035
7a	10
7b	20
7c	5.4
7d	>30
7e	9
7f	5.6
7g	>30
7h	15
7i	5.1

7j	1.3	

Non–hydrolyzable phosphate mimics (Gieβmann *et al*., 2008)

24:

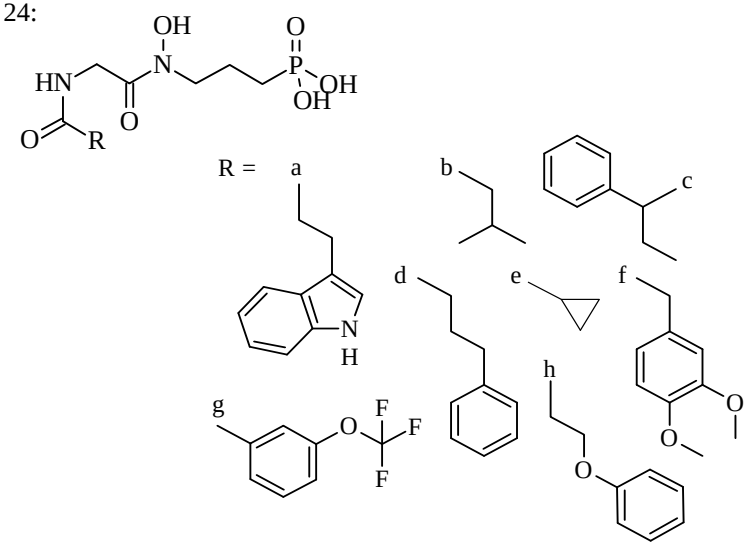

fosmidomycin	0.050	0.032
FR900098	0.051	0.018
2b	0.130	0.061
2C	13	n.d.
15	>30	n.d.
23a – i	>30	n.d.
24a	17	6.6
24b	12	9.6
24c	20	9.3
24d	19	20
24e	7.10	3.3
24f	14	12
24g	5.10	2.9
24h	1	0.400

Sulfone and sulfonamide derivatives of FR900098 (Perruchon *et al*., 2008)

fosmidomycin	0.035
FR900098	0.035
3–(acetyl(hydroxy)amino)propyl]phosphonic acid 3–methylbutyl ester	2.1
3–(acetyl(hydroxy)amino)propyl]phosphonic acid mono(2–naphthalen–1–yl–ethyl) ester	2.4
3–(acetyl(hydroxy)amino)propyl]phosphonic acid mono(2–naphthalen–2–yl–ethyl) ester	1.6
3–(acetyl(hydroxy)amino)propyl]phosphonic acid mono–n–butyl ester	3.9
3–(acetyl(hydroxy)amino)propyl]phosphonic acid mono–n–propyl ester	16
3–(acetyl(hydroxy)amino)propyl]phosphonic acid monomethyl ester	50
3–(acetyl(hydroxy)amino)propyl]phosphonic acid monophenethyl ester	0.49
3–(acetyl(hydroxy)amino)propyl]phosphonic monoethyl ester	23

Reverse analogues of fosmidomycin (Behrendt *et al*., 2010)

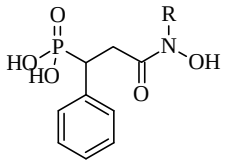

12: R = H
14: R = CH_3

fosmidomycin	0.221 ± 0.015	0.143 ± 0.016	3.71 ± 2.47	K1
FR900098	0.131 ± 0.003	0.015 ± 0.001	1.48 ± 0.84	K1
12	0.592 ± 0.025	0.012 ± 0.003	3.87 ± 1.81	K1
14	0.243 ± 0.030	0.003 ± 0.000	0.59 ± 0.20	K1

N_6–substituted adenosine derivatives of NADPH (Herforth *et al*., 2004)

lead (type IV)

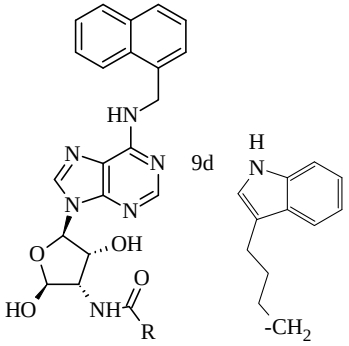

9d

		% Inhibition EcDXR		
	1	0	3.2	DD2
	6	0	12	DD2
	7	0	11	DD2
Type IV adenosine derivatives				
4–Phenylbutanamido	9a	38	18	DD2
4–(2–Thienyl)butanamido	9b	30	18	DD2
4–(2,4,–Dichlorophenoxy)butanamido	9c	41	15	DD2
4–(3–Indolyl)butanamido	9d	75	2.8	DD2
Type II adenosine derivatives				
H	10a	0	12	DD2
Acetamido	10b	0	23	DD2
Propanamido	10c	0	15	DD2
Cyclopropanamido	10d	0	11	DD2
(3–Thienyl)acetamido	10e	0	11	DD2
2–Phenylbutanamido	10f	0	6.2	DD2
4–(3–Indolyl)butanamido	10g	45	8.5	DD2
Diphenylacetamido	10h	50	6.2	DD2
4–(2,4–Dichlorophenoxy)butanamido	10i	0	10	DD2
trans–3–[(4–Chloro–3–nitro)phenyl]prop–2–enamido	10j	52	5.3	DD2
trans–3–[(3–Nitro–4–propylamino)phenyl]prop–2–enamido	10k	33	4.8	DD2
3–Methoxybenzamido	10l	0	11	DD2
(4–Cyclopropylamino–3–nitro)benzamido	10m	0	26	DD2

lead (type II)

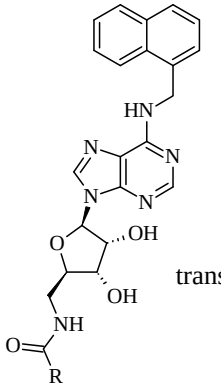

lead (type III)	4–(1–Methylethyl)amino–3–nitro)benzamido	10n	0		4.1	DD2
	3–Nitro–4–(pyrrolid–1–yl)benzamido	10o	0		15	DD2
	(4–Cyclopentylamino–3–nitro)benzamido	10p	47		4.8	DD2
	3–Nitro–4–(piperid–1–yl)benzamido	10q	0		14	DD2
	4–(Morphol–1–yl)–3–nitro]benzamido	10r	0		4.8	DD2
	(4–Dibutylamino–3–nitro)benzamido	10s	70		4.2	DD2
	[4–(2–(2–Methoxyphenyl)ethylamino)–3–nitro]benzamido	10t	58		1.3	DD2
	[4–(Morphol–1–yl)–3–(4–nitrobenzamido)]benzamido	10u	27		12	DD2
	[3–Acetamido–4–(morphol–1–yl)]benzamido	10v	0		5	DD2
	3–Acetamido–4–(piperid–1–yl)benzamido	10w	24		4.2	DD2
	3–Acetamido–4–(N–benzyl–N–ethyl)benzamido	10x	65		3.3	DD2
	4–[2–(2–Methoxyphenyl)ethylamino]–3–propanamido}benzamido	10y	0		2.7	DD2
	3–tert–Butyloxycarbonamido–4–(morphol–1–yl)]benzamido	10z	0		3.1	DD2
	(3–Acetamido–4–dibut–1–ylamino)benzamido	10a1	59		3.7	DD2
	(4–Dibut–1–ylamino–3–butanamido)benzamido	10b1	53		3.2	DD2
	[4–(1–Methylethyl)amino–3–propanamido]benzamido	10c1	0		3.2	DD2
	50–Deoxy–N6–(1–naphthylmethyl)–50–pthalimidoadenosine		0		11	DD2
	1–(6–Chloropurin–9–yl)–b–d–1,5–dideoxy–(5–phthalimido)ribofuranose		42		42	DD2
	Type III adenosine derivatives					
	H	11a	41		2.1	DD2
	4–(3–Indolyl)butanamido	11b	48		3.7	DD2
	3–Methoxyphenylacetamido	11c	0		14	DD2
	[3–Acetamido–4–(morphol–1–yl)]benzamido	11d	0		3.2	DD2
	N6–(1–Biphenylmethyl)–50–deoxy–50–phthalimidoadenosine		0		4.3	DD2

<u>DXP analogues lacking hydroxyl C3/C4</u> (Hoeffler *et al*., 2002)

19: 14:

	IC_{50} (μM) EcDXR	**IC_{50} (μM) SyDXR**
14	800	150
19	120	30

Fluoro analogues of DXP (Wong *et al*., 2004)

6: 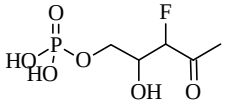

7: 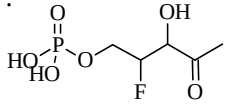

6	444	
7	773	

Fluoro analogues of DXP (Fox and Poulter, 2005)

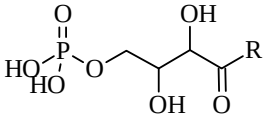

1: R = CH_2F
2: R = CHF_2
3: R = CF_3
4: R = ethyl

1	2000	
2	3400	
3	substrate	
4	6200	630

DXP analogues (Walker and Poulter, 2005)

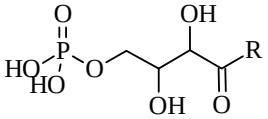

1: R = $CH_2(OH)$
2: R = NH(OH)
3: R = OMe
4: R = NH_2
5: R = OH
6: R = amide

1	310	
2	>5000	
3	1024	
4	253	90
5	551	
6	>5000	

* In some cases, IC_{50} values were not reported and the authors used % inhibition or Ki values as a measure of inhibition instead – this is clearly shown on the table, with an indication of where the reporting of IC_{50} values resumes

Numerous *in vivo* experiments with fosmidomycin have been undertaken; the first was reported by Jomaa *et al*. (1999), where mice infected with the rodent malaria parasite *P. vinckei* were treated from day 1 after infection to day 4. Even at doses as low as 5 mg/kg fosmidomycin (and FR900098), mice appeared to be free of parasites. However, since then, fosmidomycin resistance has resulted in the need for combination therapies (Borrmann *et al*., 2005). For example, fosmidomycin was used in combination with clindamycin for the treatment of acute uncomplicated malaria from *P. falciparum*. Although the drugs were well tolerated, the combination therapy involved dosages of fosmidomycin of 75 mg/kg (because of the anticipated short half–life in plasma) and an unacceptably high rate of recrudescence was reported (Wiesner *et al*., 2002). *In vitro* activity of fosmidomycin and its closest derivatives were also tested against clinical isolates of *P. falciparum*, taken from malaria–infected humans in Cameroon. The study concluded that fosmidomycin was 50–100 times less potent that other antimalarial drugs such as mefloquine, lumefantrine, atovaquone and artemisinin derivatives (Tahar and Basco, 2007).

In light of this, the need for new drug therapies arises, which are potent against malaria and do not demonstrate attributes such as poor oral bioavailability with poor resorption, as is the case with fosmidomycin (Singh *et al*., 2007). The aim of this work involved the *in vitro* and *in silico* screening of a library of 46 novel potential DXR inhibitors. The broad objectives entailed screening the compound library for DXR–inhibition potential, by way of an NADPH–dependent DXP assay, using purified PfDXR and EcDXR enzyme. Further *in vitro* analysis involved quantifying antimalarial potential of these compounds using *P. falciparum*–infected erythrocyte tissue culturing. Run in parallel to this, the compound library was screened *in silico* for qualification of potential binding affinity and theoretical ligand efficiency.

5.2 EXPERIMETNAL PROCEDURES

5.2.1 Materials, special reagents and chemicals

All general chemicals used in this study were of the highest analytical grade. The reagent and supplier information can be seen in Table **C.1**, Appendix C.

5.2.2 *In silico* docking of novel compounds into PfDXR homology model

Docking was carried out in exactly the same manner as described in Chapter **2.2.3**.

5.2.3 *In vitro* screening of novel compounds using an NADPH–dependent DXP assay

The assay, which monitors NADPH reduction, as DXP is converted to MEP, is described in full in Appendix **A10**. Screening experiments were completed in triplicate for two separate batches of PfDXR and EcDXR enzyme. Specific activity (µmol/min/mg) for each enzyme was calculated using the straight line of the graph which plotted average absorbance at 340 nm over 10 minutes (ΔA/min). Compounds were tested at a single concentration of 250 µM (in 10% DMSO) with PfDXR and EcDXR in independent experiments, in triplicate, in the same plate and under identical conditions. Initial screening was done at inhibitor concentrations between 100 and 500 µM, with 250 µM being the first concentration at which no potential inhibitor gave complete inhibition – this concentration was therefore used for screening. Specific activity for each compound was represented as a percent of the untreated sample, where the experiment containing no compound was treated as 100%.

5.2.4 *P. falciparum*–infected erythrocyte growth assays

The novel compounds were screened for their effect on the growth of *P.falciparum* in infected erythrocytes. Fresh human type–O blood was extracted and washed with complete medium (RPMI 1640 liquid with L–glutamine, 0.05 g/l gentamicin, 0.088 g/l hypoxanthine, 5 g/l Albumax II, 6 g/l HEPES, $1/20^{th}$ volume 5% $NaHCO_3$ [v/v]) at a ratio of 1:1. The sample was centrifuged at 1200 x g at room temperature for 5 minutes. The supernatant was removed and the wash step was repeated so that only red blood cells remained (Dzinjalamala *et al*., 2005). Erythrocytes were stored at 4^oC until use.

P.falciparum 3D7 parasite stocks (–80^oC) were thawed quickly at 37^oC in a water bath. Parasitized red blood cells (PRBC) were transferred to a 50 ml falcon tube and 1 volume 12% NaCl (37^oC) was added to 5 volumes PRBC in a dropwise manner with constant swirling. This was incubated at room temperature for 5 minutes before 10 ml of 1.8% NaCl (37^oC) was added dropwise. PRBCs were collected via centrifugation at 750 x g at room temperature for 5 minutes. PRBCs were then resuspended in 20 ml complete medium (37^oC) supplemented with 10% human type–O erythrocytes. Cultures were kept at 37°C under an atmosphere of 5% O_2, 3% CO_2, and 92% N_2 (Dzinjalamala *et al*., 2005).

P. falciparum–infected erythrocytes were cultivated in the manner described above and every 24 hours, parasitemia was assessed using Giemsa staining (10% Giemsa stain made up with PBS). Ring–stage parasites were synchronized weekly by the addition of 5 volumes of 5%

sorbitol (37^{o}C). This was incubated at 37^{o}C for 10 minutes before being centrifuged at 750 x g at room temperature for 3 minutes in order to collect the PRBCs (Dzinjalamala *et al*., 2005).

Drug screening was carried out using the parasite lactate dehydrogenase (pLDH) assay completed in a 96–well microtitre UV plate (Corning Costar). A 2% haematocrit and 2% parasitemia were prepared subsequent to parasitemia quantification by counting a minimum of 100 cells in a minimum of 10 views, using a 100 x magnification on a light microscope. The assay was blanked using 100 µl 2% haematocrit in 100 µl complete medium (RBC). Test samples were assayed in triplicate in a reaction containing 100 µl 2% parasitemia and 100 µl compound (250 µM in 10% DMSO). Fosmidomycin (1 µM) and selected compounds (250 µM in 10% DMSO) were tested at a single concentration of 250 µM; the rationale for testing at this concentration was such that compounds were quantified at a uniform concentration for DXR inhibition, as well as growth inhibition Controls included: chloroquine (1 µM in 10% DMSO), fosmidomycin (1 µM) and 2% parasitemia with no compound, containing 10% DMSO. Plates were kept at 37°C under an atmosphere of 5% O_2, 3% CO_2, and 92% N_2 for exactly 48 hours (Dzinjalamala *et al*., 2005). Control inhibitors chloroquine and fosmidomycin were quantified in the micromolar range, even though their IC_{50} vales are reported to be in the nanomolar range *in vitro*; this was done to ensure that a reasonable kill response of parasites/ mammalian cells was achieved.

To develop plates, 100 µl malstat (50 mM Tris–HCl, 4 g/l L–lactate, 1/500th [v/v] Triton X–100, 0.11 g/l APAD) was added to 15 µl of the cell suspension. Subsequent to this, 25 µl NBT (1.6 g/l nitro blue tetrazolium salt, 0.08 g/l phenazine ethosulphate) was added to the cell suspension. Air bubbles were removed and absorbance was measured at 620 nm (Dzinjalamala *et al*., 2005). All samples were quantified as % viability, where the 2% parasitemia control sample containing no compound, with 10% DMSO was treated at 100% viability.

5.2.5 Human cell line growth assays

The WST assay was used to confirm the anti–proliferative effects of selected compounds on Hst578T cancer cell line. The assay is based on the reduction of WST–1 by viable cells to produce a soluble formazan salt.

Plates were seeded with 5000 cells/well in 100 µl and incubated overnight at 37ºC in an atmosphere of 5% CO_2 for 16 hours. Thereafter the cells were dosed with 250 µM of the test compound (in 10% DMSO) (100 µl) in quadruplicate and incubated for 48 hours as before. After which, 10 µl of 5 mg/ml WST–1 reagent was added to each well before incubating at 37ºC in an atmosphere of 5% CO_2 for a further 4 hours before absorbance was quantified at 450 nm. The chemotherapeutic drug paclitaxel (Invitrogen) was used as a control cytotoxic compound at 250 nM concentrations (Lawson *et al.*, 2009). Other controls included a 10% DMSO solvent control and a media and compound negative control (no cells). Fosmidomycin (1 µM) and selected compounds (250 µM in 10% DMSO) were tested at a single concentration of 250 µM; again the rationale of testing at this concentration was such that compounds were quantified at a uniform concentration. The percentage of viable cells was quantified for each compound and was represented as a percent of the untreated sample containing DMSO, where the experiment containing no compound was treated as 100%. Paclitaxel and fosmidomycin were quantified against an untreated sample containing no DMSO. T–tests were quantified for each compound tested, whereby the means of two groups (control and treatment) were compared. The degrees of freedom (df) and alpha level were set at 2 and 1 respectively.

5.3 RESULTS

5.3.1 *In silico* docking of novel compounds into PfDXR homology model

AutoDock 4.2 was used to dock 48 compounds for the purpose of analysing the potential binding affinity (kcal/mol) and the relative ligand efficiency. The catalytic residues were made flexible in order to more closely represent the *in vivo* environment of the PfDXR enzyme.

The compound library can be divided into two distinct groups, namely fosmidomycin analogues (42) and analogues of known antimalarial natural products (4). The fosmidomycin analogues varied in structure in a number of ways. Firstly, changes were made to hydroxamic acid moiety to include a phenyl group. Secondly, the carbon spacer length was adjusted to include a 2–carbon spacer (201–207. 201a–207a, 201Na–207Na) and 3–carbon spacer (301–307, 301a–307a, 301Na–307Na) between the phosphonate moiety and hydroxamic acid. Lastly, changes were made to the phophonate moiety, where 201–207 and 301–307 groups included phosphonate esters; 201a–207a and 301a–307a had a typical

phosphonate moiety; and 201Na–207Na and 301Na–307Na included a negatively charged phosphonate group as a result of the dissociation of the sodium group when compounds were dissolved in water, yielding a negative charge. Novel compounds were synthesized by Mr M. Mutorwa in a collaborative effort with the Department of Chemistry, Rhodes University, Grahamstown, South Africa. All the structures are presented in Figure **5.1**

The analogues of known antimalarial natural products were derived from structures relating to isopimarane diterpenoid natural products, isolated from the Iranian tree *Platycladus orientalis* (Asili *et al*., 2004). These analogues have different phenyl side chains including 4–chlorophenyl– (140–1A), 3–chlorophenyl– (140–2A), 4–fluorophenyl– (140–3A) and 2–methyl–4–chlorophenyl– magnesium bromide (140–4AA). Novel compounds from natural products were synthesized by Mr R. Young, again, in collaboration with the Department of Chemistry, Rhodes University, Grahamstown, South Africa. They were included in the study because of the apparent lack of a phosphonate/phosphate moiety and hydroxamic acid moiety. All the structures are presented in Figure **5.1**.

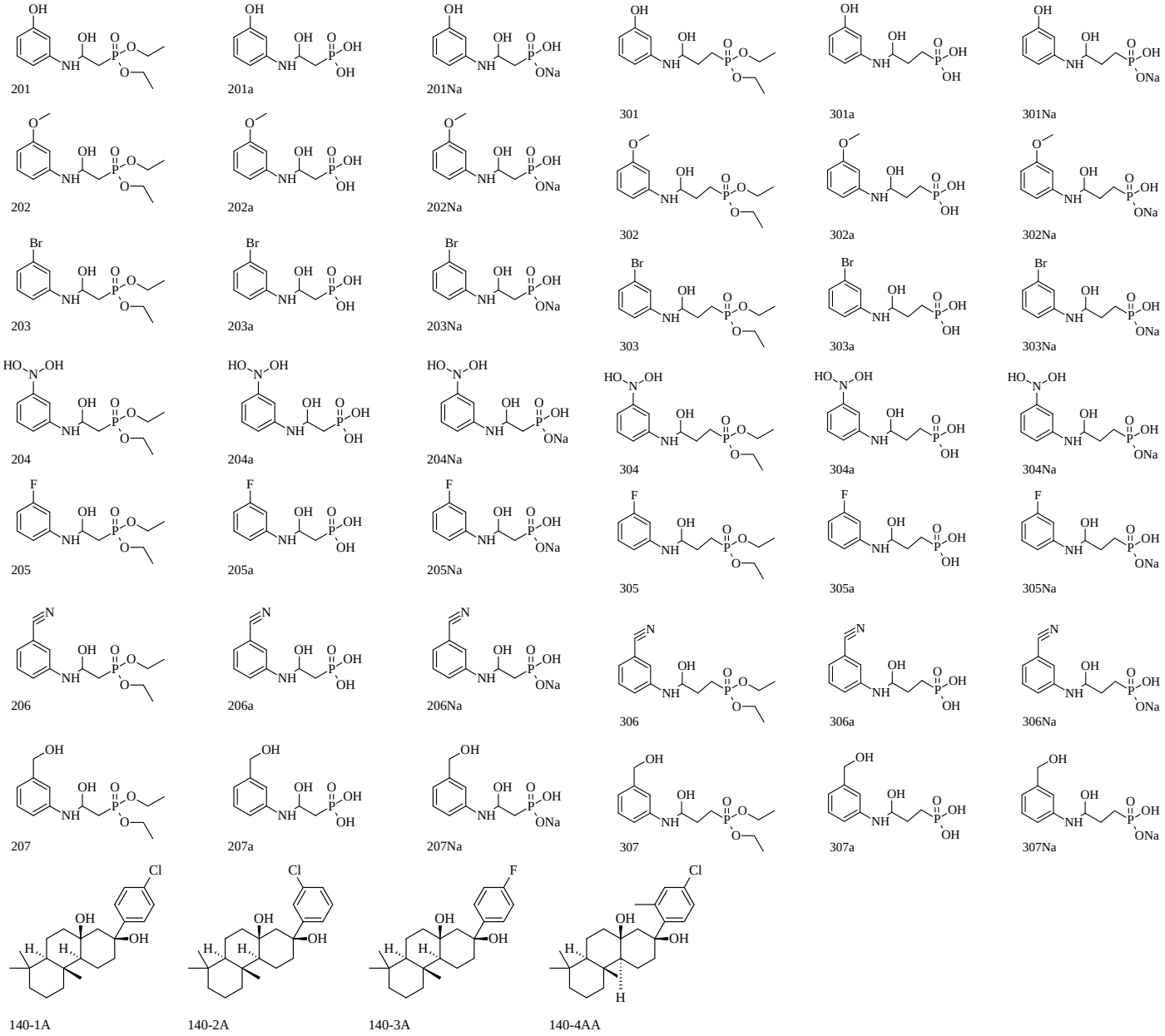

Figure 5.1: The chemical structures of novel compounds used for docking studies.
Compounds included: 201–207. 201a–207a, 201Na–207Na, 301–307, 301a–307a, 301Na–307Na (in columns down) and 140–1A, 140–2A, 140–3A, and 140–4AA (in last row). Structures were drawn using ACD/ChemSketch freeware software version 11.01.

The docking software used in this work was able to provide information including theoretical binding affinity (kcal/mol), relative ligand efficiency, theoretical inhibitor constant (pM) and potential hydrogen bonding interactions. This data is summarised in Appendix B (Table **B.1**). By simple analysis of this information, it is very difficult to gauge the efficiency of the ligands as compared to fosmidomycin; a graphical representation of this information was therefore necessary. For this purpose, the novel *in silico* screening tool developed in this work (see Chapter 2) was used. Upon visual analysis of the results of using this screening

tool, which classified DXR inhibitors into quadrants, based on the ligand's potential binding affinity (kcal/mol) and number of potential hydrogen bonding interactions, it was evident that a grouped distribution resulted. A minor modification to this plot [potential binding affinity (kcal/mol) and relative ligand efficiency] resulted in a more even spread of data points (Figure **5.2**). As expected, fosmidomycin and FR900098 demonstrated good binding affinity and good ligand efficiency, indicative of a more negative value, and resided in the bottom left quadrant (Figure **5.2**). This, coupled to the re–docking of fosmidomycin into the PfDXR homology model validated the docking process sufficiently.

The natural products analogues all demonstrated poor binding affinity and poor ligand efficiency and hence resided in the top right quadrant (Figure **5.2**). The fosmidomycin analogues that were classified as having good theoretical inhibition efficiency included: fosmidomycin, 201a, 203a, 204a, 204Na, 206Na, 301Na, 302a, 303Na, 304a, 304Na, 305a, 306a and 307Na (Figure **5.2** and Table **B.1**).

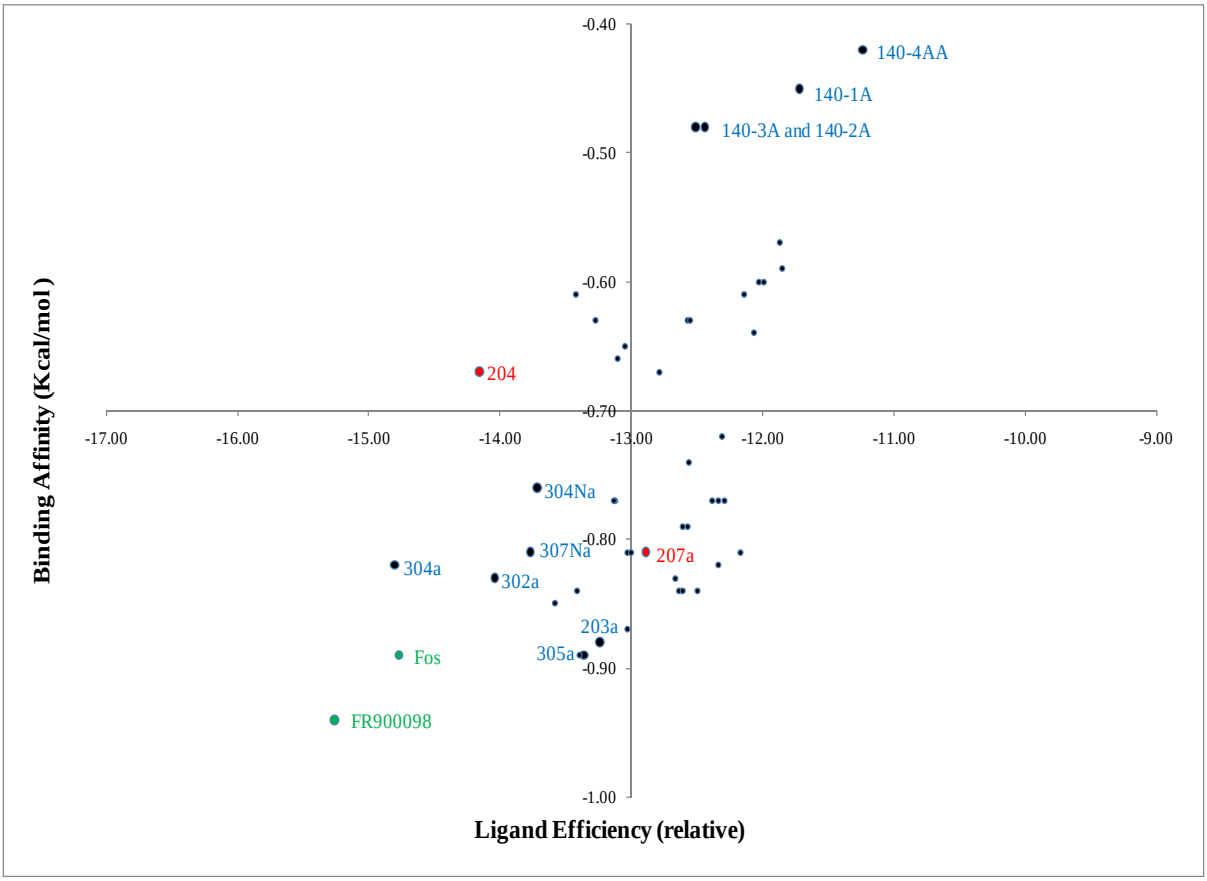

Figure 5.2: Graphical representation of the theoretical inhibition efficiency of novel compounds (legend on next page).

Graph showing the correlation between theoretical binding affinity (kcal/mol) and relative ligand efficiency for 46 potential DXR inhibitors docked into PfDXR. Inhibitors include: Fosmidomycin (coloured *green*), FR900098 (coloured *green*), 201–207, 201a–207a, 201Na–207Na, 301–307, 301a–307a, and 301Na–307Na, 140–1A, 140–2A, 140–3A and 140–4AA. The potential DXR inhibitors are classified into one of four quadrants: the top left quadrant represents compounds with good ligand efficiency but a poor inhibitor constant; the top right quadrant represents compounds poor ligand efficiency and a poor inhibitor constant; the bottom left quadrant represents compounds good ligand efficiency and a good inhibitor constant; the bottom right quadrant represents compounds poor ligand efficiency but with a good inhibitor constant.

An accumulative effect was derived from plotting binding affinity, ligand efficiency, inhibition efficiency (in the form of an inhibition constant) and potential H–bonding competence such that each factor accounted for 25% of the total score (Figure **5.3**). Compounds were directly compared to FR900098 (100%), because it demonstrated better binding properties than fosmidomycin (Figure **5.2**). From this it was evident that 304a demonstrated binding properties that were even greater than FR900098, attributed mostly to its low inhibition constant (theoretical IC_{50}). Interestingly, when all the above mentioned factors were considered, and not just the binding affinity and ligand efficiency (as in Figure **5.2**), compound 204 appeared to be one of the most efficient compounds with respect to theoretical binding. Figure **5.3** also showed that the 200 compound series demonstrated better binding properties, when compared to the 300 series; similarly, the 300 series exhibited better binding properties, when compared to the 140 series.

While 14 compounds appeared in the expected quadrant in Figure **5.2**, analysis of all 4 binding properties concluded that only 8 compounds were in fact efficient at binding the PfDXR homology model. These included: fosmidomycin, 203a, 204, 207a, 302a, 304a, 304Na, 305a and 307Na. Interestingly, 204 and 207a appear in this group, but did not reside in the expected quadrant (Figure **5.2**).

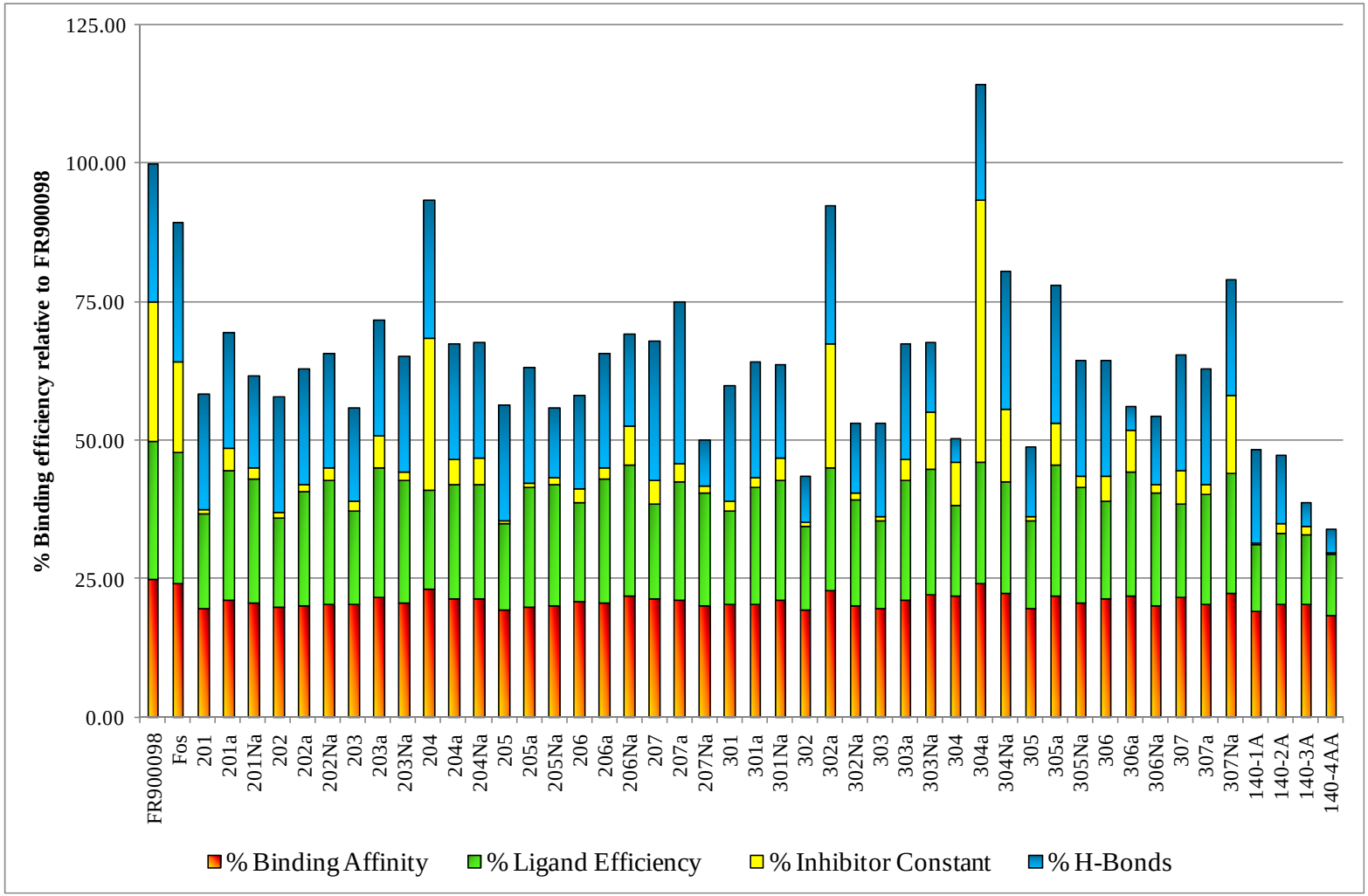

Figure 5.3: Graphical representation of the predicted *in silico* binding ability of novel compounds.
Graph showing the cumulative effect of binding affinity (in kcal/mol) and relative ligand efficiency, for 46 potential DXR inhibitors docked into PfDXR. Inhibitors include: Fosmidomycin, FR900098, 201–207, 201a–207a, 201Na–207Na, 301–307, 301a–307a, and 301Na–307Na, 140–1A, 140–2A, 140–3A and 140–4AA. The greatest values (expressed as positive values) represent those compounds which demonstrated the greatest binding ability to the PfDXR homology model.

Following the *in silico* analysis of the 200, 300 and 140 compound series, it was necessary to establish whether these compounds were effective at inhibiting the antimalarial drug target enzyme, PfDXR.

5.3.2 *In vitro* screening of novel compounds for DXR inhibition

The reduction of NADPH was monitored as a measure of enzyme activity because it is known from the literature that the DXR enzyme uses NADPH as a cofactor, as DXP is converted to MEP (Kuzuyama *et al*., 1998).

While some of the compounds were soluble in water, the phosphonate esters and natural product series were not. Dimethyl sulfoxide (DMSO) is a polar solvent that dissolves polar and non–polar compounds. It is also miscible in a wide range of organic solvents, including water (reviewed by Kvakovszky *et al*., 2007). In this study, compounds were therefore dissolved in 10% DMSO (2% DMSO in final assay). The assay was therefore tested using numerous concentrations in order to assess the threshold at which it affected enzyme activity (Figure **5.4**). It was evident that only at 25%, DMSO had an inhibitory effect on DXR. It appeared that the presence of DMSO in the assay mixture, even in very small amounts, resulted in a small degree of enzyme activation, with a slight increase in specific activity (µmol/min/mg). However, the increase was not significant enough to warrant any further investigation (Figure **5.4**). It was therefore decided that all compounds would be dissolved in 10% DMSO so that the final concentration of DMSO in the assay was 2%; this was to ensure uniformity in the assay procedure.

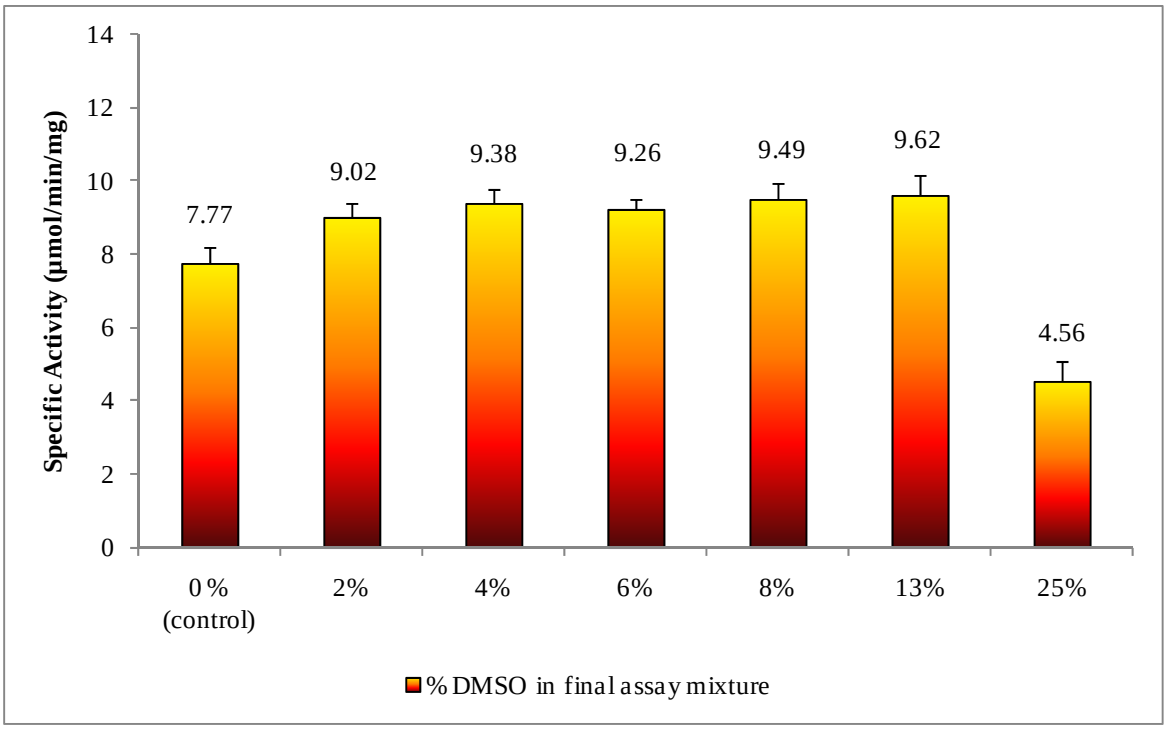

Figure 5.4: Analysis of the effects of DMSO on the activity of EcDXR.
The assay was performed under standard assay conditions with purified EcDXR enzyme. The percentages are indicative of the final% DMSO in the reaction mixture. The DMSO tolerance test was performed in triplicate subsequent to two separate batch purifications of the enzyme. Error bars represent the standard deviation for samples tested in triplicate for two separate batches of enzyme.

Following this, assays were carried out in triplicate, for PfDXR and EcDXR so that the two target enzymes could be compared directly. According to Figure **5.5**, some novel compounds tested did indeed inhibit DXR, while interestingly, some compounds had an enhancing effect on DXR.

Compounds that were shown to be effective at inhibiting PfDXR included: 202a, 203a, 207, 140–1A, 140–2A and 140–3A (Figure **5.5**). Compounds that demonstrated more than 40% inhibition for EcDXR included: 201, 201Na, 207, 301Na, 307Na, 140–1A, 140–2A and 140–3A (Figure **5.5**). From this, it was evident that the only compounds that inhibited both PfDXR and EcDXR were 207, 140–1A, 140–2A and 140–3A. The 300 series demonstrated almost no inhibitory effect toward either of the DXR enzymes. Numerous compounds demonstrated an enhancing effect on the PfDXR purified enzyme, particularly the negatively charged phosphonates of the 200 series (201Na, 202Na, 205Na, 206Na and 207Na) (Figure **5.5A**). The compounds that inhibited EcDXR exclusively were 201, 201a, 301Na and 307Na, while 202a and 203a only inhibited PfDXR. Statistical analyses using a t–test

confirmed that numerous experimental samples were significant, including the compounds that inhibited both PfDXR and EcDXR (Figure **5.5**).

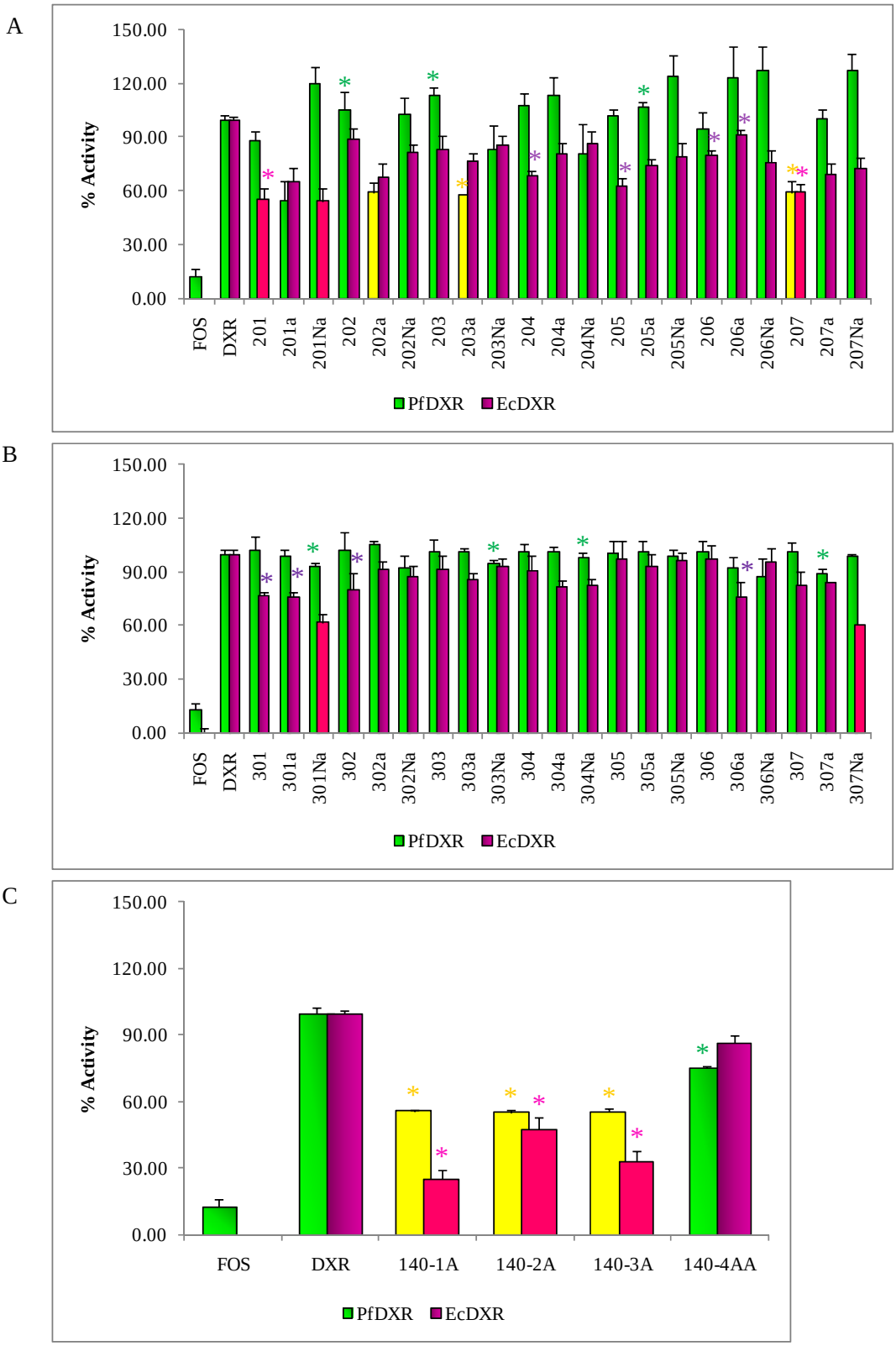

Figure 5.5: Analysis of PfDXR and EcDXR relative activity in the presence of novel compounds 201–207, 201a–207a, 201Na–207Na, 301–307, 301a–307a, 301Na–307Na, 140–1A, 140–2A, 140–3A and 140–4AA (legend on next page).

Relative percentage PfDXR inhibition (shown in *green*) and EcDXR inhibition (shown in *purple*); normalized against PfDXR or EcDXR activity respectively, in the presence of no compound, set at 100% (DXR), for (A) 201–207, 201a–207a, 201Na–207Na; (B) 301–307, 301a–307a, 301Na–307Na; (C) 140–1A, 140–2A, 140–3A, and 140–4AA. All compounds were tested at a concentration of 250 µM. 1 µM fosmidomycin (FOS) was used as a positive control for DXR inhibition. Points coloured *yellow* are representative of compounds that show more than 40% inhibition of PfDXR and points coloured *pink* are representative of compounds that show more than 40% inhibition of EcDXR (not including controls). Error bars represent the standard deviation for samples tested in triplicate for two separate batches of enzyme. '*' is indicative of statistical significance where $p < 0.005$.

Following the *in vitro* analysis of numerous compounds against the effective antimalarial drug target enzyme, it was necessary to assess whether they demonstrated antimalarial activity and to what degree.

5.3.3 *In vitro* screening of novel compounds for inhibition of *P. falciparum* growth

The *P. falciparum* 3D7 strain was cultured in type O human erythrocytes. Parasitemia was assessed daily and a pLDH assay, which was performed in duplicate for two separate experiments, was used to quantify the antimalarial effect of the compounds. A summary of the different parasite stages can be seen in Figure **B.4** (Appendix B). Parasite lactate dehydrogenase (pLDH) is maximal between 36 and 48 hours when trophozoites and shizonts predominate (Basco *et al*., 1995).

At a concentration of 250 µM, compounds that demonstrated antimalarial activity of more than 40% included: 304Na, 305Na, 307Na, 140–1A, 140–2A and 140–4AA (Figure 5.6). Control compounds used were fosmidomycin and chloroquine, which have been reported to have IC_{50} values in the nanomolar range. All samples that demonstrated possible antimalarial activity of more than 40% reduction in parasitemia, at a concentration of 250 µM, were tested for toxicity in human cells (Figure 5.6). This was accomplished by quantifying the reduction of WST–1 reagent as a measure of cell viability. Control reactions that were included in the experiment were the highly toxicity anti–cancer drug, paclataxel, chloroquine and fosmidomycin. As expected, paclataxel resulted in 60% reduction in viability (or growth inhibition), while chloroquine and fosmidomycin resulted in 87% and 44% reduction in viability respectively. Compounds 304Na, 305Na, 307Na, 140–2A, 140–3A and 140–4AA appeared to be relatively non–toxic to human cells and resulted in a reduction in viability of less than 35, while 140–1A, resulted in a reduction of 52% (Figure 5.6).

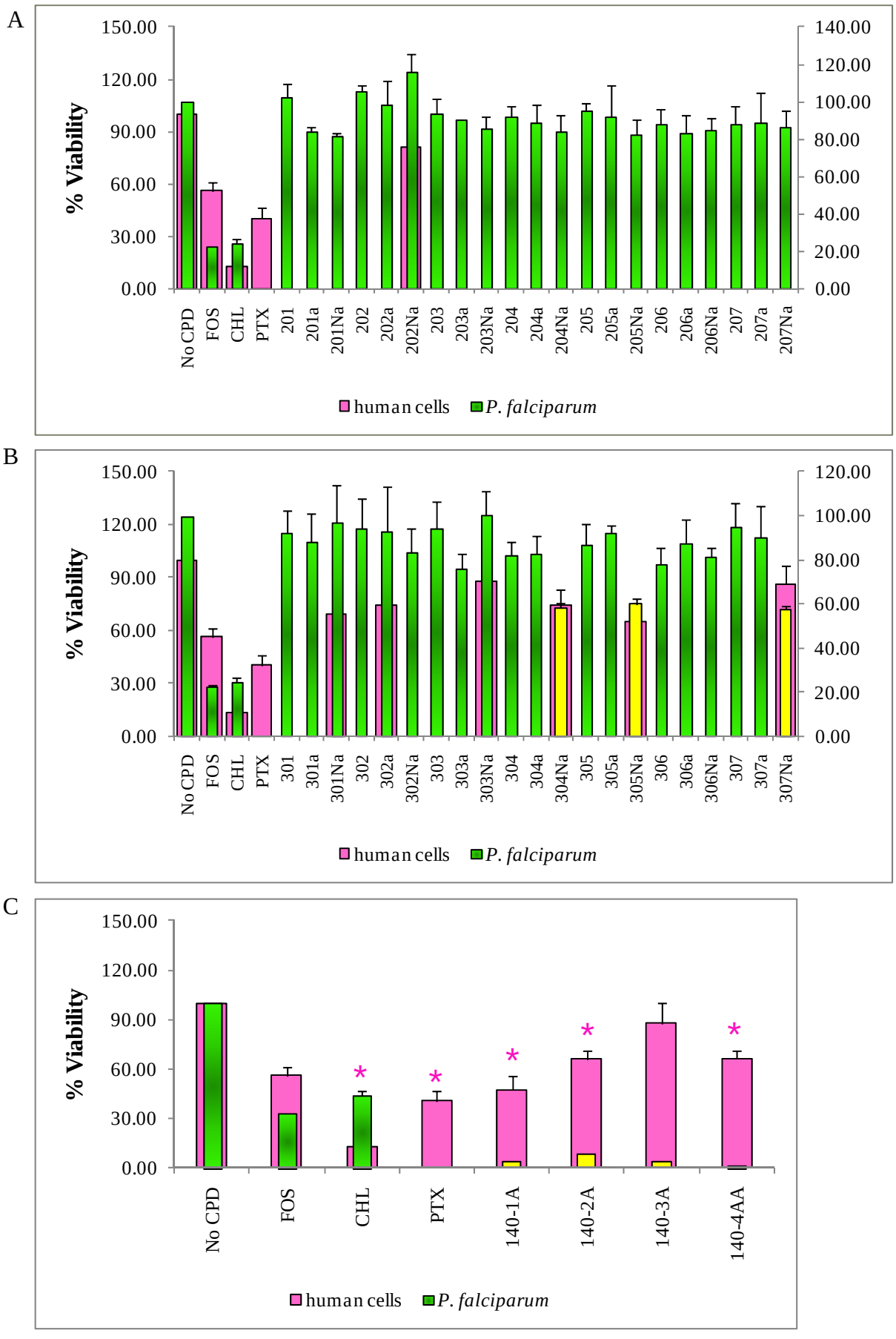

Figure 5.6: *In vitro* screening of novel compounds for growth inhibition activity (legend on next page).

The *in vitro* growth inhibition activity of novel compounds was assessed by viability assays on *P. falciparum*–infected erythrocytes and on human cells. The relative percentage parasite viability, based on pLDH activity, for all compounds is shown in *green*, while the relative percentage viability of human cells, based on the WST–1 assay, was assessed for some compounds (shown in *pink*). The pLDH assay was normalized against infected red blood cells in the presence of no compound (No CPD), for (A) novel compounds 201–207, 201a–207a, 201Na–207Na; (B) 301–307, 301a–307a, 301Na–307Na; (C) 140–1A, 140–2A, 140–3A, and 140–4AA. All compounds were tested at a concentration of 250 µM. Experimental controls include: 1 µM chloroquine (CHL), 200 nM paclataxel (PTX) and 1 µM fosmidomycin (FOS). Bars coloured *yellow* are representative of compounds that show less that 60% viability (not including controls). Error bars represent the standard deviation for samples tested in duplicate for two separate batches of enzyme. '*' is indicative of statistical significance where $p < 0.005$.

In this work all control reactions appeared to work as expected, validating the experiment. It is evident from these data that while some compounds inhibited DXR *in vitro*, they did not necessarily inhibit parasite grown *in vitro* and vice versa. The same can be said for docking studies; in some cases, compounds inhibited the growth of *P. falciparum*–infected erythrocytes and inhibited PfDXR, but did not demonstrate a good binding affinity. From these data however, one appears to be able to link structure to function with respect to drug screening (Table **5.2**).

Table 5.2: Summary of data for novel compounds for *in vitro* DXR inhibition, *in vitro* antimalarial ability and *in silico* theoretical inhibition efficiency (footnote on next page).

Sample	Inhibits Growth[b] > 40%	Good Docking[c] > 70%	Inhibits DXR[a] > 40%	Toxic to human[d] cells > 65%
FOS	YES	YES	YES	x
201	x	x	YES	
201a	x	x	x	
201Na	x	x	YES	
202	x	x	x	
202a	x	x	YES	
202Na	x	x	x	x
203	x	x	x	
203a	x	YES	YES	
203Na	x	x	x	
204	x	YES	x	
204a	x	x	x	
204Na	x	x	x	
205	x	x	x	
205a	x	x	x	
205Na	x	x	x	
206	x	x	x	
206a	x	x	x	
206Na	x	x	x	
207	x	x	YES	
207a	x	YES	x	
207Na	x	x	x	
301	x	x	x	
301a	x	x	x	
301Na	x	x	YES	x
302	x	x	x	
302a	x	YES	x	x
302Na	x	x	x	
303	x	x	x	
303a	x	x	x	
303Na	x	x	x	x
304	x	x	x	
304a	x	YES	x	
304Na	YES	YES	x	x
305	x	x	x	
305a	x	YES	x	
305Na	YES	x	x	x
306	x	x	x	
306a	x	x	x	
306Na	x	x	x	
307	x	x	x	
307a	x	x	x	
307Na	YES	YES	YES	x
140–1A	YES	x	YES	YES
140–2A	YES	x	YES	x
140–3A	YES	x	YES	x
140–4AA	YES	x	x	x

For *vitro* DXR inhibition[a], compounds that demonstrate more than 40% inhibition of PfDXR or EcDXR or both are represented as positive. Similarly, compounds that demonstrated more than 40% *in vitro* antimalarial ability[b] are represented as positive. *In silico* theoretical inhibition efficiency[c] was quantified positively for compounds that had a score of more than 14 for the sum of the binding affinity and relative ligand efficiency. Compounds that resulted in a reduction in viability[d] of more than 35% for Hst578T human cells were quantified as a positive result. A positive result is symbolized with "YES" and a negative result is symbolized with "x".

From Table **5.2**, it is evident fosmidomycin fulfilled all the desired criteria for an effective "hit" compound, as expected as it resulted in more than 40% growth inhibition of *P. falciparum*–infected erythrocytes, without being toxic to human cells. It also, docked into the PfDXR theoretical model with more than 70% of the score obtained for FR900098 and it inhibited DXR activity by more than 40% (Table **5.2**). It must also be noted that fosmidomycin was tested at a concentration that was 250 times less concentrated that other potential inhibitors, confirming its effectiveness as a DXR inhibitor. The novel compound 307Na also fulfilled all of the above mentioned criteria and it therefore represents a potential "hit" for development into an antimalarial drug (Table **5.2**).

5.4 DISCUSSION

According to Fox and Poulter (2005), fosmidomycin is a slow, tight–binding inhibitor of EcDXR. Other weaker inhibitors of DXR have been shown to be strictly competitive or non–competitive (reviewed by Singh *et al*., 2007); this type of information is critical in the rational design of potential inhibitors of DXR. In antimalarial drug discovery, numerous approaches, both novel and common, have been utilized in the design of novel antimalarial compounds, against this disease of poverty. Some of these common avenues include investigating traditional medicine leads, the use of molecular biology techniques to identify potential targets, natural product screening and structure–based drug design (Milhous, 1998). In this study, two of these avenues have been explored including structure–based drug design and natural product screening.

In the absence of an experimentally–derived PfDXR crystal structure, a homology model was designed and utilized for rigorous analysis of the PfDXR active site, for the purpose of drug design. A combinatorial approach was taken in order to hypothesize which compound properties appeared to provide the molecule with an advantage, also concentrating heavily on the literature. Numerous properties have been said to be essential in the synthesis of DXR inhibitors, including a phosphonate/phosphate moiety (Kurz *et al*., 2003_1; Kurz *et al*., 2003_2; Wiesner and Jomaa, 2007), as well as a hydroxamic group containing a charged or partially

charged nitrogen atom (Zubrzycki and Blatch, 2001). However, according to the literature, the presence of the phosphonate/phosphate moiety results in a significant reduction in lipophilicity, typical of fosmidomycin, which leads to difficulty in crossing phospholipid membranes and also adds to its poor absorption, making such compounds inefficient drugs (Deng *et al*., 2009). In a study undertaken by Haemers *et al*. (2006), a compound library was designed to include a phenyl ring, which would improve the lipophilicity of the compounds. Other structural modifications included analysing the effect of phosphonate esters versus charged and uncharged phosphonate groups. Because of the presence of a catalytic hatch, which closes over the active site after the substrate has bound (Yajima *et al*., 2002), it is likely that the small DXR active site does not easily accommodate large molecules. This, coupled to the existence of a phosphate binding pocket, may mean that the phosphonate ester group is too large to adequately bind to the DXR active site. An interesting development to the compound design process involved the inclusion of a negatively charged phosphonic acid; where the dissociation of the sodium ions in water, would yield a negatively charged group. A very small natural products screening compound group were included in this work, in order to gauge the importance of the above mentioned moieties. This group of compounds derived from natural products boasted both bulkiness and did not incorporate any of the moieties that the literature states are typical properties of a good DXR inhibitor.

Compounds were analysed both *in silico* and *in vitro* in order to gauge whether there was an overlap in structure and function. The *in silico* screening tool developed during this study (see Chapter 2) was applied for the analysis of 46 novel compounds. Compounds were docked into the PfDXR homology model and properties including binding affinity, ligand efficiency, inhibition efficiency and potential H–bonding competence were analysed. The *in silico* screening tool only took 2 of the 4 binding properties into account, and yielded 14 compounds (including fosmidomycin and FR900098) which proved effective at binding PfDXR.

The compound library was then analysed, taking into account all four factors, so that each factor accounted for 25% of the final score, where the control compound used for docking was FR900098 because it resulted in the greatest binding scores, and represents a compound (along with fosmidomycin) against which all inhibition studies are compared. The acetyl analogues of fosmidomycin were used as they show in the greatest theoretical scores for docking and in the literature; it has been shown to demonstrate better inhibitory effects for

PfDXR than fosmidomycin (Jomaa *et al*., 1999; Gieβmann *et al*., 2008; Behrendt *et al*., 2010). This more rigorous screen, allowed for the compounds to be filtered, so that they yielded a score of more than 70%. Of the 8 compounds that satisfied the criteria, two compounds (204 and 207a) did not appear in the original screened group, which took only binding affinity (kcal/mol) and ligand efficiency (relative) into account. In the case of 204, a reasonable binding affinity, with slightly lower ligand efficiency, meant that it resided in the top left quadrant; however, when the other factors were considered, it transpired that a good inhibition constant (theoretical IC_{50}) resulted in a significantly improved total score.

Upon analysis of the docked compound orientation, it was evident that there was a high degree of hydrogen bonding but the compound did not fully enter the active site, which means that some of these interactions were with non–catalytic residues. The high degree of potential bonding capacity resulted in an improved binding affinity score but the bulkiness of the molecule meant that its efficiency as a DXR inhibitor may have been compromised. In the case of 207a, its binding affinity was below the threshold of – 13 kcal/mol, but its ligand efficiency was above the threshold of – 0.7, placing it in the bottom right quadrant. Further analysis however confirmed that the high degree of hydrogen bonding resulted in an increased score that satisfied the more stringent criteria. This compound is significantly smaller than 204 and this, coupled to the presence of the critical phosphonate moiety, means that it took on a bound conformation similar to FR900098, possibly resulting in a high degree of ligand efficiency.

It is evident from the analysis that, of the compounds that yielded a score of more than 70%, most included a phosphonate group, confirming the importance of this moiety in inhibitor binding. Interestingly, more of the larger 300 series compounds appeared in this group, when compared to the 200 series. But upon analysis, it was evident that many in this group, upon docking, demonstrated changes to their minimised conformations in order to enter the active site. Compound 304a demonstrated binding properties that superseded a 100% score – this was attributed predominantly to a significantly small inhibitor constant (IC_{50}). However, upon analysis of the docking conformation, it was evident that the compound demonstrated a reverse orientation, with the NO_2 phenyl side chain protruding into the active site. This may mean that the compound required less energy to bind, resulting in a good binding score. However, it would be necessary to assess whether this compound could inhibit DXR because rigorous analysis of the active site has revealed that the phosphonate/phosphate moiety is

required for coordination of the divalent metal ion within the active site (Kuzuyama *et al*., 1998).

As expected, the 140 series compounds all resided in the top right quadrant, demonstrating poor binding affinity and poor ligand efficiency (because of their bulkiness and lack of "critical" binding groups). This screening tool is therefore useful in deciphering binding efficiency, between compound libraries, as opposed to compounds of the same library that share very similar structures. Following the *in silico* analysis, an attempt was made to link compound structure (how efficiently did it bind) with function (how well it inhibited DXR). Upon analyses of the data, it was evident that only the 140 series resulted in significant DXR inhibition for both the PfDXR and EcDXR purified enzymes, with a high degree of statistical significance. This is interesting because of the evident lack of "critical" binding groups and poor docking efficiency of the compounds. Interestingly, 140–4AA only resulted in 25 and 18% inhibition of PfDXR and EcDXR respectively, while 140–1A, 140–2A and 140–3A resulted in inhibition of ~ 50% for PfDXR and ~ 70% for EcDXR. Upon analysis of the compound structures, it may be possible that the addition CH_3 side chain on C1 (carbon 1) of the phenyl ring many have resulted in an increased bulkiness. The docking analysis also, to some degree, confirmed that 140–4AA resided in the top right quadrant when initially screened and further screening confirmed that 140–4AA achieved the poorest overall binding score. Analysis of the compound conformation concluded that the CH_3 in question resulted in an opposite orientation to that of 140–1A, 140–2A and 140–3A and had significantly less potential for hydrogen bonding interactions. Thus it may be possible that even if the compound was able to enter the PfDXR active site, it may not have bound sufficiently enough to induce a response. It may also be possible that the 140 series may be binding outside the active site and may be inhibiting DXR via the inhibition of NADPH binding; however, further kinetic analysis would need to be undertaken in order to accurately confirm this, analyses of whether the compounds were non–competitive or uncompetitive would provide some evidence in this regard.

The only other compound that exhibited some DXR inhibition for both PfDXR and EcDXR was 207. This is interesting because of the presence of the phosphonate ester group (as a replacement for the phophonate). Docking analysis revealed that 207 may dock in a similar manner to that of FR900098, whereby the phosphonate ester group exhibited potential hydrogen bonding interactions with catalytic residues Lys240 and Asn241 (x2), while the

nitrogen group interacted with Ser199 and Ser235. It may be possible that the 2^+ charge of the divalent cation could still be sufficiently coordinated by the phosphonate ester in the binding site.

Other compounds that demonstrated some inhibition ability for EcDXR (but not for PfDXR) included: 201, 201Na, 301Na and 307Na, while compounds that partially inhibited PfDXR (and not EcDXR) included 202a and 203a. Analysis of the compounds' structures, allowed for one to conclude that the 200 series boasting the shorter carbon spacer generally demonstrated slightly more inhibition potential. In general, compounds that contained fluorine or nitrogen groups at the tail end, e.g. R = NO_2, F or CN, did not bind as efficiently when compared to compounds containing oxygen groups at the tail end, e.g. R = OH, OCH_3 or CH_2OH. A preference for the OH group was also evident, which corresponds to the literature, where numerous compounds known to inhibit DXR have contained an OH group at the tail end as part of the hydroxamic acid moiety (Table **5.1**).

The antimalarial efficiency of the same compound library was tested in order to assess whether those inhibitors that targeted DXR could be used in further antimalarial drug design. As hypothesized, the 140 series all demonstrated an ability to reasonably inhibit growth of *P. falciparum*–infected erythrocytes. These compounds were derived from structures relating to isopimarane diterpenoid natural products that are known to have convincing antimalarial potential. As mentioned, further kinetic analysis would need to be done in order to determine whether the series was inhibiting DXR via the active site or via the NADPH binding motif. When analyzing the screening data from the 200 and 300 series, interestingly, fosmidomycin derivatives 304Na, 306Na and 307Na resulted in some inhibition of growth. This is surprising because the entry of antimalarial drugs into red blood cells and across 4 parasite membranes poses a difficulty in drug design because the phosphonate moiety has been associated with poor uptake into cells because of its charged nature (Knipe and Howley, 2007). It may be possible that these compounds could be mediated by a transporter explaining why they are active at inhibiting growth, despite their charged nature. The compound 307Na also inhibited EcDXR and demonstrated that it was also relatively non–toxic in human cells. It also showed good binding properties *in silico*, meaning that it fulfilled all the expected criteria of a lead compound in the rational design of novel potential antimalarial compounds.

In conclusion, the link between *in silico* and *in vitro* data may provide some evidence for more effective drug design. The fosmidomycin analogues proved to be only mildly effective at inhibiting DXR and showed very little effect against *P.falciparum* malaria. The small differences however may lend toward further predictions and improvements in structure. This is supported heavily by the existence of enzyme crystal structures and in *in silico* analysis. The efficiency of the 140 series at inhibiting *P. falciparum* growth may be an indication that there is a need to explore natural products screening as an additional approach in drug discovery, although the mechanism of inhibition should also be explored simultaneously. An even more efficient approach would be to combine natural products screening with rational drug design. It must however be noted that there may not necessarily be a link between the antimalarial activity and DXR inhibitory activity of the 140 series; it may be possible that other mechanisms are being targeted, especially given the fact that the compound were tested at very high concentrations.

CHAPTER 6
GENERAL DISCUSSION

There were two major objectives accomplished through the work done for this thesis. The first objective developed an expression system through which large yields of the problematic malarial target enzyme (PfDXR) could be purified. The second objective involved screening potential novel compounds for antimalarial activity, as well as for inhibition potential of the target enzyme in question.

Malarial enzymes are not well characterized in the literature because of their frequently recalcitrant nature and PfDXR was no exception. Numerous expression systems have been reported in the literature for the expression of problematic malarial proteins; however, the system of choice has characteristically been the bacterial expression system because of its simplicity and the fact that it is most often associated with overproduction of the target enzyme (Ahuja *et al.*, 2006). PfDXR purification is highly problematic and hence the well studied EcDXR homologue has been used primarily for DXR characterization and kinetic analysis (Reuter *et al*., 2002; Yajima *et al*., 2002; Steinbacher *et al*., 2003; Mac Sweeney *et al*., 2005). In light of this, it has taken more than a decade to crystallize PfDXR, but the structure has not yet been validated and the coordinates have not been made publically available. In the absence of an experimentally validated PfDXR crystal structure, the use of homology modelling becomes the best alternative strategy. The proposed PfDXR homology model put forward in this work was sufficiently validated using many known structure–checking programmes, as well as using ligand docking studies, where 34 known inhibitors of DXR, were docked into PfDXR, with the subsequent docking of the same inhibitors into the crystal structure of EcDXR as a control experiment. With the sufficient validation of the PfDXR homology model, the tertiary model was used to identify structural features that were unique to PfDXR. By comparing apicomplexan and non–apicomplexan DXR sequences, it was evident that PfDXR exhibited features that were unique, including differences in the NADPH binding motif, as well as differences in the catalytic hatch, which has been shown to move over the active site once the substrate has bound (Yajima *et al*., 2002). Ligand docking studies provided structural information regarding movement of the hatch upon inhibitor binding, and showed that there were significant differences in PfDXR when compared to EcDXR. It appeared, that these differences were common to numerous other

apicomplexan DXRs, warranting further analysis. Site–directed mutagenesis was therefore employed, in an effort to link these theoretical structural differences to function.

The literature reports that in EcDXR, NADPH binding occurs via Gly11, Ser12 (coordinates the pyrophosphate moiety), Gly 14, Ala35 and Gly36 (interact with the 2' phosphonate) (Reuter *et al*., 2002) and that the mutation G14D resulted in improper folding and solubility–related problems (Kuzuyama *et al*., 2000). Upon analysis of the tertiary structure of EcDXR and PfDXR, this is not surprising because of the partially buried nature of the Gly14 side chain, coupled to the drastic change in size and charge of the side chain. Sequence alignment confirmed that the PfDXR equivalent residues to Ala35 and Gly36 were Val43 and Asn44. The theoretical model of PfDXR allowed for the supposition that orientation of these residues was significantly different when compared to the EcDXR crystal structure equivalents. The rationale for mutating the two NADPH binding residues, Val43 and Asn44 was such that if the binding site mimicked that of EcDXR that the enzyme may be able to bind and utilize NADPH more efficiently, given the 10–fold increase in the maximal velocity of the *E. coli* enzyme, when compared to the unmutated PfDXR. The V43A and N44G mutations resulted in an increased K_m, which may not have been due to a lowering of affinity for substrate, but an indirect reflection of the lower affinity for NADPH. The fact that PfDXR(VN43,44AG) did not produce a more efficient DXR is probably because these two mutations were not sufficient to produce an NADPH binding site that would functionally alter the enzyme. Significant changes would have to be made to the NADPH binding motif if one wanted to more accurately make predictions. Future work in this regard would be better utilized in analysing the potential PfDXR–NADPH binding interactions, by mutating equivalent residues to those involved in NADPH binding in EcDXR so that there would be complete disruption of the motif. Possible mutant enzymes to include in future studies are: T15E (Thr10 in *E. coli*), G16E/ D (Gly11 in *E. coli*), S17R (Ser12 in *E. coli*), G19E/ D (Gly14 in *E. coli*), V43/R and N44/H. In all these cases, mutations would completely alter the size and charge of the residues in question. If a similar outcome results as has been reported in the literature for G14D (Kuzuyama *et al*., 2000), one may be able to determine whether the DXR–NADPH contacts are the same for PfDXR as have been reported in the literature for EcDXR. The PfDXR homology model presented in this work also establishes other potential interactions and mutagenesis of some of the residues that may be worth exploring. This allows assessment of whether contacts exist in PfDXR that are different from other well characterized DXR enzymes.

Efficient enzyme catalysis requires the correct active site formation and it is essential that both the divalent metal ion and NADPH cofactor are bound to DXR for the catalytic hatch to correctly close over the active site after the substrate/ inhibitor has bound (Yajima *et al.*, 2002; Steinbacher *et al.*, 2003). Mutations to the catalytic hatch residue Trp204 in SyDXR (Trp212 in *E. coli*) confirmed that there was complete disruption by the resultant Ala (W204A) and a 70–fold reduction in substrate affinity (indicative of an increased K_m) and approximately 8000–fold reduction in catalytic efficiency (k_{cat}/ K_m) (Fernandes *et al.*, 2005). In very close proximity to Trp212 (in *E. coli*) and in a region on the hatch which is highly conserved (His209 – Gly215 in *E. coli*), two very uncharacteristic differences exist, where the plant and bacterial DXRs share Asn and Ser residues (Asn211 and Ser213 in *E. coli*) while apicomplexan DXRs code for two Lys residues at the equivalent positions. Analysis of the PfDXR homology model, coupled to the docked versus undocked enzyme states, has allowed for one to hypothesize that there is significant movement of these Lys residues upon entry of the substrate/ inhibitor into the active site, with the potential for numerous intermolecular hydrogen bonding interactions being broken, upon substrate/ inhibitor entry. Mutation of these two catalytic hatch Lys residues to Asn and Ser (the *E. coli* equivalents) resulted in a decreased substrate affinity (K_m) and decreased substrate turnover (k_{cat}), with the amplified effect of this, resulted in a large reduction in the catalytic efficiency (k_{cat}/ K_m) for PfDXR(KK224,226NS) as a direct result of interfering with the substrate's affinity at the level of the active site. Similar values were reported for the W204F mutant (Fernandes *et al.*, 2005), where charge was maintained but size was modified. In light of this, future work could involve mutating both Lys residues mentioned previously in an effort to completely disrupt the catalytic hatch by introducing residues such as Ala, which has been well documented in the literature (Fernandes *et al.*, 2005; Fernandes and Proteau, 2006). It may even be possible to completely remove (by deletion mutation) or mutate a string of residues (to Gly residues) of the highly conserved catalytic hatch; in order to assess to what degree the hatch is involved in substrate specificity.

One cannot however exclude the possibility that the resultant mutant enzymes that were investigated may have resulted in localized perturbations in structure of the active site and that the reduction in activity may have been an indirect effect of a minor loss of the enzymes' structural integrity. In conclusion, structural analysis via site–directed mutagenesis can be used to better understand the structural importance of the catalytic hatch and cofactor binding

site. Even if kinetic changes are minor, the information that can be obtained from such experimental probing may allow for the origin of even greater future findings. It may however be necessary to employ additional techniques of validation in order to confidently construe that a loss in kinetic activity is a direct result of the mutation in question. Other methods of validation that could be employed in order to corroborate the findings of this work could include: circular dichroism (CD) (Greenfield, 1975), Fourier transform infrared spectroscopy (Kochan *et al*., 1995), structural determination of mutant enzymes (Håkansson, *et al*., 2006; Umeda *et al*., 2010), surface plasmon resonance (SPR) (Flatmark *et al*., 2001) or quartz crystal with microbalance and dissipation monitoring (QCMD). These methods could be used to analyze substrate binding or even cofactor binding to the target enzyme.

The PfDXR theoretical model, coupled to comparative sequence analyses with apicomplexan and non–apicomplexan DXR proteins, also allowed for the identification of structural and functional features that were unique to PfDXR, including a potential N–glycosylation site as well as a PKC phosphorylation site, which were located on the protein surface. In recent years, a greater understanding of *P.falciparum* protein trafficking network has been established in the literature (Lingelbach and Przyborski, 2006; Spork *et al*., 2009), which has helped scientists to better understand the complexity and movements of *Plasmodium* proteins in the parasite–infected erythrocyte. Glycosylation has been shown to play a role in protein folding and trafficking (Dahms *et al*., 1989) and since as early 1999, it has been hypothesized that targeting motifs might lie in the secondary or tertiary structures (Wienk *et al*., 1999; van Dooren *et al*., 2000), which makes it feasible to analyze potential motifs, as was done in this work. Nevertheless, the need to experimentally validate theoretical hypotheses remains essential. N–glycosylation has been shown in the asexual intraerythrocytic stage of the malaria parasite (Dieckmann–Schuppert *et al*., 1992), meaning that it may be realistic, in a future work plan, to include experiments that determine whether PfDXR is glycosylated *in vitro* and *in vivo*.

Coupled to structural analysis, the PfDXR theoretical model has also facilitated the screening of novel compounds for DXR inhibition. This work made use of an *in silico* approach, coupled to an *in vitro* approach which was two–tiered – compounds were analysed for DXR–inhibition potential and for *P.falciparum* growth inhibition potential. An *in silico* screening tool provided some evidence of the potential manner in which the compound under study docked into the theoretical PfDXR active site. The literature has described numerous binding

pockets including; a pocket that binds the phosphate moiety of DXP, as well as an adjacent hydrophobic binding pocket that has been shown to accommodate the N–formyl group of fosmidomycin (reviewed by Singh *et al.*, 2007). The *in silico* docking of compounds from the same library has allowed for the comparative analysis such that specific moieties were shown to bind the theoretical binding site in a manner that closely resembled fosmidomycin and FR900098. In this work, docking allowed speculation that the shorter the carbon spacer was (between the phosphonate/phosphonate ester moiety and hydroxamic acid resembling moiety), the greater the inhibition potential. The 200 series demonstrated a greater docking potential when compared to the 300 series. In the case of the 140 series, docking parameters were specified not to include the NADPH binding motif within the AutoGrid. Becasue this group of compounds contain none of the supposedly important moieties, it may be possible that these compounds effectively inhibit DXR by binding (and essentially blocking NADPH binding) at the NADPH binding site; the possibility may also exist that these compounds (and possibly others from the 200 and 300 series) may demonstrate alternative modes of action unlike fosmidomycin. The *in silico* analysis, coupled to the *in vitro* analysis of DXR inhibition potential, lends toward this theory. Future work could therefore include the improvement of the *in silico* docking analyses by extending the parameters of the AutoGrid to include the NADPH binding site. If the 140 series docks with great affinity at the NADPH binding site, it may be prudent to rationally design more analogues of known antimalarial natural products as potential NADPH binding inhibitors. Inhibitors would have to be bifunctional, *i.e.* bind both the NADPH binding site and active site, otherwise specificity issues could result in potential inhibition other NADPH enzymes. The NADPH binding site is in very close proximity to the active site and it may be plausible to synthesize an elongated ligand that binds the NADPH binding site and protrudes into the active site or adjacent hydrophobic binding pocket described by Gieβmann *et al.* (2008).

Screening for potential DXR inhibition presented some interesting results in that some compounds inhibited only EcDXR, while some compounds only inhibited PfDXR and only a single compound inhibited both enzymes (207). This experimental data suggests that the respective enzymes do not function in the same manner and potential differences in the active site architecture may exist. While comparative tertiary structure analysis hypothesized that the catalytic residues occupied almost identical positions, the catalytic behaviour of the two enzymes was not the same. From this, two conclusions can be deduced; structurally important residues occupy different positions, or the two enzymes function is significantly

different environments *in vivo*. Structurally significant residues occupy non–identical position to their equivalents, meaning that the enzymes behave in non–identical manners. This was further validated when differences in the highly conserved region of the catalytic hatch were seen when comparing PfDXR to EcDXR. Although these two enzymes only share 36% sequence similarity (Mac Sweeney *et al.*, 2005), there is a high degree of conservancy in critical areas, including the active site and surrounds. This means that these two enzymes may exist in very difference environments *in vivo*.

In the malaria parasite, DXP is not only an intermediate in the biosynthesis of IPP and DMAPP; it is also involved in the biosynthesis of thiamin in vitamin B1 synthesis and pyridoxine in vitamin B6 synthesis (Hill *et al*., 1996; Cane *et al*, 1999; Cane *et al*., 2000; White, 1978). It therefore may be possible that DXP is limiting in the parasite when compared to bacteria, accounting for the apparent differences in the kinetic behaviour of the enzymes, where EcDXR very clearly demonstrated a greater V_{max}. This may also be the reason why PfDXR showed a greater substrate affinity for DXP, evident in the reduced K_m when compared to EcDXR. The similarity in the enzymes' catalytic efficiency (k_{cat}/K_m) means that the 10–fold greater reaction velocity for EcDXR was due to its ability to turn over more substrate (k_{cat}), indicating that DXP may not be limiting in the *E. coli* homologue, when compared to the malarial equivalent.

While DXR inhibition was accurately quantified using and NADPH–dependent enzyme assay *in vitro*, it was necessary to assess whether potential DXR inhibitors could cross the parasite membrane, a vital consideration in antimalarial drug design. According to the literature, the two negatively charged oxygens of the phosphonate moiety are necessary for good inhibition of DXR (Perruchon *et al.*, 2008), however, in drug discovery, phosphonate moieties are typically avoided because of their non–lipophilic nature (Foye *et al.*, 2008). In this work, compounds were synthesized to include an aromatic group, which may have assisted in the ability of compounds to cross the parasite membrane (Haemers *et al.*, 2006; Foye *et al.*, 2008). The literature states that the high water solubility of fosmidomycin adds to its poor bioavailability (Na–Bangchang *et al.*, 2008). It is therefore surprising that despite all its structural flaws, fosmidomycin was still able to cross the parasite membrane and inhibit growth of *P. falciparum*. In this work, only three compounds demonstrated a reasonable reduction in parasite viability, namely 304Na, 305Na and 307Na. In all these cases, the dissociation of the sodium ion in water yielded a charged phosphonate group, which appeared

to have some sort of positive effect with regards to uptake of the compound across the numerous membranes, which was perchance improved by the presence of the aromatic group. The 140 series are analogues of known antimalarial natural products, so it was not surprising they resulted in almost complete loss of parasite viability.

From the parallel *in silico* and *in vitro* drug screening, it was evident that only a single compound demonstrated reasonable potential binding to DXR (determined using *in silico* docking), inhibited DXR *in vitro*, and inhibited *P.falciparum* growth (307Na). Its potential as a lead compound in antimalarial drug development was therefore feasible. However, it was first necessary to determine whether it was toxic to human cells. The compound resulted in less than 15 % reduction in cell viability of the human cancer cell line Hst578T, meaning that it was non–toxic to human cells. In future work, a library of 307Na analogues could be synthesized to improve upon the overall inhibition potential of the compound, especially the inhibition of PfDXR. At such an early stage in the drug discovery process, the high concentration of compound that was used to test for DXR inhibition (250 µM) is not of concern because the same concentration tested in *P.falciparum* growth inhibition (250 µM) is 4 times greater than that used typically for chloroquine in drug screening experiments done at the Department of Pharmacology, University of Cape Town. Future work would hence include the determination of IC_{50} values for novel 307Na analogues in growth assays against *P.falciparum* as well as in human cells. The use of other human cell lines may also be more relevant than using a cancerous line; for example compound could be tested in human non–malignant Chang liver cells (Sui *et al*., 2008).

In conclusion, two outcomes were evident from this work. Firstly, analogues of known antimalarial natural products can be screened against malaria, which may then lead towards the rational design of novel compounds that are effective against a specific antimalarial drug target enzyme, such as PfDXR. It must however be noted that the mechanism of action of potential DXR inhibitors needs to be thoroughly analysed in order to understand the complexities of the target enzyme for future drug design. Secondly, the rational design of novel compounds against a specific antimalarial drug target enzyme can be untaken by adopting a coupled *in silico* and *in vitro* approach to drug discovery. While an *in vitro* approach to drug discovery provides vial information about the potential inhibitors under investigation, the *in silico* analysis of potential hits may provide one with information that can result in the structural improvement of existing inhibitors that are more specific to the target enzyme in question.

Since an experimental purification strategy for PfDXR has been developed in this work, future work should include the determination of the x-ray crystal structure of PfDXR. The continuation of the rational design of novel DXR inhibitors can be continued using the parallel approach proposed in the work. Once a ‘hit’ compound has been established, the crystal structure of PfDXR with the appropriate inhibitor bound may provide the evidence which will bridge the gap in research short fallings that are evident in this work.

CHAPTER 7
ADDITIONAL INFORMATION

7.1 REFERENCES

7.1.1 Internet

Bloland, P.B. (2001) World Health Organization. Drug resistance and malaria (available online at: http://www.who.int/csr/resources/publications/drugresist/malaria.pdf).

Cann, A.J. (1996) Biology of *Plasmodium parasites* and anopheles mosquitoes (available online at: http://www.wehi.edu.au/MalDB–www/intro.html).

DeLano, W.L. (2002) The PyMOL molecular graphics system. DeLano Scientific, San Carlos (available online at: http://www.pymol.org).

European Commission (2009) (available online at: http://ec.europa.eu/research/health/infectious–diseases/poverty–diseases/projects_en.html).

European Molecular Biology Laboratory, EMBL (2008) European Bioinformatics Institute (available online at http://www.ebi.ac.uk/interpro/DisplayIproEntry?ac=IPR001495).

GSK (2009) World's largest malaria vaccine trial now underway in seven African countries (available online at: http://www.gsk.com/media/pressreleases/2009/2009_pressrelease_10124.htm).

Jomaa, H., Irth, H., Van Calenbergh, S. (2007) Infectious diseases (available online at: http://ec.europa.eu/research/health/poverty–diseases/projects/102_en.htm).

MIM, (2009) Sessions Report, Symposium 41. (available online at: http://www.tropika.net/svc/specials/mim2009/session–reports/symposium–41).

National Center for Biotechnology Information, NCBI (2010) (available online at: http://www.ncbi.nlm.nih.gov/gquery/?term=1–deoxy–D–xylulose+5–phosphate+reductoisomerase).

Osipiuk, J., Mulligan, R., Stam, J., Anderson, W.F., Joachimiak, A. (2009) 1–deoxy–D–xylulose 5–phosphate reductoisomerase from Yersinia pestis (available online at: http://www.rcsb.org/pdb/results/results.do?outformat=&qrid=43631711&tabtoshow=Current)

SAMI, South Africa Malaria Initiative (2007) Socio–economic impact of malaria and the status of malaria research in South Africa (available online at: http://www.acgt.co.za/sami/).

WHO (2010_1) World Health Organisation. Malaria: Fact sheet number 94 (available online at: http://www.who.int/mediacentre/factsheets/fs094/en/print.html).

WHO (2010_2) Initiative for vaccine research (IVR) (available online at: http://www.who.int/vaccine_research/diseases/soa_parasitic/en/index4.html).

WHO (2010_3) *International travel and health,* Annexe III, World Health Organization, Geneva (available online at: http://www.searo.who.int/LinkFiles/Important_Documents_Malaria_Prevention.pdf).

WHO (2010_4) *Media centre*, World Health Organization, Geneva (available online at: http://www.who.int/mediacentre/news/releases/2010/malaria_20101118/en/index.html).

7.1.2 Books

Bruce–Chwatt, L.J., Black, R.H., Canfield, C.J., Clyde, D.F., Peters, W., Wernsdorfer, W.H. (1986) *Chemotherapy of malaria*. Second Edition. World Health Organization, Geneva, 102.

Cowman, A.F. (1998) The molecular basis of resistance to the sulfones, sulfonamides, and dihydrofolate reductase inhibitors, *Malaria: parasite biology, pathogenesis, and protection*. American Society for Microbiology, Washington DC, 303–316.

Foye, W.O., Lemke, T.L., Williams, D.A. (2008) Drugs affecting neutrotransmission and enzymes. *Foye's principals of medicinal chemistry*. Sixth Edition. Lippincott, Williams and Wilkins, Baltimore, 472.

Henriksson, L M. (2007_2). Structural and functional studies of peptidyl–prolyl *cis–trans* isomerase A and 1–deoxy–D–xylulose–5–phosphate reductoisomerase from *Mycobacterium tuberculosis*. Acta Universitatis Upsaliensis. *Digital Comprehensive Summaries of Uppsala Dissertations from the Faculty of Science and Technology* 351, 103.

Knipe, D.N., Howley, P.M. (2007) General virology. *Fields Virology*. Fifth Edition. Lippincott, Williams and Wilkins, Philadelphia, 460.

Milhous, W.K., Kyle, D.E. (1998) Introduction to the modes of action and mechanisms of resistance to antimalarials. *Malaria: parasite biology, pathogenesis, and protection*. American Society for Microbiology, Washington DC, 317–330.

Plowe, C.V. (2001) Folate antagonists and mechanisms of resistance. *Antimalarial chemotherapy: mechanisms of action, resistance, and new directions in drug discovery*. Humana Press, Totowa, 173–190.

Smith, C.A. Wood, E.J. (1991) The importance of kinetic parameters. *Biological molecules*. First Edition. Chapman and Hall, London, 90.

Vial, H.J., Calas, M. (2001) *Antimalarial chemotherapy: mechanisms of action, resistance, and new directions in drug discovery*. Totowa, NJ, Humana Press, 347–365.

7.1.3 Journals

Acharya, P., Kumar, R., Tatu, U. (2007) Chaperoning a cellular upheaval in malaria: heat shock proteins in *Plasmodium falciparum*. *Mol. Biochem. Parasitol.* 153, 85–94.

Ahn, T., Yang, S., Yun, C. (2004) Enhanced expression of human cytochrome P450 1A2 by co–expression with human molecular chaperone Hsp70. *Toxicol. Lett.* 153, 267–272.

Ahuja, S., Ahuja, S., Chen, Q., Wahlgren, M. (2006) Prediction of solubility on recombinant expression of *Plasmodium falciparum* erythrocyte membrane protein 1 domains in *Escherichia coli. Malaria J.* 5, 52–60.

Altincicek, B., Hintz, M., Sanderbrand, S., Wiesner, J., Beck, E., Jomaa, H. (2000) Tools for discovery of inhibitors of the 1–deoxy–D–xylulose 5–phosphate (DXP) synthase and DXP reductoisomerase: an approach with enzymes from the pathogenic bacterium *Pseudomonas aeruginosa*. *FEMS Microbiol. Lett.* 190, 329–333.

Ambroise–Thomas, P., Rossignol, J.F. (1986) Chemotherapy of resistant *falciparum* malaria. *Parasitol. Today* 2, 79–80.

Amrein, K.E., Takacs, B., Stieger, M., Molnos, J., Flint, N.A., Burn, P. (1995) Purification and characterization of recombinant human p50csk protein–tyrosine kinase from *an Escherichia coli* expression system overproducing the bacterial chaperones GroES and GroEL. *Proc. Natl. Acad. Sci. U.S.A.* 92, 1048–1052.

Angov, E., Hillier, C.J., Kincaid, R.L., Lyon, J.A. (2008) Heterologous protein expression is enhanced by harmonizing the codon usage frequencies of the target gene with those of the expression host. *PLoS ONE.* 3, 2189.

Argyrou, A., Blanchard, J.S. (2004) Kinetic and chemical mechanism of *Mycobacterium tuberculosis* 1–deoxy–D–xylulose–5–phosphate isomeroreductase. *Biochem.* 43, 4375–4384.

Asili, J., Lambert, M., Ziegler, H.L., Staerk, D., Sairafianpour, M., Witt, M., Asghari, G., Ibrahimi, I. S., Jaroszewski, J. W. (2004). Labdanes and isopimaranes from Platycladus orientalis and their effects on erythrocyte membrane and on *Plasmodium falciparum* growth in the erythrocyte host cells. *J. Nat. Prod.* 67, 631–637.

Baca, A.M., Hol, W.G.J. (2000) Overcoming codon bias: a method for high–level overexpression of *Plasmodium and* other AT–rich parasite genes in *Escherichia coli*. *Int. J. Parasitol.* 30, 113–118.

Baker, D., Sali, A. (2001) Protein structure prediction and structural genomics. *Science* 294, 93–96.

Banerjee, R., Liu, J., Beatty, W., Pelosof, L., Klemba, M., Goldberg, D.E. (2002) Four plasmepsins are active in the *Plasmodium falciparum* food vacuole, including a protease with an active–site histidine. *Proc. Natl. Acad. Sci. USA* 99, 990–995.

Bardsley, W.G., Kavanagh, J., Waight, R.D. (1980) Deviations from Michaelis–Menten kinetics. *Biochem. J.* 187, 739–765.

Basco, L.K., Marquet, F., Makler, M., Le Bras, J. (1995) *Plasmodium falciparum* and *Plasmodium vivax*: lactate dehydrogenase activity and its application for *in vitro* drug susceptibility assay. *Exp. Parasitol.* 80, 260–271.

Bastos, M.S., da Silva–Nunes, M., Malafronte, R.S., Hellena, E., Hoffmann, E., Wunderlich, G., Moraes, S.L., Ferreira. M.U. (2007) Antigenic polymorphism and naturally acquired antibodies to *Plasmodium vivax* merozoite surface protein 1 in rural Amazonians. *Clin. Vaccine Immunol.* 14(10), 1249–1259.

Becker, J.V., Mtwisha, L., Crampton, B.G., Stoychev, S., van Brummelen, A.C., Reeksting, S., Louw, A.I., Birkholtz, L.M., Mancama, D.T. (2010) *Plasmodium falciparum* spermidine synthase inhibition results in unique perturbation–specific effects observed on transcript, protein and metabolite levels. *BMC Genomics* 11, 235–251.

Becker, K., Kirk, K. (2004) Of malaria, metabolism and membrane transport. *Trends parasit.* 20(12), 590–596.

Behrendt, C.T., Kunfermann, A., Illarionova, V., Matheeussen, A., Grüwert, T., Groll, M., Rohdich, F., Bacher, A., Eisenreich, W., Fischer, M., Maes, L., Kurz, T. (2010) Synthesis and antiplasmodial activity of highly active reverse analogues of the antimalarial drug candidate fosmidomycin. *Chem. Med. Chem.* 5, 1–4.

Bennett, T.N., Patel, J., Ferdig, M.T., Roepe, P.D. (2007) *Plasmodium falciparum* Na+/H+ exchanger activity and quinine resistance. *Mol Biochem Parasitol.* 153(1), 48–58.

Bhattacharjee, S., van Ooij, C., Balu, B., Adams, J.H., Haldar, K. (2008) Maurer's clefts of *Plasmodium falciparum* are secretory organelles that concentrate virulence protein reporters for delivery to the host erythrocyte. *Blood* 111, 2418–2426.

Bhisutthibhan, J., Pan, X. Q., Hossler, P.A., Walker, D.J., Yowell, C.A., Carlton, J., Dame, J.B., Meshnick, S.R. (1998) The *Plasmodium falciparum* translationally controlled tumor protein homolog and its reaction with the antimalarial drug artemisinin. *J. Biol. Chem.* 273, 16192–16198.

Billman–Jacobe, H. (1996) Expression in bacteria other than *Escherichia coli. Curr. Opin. Biotechnol*. 7, 500–504.

Birkholtz, L., Blatch, G.L., Coetzer, T., Hoppe, H., Human, E., Morris, E., Ngcete, Z., Oldfield, L., Roth, R., Shonhai, A., Stephens, L.L., Louw, A.I. (2008) Heterologous expression of plasmodial proteins for structural studies and functional annotation. *Malaria J.* 7, 197.

Bitonti, A., Dumont, J., Bush, T., Edwards, M., Stemerick, D., McCann, P., Sjoerdsma, A. (1989) Bis(benzyl)polyamine analogs inhibit the growth of chloroquine–resistant human malaria parasites (*Plasmodium falciparum*) *in vitro* and in combination with α–difluoromethylornithine cure murine malaria. *Proc. Natl. Acad. Sci. USA.* 86(2), 651–655.

Bormann, S., Adegnika, A.A., Moussavou, F., Oyakhirome, S., Esser, G., Matsiegui, P.B., Ramharter, M., Lundgren, I., Kombila, M., Issifou, S., Hutchinson, D., Wiesner, J., Jomaa, H., Kremsner, P.G. (2005) Short–course regimens of artesunate–fosmidomycin in treatment of uncomplicated *Plasmodium falciparum* malaria. *Antimicrob. Agents Chemother.* 49, 3749–3754.

Boshoff, A., Nicoll, W.S., Hennessy, F., Ludewig, M., Daniel, S., Modisakeng, K.W., Shonhai, A., McNamara, C., Bradley, G., Blatch, G.L. (2004) Molecular chaperones in biology, medicine and protein biotechnology. *S. Afr. J. Sci.* 100, 665–677.

Botha, M., Pesce, E.R., Blatch, G.L. (2007) The Hsp40 proteins of *Plasmodium falciparum* and other apicomplexa: Regulating chaperone power in the parasite and the host. *Int. J. Biochem. Cell Biol.* 39, 1781–1803.

Bradford, M. (1976) A rapid and sensitive method for the quantification of microgram quantities of protein using the principle of protein–dye binding. *Anal. Biochem.* 72, 248.

Bray, P.G., Bray, P.G., Brewer, J., Schijns, V. (2009) The development of modern vaccines. *Pharm J.* 282, 679.

Bukau, B., Weissman, J., Horwich, A. (2006) Molecular chaperones and protein quality control. *Cell* 125, 443–451.

Burston, S.G., Clarke, A.R. (1995) Molecular chaperones: physical and mechanistic properties. *Essays Biochem.* 29, 125–136.

Butler, M.S. (2004) The role of natural product chemistry in drug discovery. *J. Nat. Prod.* 67, 2141–2153.

Cameron A., Read J., Tranter R., Winter V., Sessions R., Brady R.L. (2004) Identification and activity of a series of azolebased compounds with lactate dehydrogenase directed antimalarial activity. *J. Biol. Chem.* 279, 31429–31439.

Cane, D.E., Chow, C., Lillo, A., Kang, I. (2001) Molecular cloning, expression and characterization of the first three genes in the mevalonate–independent isoprenoid pathway in *Streptomyces coelicolor*. *Bioorg. Med. Chem.* 9, 1467–1477.

Cane, D.E., Du, S., Robinson, J.K., Hsiung, Y., Spenser, I.D. (1999) Biosynthesis of vitamin B_6: Enzymatic conversion of 1–deoxy–D–xylulose–5–phosphate to pyridoxol phosphate. *J. Am. Chem. Soc.* 121, 7722–7723.

Cane, D.E., Du, S., Spenser, I.D. (2000) Biosynthesis of vitamin B_6: Origin of the oxygen atoms of pyridoxol phosphate. *J. Am. Chem. Soc.* 122, 4213–4214.

Carrió, M.M., Villaverde, A. (2002) Construction and deconstruction of bacterial inclusion bodies. *J Biotechnol.* 96, 3–12.

Castelli, F., Odolini, S., Autino, B., Foca, E., Russo, R. (2010) Malaria prophylaxis: A comprehensive review. *Pharmaceuticals 3*(10), 3212–3239.

Cedrone, F., Ménez, A., Quéméneur, E. (2000). Tailoring new enzyme functions by rational redesign. *Curr. Opin. Str. Biol.* 10, 405–410.

Chakrabarti, D., Da Silva, T., Barger, J., Paquette, S., Patel, H., Patterson, S. Allen, C. M. (2002) Protein farnesyltransferase and protein prenylation in *Plasmodium falciparum*. *J. Biol. Chem.* 277, 42066–42073.

Chang, A., Scheer, M., Grote, A., Schomburg, I., Schomburg, D. (2009) BRENDA, AMENDA and FRENDA the enzyme information system: new content and tools in (2009) *Nucl. Acids Res.* 37, 588–592.

Cheetham, M.E., Caplan, A.J. (1998) Structure, function and evolution of DnaJ: conservation and adaptation of chaperone function. *Cell Stress Chap.* 3, 28–36.

Chiang, A.N., Valderramos, J.C., Balachandran, R., Chovatiya, R.J., Mead, B.P., Scneider, C., Bell, S.L., Klein, M.G., Huryn, D.M., Chen, X.S., Day, B.W., Fidock, D.A., Wipf, P., Brodsky, J.L. (2009) Select pyrimidinones inhibit the propagation of the malarial parasite, *Plasmodium falciparum*. *Bioorg*. *Med*. *Chem*. 17, 1527–1533.

Christian, D., Laurent, M. (2007) Antimalarial drug discovery: targeting protein kinases. *Expert. Opin. Ther. Targets* 11, 279–290.

Clarke, P.R., Hardie, D.G. (1990) Regulation of HMG–CoA reductase: identification of the site phosphorylated by the AMP–activated protein kinase *in vitro* and in intact rat liver. *Embo. J.* 9, 2439–2446.

Cordoba, E., Salmi, M., León, P. (2009) Unravelling the regulatory mechanisms that modulate the MEP pathway in higher plants. *J. Exp. Bot.* 60(10), 2933–2943.

Courtois, M., Mincheva, Z., Andreu, F., Rideau, M., Viaud–Massuard, M.C. (2004) Synthesis and biological evaluation with plant cells of new fosmidomycin analogues containing a benzoxazolone or oxazolopyridinone ring. *J. Enzyme Inhib. Med. Chem.* 19, 559–565.

Cunnea, P.M., Miranda–Vizuete, A., Bertoli, G., Simmen, T., Damdimopoulos, A.E., Hermann, S., Leinonen, S., Huikko, M.P., Gustafsson, J.A., Sitia, R., Spyrou, G. (2003) ERdj5, an endoplasmic reticulum (ER)–resident protein containing DnaJ and thioredoxin domains, is expressed in secretory cells or following ER stress. *J. Biol. Chem.* 278, 1059–1066.

Dahms, N.M., Lobel, P., Kornfeld, S. (1989) Mannose 6–phosphate receptors and lysosomal enzyme targeting. *J. Biol. Chem*. 264, 12115–12118.

Dale, G.E., Broger, C., Langen, H., D'Arcy, A., Stuber, D. (1994_1) Improving protein solubility through rationally designed amino acid replacements: solubilization of the trimethoprim–resistant type S1 dihydrofolate reductase. *Protein Eng.* 7, 933–939.

Dale, G.E., Schonfeld, H.J., Langen, H., Stieger, M. (1994_2) Increased solubility of trimethoprim–resistant type S1 DHFR from Staphylococcus aureus in *Escherichia coli* cells overproducing the chaperonins GroEL and GroES. *Protein Eng.* 7, 925–931.

De, D., Krogstad, F.M., Byers, L.D., Krogstad, D.J. (1998) Structure–activity relationships for antiplasmodial activity among 7– substituted 4–aminoquinolines. *J. Med. Chem.* 41, 4918–4926.

de Marco, A. (2007_1) Protocol for preparing proteins with improved solubility by co–expressing with molecular chaperones in *Escherichia coli*. *Nat. Protocol.* 2(10), 2632–2639.

de Marco, A., de Marco, V. (2004) Bacteria co–transformed with recombinant proteins and chaperones cloned in independent plasmids are suitable for expression tuning. *J.Biotechnol.* 109, 45–52.

de Marco, A., Deuerling, E., Mogk, A., Tomoyasu, T., Bukau, B. (2007_2). Chaperone–based procedure to increase yields of soluble recombinant proteins produced in *E. coli. BMC Biotechnol.* 7, 32.

de Marco, A., Volrath, S., Bruyere, T., Law, M., Fonne–Pfister, R. (2000) Recombinant maize protoporphyrinogen IX oxidase expressed in *Escherichia coli* forms complexes with GroEL and DnaK chaperones. *Protein Expr. Purif.* 20, 81–86.

Deck, L.M., Royer, R.E., Chamblee, B.B., Hernandez, V.M., Malone, R.R., Torres, J.E., Hunsaker, L.A., Piper, R.C., Makler, M.T., Vander Jagt, D.L. (1998) Selective inhibitors of human lactate dehydrogenases and lactate dehydrogenase from the malarial parasite *Plasmodium falciparum*. *J. Med. Chem.* 41, 3879–3887.

Deng, L., Sundriyal, S., Rubio, V., Shi, Z.Z., Song, Y. (2009) Coordination chemistry based approach to lipophilic inhibitors of 1–deoxy–D–xylulose–5–phosphate reductoisomerase. *J. Med. Chem.* 52, 6539 –6542.

Depetrillo, J.C., Singer, C., Bergagnini, I.A., Kolakowski, P., Edwards, B., Smith, M.A. (2010) Assessment of adherence to atovaquone–proguanil prophylaxis in travellers. *Journal of Travel Medicine* 17, 217–220.

Deuerling, E., Bukau, B. (2004) Chaperone–assisted folding of newly synthesized proteins in the cytosol. *Crit. Rev. Biochem. Mol. Biol*. 39, 261–277.

Deuerling, E., Schulze–Specking, A., Tomoyasu, T., Mogk, A., Bukau, B. (1999) Trigger factor and DnaK cooperate in folding of newly synthesized proteins. *Nature* 400(6745), 693–696.

Devreux, V., Wiesner, J., Goeman, J.L., Van der Eycken, J., Jomaa, H., Van Calenbergh, S. (2006) Synthesis and biological evaluation of cyclopropyl analogues of fosmidomycin as potent *Plasmodium falciparum* growth inhibitors. *J. Med. Chem*. 49, 2656–2660.

Dharia, N.V., Sidhu, A.B.S., Cassera, M.B., Westenberger, S.J., Bopp, S.E.R., Eastman, R.T., Plouffe, D., Batalov, S., Park, D.J., Volkman, S.K., Wirth, D.F., Zhou, Y., Fidock, D.A., Winzeler, E.A. (2009) Use of high–density tiling microarrays to identify mutations globally and elucidate mechanisms of drug resistance in *Plasmodium falciparum*. *Genome Biol.* 10(2), R21.

Dhiman, R.K, Schaeffer, M.L., Bailey, A.M., Testa, C.A., Scherman, H., Crick, D.C. (2005) 1–Deoxy–D–xylulose–5–phosphate reductoisomerase (IspC) from *Mycobacterium tuberculosis*: towards understanding mycobacterial resistance to fosmidomycin. *J. Bacteriol.* 187(24), 8395–8402.

Dieckmann–Schuppert, A., Bender, S., Odenthal–Schnittler, M., Bause, E., Schwarz, R.T. (1992) Apparent lack of N–glycosylation in the asexual intraerythrocytic stage of *Plasmodium falciparum*. *Eur J. Biochem.* 205, 815–825.

Disch, A., Schwender, J., Müller, C., Lichtenthaler, H.K., Rohmer, M. (1998) Distribution of the mevalonate and glyceraldehyde phosphate/pyruvate pathways for isoprenoid biosynthesis in unicellular algae and the cyanobacterium *Synechocystis* PCC 6714 . *Biochem. J.* 333, 381–388.

Dondorp, A.M., Nosten, F., Yi, P., Das, D., Phyo, A.P., Tarning, J., Lwin, K.M., Ariey, F., Hanpithakpong, W., Lee, S.J., Ringwald, P., Silamut, K., Imwong, M., Chotivanich, K., Lim, P., Herdman, T., An, S.S., Yeung, S., Singhasivanon, P., Day, N.P., Lindegardh, N., Socheat, D., White, N.J. (2009) Artemisinin resistance in *Plasmodium falciparum* malaria. *N. Engl. J. Med.*, 361(5),455–467.

Doolan, D.L., Hoffman, S.L. (2001) DNA–based vaccines against malaria: status and promise of the multi–stage malaria DNA vaccine operation. *Int. J. Parasitol.* 31, 753–762.

Druilhel, P., Spertini, F., Soesoe1, D., Corradin, G., Mejia, P., Singh, M., Audran, R., Bouzidi, A., Oeuvray1, C., Roussilhon1, C. (2005) A malaria vaccine that elicits in humans antibodies able to kill *Plasmodium falciparum*. *PLoS Med.* 2(11), 1135–1144.

Dubey, V.S. (2002) Mevalonate–independent pathway of isoprenoids synthesis: A potential target in some human pathogens. *Curr. Sci.* 83(6), 685–688.

Dzinjalamala, F.K., Macheso, A., Kublin, J.G., Taylor, T.E., Barnes, K.I., Molyneux, M.E., Plowe, C.V. and Smith, P. (2005) Blood folate concentrations and *in vivo* sulfadoxine–pyrimethamine failure in Malawian children with uncomplicated *Plasmodium falciparum* malaria. *Am. J. Trop. Med. Hyg.* 72, 267–272.

Eggleson, K.K., Duffin, K.L. and Goldberg, D.E. (1999) Identification and characterization of falcilysin, a metallopeptidase involved in hemoglobin catabolism within the malaria parasite *Plasmodium falciparum*. *J. Biol. Chem.* 274, 32411–32417.

Eisenthal, R. (1974) The direct linear plot. *Biochem. J.* 139, 715–720.

Engprasert, S., Taura, F., Shoyama, Y. (2005) Molecular cloning, expression and characterization of recombinant 1–deoxy–D–xylulose–5–phosphate reductoisomerase from *Coleus forskohlii* Briq. *Plant Sci.* 169, 287–294.

Fatumo, S., Plaimas, K., Mallm, J.P., Schramm, G., Adebiyi, E., Oswald, E., Eils, R, Kònig, R. (2009) Estimating novel potential drug targets of *Plasmodium falciparum* by analysing the metabolic network of knock–out strains *in silico*. *Infect. Gen. Evol.* 9, 351–358.

Fernandes, R.P.M., Phaosiri, C., Proteau, P.J., (2005) Mutation in the flexible loop of 1–deoxy–D–xylulose 5–phosphate reductoisomerase broadens substrate utilization. *Arch. Biochem. Biophys.* 444, 159–164.

Ferreira, M.U., da Silva–Nunes, M., Wunderlich, G. (2004) Antigenic diversity and immune evasion by malaria parasites. *Clin. Diagn. Lab. Immunol*. 11, 987–995.

Fink, A.L. (1999) Chaperone–mediated protein folding. Physiol. Rev. *79, 425.*

Fidock, D.A. (2010) Priming the antimalarial pipeline. *Nature Drug Disc.*, 467, 297–298.

Flatmark, T., Jorunn, Stokka, A.J., Berge, S.V. (2001) Use of surface plasmon resonance for real–time measurements of the global conformational transition in human phenylalanine hydroxylase in response to substrate binding and catalytic activation. *Anal. Biochem.* 294, 95–101.

Flick, K., Ahuja, S., Chene, A., Bejarano, M.T., Chen, Q. (2004) Optimized expression of *Plasmodium falciparum* erythrocyte membrane protein 1 domains in *Escherichia coli*. *Malaria J.* 3(50).

Flitsch, W., Lubisch, W., Rosche, J. (1987) Synthetic routes to 1–substituted butadienylphosphonates. *Liebigs Ann. Chem.* 8, 661–664.

Fournillier, A., Wychowski, C., Boucreux, D., Baumert, T.F., Meunier, J.C., Jacobs, D., Muguet, S., Depla, E., Inchauspe, G. (2001) Induction of hepatitis C virus E1 envelope protein–specific immune response can be enhanced by mutation of N–glycosylation sites. *J. Virol*. 75, 12088–12097.

Fox, D.T., Poulter, C.D. (2005) Mechanistic studies with 2–C–methyl–D–erythritol 4–phosphate synthase from *Escherichia coli. Biochem.* 44(23), 8360–8368.

Gardner, M.J., Tettelin, H., Carucci, D.J., Cummings, L.M., Aravind, L., Koonin, E.V., Shallom, S., Mason, T., Yu, K., Fujii, C., Pederson, J., Shen, K., Jing, J., Aston, C., Lai, Z., Schwartz, D.C., Pertea, M., Salzberg, S., Zhou, L., Sutton, G.G, Clayton, R., White, O., Smith, H.O., Fraser, C.M., Adams, M.D., Venter, J.C., Hoffman, S.L. (1998) Chromosome 2 sequence of the human malaria parasite *Plasmodium falciparum*. *Science* 282, 1126–1132.

Geisse, S., Gram, H., Kleuser, B., Kocher, H.P. (1996) Eukaryotic expression systems: A comparison. *Protein Expr. Pur.* 8, 271–282.

Georgiou, G., Valax, P. (1996) Expression of correctly folded proteins in *Escherichia coli*. *Curr. Opin. Biotechnol.* 7, 190–197.

Gero, A.M., Dunn, C.G., Brown, D.M., Pulenthiran, K., Gorovits, E.L., Bakos, T. Weis, A.L. (2003) New malaria chemotherapy developed by utilization of a unique parasite transport system. *Curr. Pharm. Des.* 9, 867–877.

Geyer, J.A., Prigge, S.T., Waters, N.C. (2005) Targeting malaria with specific CDK inhibitors. *Biochim. Biophys. Acta* 1754, 160–170.

Gieβmann, D., Heidler, P., Haemers, T., Van Calenbergh, S., Reichenberg. A., Jomaa, H., Weidemeyerd, C., Sanderbrand, S., Wiesner, J., Link, A. (2008) Towards new antimalarial drugs: synthesis of non–hydrolyzable phosphate mimics as feed for a predictive QSAR study on 1–deoxy–D–xylulose–5–phosphate reductoisomerase inhibitors. *Chem. Biodiv*. 5, 643–656.

Girard, M.P., Reed, Z.H., Friede, M., Kieny, M.P. (2007) A review of human vaccine research and development: malaria. *Vaccine* 25(9), 1567–1580.

Goble, J.L., Adendorff, M.R., de Beer, T.A.P., Stephens, L.L., Blatch, G.L. (2010) The malarial drug target *Plasmodium falciparum* 1–deoxy–D–xylulose–5–phosphate reductoisomerase (*Pf*DXR): development of a 3–D model for identification of novel, structural and functional features and for inhibitor screening. *Protein Pept. Lett.*17, 109–120.

Gowda, D.C., Davidson, E.A. (1999) Protein glycosylation in the malaria parasite. *Parasitol. Today* 15, 147–152.

Gräslund, S., Nordlund, P., Weigelt, J., Hallberg, B.M., Bray, J., Gileadi, O., Knapp, S., Oppermann, U., Arrowsmith, C., Hui, R., Ming, J., dhe–Paganon, S., Park, H.W., Savchenko, A., Yee, A., Edwards, A., Vincentelli, R., Cambillau, C., Kim, R., Kim, S.H., Rao, Z., Shi, Y., Terwilliger, T.C., Kim, C.Y., Hung, L.W., Waldo, G.S., Peleg, Y., Albeck, S., Unger, T., Dym, O., Prilusky, J., Sussman, J.L., Stevens, R.C., Lesley, S.A., Wilson, I.A., Joachimiak,

A., Collart, F., Dementieva, I., Donnelly, M.I., Eschenfeldt, W.H., Kim, Y., Stols, L., Wu, R., Zhou, M., Burley, S.K., Emtage, J.S., Sauder, J.M., Thompson, D., Bain, K., Luz, J., Gheyi, T., Zhang, F., Atwell, S., Almo, S.C., Bonanno, J.B., Fiser, A., Swaminathan, S., Studier, F.W., Chance, M.R., Sali, A., Acton, T.B., Xiao, R., Zhao, L., Ma, L.C., Hunt, J.F., Tong, L., Cunningham, K., Inouye, M., Anderson, S., Janjua, H., Shastry, R., Ho, C.K., Wang, D., Wang, H., Jiang, M., Montelione, G.T., Stuart, D.I., Owens, R.J., Daenke, S., Schütz, A., Heinemann, U., Yokoyama, S., Büssow, K., Gunsalus, K.C. (2008) Protein production and purification. *Nat. Methods* 5, 135–146.

Greenfield, N.J. (1975) Circular dichroism studies of dihydrofolate reductase from a methotrexate–resistant strain of *Escherichia coli* B, MB 1428: ternary complexes. *Biochim. Biophys. Acta* 403, 42–36.

Grolle, S., Bringer–Meyer, S., Sahm, H. (2000) Isolation of the dxr gene of *Zymomonas mobilis* and characterization of the 1–deoxy–D–xylulose 5–phosphate reductoisomerase. *FEMS Microbiol. Lett*. 191, 131–137.

Haacke, A., Fendrich, G., Ramage, P., Geiser M. (2009) Chaperone over–expression in *Escherichia coli*: Apparent increased yields of soluble recombinant protein kinases are due mainly to soluble aggregates. *Protein Expr. Purif.* 64, 185–193.

Haemers, T., Wiesner, J., Van Poecke, S., Goeman, J., Henschker, D., Beck, E., Jomaa, H., Van Calenbergh, S. (2006) Synthesis of α–substituted fosmidomycin analogues as highly potent *Plasmodium falciparum* growth inhibitors. *Bioorg. Med. Chem. Lett.*16, 1888–1891.

Håkansson, K.O., Østergaard, H., Winther, J.R. (2006) Crystallization of mutant forms of glutaredoxin Grx1p from yeast. *Acta Crystallogr. Sect. F. Struct. Biol. Cryst. Commun*. 62, 920–922.

Hanning, G., Makrides, S.C. (1998) Strategies for optimizing heterologous protein expression in *Escherichia coli*. *Tibtechnology* 16, 54–60.

Haque, T.S., Skillman, A.G., Lee, C.E., Habashita, H., Gluzman, I.Y., Ewing, T.J., Goldberg, D.E., Kuntz, I. D. and Ellman, J.A. (1999) Potent, low–molecular–weight non–peptide inhibitors of malarial aspartyl protease plasmepsin II. *J. Med. Chem.* 42, 1428–1440.

Hardcastle, I.R., Golding, B.T., Griffin, R.J. (2002) Designing inhibitors of cyclin–dependent kinases. *Ann. Rev. Pharmacol. Toxicol.* 42, 325–348.

Harrison, C. (2003) GrpE, a nucleotide exchange factor for DnaK. *Cell Stress Chap.* 8(3), 218–24.

Harvey, R.G. (1966) Reactions of triethylphosphite with activated olefins. *Tetrahedron* 22, 2561.

Hayhurst, A., Harris, W.J. (1999) *Escherichia coli* Skp chaperone coexpression improves solubility and phage display of single–chain antibody fragments. *Protein Expr. Purif.* 15, 336–343.

Henriksson, L.M., Bjorkelid, C., Mowbray, S.L., Unge, T. (2006) The 1.9 a resolution structure of *Mycobacterium tuberculosis* 1–deoxy–D–xylulose 5–phosphate reductoisomerase, a potential drug target. *Acta Crystallogr*. 62, 807.

Henriksson, L.M., Unge, T., Jones, T.A., Mowbray, S.L. (2007_1) Structures of *Mycobacterium tuberculosis* 1–deoxy–D–xylulose–5–phosphate reductoisomerase provide new insights into catalysis. *J. Biol. Chem.* 282, 19905.

Herforth, C., Wiesner, J., Heidler, P., Sanderbrand, S., Van Calenbergh, S., Jomaa, H., Link, A. (2004) Antimalarial activity of N6–substituted adenosine derivatives. Part 3. *Bioorg. Med. Chem.* 12, 755–762.

Hill, R.E., Himmeldirk, K., Kennedy, I.A., Pauloski, R.M., Sayer, B.G., Wolf, E., Spenser, I.D. (1996) A 13C NMR investigation of the biosynthesis of pyridoxol in *Escherichia coli*. *J. Biol. Chem.* 271, 30426–30435.

Hiller, N.L., Bhattacharjee, S., van Ooij, C., Liolios, K., Harrison, T., Lopez–Estrano, C., Haldar. K. (2004) A host–targeting signal in virulence proteins reveals a secretome in malarial infection. *Science*, 306, 1897–1898.

Hoeffler, J.F., Tritsch, D., Grosdemange–Billiard, C., Rohmer, M. (2002) Isoprenoid biosynthesis via the methylerythritol phosphate pathway: mechanistic investigations of the 1–deoxy–D–xylulose–5–phosphate reductoisomerase. *Eur. J. Biochem.* 269, 4446–4457.

Hoppe, H.C., van Schalkwyk, D.A., Wiehart, U.I.M., Meredith, S.A., Egan, J., Weber, B.W. (2004) Antimalarial quinolines and artemisinin inhibit endocytosis in *Plasmodium falciparum*. *Antimicrob. Agents Chemother*. 48(7), 2370–2378.

Horton, R. (2003) Medical journals: evidence of bias against the diseases of poverty. *Lancet* 361, 712–713.

Hosoda A., Kimata Y., Tsuru A., Kohno K. (2003) A novel endoplasmic reticulum–resident protein containing both a BiP–interacting J–domain and thioredoxin–like motifs. *J. Biol. Chem*. 278, 2669–2676

Houry, W.A. (2001) Chaperone–assisted protein folding in the cell cytoplasm. *Curr. Protein Pept. Sci.* 2, 227–44.

Hu, X., O'Hara, L., White, S., Magner, E., Kane, M., Wall, J.G. (2007) Optimisation of production of domoic acid–binding scFv antibody fragment in *Escherichia coli* using molecular chaperones and functional immobilisation on a mesoporous silicate support. *Protein Expr. Purif.* 52, 194–201.

Hunter, W.M. (2007) The non–mevalonate pathway of isoprenoid precursor biosynthesis. *J. Biol. Chem.* 282(30), 21573–21577.

Hyde, J.E. (2005) Exploring the folate pathway in *Plasmodium falciparum*. *Acta Trop*. 94, 191–206.

Hyde, J.E., Dittrich, S., Wang, P., Sims, P.F., de Crécy–Lagard, V., Hanson, A.D. (2008) *Plasmodium falciparum*: a paradigm for alternative folate biosynthesis in diverse microorganisms? *Trends Parasitol.* 24, 502–508.

Jawaid, S, Seidle, H, Zhou, W, Abdirahman, H, Abadeer, M, *et al*. (2009) Kinetic characterization and phosphoregulation of the *Francisella tularensis* 1–deoxy–D–xylulose 5–phosphate reductoisomerase (MEP Synthase). *PLoS ONE* 4, 8288.

Jiang, L., Lee, P.C., White, J., Rathod, P.K. (2000) Potent and selective activity of a combination of thymidine and 1843U89, a folate–based thymidylate synthase inhibitor, against *Plasmodium falciparum*. *Antimicrob*. *Agents Chemother*. 44(4), 1047–1050.

Jirage, D., Keenan, S.M., Waters, N.C. (2010) Exploring Novel Targets for Antimalarial Drug Discovery: Plasmodial Protein Kinases. *Infect. Disord. Drug Targets* 10, 134–146.

Johnson, D.J., Owen, A., Plant, N., Bray, P.G., Ward, S.A. (2008) Drug–regulated expression of *Plasmodium falciparum* P–glycoprotein homologue 1: a putative role for nuclear receptors. *Antimicrob. Agents Chemother.* 52, 1438–1445.

Jomaa, H., Wiesner, J., Sanderbrand, S., Altincicek, B., Weidemeyer, C., Hintz, M., Türbachova, I., Eberl, M., Zeidler, J., Lichtenthaler, H.K., Soldati, D., Beck, E. (1999) Inhibitors of the nonmevalonate pathway of isoprenoid biosynthesis as antimalarial drugs. *Science* 285, 1573–1576.

Kappe, S.H.I., Kaiser, K., Matuschewski, K. (2003) The *Plasmodium* sporozoite journey: a rite of passage. *Trends Parasitol.* 19, 135–143.

Karsten, V., Qi, H., Beckers, C.J.M., Reddy, A., Dubremetz, J.F., Webster, P., Joiner, K.A. (1998) The protozoan parasite Toxoplasma gondii targets proteins to dense granules and the vacuolar space using both conserved and unusual mechanisms. *J. Cell. Biol*. 141, 1323–1333.

Keenan, S.M., Geyer, J.A., Welsh, W.J., Prigge, S.T., Waters, N.C. (2005) Rational inhibitor design and iterative screening in the identification of selective plasmodial cyclin dependent kinase inhibitors. *Comb. Chem. High Throughput Screen.* 8, 27–38.

Keough, D.T., Ng, A.L., Winzor, D.J., Emmerson, B.T., de Jersey, J. (1999) Purification and characterization of *Plasmodium falciparum* hypoxanthine–guanine–xanthine phosphoribosyltransferase and comparison with the human enzyme. *Mol. Biochem. Parasitol.* 98, 29–41.

Kesselheim, A.S. (2008) Drug development for neglected diseases — the trouble with FDA review vouchers. *N. Engl. J. Med.* 359, 1981–1983.

Kim, S.M., Kuzuyama, T., Chang, Y.J., Song, K.S., Kim, S.U. (2006) Identification of class 2 1–deoxy–D–xylulose 5–phosphate synthase and 1–deoxy–D–xylulose 5–phosphate reductoisomerase genes from *Ginkgo biloba* and their transcription in embryo culture with respect to ginkgolide biosynthesis. *Planta. Med. 7*2(3), 234–240.

Kishimoto, A., Nishiyama, K., Nakanishi, H., Uratsuji, Y., Nomura, H., Takeyama, Y., Nishizuka, Y. (1985) Studies on the phosphorylation of myelin basic protein by protein kinase C and adenosine 3':5'–monophosphate–dependent protein kinase. *J. Biol. Chem*. 260, 12492–12499.

Klemba, M., Gluzman, I., Goldberg, D.E. (2004) A *Plasmodium falciparum* dipeptidyl aminopeptidase I participates in vacuolar hemoglobin degradation. *J. Biol. Chem*. 279, 43000–43007.

Knockaert, M., Greengard, P., Meijer, L. (2002) Pharmacological inhibitors of cyclin–dependent kinases. *Trends Pharmacol. Sci*. 23, 417–425.

Kochan, Z., Karbowska, J., Bukato, G., Zydowo, M.M., Bertoli, E., Tanfani, F., Swierczyński, J. (1995) A comparison of the secondary structure of human brain mitochondrial and cytosolic 'malic' enzyme investigated by Fourier–transform infrared spectroscopy. *Biochem. J*. 309, 607–611.

Köhler, S., Delwiche, C.F., Denny, P.W., Tilney, L.G., Webster, P., Wilson, R.J.M., Palmer, J.D., Roos, D.S. (1997) A plastid of probable green algal origin in apicomplexan parasites. *Science* 275, 1485–1488.

Koppisch, A.T., Fox, D.T., Blagg, B.S., Poulter, C.D. (2002) *E. coli* MEP synthase: steady–state kinetic analysis and substrate binding. *Biochem.* 41, 236–243.

Kost, T.A, Condreary, J.P., Jarvis, D.L. (2005) Baculovirus as versatile vectors for protein expression in insect and mammalian cells. *Nat. Biotechnol.* 23, 567–575.

Kroemer, R.T., Doughty, S.W., Robinson, A.J. (1996) Prediction of the three–dimensional structure of human interleukin–7 by homology modelling. *Protein Eng.* 9, 493–498.

Kumar, N., Koski, G., Harada, M., Aikawa, M., Zheng, H. (1991) Induction and localization of *Plasmodium falciparum* stress proteins related to the heat shock protein 70 family. *Mol. Biochem. Parasitol.* 48, 47–58.

Kumar, N., Zheng, H. (1992) Nucleotide sequence of a *Plasmodium falciparum* stress protein with similarity to mammalian 78–kDa glucose–related protein. *Mol. Biochem. Parasitol.* 56, 353–356.

Kumar, R., Adams, B., Musiyenko, A., Shulyayeva, O., Barik, A. (2005) The FK506–binding protein of the malaria parasite, *Plasmodium falciparum*, is a FK506–sensitive chaperone with FK506 independent calcineurin–inhibitory activity. *Mol. Biochem. Parasitol*.141, 163–173.

Kuntz, L., Tritsch, D., Grosdemange–Billiard, C., Hemmerlin, A., Willem, A., Bacht, T. J., Rohmer, M. (2005) Isoprenoid biosynthesis as a target for antibacterial and antiparasitic drugs: phosphonohydroxamic acids as inhibitors of deoxyxylulose phosphate reducto–isomerase. *Biochem. J*. 386, 127–135.

Kurz, T., Geffken, D., Wackendorff, C. (2003_1) Hydroxyurea analogues of fosmidomycin. *Z. Naturforsch.* 58B, 106–110.

Kurz, T., Geffken, D., Wackendorff, C. (2003_2) Carboxylic acid analogues of fosmidomycin. *Z. Naturforsch* .58B, 457–461.

Kuzuyama, T., Takahashi, S., Takagi, M. Seto, H. (2000) Characterization of 1–deoxy–D–xylulose 5–phosphate reductoisomerase, an enzyme involved in isopentenyl diphosphate biosynthesis and identification of its catalytic amino acid residues. *J. Biol. Chem.* 275, 19928–19932.

Kvakovszky, G., McKim, A.S., Moore, J. (2007) A review of microelectronic manufacturing applications using DMSO–based chemistries. *ECS Transact.*11 (2), 227–234.

LaCount, D.J., Vignali, M., Chettier, R., Phansalkar, A., Bell R., Hesselberth, J.R., Schoenfeld, L.W., Ota, I., Sahasrabudhe, S., Kurschner, C., Fields, S., Hughes, R.E. (2005) A protein interaction network of the malaria parasite *Plasmodium falciparum*. *Nature* 438, 103–107.

Laemmli, U.K. (1970) Cleavage of structural proteins during the assembly of the head of bacteriophage T4. *Nature* 227, 680–685.

Laskowski, R.A., MacArthur, M.W., Moss, D.S., Thornton, J.M. (1993) PROCHECK: a program to check the stereochemical quality of protein structures. *J. Appl. Crystallogr*. 26, 283–291.

Lawson, J.C., Blatch, G.L., Edkins, A.L. (2009) Cancer stem cells in breast cancer and metastasis. *Breast Cancer Res. Treat.* 118, 41–54.

Le Cabec, V., Cowland, J.B., Calafat, J., Borregaard, N. (1996) Targeting of proteins to granule subsets is determined by timing and not by sorting – the specific granule protein NGAL is localized to azurophil granules when expressed in HL–60 cells. *Proc. Natl. Acad. Sci. U. S. A.* 93, 6454–6457.

Lee, C.S., Salcedo, E., Wang, Q., Wang, P., Sims, P.F., Hyde, J.E. (2001) Characterization of three genes encoding enzymes of the folate biosynthetic pathway in *Plasmodium falciparum*. *Parasitol.* 122(1), 1–13.

Liao, Z., Chen, R., Chen, M., Yang, C., Wang, Q., Gong, Y. (2007) A new 1–deoxy–D–xylulose 5–phosphate reductoisomerase gene encoding the committed–step enzyme in the MEP pathway from *Rauvolfia verticillata. Z. Naturforsch. C* 62, 296–304.

Lilie, H., Schwarz, E., Rudolph, R. (1998) Advances in refolding of proteins produced in *E. coli*. *Curr. Opin. Biotechnol.* 9, 497–501.

Ling, Y., Sahota, G., Odeh, S., Chan, J.M.W., Araujo, F.G., Moreno, S.N.J., Oldfield, E. (2005) Bisphosphonate inhibitors of *Toxoplasma gondi* growth: *In vitro*, QSAR, and *in vivo* investigations. *J. Med. Chem*. 48, 3130–3140.

Lingelbach, K., Przyborski, J.M. (2006) The long and winding road: protein trafficking mechanisms in the *Plasmodium falciparum* infected erythrocyte. *Mol. Biol. Parasitol.* 147, 1–8.

Mac Sweeney, A., Lange, R., Fernandes, R.P., Schulz, H., Dale, G.E., Douangamath, A., Proteau, P.J., Oefner, C. (2005) The crystal structure of *E. coli* 1–deoxy–D–xylulose–5–phosphate reductoisomerase in a ternary complex with the antimalarial compound fosmidomycin and NADPH reveals a tight–binding closed enzyme conformation. *J. Mol. Biol.* 345, 115–127.

Macreadie, I., Ginsburg, H., Sirawaraporn, W., Tilley, L. (2000) Antimalarial drug development and new targets. *Parasitol. Today* 16, 438–444.

Makrides, S.C. (1996) Strategies for achieving high–level expression of genes in *Escherichia coli*. *Microbiol. Rev*. 60, 512–538.

Malkin, E.M., Diemert, D.J., McArthur, J.H., Perreault, J.R., Miles, A.P., Giersing, B.K., Mullen, G.E., Orcutt, A., Muratova, O., Awkal, M., Zhou, H., Wang, J., Stowers, A., Long, C.A., Mahanty, S., Miller, L.H., Saul, A., Durbin, A.P. (2005) Phase 1 clinical trial of apical membrane antigen 1: an asexual blood–stage vaccine for *Plasmodium falciparum* malaria. *Infect Immun.* 73, 3677–3685.

Manning, G., Plowman, G.D., Hunter, T., Sudarsanam, S. (2002) Evolution of protein kinase signaling from yeast to man. *Trends Biochem. Sci*. 27, 514–20.

Marshall, R.D. (1972) Glycoproteins. *Annu. Rev. Biochem*. 41, 673–702.

Martin, R.E., Ginsburg, H., Kirk, K. (2009) Membrane transport proteins of the malaria parasite. *Mol. Microbiol*. 74, 519–28.

Martin, R.E., Marchetti, R.V., Cowan, A.I., Howitt, S.M., Bröer, S., Kirk, K. (2009) Chloroquine transport via the malaria parasite's 'Chloroquine Resistance Transporter'. *Science* 325, 1680–1682.

Martínez–Torrecuadrada, J.L., Romero, S., Núñez, A., Alfonso, P., Sánchez–Céspedes, M., Casal, J.I. (2005) An efficient expression system for the production of functionally active human LKB1. *J. Biotechnol.* 115, 23–34.

Matambo, T.S., Odunuga, O.O., Boshoff, A., Blatch, G.L. (2004) Overproduction, purification and characterization of the *Plasmodium falciparum* heat shock protein 70. *Protein Expr. Purif.* 33, 214–222.

Mather, M.W., Henry, K.W., Vaidya, A.B. (2007) Mitochondrial drug targets in apicomplexan parasites. *Curr. Drug Targets* 8, 49–60.

Mayer, M.P., Rüdiger, S., Bukau, B. (2000) Molecular basis for interactions of the DnaK chaperone with substrates. *Biol. Chem.* 381, 877–885.

McConkey, G.A. (1999) Targeting the shikimate pathway in the malaria parasite *Plasmodium falciparum*. *Antimicrob. Agents Chemother*. 43, 175–177.

McFadden, G.I. (1999_1) Plastids and protein targeting. *J. Euk. Microbiol*. 46, 339–346.

McFadden, G.I. (1999_2) Endosymbiosis and evolution of the plant cell. *Curr. Opin. Plant Biol*. 2, 513–519.

Mehlin, C., Boni, E., Buckner, F.S., Engel, L., Feis, T, Gelb, M.H., Haji, L., Kim, D., Liu, C., Mueller, N., Myler, P.J., Reddy, J.T., Sampson, J.N., Subramanian, E., Van Voorhis, W.C., Worthey, E., Zucker, F., Hol, W.G.J. (2006) Heterologous expression of proteins from *Plasmodium falciparum*: Results from 1000 genes. *Mol. Biochem. Parasitol.* 148, 144–160.

Merckle, L., de Andres–Gomez, A., Dick, B., Cox, R.J, Godfrey, C.R. (2005) A fragment–based approach to understanding inhibition of 1–deoxy–D–xylulose–5–phosphate reductoisomerase *Chem. Biochem.* 6, 1866–18674.

Meyer, O., Grosdemange–Billiard, C., Tritsch, D., Rohmer, M. (2003) Isoprenoid biosynthesis via the MEP pathway. Synthesis of (3R,4S)–3,4–dihydroxy–5–oxohexylphosphonic acid, an isosteric analogue of 1–deoxy–D–xylulose 5–phosphate, the substrate of the 1–deoxy–D–xylulose 5–phosphate reducto–isomerase. *Org. Biomol. Chem*. 1, 4367–4372.

Michaelis, L., Menten, M.L. (1913). *Kinetik der Invertinwirkung Biochem. Z.* 49, 333–369.

Midorikawa, Y., Haque, Q.M. (1997) 15–Deoxyspergualin, an immunosuppressive agent, used in organ transplantation showed suppressive effects on malarial parasites. *Chemotherapy* 43, 31–35.

Midorikawa, Y., Haque, Q.M., Nakazawa, S. (1998) Inhibition of malaria–infected erythrocytes by deoxyspergualin: effect on *in vitro* growth of malaria cultures. *Chemotherapy* 48, 409–413.

Mincheva, Z., Curtois, M., Creche, J., Ridaeu, M., Viaud–Massard, M.C. (2003) One–pot synthesis of functionalized 4,5–dihydroisoxazole derivatives *via* nitrile oxides and biological evaluation with plant cells. *Bioorg. Med. Chem*. 12, 191–197.

Misra, G., Ramachandran, R. (2009) Hsp70–1 from *Plasmodium falciparum*: protein stability, domain analysis and chaperone activity. *R. Biophysical Chem.* 142(1–3), 55–64.

Moore, J.T., Arvinder, U., Maley, F., Maley, G.F. (1993) Overcoming inclusion body formation in a high level expression system. *Protein Expr. Purif.* 4, 160–163.

Morgan D.O. (1997) Cyclin–dependent kinases: engines, clocks, and microprocessors. *Annu. Rev. Cell Dev. Biol.* 13, 261–291.

Morris, G.M., Goodsell, D.S., Halliday, R.S., Huey, R., Hart, W.E., Belew, R.K., Olson, A.J. (1998) Automated docking using a lamarckian genetic algorithm and empirical binding free energy function. *J. Comput. Chem.* 19, 1639–1662.

Morton, C.L., Potter, P.M. (2000) Comparison of *Escherichia coli*, *Saccharomyces cerevisiae*, *Pichia pastoris*, *Spodoptera frugiperda*, and COS7 cells for recombinant gene expression. *Mol. Biotechnol.* 16, 193–202.

Moura, P.A., Dame, J.B., Fidock, D.A. (2009) Role of Plasmodium falciparum digestive vacuole plasmepsins in the specificity and antimalarial mode of action of cysteine and aspartic protease inhibitors. *Antimicrob. Agents Chemother*. 53, 4968–4978.

Müller, I.B., Das, R., Kai, G., Lüersen, K., Wrenger, C., Walter, R.D. (2008) Assessing the polyamine metabolism of *Plasmodium falciparum* as chemotherapeutic target. *Mol. Biochem. Parasitol.* 160, 1–7.

Murakawa, T., Sakamoto, H., Fukada, S., Konishi, T., Nishida, M. (1982). Pharmacokinetics of fosmidomycin, a new phosphonic acid antibiotic. *Antimicrob. Agents Chemother*. 21(2), 224–230.

Na–Bangchang, K., Ruengweerayut, R., Karbwang, J., Chauemung, A., Hutchinson, D. (2007) Pharmacokinetics and pharmacodynamics of fosmidomycin monotherapy and combination therapy with clindamycin in the treatment of multidrug resistant *falciparum* malaria. *Malaria J.* 6, 70.

Narum, D.L., Kumar, S., Rogers, W.O., Fuhrmann, S.R., Liang, H., Oakley, M., Taye, A., Sim, B.K.L., Hoffman, S.L. (2001) Codon optimization of gene fragments encoding *Plasmodium falciparum* merzoite proteins enhances DNA vaccine protein expression and immunogenicity in mice. *Infect. Immun.* 69, 7250–7253.

Ndugwa, R.P., Müller, O., Kouyaté, B., Becher, H., Ramroth, H. (2007) Improving malaria mortality estimates for rural Africa by adding further studies. *Int. J. Epidemiol*. 36, 242–247.

Nicoll, W.S., Boshoff, A., Ludewig, M.H., Hennessy, F., Jung, M., Blatch, G.L. (2006) Approaches to the isolation and characterization of molecular chaperones. *Protein Expr. Pur*. 46, 1–15.

Nishihara, K., Kanemori, M., Kitagawa, M., Yangi, H., Yura, T. (1998) Chaperone co–expression and synergistic roles of DnaK–DnaJ–GrpE and GroEL–GroES in assisting folding of an allergen of Japanese cedar pollen, Cryj2 in *Escherichia coli*. *Appl. Environ. Microbiol.* 64, 1694–1699.

Nishihara, K., Kanemori, M., Yanagi, H., Yura, T. (2000) Overexpression of trigger factor prevents aggregation of recombinant proteins in *Escherichia coli*. *Appl. Environ. Microbiol.* 66, 884–889.

Nyalwidhe, J., Lingelbach, K. (2006) Proteases and chaperones are the most abundant proteins in the parasitophorous vacuole of *Plasmodium falciparum*–infected erythrocytes. *Proteom.* 6, 1563–1573.

Odom, A.R., Van Voorhis, W.C. (2010) Functional genetic analysis of the *Plasmodium falciparum* deoxyxylulose 5–phosphate reductoisomerase gene. *Mol. Biochem. Parasitol*. 170: 108–111.

Okita, B., Arcuri, E., Turner, K., Sharr, D., Del Tito, B., Swanson, J., Shatzman, A., Zabriskie, D. (2004) Effect of induction temperature on the production of malaria antigens in recombinant *E. coli*. *Biotechnol. Boeing.* 34, 854–862.

Okuhara, M., Kuroda, Y., Goto, T., Okamoto, M., Terano, H., Kohsaka, M., Aoki, H., Imanaka, H. (1980) Studies on new phosphonic acid antibiotics: III. Isolation and characterization of FR–31564, FR–32863 and FR–33289. *J. Antibiot.* 33, 24–28.

Olliaro, P.L., Yuthavong, Y. (1999) An overview of chemotherapeutic targets for antimalarial drug discovery. *Pharmacol. Ther*. 81, 91–110.

Ortmann, R., Wiesner, J, Reichenberg, A., Henschker, D., Beck, E., Jomaa, H., Schlitzer, M. (2003) Acyloxyalkyl ester prodrugs of FR900098 with improved *in vivo* antimalarial activity. *Bioorg. Med. Chem. Lett. 13*, 2163–2166.

Ortmann, R., Wiesner, J., Reichenberg, A., Henschker, D., Beck, E., Jomaa, H., Schlitzer, M. (2005) Alkoxycarbonyloxyethyl ester prodrugs of FR900098 with improved *in vivo* antimalarial activity. *Arch. Pharm. (Weinheim)* 338, 305–314.

Ortmann, R., Wiesner, J., Silber, S., Klebe, G., Jomaa, J., Shlitzer, M. (2007) Novel deoxyxylulosephosphate–reductoisomerase inhibitors: fosmidomycin derivatives with spacious acyl residues. *Arch. Pharm. Chem. Life Sci.* 340, 483 – 490.

Palmer, J. D. (1992) Green ancestry of malarial parasites? *Curr. Biol.* 2, 318–320.

Parker, S.E., Monteit, D., Horton, H., Hof, R., Hernandez, P., Vilalta, A., Hartikka, J., Hobart, P., Bentley, C.E., Chang, A., Hedstrom, R., Rogers, W.O., Kumar, S., Hoffman, S.L., Norman, J.A. (2001) Safety of a GM–CSF adjuvant–plasmid DNA malaria vaccine. *Gene Therap.* 8(13), 1011–1023.

Perruchon, J., Ortmann, R., Altenkämper, M., Silber, K., Wiesner, J., Jomaa, H., Klebe, G., Schlitzer, M. (2008) Studies addressing the importance of charge in the binding of fosmidomycin–like molecules to deoxyxylulosephosphate reductoisomerase. *Chem. Med. Chem.* 3, 1232–1241.

Pesce E.R., Acharya P., Tatu U., Nicoll W.S., Shonhai A., Hoppe H.C., and Blatch, G.L. (2008) The *Plasmodium falciparum* heat shock protein 40, Pfj4, associates with heat shock protein 70 and shows similar heat induction and localisation patterns. *Int. J. Biochem. Cell Biol.* 40, 2914–2926.

Pesce, E.R., Cockburn, I.L., Goble, J.L., Stephens, L.L., Blatch, G.L. (2010) Malaria heat shock proteins: drug targets that chaperone other drug targets. *Infect. Disord. Drug* Targets 10, 147–157.

Phaosiri C, Proteau P.J. (2004) Substrate analogs for the investigation of deoxyxylulose 5–phosphate reductoisomerase inhibition: synthesis and evaluation. *Bioorg. Med. Chem. Lett.* 14(21), 5309–5312.

Powers, M.V., Workman, P. (2007) Inhibitors of the heat shock response: biology and pharmacology. *FEBS Lett*. 581, 3758–3769.

Proudfoot, A.E., Goffin, L., Payton, M.A., Wells, T.N., Bernard, A.R. (1996) *In vivo* and *in vitro* folding of a recombinant metalloenzyme, phosphomannose isomerase. *Biochem. J*. 318, 437–442.

Querol, J., Campos, N., Imperial, S., Boronat, A., Rodríguez–Concepción, M. (2002) Functional analysis of the *Arabidopsis thaliana* GCPE protein involved in plastid isoprenoid biosynthesis. *FEBS Lett.* 514, 343–346.

Ralph, S.A., van Dooren, G.G., Waller, R.F., Crawford, R.J., Fraunholz, M.J., Foth, B.J., Tonkin, C.J., Roos, D.F., McFadden, G.I. (2004) Metabolic maps and functions of the *Plasmodium falciparum* apicoplast. *Nature Rev.* 2, 203–216.

Rangarajan, P.N., Padmanaban, P. (2001) Emerging targets for antimalarial drugs. *Expert Opin. Therap. Targets* 5, 423–441.

Rayavara, K., Desai, S.A. (2008) Genetic disruption of a mechanosensitive ion channel in *Plasmodium falciparum*. *Am. J. Trop. Med. Hyg.* 79, 65–66.

Reichenberg, A., Wiesner, J., Weidemeyer, C., Dreiseidler, E., Sanderbrand, S., Altincicek, B., Beck, E., Schlitzer, M., Jomaa, H. (2001) Diaryl ester prodrugs of FR900098 with improved *in vivo* antimalarial activity. *Bioorg. Med. Chem. Lett.* 11, 833–835.

Reuter, K., Sanderbrand, S., Jomaa, H., Wiesner, J., Steinbrecher, I., Beck, E., Hintz, M., Klebe, G., Stubbs, M. (2002) Crystal structure of 1–deoxy–D–xylulose 5–phosphate reductoisomerase, a crucial enzyme in the nonmevalonate pathway of isoprenoid biosynthesis. *J. Biol. Chem.* 277, 5378–5384.

Ricagno, S., Grolle, S., Bringer–Meyer, S., Sahm, H., Lindqvist, Y., Schneider, G. (2004) Crystal structure of 1–deoxy–D–xylulose–5–phosphate reductoisomerase from *Zymomonas mobilis* at 1.9–A resolution. *Biochim.Biophys.Acta* 1698, 37–44.

Robert, A., Meunier, B. (1998) Is alkylation the main mechanism of action of the antimalarial drug artemisinin? *Chem. Soc. Rev*. 27, 273–279.

Rodriguez–Concepcion, M., Campos, N., Lois, L.M., Maldonado, C., Hoeffler, J.F., Grosdemange–Billiard, C., Rohmer, M, Boronat, A. (2000) Genetic evidence of branching in the isoprenoid pathway for the production of isopentenyl diphosphate and dimethylallyl diphosphate in *Escherichia coli*. *FEBS Lett.* 473, 328–332.

Rohdich, F., Lauw, S., Kaiser, J., Feicht, R., Koehler, P., Bacher, A., Eisenreich, W. (2005) Isoprenoid biosynthesis in plants–2C–methyl–D–erythritol–4–phosphate synthase (IspC protein) of *Arabidopsis thaliana.* *FEBS J.* 273, 4446–4458.

Rohmer, M., Grosdemange, B.C., Seemann, M., Tritsch, D. (2004) Isoprenoid biosynthesis as a novel target for antibacterial and antiparasitic drugs. *Curr. Opin. Investig. Drugs* 5, 154–162.

Rosenthal, P.J. (2003) Antimalarial drug discovery: old and new approaches. *J. Exp. Biol.* 206, 3735–3744.

Rüdiger, S., Germoth, L., Schnieider–Mergener, J., Bakau, B. (1997) Substrate specificity of the DnaK chaperones determined by screening cellulose–bound peptide libraries. *EMBO J.* 16, 1501–1507.

Sadasivaiah, S., Tozan, Y., Breman, J.G. (2007) Dichlorodiphenyltrichloroethane (DDT) for indoor residual spraying in Africa: how can it be used for malaria control? *Am. J. Trop. Med. Hyg*. 77(Suppl. 6), 249–263.

Sahu, N.K., Sahu, S., Kohli, D.V. (2008) Novel molecular targets for antimalarial drug development. *Chem Biol. Drug Des.* 71, 287–297.

Sali, A., Blundell, T.L. (1993) Comparative protein modelling by satisfaction of spatial restraints. *J. Mol. Biol.* 234, 779–815.

Sareen, D., Sharma, R., Vohra, R.M. (2001) Chaperone–assisted overexpression of an active D–carbamoylase from *Agrobacterium tumefaciens* AM 10. *Protein Expr. Purif.* 23, 374.

Sargeant, T.J., Marti, M., Caler, E., Calrton, J.M., Simpson, K., Speed, T.P., Cowman, A.F. (2006). Lineage–specific expansion of proteins exported to erythrocytes in malaria parasites. *Genome Biol.* 7, R12.1–R12.22.

Sato, S., Wilson, R.J. (2002) The genome of *Plasmodium falciparum* encodes an active delta–aminolevulinic acid dehydratase. *Curr. Genet.* 40, 391–398.

Schlieker, C., Bukau, B., Mogk, A. (2002) Prevention and reversion of protein aggregation by molecular chaperones in the *E. coli* cytosol: implications for their applicability in biotechnology. *J. Biotechnol.* 96, 13–21.

Schrodel, A., Volz, J., de Marco, A. (2005) Fusion tags and chaperone co–expression modulate both the solubility and the inclusion body features of the recombinant CLIPB14 serine protease. *J. Biotechnol.* 120, 2–10.

Schwartzbach, S.D., Osafune, T., Loffelhardt, W. (1998) Protein import into cyanelles and complex chloroplasts. *Plant Mol. Biol*. 38, 247.

Schwender, J., Muller, C., Zeidler, J., Lichtenthaler, H.K. (1999) Cloning and heterologous expression of a cDNA encoding 1–deoxy–D–xylulose–5–phosphate reductoisomerase of *Arabidopsis thaliana*. *FEBS Lett.* 455, 140–144.

Seemann, M., Janthawornpong, K., Schweizer, J., Böttger, L.H., Janoschka, A., Ahrens–Botzong, A., Tambou, E.N., Rotthaus, O., Trautwein, A.X., Rohmer, M., Schünemann, V. (2009) Isoprenoid biosynthesis via the MEP pathway: *In vivo* Mössbauer spectroscopy identifies a $[4Fe–4S]^{2+}$ center with unusual coordination sphere in the LytB protein. *J. Am. Chem. Soc.* 131, 13184–13185.

Semenov, A., Olson, J.E. and Rosenthal, P.J. (1998) Antimalarial synergy of cysteine and aspartic protease inhibitors. *Antimicrob. Agents Chemother.* 42, 2254–2258.

Shenai, B.R., Sijwali, P.S., Singh, A. and Rosenthal, P.J. (2000) Characterization of native and recombinant falcipain–2, a principal trophozoite cysteine protease and essential hemoglobinase of *Plasmodium falciparum*. *J. Biol. Chem.* 275, 29000–29010.

Shonhai, A., Boshoff, A., Blatch, G.L. (2007) The structural and functional diversity of Hsp70 proteins from *Plasmodium falciparum*. *Protein Sci. 16*, 1803–1818.

Silber, K., Heidler, P., Kurz, T., Klebe, G. (2005) AFMoC enhances predictivity of 3D QSAR: A case study with DOXP–reductoisomerase. *J. Med. Chem*. 48, 3547–3563.

Singh, A., Rosenthal, P.J. (2001) Comparison of efficacies of cysteine protease inhibitors against five strains of *Plasmodium falciparum. Antimicrob. Agents Chemother*. 45, 949–951.

Singh, B., Sung, L.K., Matusop, A., Radhakrishnan, A., Shamsul, S.S.G, Cox–Singh, J., Thomas, A., Conway, D.J. (2004) A large focus of naturally acquired *Plasmodium knowlesi* infections in human beings. *Lancet* 363(9414), 1017–1024.

Singh, N., Chevé, G., Avery, M.A., McCurdy, C.R. (2006) Comparative protein modeling of 1–deoxy–D–xylulose–5–phosphate reductoisomerase enzyme from *Plasmodium falciparum*: a potential target for antimalarial drug discovery. *J. Chem. Inf. Model*. 46, 1360–1370.

Singh, N., Chevé, G., Avery, M.A., McCurdy, C.R. (2007) Targeting the methyl erythritol phosphate (MEP) pathway for novel antimalarial, antibacterial and herbicidal drug discovery: inhibition of 1–deoxy–D–xylulose–5–phosphate reductoisomerase (DXR) enzyme. *Curr. Pharm. Des.* 13, 1161–1177.

Solit, D.B., Chiosis, G. (2008) Development and application of Hsp90 inhibitors. *Drug Discov. Today* 13, 38–43.

Spehr, V., Frahm, D., Meyer, T.F. (2000) Improvement of the T7 expression system by the use of T7 lysozyme. *Gene* 257, 259–267

Spork, S., Hiss, J.A., Mandel, K., Sommer, M., Kooij, T.W.A., Chu, T., Schneider, G., Maier, U.G., Przyborski, J.M. (2009) An unusual ERAD–like complex is targeted to the apicoplast of *Plasmodium falciparum*. *Eukaryot. Cell* 8, 1134–1145.

Sridaran, S., McClintock, S.K., Syphard, L.M., Herman, K.M., Barnwell, J.W., Udhayakumar, V. (2010) Anti–folate drug resistance in Africa: meta–analysis of reported dihydrofolate reductase (dhfr) and dihydropteroate synthase (dhps) mutant genotype frequencies in African *Plasmodium falciparum* parasite populations. *Malaria J.* 9, 247.

Steinbacher, S., Kaiser, J., Eisenreich, W., Huber, R., Bacher, A., Rohdich, F. (2003) Structural basis of fosmidomycin action revealed by the complex with 2–C–methyl–D–erythritol 4–phosphate synthase (IspC). Implications for the catalytic mechanism and anti–malaria drug development. *J. Biol. Chem.* 278, 18401–18407.

Sui, S., Wang, J., Yang, B., Song, L., Zhang, J., Chen, M., Liu, J., Lu, Z., Cai, Y., Chen, S., Bi, W., Zhu, Y., He, F., Qian, X. (2008) Phosphoproteome analysis of the human Chang liver cells using SCX and a complementary mass spectrometric strategy. *Proteom.* 8, 2024–2034.

Surolia, N., Surolia, A. (2001) Triclosan offers protection against blood stages of malaria by inhibiting enoyl–ACP reductase of *Plasmodium falciparum*. *Nat. Med.* 7, 167–173.

Szabo, A., Langer, T., Schröder, H., Flanagan, J., Flanagan, J., Bukau, B., Hartl, F.U. (1994) The ATP hydrolysis–dependent reaction cycle of the *Escherichia coli* Hsp70 system – DnaK, DnaJ and GrpE. *Proc. Natl. Acad. Sci.* 91, 10345–10349.

Tahar, R., Basco, L.K. (2007) Molecular epidemiology of malaria in Cameroon. XXV. *In vitro* activity of fosmidomycin and its derivatives against fresh clinical isolates of *Plasmodium falciparum* and sequence analysis of 1–deoxy–D–xylulose–5–phosphate reductoisomerase. *Am. J. Trop. Med. Hyg.* 77(2), 214–220.

Takahashi, S., Kuzuyama, T., Watanabe, H., Seto, H. (1998) A 1–deoxy–D–xyulose 5–phosphate reductoisomerase catalyzing the formation of 2–C–methyl–D–erythritol 4–phosphate in an alternative nonmevalonate pathway for terpenoid biosynthesis. *Proc. Natl Acad. Sci.* 95, 9879–9884.

Takenoya, M., Ohtaki, A., Noguchi, K., Endo, K., Sasaki, Y., Ohsawa, K., Yajima, S., Yohda, M. (2010) Crystal structure of 1–deoxy–D–xylulose 5–phosphate reductoisomerase from the hyperthermophile *Thermotoga maritima* for insights into the coordination of conformational changes and an inhibitor binding. *J. Struct. Biol*. 170, 532–539.

Tavaria, M., Gabriele, T., Kola, I., Anderson, R.L. (1996) A hitchhiker's guide to the human Hsp70 family. *Cell Stress Chap.* 1, 23–28.

Taylor–Robinson, A.W. (2002) Exoerythrocytic malaria vaccine development: understanding host–parasite immunobiology underscores strategic success. *Expert Rev. Vaccines,* 1(3), 317–340.

Tekwani, B.L., Walker, L.A. (2005) Targeting the hemozoin synthesis pathway for new antimalarial drug discovery: technologies for *in vitro* beta–hematin formation assay. *Comb. Chem. High Throughput Screen.* 8, 63–79.

Templeton, T.J., Iyer, L.M., Anantharaman, V., Enomoto, S., Abrahante, J.E., Subramanian, G.M., Hoffman, S.L., Abrahamsen, M.S., Aravind, L. (2004) Comparative analysis of apicomplexa and genomic diversity in eukaryotes. *Genome Res.* 4, 1686–1695.

Thompson, J.D., Gibson, T.J., Plewniak, F., Jeanmougin, F., Higgins, D.G. (1997) The CLUSTAL X windows interface: flexible strategies for multiple sequence alignment aided by quality analysis tools. *Nucl. Acids Res.* 24, 4876–4882.

Thompson, J.D., Higgins, D.G., Gibson, T.J. (1994) CLUSTAL W: Improving the sensitivity of progressive multiple sequence alignment through sequence weighting, position–specific gap penalties and weight matrix choice. *Nucl. Acids Res*. 22, 4673–4680.

Trouiller, P., Olliaro, P., Torreele, E., Orbinski, J., Laing, R., and Ford, N. (2002) Drug development for neglected diseases: a deficient market and a public–health policy failure. *Lancet* 359, 2188–2194.

Tuteja, R. (2007) Unraveling the components of protein translocation pathway in human malaria parasite *Plasmodium falciparum. Arch. Biochem. Biophys*. 467, 249–260.

Umeda, T., Tanaka, N., Kusakabe, Y., Nakanishi, M., Kitade, Y. Nakamura, K.T. (2010) Crystallization and preliminary X–ray crystallographic study of 1–deoxy–D–xylulose 5–phosphate reductoisomerase from *Plasmodium falciparum. Acta Cryst.* F66, 330–332.

van Dongen, M., Weigelt, J., Uppenberg, J., Schultz, J., Wikström, M. (2002) Structure–based screening and design in drug discovery. *Drug Discov. Today* 7, 471–478.

van Dooren, G.G., Waller, R.F., Joiner, K.A., Roos, D.S., McFadden, G.I. (2000) Traffic Jams: protein transport in *Plasmodium falciparum. Parasitol. Today* 16, 421–427.

Verma, R., Boleti, E., George, A.J.T. (1998) Antibody engineering: comparison of bacterial, yeast, insect and mammalian expression systems. *J. Immunol. Meth*. 216, 165–181.

Vial, H.J., Philippot, J.R., Wallach, D.F. (1984) A re–evaluation of the status of cholesterol in erythrocytes infected by *Plasmodium knowlesi* and *P. falciparum*. *Mol. Biochem. Parasitol.* 13(1), 53–65.

Vincensini, L., Richert, S., Blisnick, T., Van Dorsselaer, A., Leize–Wagner, E., Rabilloud, T., Braun–Brenton, C. (2005). Proteomic analysis identifies novel proteins of the Maurer's clefts, a secretory compartment delivering *Plasmodium falciparum* proteins to the surface of its host cell. *Mol. Cell. Proteom.* 4, 582–593.

von Heijne, G. (1985) Signal sequences: the limits of variation. *J. Mol. Biol*. 184, 99–105.

Vriend, G. (1990) WHAT IF: a molecular modelling and drug design program. *J. Mol. Graph*. 8, 52–56.

Vythilingam, I., Tan, C.H., Asmad, M., Chan, S.T., Lee, K.S., Singh, B. (2006) Natural transmission of *Plasmodium knowlesi* to humans by *Anopheles latens* in Sarawak, Malaysia. *Trans. Roy. Soc. Trop. Med. Hyg*. 100, 1087–1088.

Walker, J.R., Poulter, C.D. (2005) Synthesis and evaluation of 1–deoxy–D–xylulose 5–phosphate analogues as chelation–based inhibitors of methylerythritol phosphate synthase. *J. Org. Chem.* 70, 9955–9959.

Wall, J.G., Pluckthun, A. (1995) Effects of overexpressing folding modulators on the *in vivo* folding of heterologous proteins in *Escherichia coli*. *Curr. Opin. Biotechnol*. 6, 507–516.

Waller, R.F., Keeling, P.J., Donald, R.G.K., Striepen, B., Handman, E., Lang–Unnasch, N., Cowman A.F., Besra, G.S., Roos, D.S., McFadden, G.I. (1998) Nuclear–encoded proteins target to the plastid in *Toxoplasma gondii* and *Plasmodium falciparum*. *Proc. Natl. Acad. Sci. U. S. A., 95*, 12352–1235.

Waller, R.F., Ralph, S.A., Reed, M.B., Su, V., Douglas, J.D., Minnikin, D.E., Cowman, A.F., Besra, G.S., McFadden, G.I. (2003) A type II pathway for fatty acid biosynthesis presents drug targets in *Plasmodium falciparum*. *Antimicrob. Agents Chemother*. 47, 297–301.

Ward, S.A. (2008) Drug–regulated expression of *Plasmodium falciparum* P–glycoprotein homologue 1: a putative role for nuclear receptors. *Antimicrob. Agents Chemother.*

Watanabe, Y.H., Motohashi, K., Taguchi, H., Yoshida, M. (2005) Heat–inactivated proteins managed by DnaKJ–GrpE–ClpB chaperones are released as a chaperonin–recognizable non–native form. *J. Biol. Chem*. 275, 12388–12392.

Waters, N.C., Geyer, J.A. (2003) Cyclin–dependent protein kinases as therapeutic drug targets for antimalarial drug development. *Expert Opin. Ther. Targets* 7, 7–17.

Weissman, J.S., Hohl, C.M., Kovalenko, O., Kashi, Y., Chen, S., Braig, K., Saibil, H.R., Fenton, W.A., Horwich, A.L. (1995) Mechanism of GroEL action: productive release of polypeptide from a sequestered position under GroES. *Cell* 83, 577–587.

White, R.H. (1978) Stable isotope studies on the biosynthesis of the thiazole moiety of thiamin in *Escherichia coli*. *Biochem.* 17, 3833–3840.

Wienk, H.L.J., Czisch, M., de Kruijff, B. (1999) The structural flexibility of the preferredoxin transit peptide. *FEBS Lett.* 453, 318–326.

Wiesner, J., Henschker, D., Hutchinson, D.B., Beck, E, Jomaa, H. (2002). *In vitro* and *in vivo* synergy of fosmidomycin, a novel antimalarial drug, with clindamycin. *Antimicrob. Agents Chemother.* 46(9), 2889–2894.

Wiesner, J., Jomaa, H. (2007) Isoprenoid biosynthesis of the apicoplast as drug target, *Curr. Drug Targets* 8, 3–13.

Williams, T.N., Mwangi, T.W., Roberts. D.J., Alexander, N.D., Weatherall, D.J., Wambua, S., Kortok, M., Snow, R.W., Marsh, K. (2005) An Immune Basis for Malaria Protection by the Sickle Cell Trait. *PLoS Med.* 2(5), 442–445.

Williamson, C.K. (2008) New antimalarials targeting both the asexual and gametocyte stages. ***Drugs Fut***., 33(12), 1033.

Wilson, R.J.M., Denny, P.W., Preiser, P.R., Rangachari, K., Roberts, K., Roy, A., Whyte, A., Strath, M., Moore, D.J., Moore, P.W., Williamson, D.H. (1996) Complete gene map of the plastid–like DNA of the malaria parasite *Plasmodium falciparum. J. Mol. Biol.* 261, 155–172.

Wilson, R.J.M., Gardner, M.J., Feagin, J.E., Williamson, D.H. (1991) Have malaria parasites three genomes? *Parasitol. Today* 7, 134–136.

Wirth, D.F. (2002) The parasite genome: biological revelations. *Nature* 419, 495–496.

Wong, A., Munos, J.W., Devasthali, V., Johnson, K.A., Liu, H.W. (2004) Study of 1–deoxy–D–xylulose–5–phosphate reductoisomerase, synthesis and evaluation of fluorinated substrate analogues. *Org. Lett.* 6, 3625–3628.

Wong, U., Cox, R.J. (2007) The chemical mechanism of D–1–deoxyxylulose–5–phosphate reductoisomerase from *Escherichia coli*. *Angew. Chem. Int. Ed. Engl.* 46, 4926–4929.

Wongsrichanala, I.C., Pickard, A.L., Wernsdorfer, W.H., Meshnick, S.R. (2002) Epidemiology of drug–resistant malaria. *Lancet Infect. Dis.* 2, 209–218.

Woo, Y.H., Fernandes, R.P., Proteau, P.J. (2006) Evaluation of fosmidomycin analogs as inhibitors of the *Synechocystis* sp. PCC6803 1–deoxy–Dxylulose–5–phosphate reductoisomerase. *Bioorg. Med. Chem.* 14, 2375–2385.

Woodgett, J.R., Gould, K.L., Hunter, T. (1986) Substrate specificity of protein kinase C. Use of synthetic peptides corresponding to physiological sites as probes for substrate recognition requirements. *Eur. J. Biochem.* 161, 177–184.

Wright, C.W. (2005) Plant derived antimalarial agents: new leads and challenges. *Phytochem. Rev*. 4, 55–61.

Xiao, Z., Waters, N.C., Woodard, C.L., Li, Z., Li, P.K. (2001) Design and synthesis of Pfmrk inhibitors as potential antimalarial agents. *Bioorg. Med. Chem. Lett.* 11, 2875–2878.

Yajima, S., Nonaka, T., Kuzuyama, T., Seto, H., Ohsawa, K. (2002) Crystal structure of 1–deoxy–D–xylulose 5–phosphate reductoisomerase complexed with cofactors: implications of a flexible loop movement upon substrate binding. *J. Biochem. (Tokyo)* 131, 313–317.

Yeh, I., Hanekamp, T., Tsoka, S., Karp, P.D., Altman, R.B. (2004) Computational analysis of *Plasmodium falciparum* metabolism: organizing genomic information to facilitate drug discovery. *Genome Res*. 14, 917–924.

Yin, X., Proteau, P.J. (2003) Characterization of native and histidine–tagged deoxyxylulose 5–phosphate reductoisomerase from the cyanobacterium *Synechocystis* sp. PCC6803. *Biochim Biophys. Acta* 1652, 75–81.

Yokoyama, N., Hirata, M., Ohtsuka, K., Nishiyama, Y., Fujii, K., Fujita, M., Kuzushima, K., Kiyono, T., Tsurumi, T. (2000) Expression of human chaperones Hsp70 and Hsdj or Hsp40 cofactor increases solubility of overexpressed target proteins in insect cells. *Biochim Biophys. Acta* 1493, 119–124.

Zang, L., Wu, G., Tate, C.G., Lookene, A., Olivercroner, A. (2003) Calreticulin promotes folding/dimerisation of human lipoprotein lipase expressed in insect cells (Sf21). *J. Biol. Chem.* 278, 29344–29351.

Zubrzycki, I.Z., Blatch, G.L. (2001) DFT study of a substrate and inhibitors of 1–deoxy–D–xylulose–5–phosphate reductoisomerase – the potential novel target molecule for anti–malaria drug development. *J. Mol. Model*. 7, 378–383.

7.2 APPENDICES

7.2.1 Appendix A – General experimental procedures

A1: Transformation of plasmid DNA into *E.coli* cells

Aliquots of 100 µl competent cells, either M15 cells, XL1 Blue cells; or 50 µl super–competent *E. coli* JM 109 cells were incubated with plasmid DNA (200–500 ng) on ice for 20 minutes. The cells were then heat–shocked at 42^{o}C for 45 seconds and incubated on ice for a further 2 minutes. Sterile 2x YT both (900 µl) was heated to 37^{o}C in a heating block and added to the transformation reaction. This was incubated at 37^{o}C for 1 hour, with agitation. From the transformation mixture, 150 µl was inoculated into 25 ml 2xYT containing appropriate antibiotic; the final concentrations for antibiotics were as follows: 100 µg/ml ampicillin, 50 µg/ml kanamycin, 34 µg/ml chloramphenicol. The inoculum was then incubated at 37^{o}C with shaking on a platform (180–200 rpm) for 12–16 hours; this is termed *the population effect*. The remaining transformation mixture was centrifuged at 13 000 rpm at room temperature for 1 minute and the pellet resuspended in a small amount of broth (100 µl). This was then spread–plated onto a 2x YT broth agar plate (1.6% tryptone, 1% yeast extract, 0.5% NaCl, 1.5% agar) containing the appropriate antibiotic. The plate was then inverted and incubated at 37^{o}C overnight.

A2: Preparation of *E.coli* competent cells

A transformant was inoculated into 5 ml 2X YT broth culture and incubated for 12–16 hours at 37^{o}C. A volume of overnight culture was then inoculated into 25 ml 2X YT broth such that the OD_{600nm} was 0.1 AU. The culture was grown at 37^{o}C with shaking on a platform (180–200 rpm) for 3–4 hours or until the OD_{600} was between 0.6 and 0.8 AU. The culture was the pelleted using JA14 rotor at 5000 rpm for 10 minutes at 4^{o}C. The pellet was then resuspended in 4 ml RF 1 solution (100 mM KCl, 50 mM $MnCl_2$, 30 mM CH_3COOK, 10 mM $CaCl_2$, 15% glycerol, pH 5.8) and incubated on ice for 20 minutes. The cells were again centrifuged at 5000 rpm at 4^{o}C for 10 minutes and resuspended in 1.5 ml RF 2 solution (10 mM Mops, 10 mM KCl,, 75 mM $CaCl_2$, 15% glycerol, pH 6.8). The mixture was aliquoted and stored at –80^{o}C until use. Competent cells that were made included: 1) XL1 Blue, which were inoculated from and old stock into 5 ml 2X YT broth; 2) M15, which was prepared in the same manner as XL1 Blue; 3) XL1 containing pMRBAD–PfHsp70 plasmid DNA, which were inoculated from a transformation in which XL1 blue cells were transformed with pMRBAD–PfHsp70; 4) XL1 containing pGro7 plasmid DNA, which were prepared in the

same manner as XL1 containing pMRBAD–PfHsp70; 4) XL1 containing pKJE7 plasmid DNA, which were prepared in the same manner as XL1 containing pMRBAD–PfHsp70; 5) XL1 containing pG–KJE8 plasmid DNA, which were prepared in the same manner as XL1 containing pMRBAD–PfHsp70.

A3: Diagnostic restriction enzyme analysis

Restriction enzyme analysis was used in confirmation and identification of purified plasmid DNA. Restriction analysis of approximately 100–200 ng double stranded plasmid DNA was achieved by digestion with 10 units of restriction enzyme in the presence of the relevant buffer. The reactions were made up to 20 µl using sterile milli–Q water and incubated at 37^{o}C for 6 hours. An uncut negative control was prepared for each enzyme reaction which contained no enzyme. Buffers used for digestion with the various enzymes included: buffer 2 (50 mM NaCl, 10 mM Tris–HCl, 10 mM $MgCl_2$, 1 mM dithiothreitol, pH 7.9 @ 25°C); buffer 3 (100 mM NaCl, 50 mM Tris–HCl, 10 mM $MgCl_2$, 1 mM dithiothreitol, pH 7.9 @ 25°C); and buffer 4 (50 mM potassium acetate, 20 mM Tris–acetate, 10 mM magnesium acetate, 1 mM dithiothreitol, pH 7.9 @ 25°C) (New England Biolabs). Plasmid DNA was linearized and double digested using the enzyme/buffer combinations summarized in Table **A.1**.

Table A.1: Enzymes and relevant buffers used in restriction enzyme analysis of plasmid DNA.

Plasmid	**Enzyme**	**Buffer**
pMRBAD–PfHsp70	Linearization with *Nco*I	Buffer 4
	Double digestion with *Aat*II and *Nco*I	
pGEMT–hPfDXR	Linearization with *Bam*HI	Buffer 3
	Double digestion with *Sal*I and *Bam*HI	
pQE30–PfDXR	Linearization with *Bam*HI	Buffer 3
	Double digestion with *Sal*I and *Bam*HI	
pQE9–EcDXR	Linearization with *Bam*HI	Buffer 2
	Double digestion with *Hind*III and *Bam*HI	

A4: Agarose gel electrophoresis

An agarose gel loading buffer (30% glycerol, 0.25% bromophenol blue) was added to each restriction digest (20 µl) in order to stop the reaction. The samples were then resolved on a 0.8% agarose gel containing 0.5 µg/ml ethidium bromide in the presence of 0.5 x TBE buffer (45 mM Tris, 45 mM borate, 1 mM EDTA, pH 8.3) at 100 V. Lamba (λ) DNA was digested with *Pst*I restriction enzyme and resolved as a molecular weight marker. Agarose gels were

visualised using ultraviolet (UV) light in a BioRad Universal Hood II Chemi/ Gel Doc system.

A5: DNA sequencing of plasmid DNA

Purified plasmid DNA (~400 ng) was added to a cycle sequence reaction, containing 3.2 pmol primer; either hPfDXR*Bam*HIF (forward), hPfDXR*Sal*IR (reverse), pQE1F (forward), or pQE1R (reverse). The cycle sequence reactions (final volume 20 µl) were prepared using the ABI PRISM® BigDye™ Terminator Cycle Sequencing Ready Reaction Kit (Fermentas), according to the manufacturer's conditions. Parameters for DNA amplification include: 1 cycle of 5 minutes at 95°C; followed by 30 cycles of denaturation, annealing and extension (30 seconds at 95°C, 30 seconds at 55–57°C and 30 seconds at 72°C); 1 cycle of 7 minutes at 72°C; followed by a hold at 4°C. The annealing temperature used for hPfDXR*Bam*HI and hPfDXR*Sal*IR primers was 57°C, and 55°C for pQE1F and pQE1R primers. DNA Sequencing Clean–up Kit™ (Zymo Research) was used in order to remove any unincorporated nucleotides and in order to concentrate the cycle sequencing reaction termination products; this was carried out according to the manufacturer's instructions.

A6: Sodium dodecyl sulphate polyacrylamide gel electrophoresis (SDS–PAGE)

Samples were treated with sodium dodecyl sulphate (SDS) polyacrylamide gel (PAGE) loading buffer (62.5 mM Tris–HCl pH 6.8, 26% [v/v] glycerol, 10% [w/v] SDS, 0.05% [w/v]bromophenol blue), containing [v/v] 5% β–mercaptoethanol (added fresh). Samples were boiled at 100°C for 15 minutes and analyzed by SDS–PAGE at 120 volts for 1.5 hours in SDS–PAGE running buffer (25 mM Tris, 192 mM glycine, 0.1% SDS, pH 8.3. The resolution of proteins was carried out using 12% acrylamide resolving gel and 4% acrylamide stacking gel using the concept of staggered buffering system (Laemmli, 1970). The electrophoresis was conducted using the Biorad Mini–protein 3 electrophoresis system (Biorad, USA). Protein was visualized after staining with coomassie stain (0.2% [w/v] Coomassie Brilliant Blue R–250, 40% [v/v] methanol, 7% [v/v] glacial acetic acid) and destaining with a strong destain solution (40% methanol, 7% glacial acetic acid).

A7: Western analysis and chemiluminescence–based immunodetection

The protein samples that were separated via SDS–PAGE were electrophoretically transferred onto a Hybond™–c extra nitrocellulose membrane, after being equilibrated in western transfer buffer (25 mM Tris, 192 mM glycine, 20% methanol, 4°C). Transfer took place at

100V for 1.5 hours using Biorad Western transfer apparatus (Biorad, USA). Transfer was visualised by incubating the membrane with ponceau S stain (0.5% Ponceau S, 1% glacial acetic acid) for 2 minutes before destaining with TBS (50 mM Tris–HCl, 150 mM NaCl, pH 7.5), followed by sterile water. The membrane was then incubated overnight at 4^{o}C in a blocking solution (5% [w/v] non–fat milk powder in TBS), as to prevent non–specific binding of suitable antibody. Detection of the PfDXR His–tagged protein was performed by incubating the membrane with mouse monoclonal anti–His antibody (1 in 3 000 dilution in blocking solution), followed by a goat polyclonal anti–mouse IgG secondary antibody, peroxidase–linked species–specific whole antibody (diluted 1 in 5 000 in blocking solution), each for 1 hour. Non–specifically bound primary and secondary antibody was removed from the membrane by washing three times for 20 minutes with TBS–tween (0.1% [v/v] Tween–20 in TBS), after each antibody incubation at room temperature, with shaking on a platform (30–50 rpm). The membrane was then incubated with ECL Advance Western Blotting Kit solution A (Tris buffer in 3.2% [v/v] ethanol) (250 µl) and solution B (Proprietary substrate in Tris buffer) (250 µl); Amersham Biosciences. The protein was then visualized using the BioRad Chemi/ Gel Doc system. The membrane was then incubated overnight at 4^{o}C in a blocking solution (5% [w/v] non–fat milk powder in TBS). Detection of the PfHsp70 protein was performed by incubating the membrane with rabbit polyclonal anti–PfHsp70 antibody (diluted 1 in 3 000 in blocking solution), followed by a donkey anti–rabbit IgG horseradish peroxidase–linked species–specific whole antibody (diluted 1 in 5 000 in blocking solution). The membrane was treated in the same way as described above for PfDXR His–tagged protein detection. The protein was then visualized using the BioRad Chemi/ Gel Doc system.

A8: His–spin protein miniprep™

Into 10 Zymo–Spin P1 columns (Zymo Research), 250 µl of His–affinity gel (Nickel–charged agarose in 30% [v/v] 20 mM sodium phosphate buffer pH 7.7, 100 mM NaCl, 10 mM imidazole, 20% [v/v] ethanol) was transferred. The columns were centrifuged for 15 seconds at 4^{o}C at 12 000 x g so that the affinity gel was completely drained. Subsequent to centrifugation, 300 µl of protein sample was then added to each of the ten columns, the affinity gel was resuspended and the resuspension was incubated at 4^{o}C for 2 minutes. The columns were centrifuged for 15 seconds at 4^{o}C at 12 000 x g. The flow through was discarded and the previous step repeated until all the protein sample had been passed through the columns. The affinity gel with bound protein was then washed with 250 µl His–wash buffer (50 mM sodium phosphate buffer pH 7.7, 300 mM NaCl, 50 mM imidazole, 0.03%

Triton X–100) and centrifuged for 15 seconds at 4°C at 12 000 x g. The flow through was discarded and the wash step repeated. Each Zymo–Spin P1 column was then placed in a sterile microcentrifuge tube and 150 µl His–elution buffer (50 mM sodium phosphate buffer pH 7.7, 300 mM NaCl, 250 mM imidazole) was added to each column. The gel was resuspended and incubated at 4°C for 1 minute. The protein was then eluted by centrifugation for 15 seconds at 4°C at 12 000 x g. Eluates from the 10 columns were then pooled and stored at 4°C for no longer then 1 hour until buffer exchange was carried out.

A9: Bradford's protein assay

The Bradford's protein assay was adapted from Bradford, 1976. The sample (5% [v/v]) was incubated with Bradford's reagent for 5 minutes at room temperature in a final reaction volume of 210 µl. Subsequent to incubation, protein was quantified at a wavelength of 595 nm using a Microtitre Plate Reader (Bio–Tek Instruments), in a 96–well microtitre plate. The protein concentration was quantified using a bovine serum albumin (BSA) standard curve (0–300 µg/ml).

A10: NADPH–dependent DXP enzyme assay

The assay, which converts NADPH to NADP+ was performed in a reaction mixture containing 100 mM Tris–HCl (pH 7.5), 1 mM $MnCl_2$, 0.3 mM DXP substrate, 0.3 mM NADPH (Jomaa *et al*., 1999) and DXR (5 – 20 µg/ml), made a final volume of 200 µl with assay buffer. Samples were incubated at 37°C for 5 minutes before the reaction was initiated by adding 20 µg/ml purified PfDXR or 5 µg/ml purified EcDXR. The oxidation of NADPH was monitored at 340 nm using a PowerWave™ microtitre plate reader, using a flat–bottomed 96–well microtitre plate, adjusted to 37°C. Reactions were blanked against a reaction containing water with 2 % DMSO (no enzyme). Activity of DXR was expressed in units per mg of protein where 1 unit is defined as the amount of enzyme that causes oxidation of 1 µmol of NADPH per minute; the extinction coefficient for NADPH used in this work was 0.00622 $\mu M^{-1}.cm^{-1}$ at 340 nm. Control reactions that were included prior to assay analysis included: no enzyme; denatured enzyme (boiled); no NADPH; and no divalent ion.

7.2.2 Appendix B – Addition figures and tables

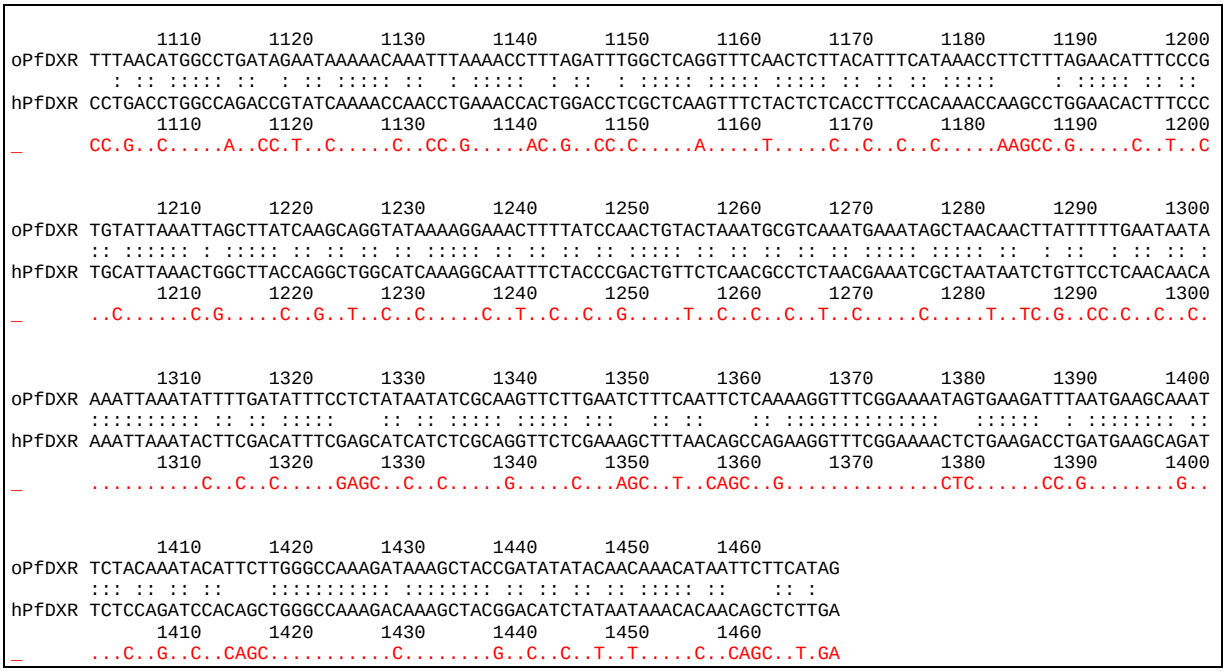

Figure B.1: Comparative sequence analysis showing codon harmonisation of the *P. falciparum* DXR gene.
Global sequence alignment of the full length PfDXR codon optimised gene versus the PfDXR codon harmonised gene using GENESTREAM. The consensus sequence characterizes identical nucleotides as '**:**', with 71.1% identity between the codon optimised and codon harmonised gene. The leader signal peptide sequence (213 nucleotides) is highlighted in *green*, while differences in the nucleotide sequence are shown in *red*.

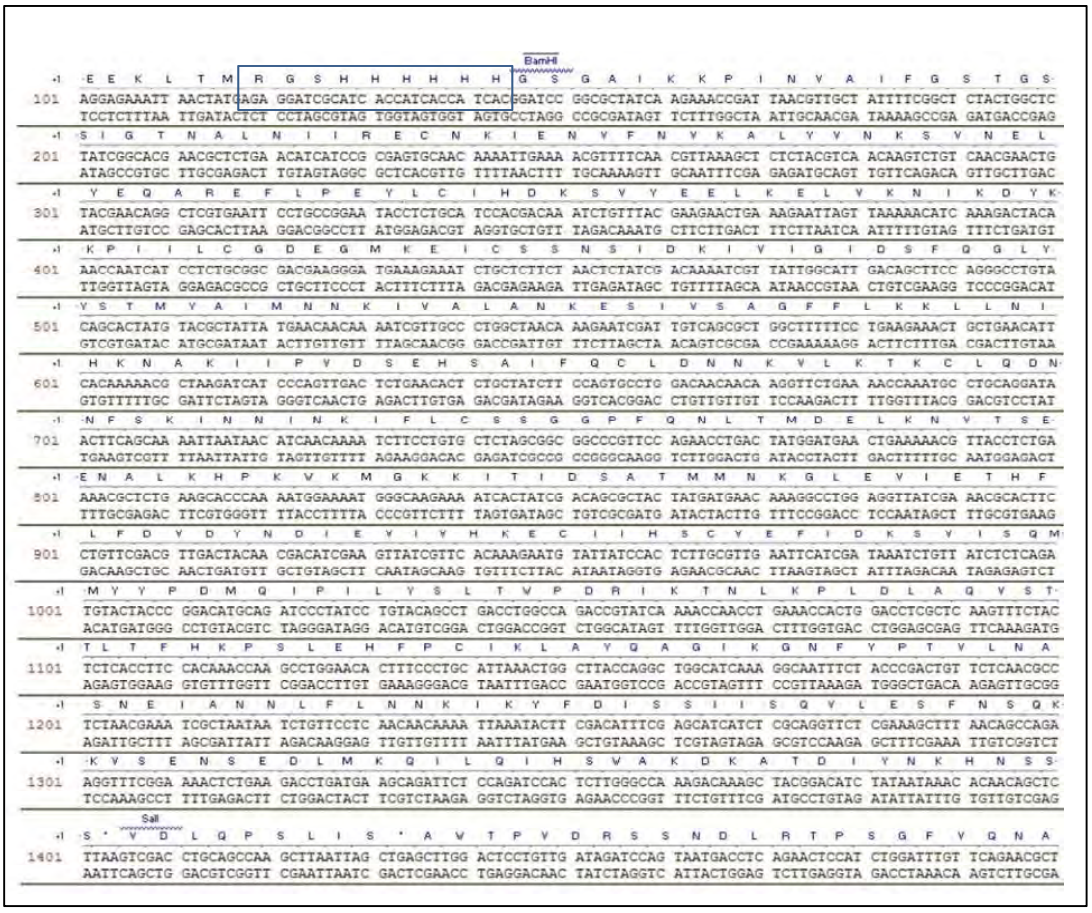

Figure B.2: Sequencing and verification of the pQE30–hPfDXR plasmid construct.
Fragment of the pQE30–hPfDXR nucleic acid sequence (1 to 1499), with the translated amino acid sequence shown in *blue*. The sequence coding for the N–terminal Histidine tag (His_6–tag) is highlighted in *pale yellow* and the restriction sites, *Bam*HI and *Sal*I are shown. The nucleotide bases, adenine (A), guanine (G), cytosine (C) and thymine (T) are shown in black. The ATG start codon is located at position 115 and the TAA stop codon, at position 1404.

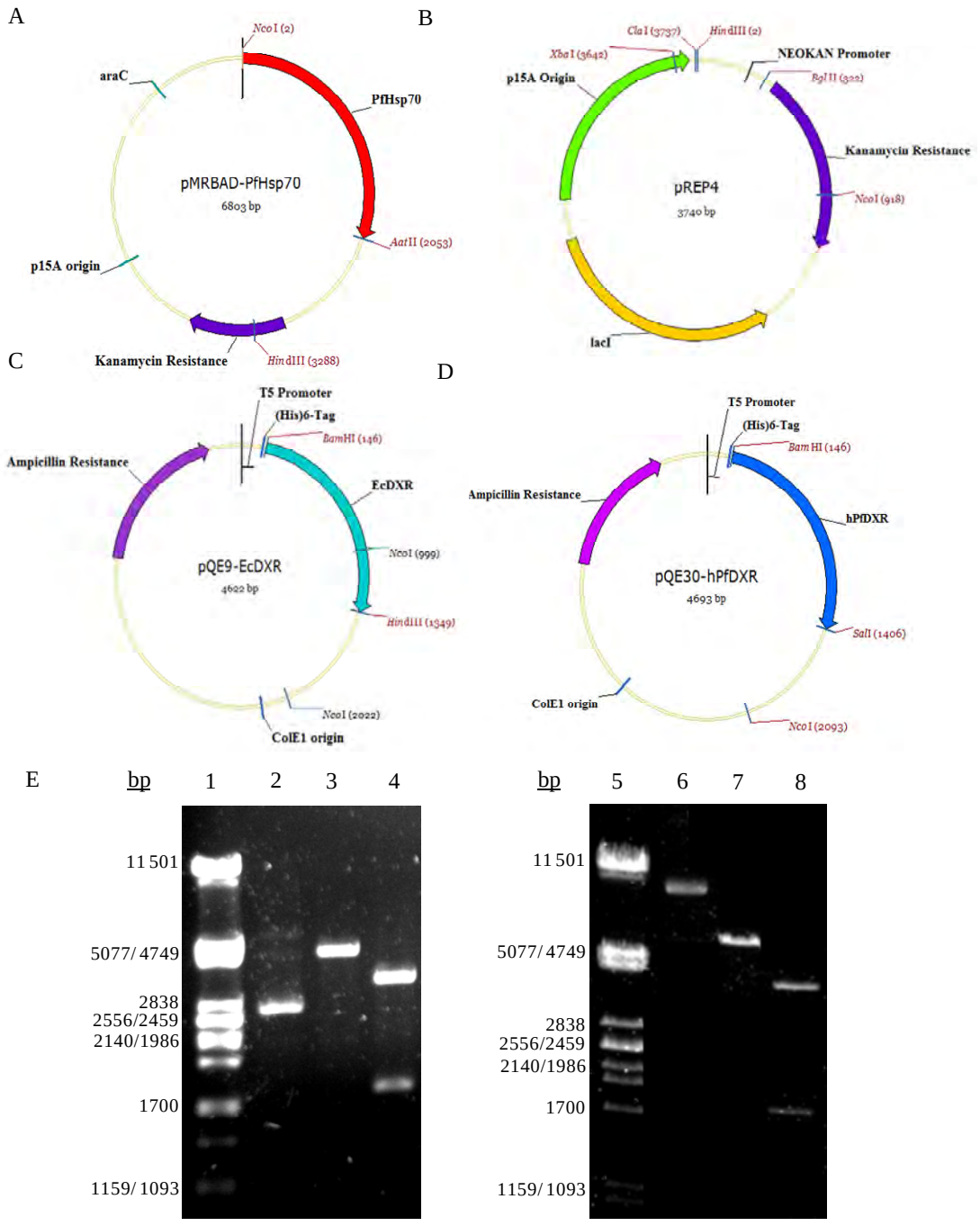

Figure B.3: Restriction analysis and verification of pQE30–hPfDXR and pMRBAD–PfHsp70 plasmid constructs.

(A) Plasmid map of pMRBAD–PfHsp70 showing the diagnostic restriction enzyme sites, encoding the malarial chaperone PfHsp70. (B) Plasmid map of pREP4, encoding the *lac*I repressor protein, purchased from Qiagen. (C) Plasmid map of pQE9–EcDXR showing the diagnostic restriction enzyme sites, encoding EcDXR. (D) Plasmid map of pQE30–hPfDXR showing the diagnostic restriction enzyme sites, encoding PfDXR. (E) 0.8% Agarose gel showing confirmation of the pQE30–hPfDXR and pMRBAD–PfHsp70 plasmid by diagnostic restriction enzyme analysis: lane 1 and 5: Lambda DNA restricted with *Pst*I restriction enzyme used as a DNA ladder quantified in base pairs (bp); lane 2: Uncut pQE30–hPfDXR showing mostly supercoiled parental DNA; lane 3: *Bam*HI linearized pQE30–hPfDXR DNA produces a 4691 bp product; lane 4: pQE30–hPfDXR DNA double digested with *Bam*HI and *Sal*I to release the 1290 bp hPfDXR coding region and the 3401 bp vector fragment. lane 6: Uncut pMRBAD–PfHsp70 showing mostly circular parental DNA; lane 7: *Nco*I linearized pMRBAD–PfHsp70 DNA produces a 6803 bp product; lane 8: pMRBAD–PfHsp70 DNA double digested with *Nco*I and *Aat*II to release the 2045 bp PfHsp70 coding region and the 4758 bp vector fragment.

Table B.1: Summary of information generated from AutoDock 4.2 for 46 novel compounds docked into the PfDXR homology model.

Ligand	H–Bonding Interactions with Catalytic Residues	# H–Bonds (Total)	Binding Affinity (kcal/mol)	Ligand Efficiency (relative)	Inhibition Constant (pM)
FR900098	Ser199(OG), Asn240(OD1), Lys241(HZ1), Lys241(HZ3)	5	–15.26	–0.94	45.59
Fos	Ser235(HG), Lys241(HZ2)	5	–14.77	–0.89	69.34
201	Ser199(HG), Ser235(HG), Asn240(OD1), Lys241(HZ1)	5	–12.07	–0.64	1430.00
201a	Ser199(OG), Ser235(HG), Lys241(HZ1)	5	–13.03	–0.87	279.89
201Na	Ser199(OG), Ser235(HG), Asn240(OD1), Lys241(HZ3)	4	–12.64	–0.84	545.99
202	Asn240(OD1), Lys241(HZ1), Lys241(HZ2)	5	–12.14	–0.61	1260.00
202a	Ser199(OG), Ser235(HG), Asn240(OD1), Lys241(HZ1), Lys241(HZ2)	5	–12.38	–0.77	846.39
202Na	Ser199(OG), Ser235 (OD), Asn(OG1), Lys241(HZ2)	5	–12.50	–0.84	524.06
203	Ser199(OG), Ser235(HG), Asn240(OD1), Lys241(HZ1)	4	–12.57	–0.63	631.57
203a	Ser235(HG), Asn240(OD1), Lys241(HZ1)	5	–13.24	–0.88	196.30
203Na	Ser199(OG), Ser235(HG), Asn240(OD1), Lys241(HZ2)	5	–12.66	–0.83	752.66
204	Ser199(OG), Ser235(HG), Asn240(OD1), Lys241(HZ2)	6	–14.16	–0.67	41.56
204a	Ser199(OG), Ser235(HG), Asn240(OD1)	5	–13.12	–0.77	242.77
204Na	Ser199(OG), Asn240(OD1), Lys241(HZ1)	5	–13.13	–0.77	238.64
205	Ser199(OG), Ser235(HG), Asn240(OD1), Lys241(HZ3)	5	–11.85	–0.59	2060.00
205a	Ser199(OD), Asn240(OD1)	5	–12.17	–0.81	1190.00
205Na	Ser199(HG), Asn240(OD1)	3	–12.34	–0.82	899.72
206	Ser199(OG), Asn240(OD1), Lys241(HZ3)	4	–12.79	–0.67	424.74
206a	Ser199(OG), Ser235(HG)	5	–12.61	–0.84	571.51
206Na	Ser199(OG), Asn240(OD1), Lys241(HZ3)	4	–13.36	–0.89	161.97
207	Ser199(HN), Ser235(HN), Asn240(OD1), Lys241(HZ2), Lys241(HZ3)	6	–13.05	–0.65	270.92
207a	Ser199(OG), Asn240(OD1), Lys241(HZ1)	7	–12.89	–0.81	356.64
207Na	Asn240(OD1)	2	–12.29	–0.77	977.10

301	Ser199(OG), Ser235(HG), Asn240(OD1), Lys241(HZ1)	5	–12.55	–0.63	633.79
301a	Asn240(OD1)	5	–12.57	–0.79	614.36
301Na	Asn240(OD1), Lys241(HZ3)	4	–13.03	–0.81	281.95
302	Ser199(OG), Asn240(OD1)	2	–11.87	–0.57	1980.00
302a	Ser199(OG), Ser235(HG), Asn240(OD1), Lys241(HZ1)	6	–14.04	–0.83	51.14
302Na	Ser199(OG), Ser235(HG)	3	–12.31	–0.72	944.39
303	Ser199(OG), Ser235(HG), Asn240(OD1), Lys241(HZ1)	4	–12.03	–0.60	1520.00
303a	Ser199(OG), Lys241(HZ2)	5	–13.00	–0.81	295.66
303Na	Ser235(HG), Asn240(OD1)	3	–13.58	–0.85	110.20
304	Lys241(HZ2)	1	–13.42	–0.61	144.64
304a	Ser199(HG), Ser235(HG), Asn240(OD1), Lys241(HZ1)	5	–14.80	–0.82	14.11
304Na	Asn240(OD1), Lys241(HZ1), Lys241(HZ3)	6	–13.72	–0.76	88.20
305	Ser199(OG), Asn240(OD1), Lys241(HZ1), Lys241(HZ3)	3	–11.99	–0.60	1610.00
305a	Ser199(OG), Asn240(OD1), Lys241(HZ2)	6	–13.39	–0.89	153.23
305Na	Ser199(OG), Asn240(OD1), Lys241(HZ1), Lys241(HZ2)	5	–12.61	–0.79	570.14
306	Ser199(HG), Asn240(OD1), Lys241(HZ3)	5	–13.10	–0.66	250.98
306a	Ser199 (HN)	1	–13.41	–0.84	148.74
306Na	Asn240(OD1), Lys241(HZ2)	3	–12.34	–0.77	899.07
307	Ser199(OG), Ser235(HG), Asn240(OD1)	5	–13.27	–0.63	186.20
307a	Ser235 (HG), Asn240(OD1), Lys241(HZ2)	5	–12.56	–0.74	624.48
307Na	Asn240(OD1), Lys241(HZ2)	5	–13.77	–0.81	80.93
140–1A	Ser199(OG), Asn240(OD1), Lys241(HZ1)	4	–11.72	–0.45	2550.00
140–2A	Ser199(OG), Asn240(OD1), Lys241(HZ1)	3	–12.51	–0.48	674.96
140–3A	Asn240(OD1)	1	–12.44	–0.48	756.88
140–4AA	Asn240(OD1)	1	–11.24	–0.42	5750.00

Information includes theoretical binding affinity (kcal/mol), relative ligand efficiency, theoretical inhibitor constant (pM) and potential hydrogen bonding interactions with flexible residues only. H = hydrogen, O = oxygen, D = delta, G = gamma, Z = zeta, named according to the atom position on the flexible residue.

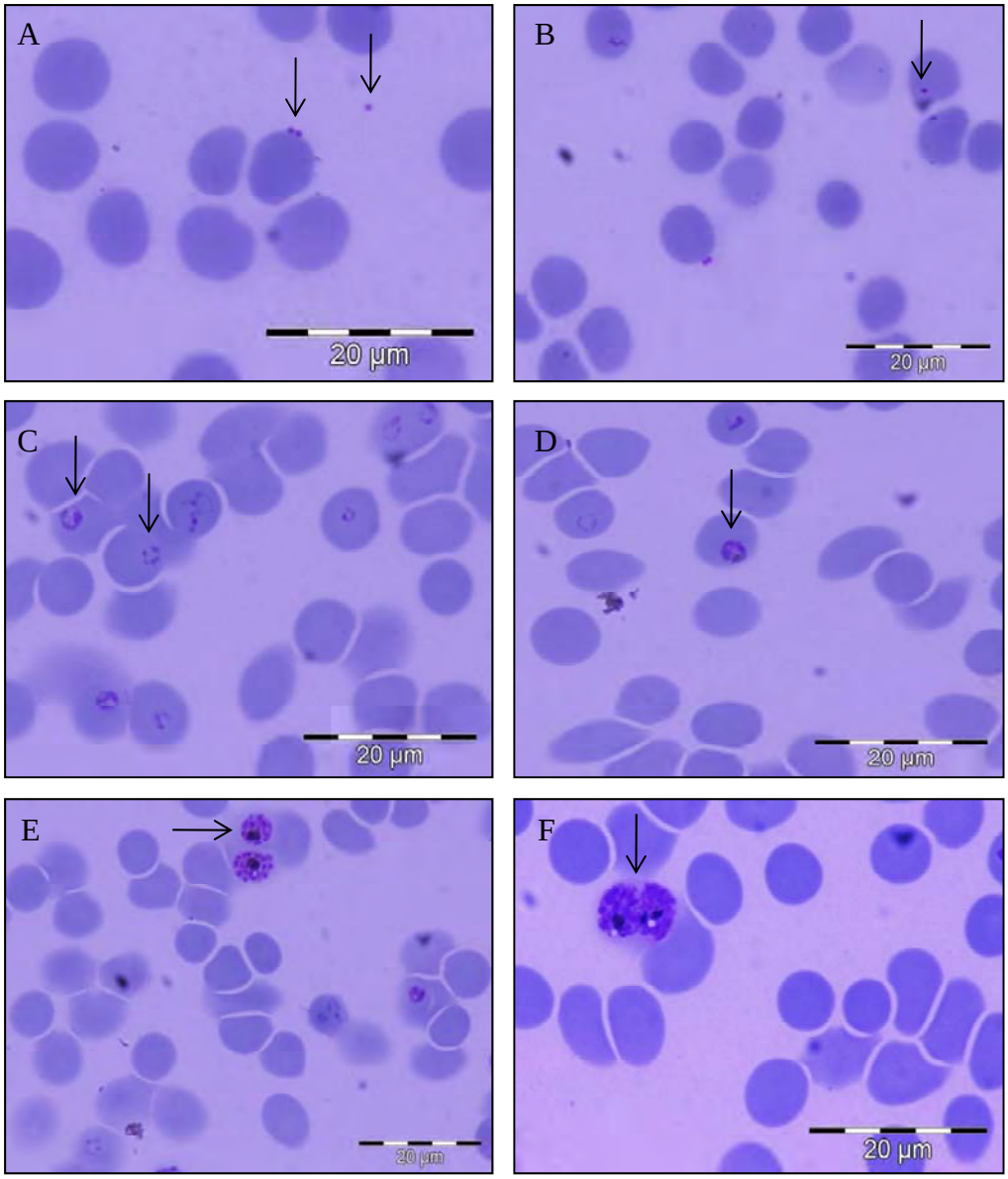

Figure B.4: Giemsa–stained *P. falciparum*–infected erythrocytes at different stages of infection.
Red blood cells infected with *P. falciparum* 3D7 malaria parasites. Free merozoites travel to an erythrocyte and are taken into the erythrocyte (A), in the erythrocyte, the early ring stage parasite (B) is distinguishable from the late ring stage when the merozoite spreads itself into a thin biconcave disc (C). The early trophozoite is distinguishable from the ring when the cytoplasm of the parasite has begun to expand but no haemozoin crystals are visible (D). The shizont (E) contains haemozoin and is distinguishable by the presence of numerous nuclei. (F) The incidence of multiple infections was a common occurrence.

7.2.3 Appendix C – General reagents and chemicals

Table C.1: Reagents and chemicals used for this work, as well as the relevant suppliers.

REAGENT	SUPPLIER
Agar	Oxoid, UK
Acetic acid	Merck, Germany
Agarose	Whitehead Scientific, South Africa
Ammonium persulphate	Saarchem, South Africa
Ampicillin	Sigma–Aldrich, USA
Bis/acrylamide	Biorad, South Africa
Bradford's reagent	Sigma–Aldrich, USA
Bromophenol blue	Sigma–Aldrich, USA
BSA	Roche, Germany
Calcium chloride	Merck, Germany
Chloramphenicol	Sigma–Aldrich, USA
Coomassie brilliant blue R250	Saarchem, South Africa
Cobalt chloride	Saarchem, South Africa
dNTP mix	Roche, Germany
DOXP substrate	Sigma–Aldrich, USA
Ethanol	Merck, Germany
Ethidium bromide	Sigma–Aldrich, USA
Glycerol	Merck, Germany
Glycine	Sigma–Aldrich, USA
Hybond c–extra nitrocellulose membrane	Amersham, USA
Hydrochloric acid	Merck, Germany
Imidazole	Sigma–Aldrich, USA
IPTG	Peqlab, Germany
Magnesium chloride	Saarchem, South Africa
Manganese chloride	Saarchem, South Africa
β–Mercaptoethanol	Merck, Germany
Methanol	Merck, Germany
Potassium chloride	Merck, Germany
Potassium dihydrogen phosphate	Merck, Germany
Lamda DNA	Promega, USA
Lysozyme	Roche, Germany
Phenylmethylsufonyl fluoride	Sigma–Aldrich, USA
Ponceau S	Sigma–Aldrich, USA
Protein Marker IV	Peqlab, Germany
Sodium chloride	Merck, Germany

Sodium dodecyl sulphate	Saarchem, South Africa
Sodium hydroxide	Merck, Germany
Trizama base	Oxoid, UK
Tryptone	Oxoid, UK
Tween 20	Saarchem, South Africa